Weissel, J., Peirce, J., Taylor, E., Alt, J., et al., 1991
Proceedings of the Ocean Drilling Program, Scientific Results, Vol. 121

39. CONSTRAINTS ON THE INDIA-ASIA CONVERGENCE: PALEOMAGNETIC RESULTS FROM NINETYEAST RIDGE[1]

Chris T. Klootwijk,[2] Jeff S. Gee,[3] John W. Peirce,[4] and Guy M. Smith[5]

ABSTRACT

This study details the Late Cretaceous and Tertiary northward movement of the Indian plate. Breaks in India's northward movement rate are identified, dated, and correlated with the evolution of the India-Asia convergence. Paleolatitudinal constraints on the origin of Ninetyeast Ridge are discussed, and limited magnetostratigraphic detail is provided.

Nearly 1500 sediment and basement samples from Sites 756, 757, and 758 on Ninetyeast Ridge were studied through detailed alternating field and thermal demagnetization. Primary and various secondary magnetization components were identified. Breakpoint intervals in the primary paleolatitude pattern for common-Site 758 were identified at 2.7, 6.7, 18.5, about 53, 63.5–67, and 68–74.5 Ma. Only the breakpoint interval at about 53 Ma reliably reflects a reduction in India's northward movement rate. The onset of this probably gradual slowdown was dated at 55 Ma (minimal age) based on the intersection of weighted linear regression lines. At the location of common-Site 758, northward movement slowed from 18–19.5 cm/yr (from at least 65 to 55 Ma) to 4.5 cm/yr (from 55 to at least 20 Ma). Reanalysis of earlier DSDP/ODP paleolatitude data from the Indian plate gives a comparable date (53 Ma) for this reduction in northward velocity.

Comparison of our Ninetyeast Ridge data and Himalayan paleomagnetic data indicates that the initial contact of Greater India and Asia may have already been established by Cretaceous/Tertiary boundary time. The geological record of the convergence zone and the Indian plate supports the notion that the Deccan Traps extrusion may have resulted from the ensuing deformation of the Indian plate. We interpret the breakpoint at 55+ Ma to reflect completion of the eastward progressive India-Asia suturing process.

Neogene phases in the evolution of the convergence zone were correlated with significant changes in the susceptibility, NRM intensity, and lithostratigraphic profile of Site 758. These changes are interpreted to reflect and postdate tectonic phases in the evolution of the wider Himalayan and southern Tibetan region. The changes were dated and interpreted as follows: 17.5 Ma, initial uplift of the Higher Himalaya following initiation of intercontinental underthrusting; 10–10.4 Ma, increased uplift and onset of Middle Siwaliks sedimentation; 8.8 Ma, probable reduction in influx corresponding with the Nagri Formation to Dhok Pathan Formation changeover; 6.5 Ma, major tectonic phase evident throughout the wider Himalayan region and northern Indian Ocean; 5.1–5.4 Ma, onset of oroclinal bending of the Himalayan Arc, of extensional tectonism in southern Tibet, and of Upper Siwalik sedimentation; 2.5–2.7 and 1.9 Ma, major phases of uplift of the Himalayan and Tibetan region culminating in the present-day high relief.

The basal ash sequence and upper flow sequence of Site 758 and the basal ash sequence of Site 757 indicate paleolatitudes at about 50°S. These support a Kerguelen hot spot origin for Ninetyeast Ridge. Consistently aberrant inclinations in the basalt sequence of Site 757 may be related to a southward ridge jump at about the time (58 Ma) that these basalts were erupted. The basalt sequence of Site 756 indicates a lower paleolatitude (about 43°S), as do parts of the basalt sequence of Site 758 which also have reversed polarity overprints. The low paleolatitudes for Site 756 may be explained by late-stage volcanism north of the Kerguelen hot spot or the influence of the Amsterdam–St. Paul hot spot.

INTRODUCTION

The Indian continent has moved northward over more than 70° of latitude since its Early Cretaceous separation from Australia and Antarctica. The magnitude and progress of this northward movement are well documented from seafloor-spreading analyses of the Indian Ocean (e.g., McKenzie and Sclater, 1971; Sclater and Fisher, 1974; Johnson et al., 1976, 1980; Norton and Sclater, 1979; Patriat et al., 1982; Fisher and Sclater, 1983; Patriat and Achache, 1984; Veevers, 1984; Molnar et al., 1988; Patriat and Ségoufin, 1988; Powell et al., 1988; Royer et al., 1988; Royer and Sandwell, 1989). Suturing of Greater India and Asia is generally thought to have been completed by 55–50 Ma. We will suggest, however, that initial contact may have already been established by Cretaceous/Tertiary boundary time. India's indentation into southern Asia has progressed since initial contact, throughout the Cenozoic, and continues today. Wide regions of southern Asia have been deformed (e.g., Molnar and Tapponnier, 1975, 1977, 1978; Tapponnier and Molnar, 1976, 1977; Tapponnier et al., 1982, 1986, 1990; Peltzer et al., 1982; Armijo et al., 1986, 1989), culminating in the Neogene uplift of the Higher Himalaya and finally the Pliocene-Pleistocene uplift of the wider Himalayan region and the Tibetan Plateau.

Geological investigations of the Himalayan-Tibetan convergence zone have increased dramatically over the last decade, resulting in a wealth of new data and insights. Any successful interpretation of the evolution of the India-Asia convergence needs to link the direct geological record of the Himalayan-Tibetan convergence zone and its more indirect sedimentary record in the Bengal and Indus fans with the relative motion record preserved in the Indian Ocean seafloor and also with the paleomagnetic record of the convergence zone, the Indian continent, and the oceanic part of the Indian plate (Fig. 1). Ours is, perhaps, the first study to benefit from an integrated primary knowledge of the paleomagnetic record from the latter three regions.

[1] Weissel, J., Peirce, J., Taylor, E., Alt, J., et al., 1991. *Proc. ODP, Sci. Results,* 121: College Station, TX (Ocean Drilling Program).
[2] Bureau of Mineral Resources, Geology and Geophysics, P.O. Box 378, Canberra ACT 2601, Australia.
[3] Scripps Institution of Oceanography, La Jolla, CA 92039, U.S.A.
[4] Geophysical Exploration and Development Corporation, Calgary, Alberta T2P 0Z3, Canada.
[5] Department of Earth and Atmospheric Sciences, St. Louis University, P.O. Box 8099, Laclede Sta., St. Louis, MO 63103, U.S.A.

The evolution of the India-Asia convergence has been a matter of debate ever since Molnar and Tapponnier (1975) analyzed the neotectonic evolution of southern Asia in terms of a rigid die (India) penetrating into a deformable plastic medium (Asia). Questions under discussion are the time and latitude of initial collision and suturing and the magnitude and mode of India's subsequent indentation into Asia. Paleomagnetism is ideally suited to address these questions because India's Late Cretaceous and Tertiary large-scale northward movement has been nearly exclusively latitudinal and is, therefore, well resolvable from paleolatitude observations. Unambiguous answers, however, have not been obtained so far from paleomagnetic studies that have concentrated either on a direct comparison of the paleolatitudinal evolution of northern India and southern Tibet or on the paleolatitudinal record from Deep Sea Drilling Project (DSDP) and Ocean Drilling Program (ODP) cores.

There are numerous reasons for the lack of consensus regarding the India-Asia convergence history. The complexity and limited availability of paleomagnetic data is one cause. In particular, the autochthonous Tertiary sequences on the Indian shield are limited in extent and suitability for paleomagnetic studies, and data are limited to the voluminous Deccan Traps of presumed Cretaceous/Tertiary boundary age. Furthermore, the paleomagnetic record from the more internal Himalayan region is complex, with numerous overprints and only sparse radiometric age control. Finally, the less complexly magnetized and well-developed, but largely allochthonous, Tertiary and upper Mesozoic sequences in Baluchistan, the Western Himalayan Syntaxis, the Himalayan foothills, and the Indo-Burman/Indo-Sinian ranges have not gained the attention they deserve. A notable exception is the series of highly successful magnetostratigraphic studies of the Siwaliks in the Potwar Plateau/Salt Range region of northern Pakistan and the Jammu region of northwestern India.

Conflicting results from the available paleomagnetic data further complicate the issue. Constraints from continental paleomagnetic data on the time and latitude of the India-Asia collision have been dominated by data from the Deccan Traps of presumed Cretaceous/Tertiary boundary age in central India and data from Upper Cretaceous and lower Tertiary sequences in southern Tibet. Results from the Deccan Traps have been generally interpreted in terms of a moderate southern paleolatitude (~27°S-33°S for Bombay [arbitrary locality]) during their extrusion. In contrast, the southern Tibetan data have been generally interpreted in terms of a paleoposition of about 15°N during the Late Cretaceous and earliest Tertiary. Such interpretations leave a wide oceanic gap at that time between southern Tibet and Greater India, even if one considers a Greater India of far northern extent (e.g., Powell and Conaghan, 1973, 1975; Veevers et al., 1975; Powell, 1979, 1986; Klootwijk and Bingham, 1980; Klootwijk et al., 1985, 1986b). Such paleomagnetic data have reinforced the notion that collision occurred at about the Paleocene/Eocene time boundary. It can be questioned, however, whether or not these paleomagnetic data sets fairly represent the paleopositions of India and southern Tibet, as will be discussed subsequently ("Some Problematic Paleomagnetic Data"). Exclusion of these data allows interpretations for an earlier initial contact between Greater India and southern Asia (Klootwijk et al., 1985, 1986b; Jaeger et al., 1989), and a few authors have suggested that contact between India and Asia had already occurred perhaps as early as Cretaceous/Tertiary boundary time (Klootwijk et al., 1986a; Jaeger et al., 1989).

An earlier analysis of paleolatitude observations from DSDP cores from Ninetyeast Ridge (Peirce, 1978) indicated a slowdown in the northward motion of the Indian plate at about 40 Ma, in line with the then-popular model of India-Asia convergence (Molnar and Tapponnier, 1975). Peirce pointed out, however, the possibility of an earlier slowdown. Perhaps the most detailed estimate of the slowdown in India's northward movement is that of Patriat and Achache (1984). This elegant absolute motion study, based on a mantle-fixed hot-spot reference frame (Morgan, 1983) and Africa-India relative motion data (Patriat, 1983), estimated collision to have occurred at the time of Chron 20 (then dated at 50 Ma), based on large fluctuations in direction and magnitude of Indian Ocean spreading. Klootwijk et al. (1985) have pointed out, however, that these data can also be interpreted in terms of final suturing of Greater India and southern Asia at about 55 Ma, with an earlier initial contact in northwestern Greater India.

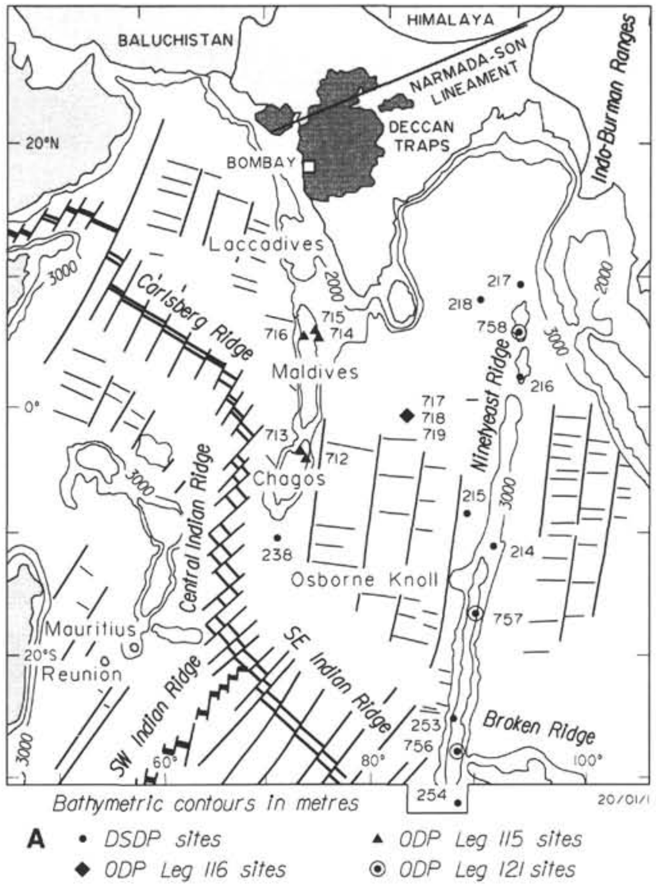

Figure 1. **A.** Overview of Peninsular India and Central Indian Ocean features with DSDP and ODP drilling sites labeled, redrawn from Shipboard Scientific Party (1988d, fig. 1). **B, C.** Overview of the India-Asia convergence zone, modified from Klootwijk et al. (1985, 1986a). Magnitude and sense of rotation, as inferred from paleomagnetic data and indicated by the azimuthal angle of the arrows, are given for segments of (B) the Himalayan Arc and the Lhasa Block with respect to the Indian shield and (C) the Western Himalayan–Pamir Syntaxis with respect to the Indian Shield (solid symbols) or Eurasia (open symbols). Paleomagnetic data 1–11 in Figure 1B are summarized in Klootwijk et al. (1985, table 1, 1986a); data for 12 according to Bossart et al. (1989).

The present study on the paleolatitudinal evolution of ODP Leg 121 Sites 756, 757, and 758 on Ninetyeast Ridge is a sequel to Peirce's (1978) study of DSDP sites on or directly west of this ridge. Our data indicate that India's northward motion slowed dramatically at or just before 55 Ma. We interpret this slowdown as the completion of suturing. We argue that initial contact between northwestern Greater India and Asia was already established by Cretaceous/Tertiary boundary time. The combined paleomagnetic record of the Leg 121 sites records the progression of continental convergence and evolution of the Himalayan-Tibetan convergence zone during the Paleogene. The Neogene evo-

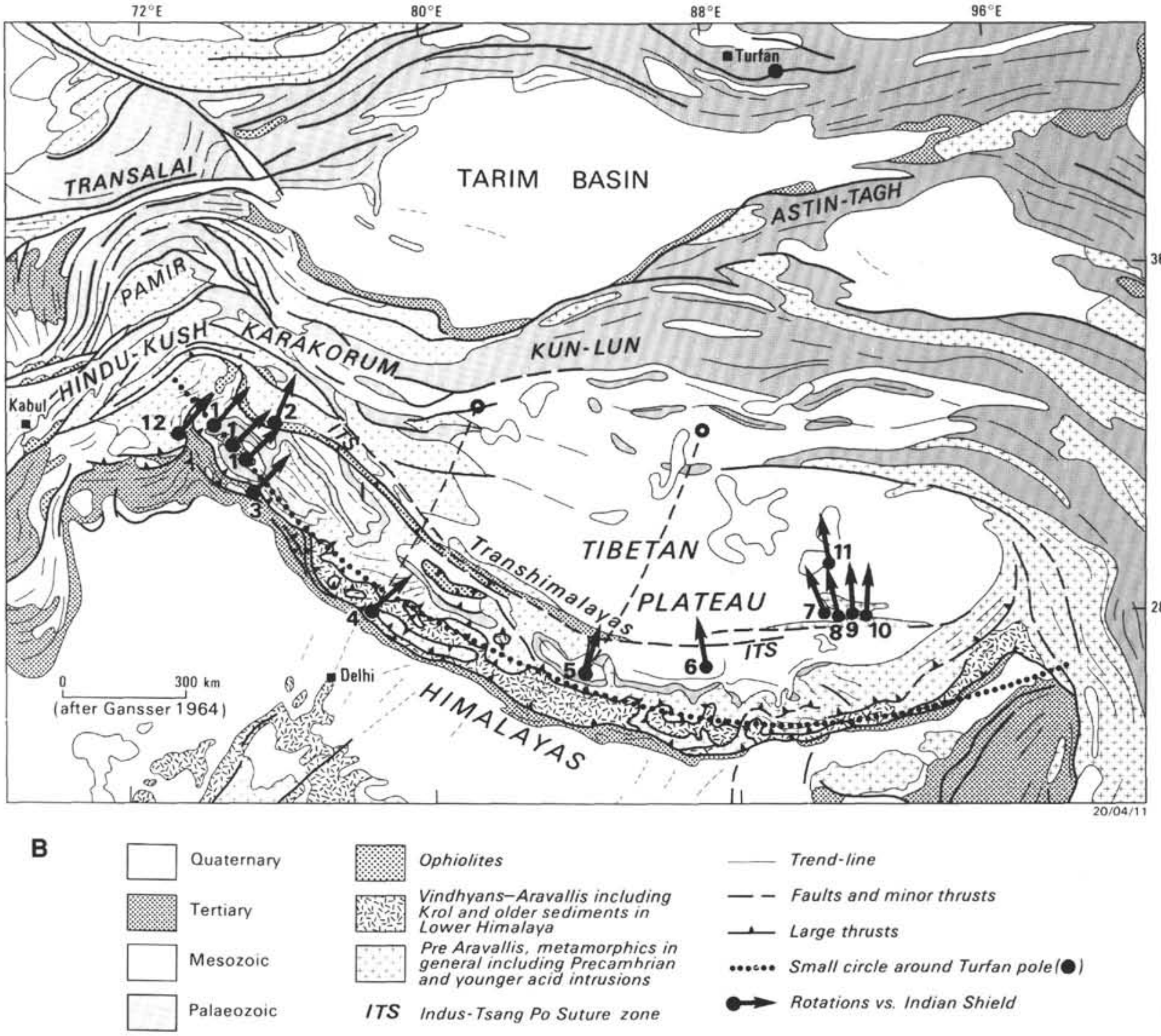

Figure 1 (continued).

lution is deduced from the magnetic and lithostratigraphic record of Site 758, which at 5°N is the site closest to the Bengal Fan. The paleomagnetic record of the ash and basalt sequences from Sites 757 and 758 supports Peirce's (1978) conclusion that Ninetyeast Ridge was formed at the Kerguelen hot spot (~49°S). However, substantial overprinting has occurred at Site 758, which may be related to the Amsterdam–St. Paul hot spot. Tectonism associated with a southward ridge jump has disturbed the sequence of Site 757. The shallower than expected paleolatitude of Site 756 basement (~43°S) may be related to the Amsterdam–St. Paul hot spot. Isotope geochemistry indicates involvement of this hot spot, indeed. Alternatively, these lower paleolatitudes may indicate a northward shift of the Kerguelen hot spot or perhaps a later episode of volcanism after the area had moved off the Kerguelen hot spot.

A splendid magnetostratigraphic profile has been obtained from the terrigenous clay-rich sequence covering the top hundred meters of Site 758, which was doubly recovered with the advanced hydraulic piston corer (APC). However, the magnetostratigraphic value of the other sedimentary samples was limited, primarily by the systematic overprinting of the carbonate-rich sediments during drilling and shipboard handling of cores and samples. The resulting paleomagnetic record is too disjointed for fruitful magnetostratigraphic interpretation.

METHODS

Sampling

A total of 1494 samples was taken, as detailed in Table 1. Soft sediments were sampled by pushing Mineral Research 7-cm^3 plastic cubes into the working half of the core section, using a plastic jig for proper alignment along the core axis. Prior to on-board sampling all cubes were demagnetized at 20 or 60 mT with the Schonstedt GSD-1 AF-demagnetizer. Harder sediments, consolidated ashes, and basalts were sliced, with a twin-bladed saw, into 10.6-cm^3 cubes. Slicing the cube samples proved faster and allowed for more accurate alignment of the sample axis with the core axis than drilling minicores. We typically took two samples per section from the sediments and ashes and increased this to three samples per section, wherever possible, in the crucial 40–55-Ma interval. We took up to six samples per cooling unit from the basalt sections. Sections 121-758A-4H-3, 121-758A-4H-4, and 121-758B-4H-1 were sampled at about 10-cm intervals in an effort to locate the Réunion subchrons.

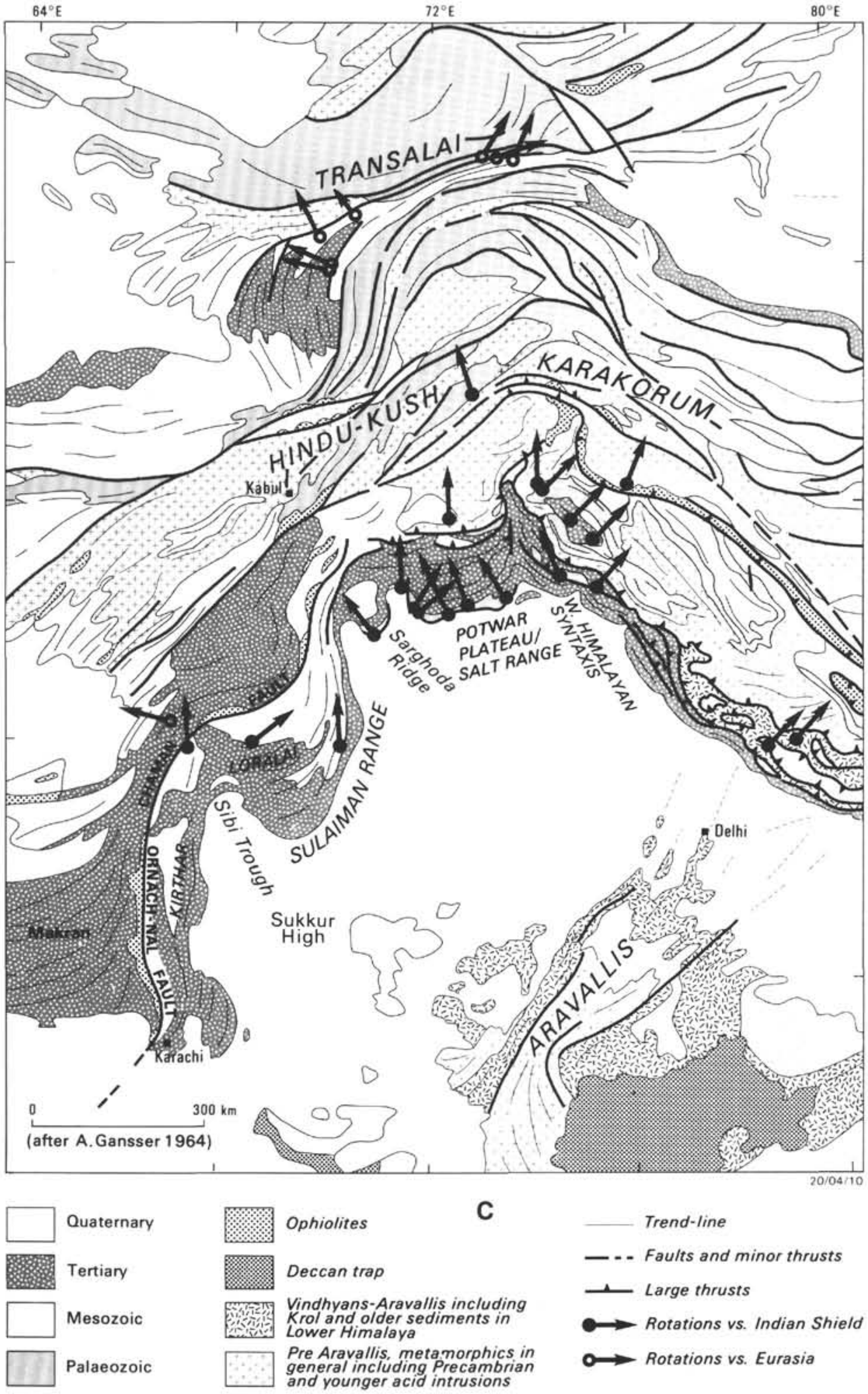

Figure 1 (continued).

Other than as an occasional check, progressive demagnetization treatment of the samples was deferred to shorebased studies. This was done because of the lower accuracy of the MOLSPIN magnetometer compared with that of the shorebased cryogenic magnetometers and because of indications of pickup of anhysteretic remanent magnetization (ARM) with the on-board Schonstedt AF-demagnetizer above 15-mT peak field (Shipboard Scientific Party, 1989b).

Demagnetization Treatment

All sediment samples were stored in a refrigerator at a nominal 4°C. Ash and basalt samples were stored in mu-metal boxes in

Table 1. Sample and measurement distribution.

	Sample distribution											Measurement distribution				
	Sediments			Tuff/Ash			Basement			Total		Pilot samples		Bulk samples		
Hole	H	X	R	W	X	R	X	N	R	Hole	Site	AF	TH	AF	TH	Steps
756B	137	—	—	—	—	—	—	—	—	137		30	—	98	0	2,172
756C	—	49	—	—	—	—	—	8	—	57		19	2	34	6	1,074
756D	—	—	—	—	—	—	—	—	54	54		14	14	0	40	1,477
											248					
757B	235	32	—	—	59	—	4	2	—	332		106	14	195	40	5,656
757C	—	—	70	4	—	3	—	—	76	153		44	21	50	62	3,411
											485					
758A	155	223	5	—	—	31	—	—	202	616		191	49	280	151	11,563
758B	145	—	—	—	—	—	—	—	—	145		42	—	103	—	2,550
											761					
												455	100	760	299	27,903

Note: H = advanced hydraulic piston core; X = extended core barrel; R = rotary barrel; W = wash-core recovery; N = Navi-drill core; AF = alternating field demagnetization; TH = thermal demagnetization.

fields of less than 100 nT. After initial natural remanent magnetization (NRM) measurements, 455 pilot samples were selected for progressive alternating field (AF) demagnetization in 11–22 steps up to 100 mT, using a Schonstedt GDS-5 AF-demagnetizer with a two-axis tumbler and a fast-reversing clutch. A further 100 pilot samples were selected for pilot thermal demagnetization in 24 steps up to 675°C. All heatings were carried out in large-volume furnaces with a feedback-controlled 10-set Rubens-Helmholtz coil system (McElhinny et al., 1971), reducing the ambient field to less than 5 nT over the furnace space during the heating/cooling cycle. Heatings (0.75–1 hr) were carried out in an inert argon gas environment, with forced cooling in air (0.5 hr). The onset of significant chemical changes was monitored through bulk susceptibility measurements on a DIGICO bridge.

The NRM of all pilot samples was remeasured after an interval of about 3 months in order to monitor viscous magnetization acquisition. Measurements were made on a two-axis ScT cryogenic magnetometer and a DIGICO spinner. Both magnetometers are housed in six-coil Helmholtz systems that reduce the ambient field at the sample insert to about 1000 nT. The magnetometers are linked to a data base housed on a controlling HP-A600 system, which allows for on-line inspection of Zijderveld (1967) plots. This feature has proven most useful in selecting the most appropriate demagnetization steps.

Analysis of the pilot samples showed considerable complexity in magnetization content. The bulk of the sediment and most of the ash samples, therefore, were AF demagnetized in as much detail as the pilot samples, albeit a few of the initial demagnetization steps were skipped occasionally. All of the remaining basalt and a few of the more robust ash samples were demagnetized thermally in 25 steps up to 685°C. Thermal treatment of the basalt samples showed better separation of components than AF demagnetization. Thermal demagnetization of all previously AF-demagnetized pilot basalt and ash samples was carried out in similar detail.

Considerable care was taken throughout this study to demagnetize the samples in as much detail as deemed necessary from on-line inspection of Zijderveld plots. Some 27,900 measurements were made on the 1494 samples (Table 1). This amounts to an average of 19 measurement steps per sample.

Analysis of Demagnetization Data

Measurements were stored on an IMAGE-database, housed on an HP-1000F system (Giddings, 1984; Giddings et al., 1985). All samples were analyzed individually for linear directions, planar elements, and Hoffman-Day directions with the use of an interactive graphics program (Giddings, 1985), based in part on Kirschvink's (1980) principal component analysis (PCA) method. Analysis was routinely carried out in the sample reference frame. We also analyzed samples from oriented APC cores (Holes 757B, 758A, and 758B) in the geographic reference frame after correction for the drift of the drill string and azimuthal rotation of the cores.

The samples generally showed a complex multicomponent magnetization pattern. We have followed a two-cycle procedure for directional analysis. In the first cycle, Zijderveld and equal-area plots of demagnetization series for individual samples were scrutinized with the interactive graphics PCA program, and all linear and Hoffman-Day components were determined which showed a good fit to the data. Based on experience (CTK), such a scrutiny of individual samples by a skilled operator, although necessarily somewhat subjective, is preferable to a batch-type analysis of samples following more objective, but preset and rigid, acceptance criteria. In the second cycle all linear and Hoffman-Day components were analyzed for directional groupings and common AF and thermal stability ranges, followed with a directional interpretation of the characteristic groupings.

A combination of methods was used in this second-cycle interpretation:

1. Equal-area plots of initial NRM directions (Fig. 2) and density distribution plots of all analyzed components from the pilot samples were scrutinized for overprints, particularly through a search for unwarranted directional groupings throughout unoriented cores.

2. Analyzed components of all pilot and bulk samples were plotted for each hole against depth (declination and inclination plots for both linear and Hoffman-Day directions) and were compared with obvious overprint directions and expected primary directions at the site. The latter comparison proved particularly useful in the identification of primary magnetization components through extended core sequences, such as from Site 758. This site has undergone more than 80 m.y. of continual northward drift over 50° of latitude, expressed in an inclination shift of more than 70°. We do not believe that such a comparison between observed and expected directions introduced any significant bias in the identification process. The primary and multiple overprint components (A–G, discussed in the following section) generally formed directionally discrete groupings with, for some of the components, unique and discrete stability spectra. This comparison merely served as a tool in identifying the primary magnetizations from amongst all earlier determined component directions throughout a core sequence.

In the absence of a detailed set of paleomagnetic pole positions for the Indian plate for the period of interest (0–85 Ma), expected

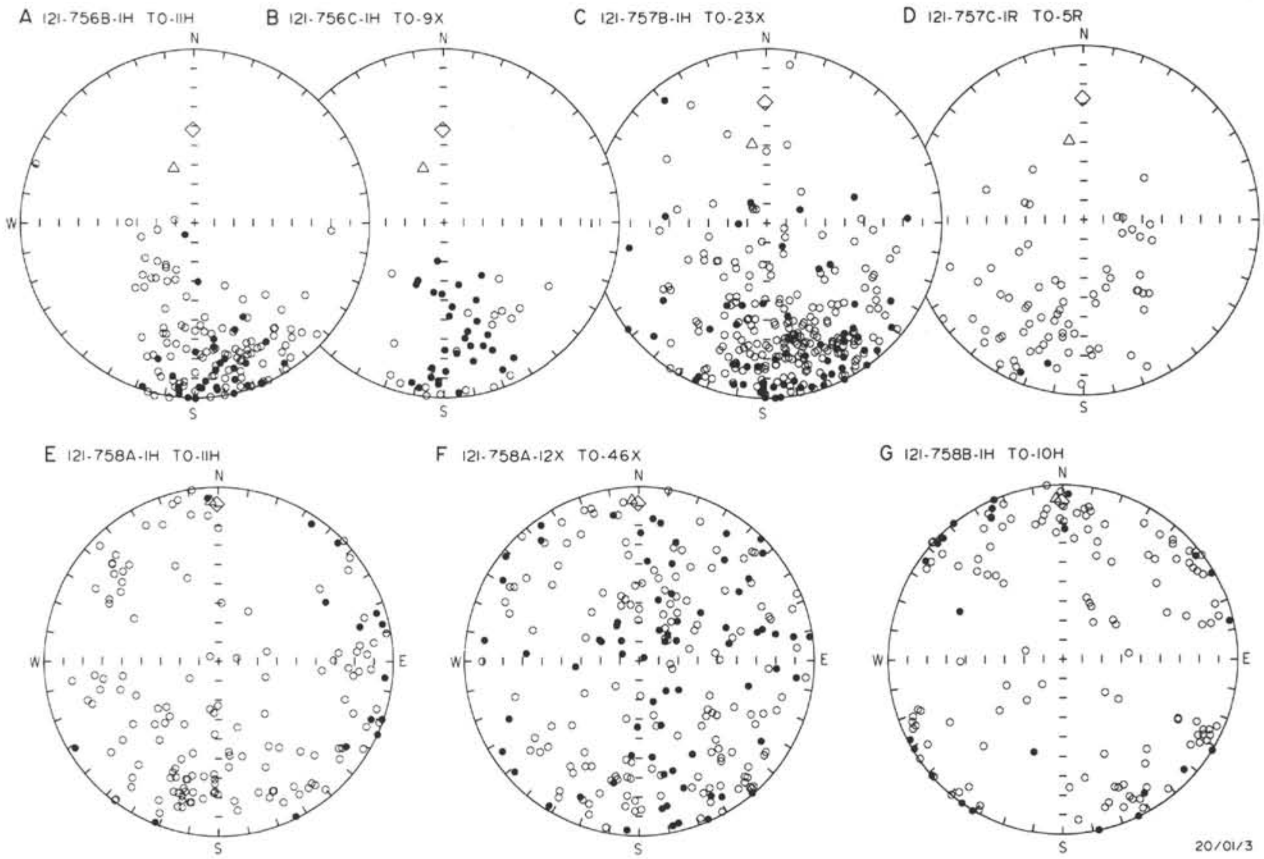

Figure 2. Initial NRM directions of sediment samples in equal-area projection. Solid symbols indicate downward-pointing directions and open symbols indicate upward-pointing directions. The present local field direction and the axial dipole field direction are indicated by a triangle and a diamond, respectively. Presence of the "180 degree" component is evident in Figures 2A–2D.

directions were obtained from an apparent polar wander path (APWP), which was simulated following the method described in Klootwijk et al. (1985). This APWP is derived from a recently refined set of Eulerian rotation poles (P. Patriat, pers. comm., 1989), which describes India's absolute motion on the basis of India-Africa relative motion data (Patriat et al., 1982; P. Patriat, pers. comm., 1983; Patriat and Achache, 1984; Patriat and Ségoufin, 1988) and Africa's motion with respect to a mantle-fixed hot-spot reference frame (Morgan, 1983). The Eulerian rotation poles, dated according to the Berggren et al. (1985) time scale, and the derived paleomagnetic pole positions for the Indian plate are listed in Table 2. This set of pole positions was linearly

Table 2. Simulated pole positions.

		Euler pole[a]			South Pole position	
Anomaly	Age (Ma)	Latitude (N, degrees)	Longitude (E, degrees)	Angle (degrees)	Latitude (S, degrees)	Longitude (E, degrees)
5	10.54	22.2	36.6	8.28	82.3	128.2
6	20.45	30.4	25.3	13.84	78.1	118.9
8	27.74	28.2	26.8	18.88	73.4	121.3
13	35.29	23.8	32.6	24.62	67.5	127.8
18	42.73	26.9	28.8	27.57	65.4	125.3
20	46.17	28.4	26.4	29.03	64.5	123.5
21	50.34	23.4	27.7	32.62	60.1	124.4
22	52.62	33.5	14.5	30.79	64.4	113.3
23	54.70	24.5	20.8	35.28	58.3	118.9
24	56.14	24.8	17.9	37.00	56.5	116.0
25	58.64	25.4	13.5	39.48	54.5	112.3
26	60.75	24.7	11.7	41.64	52.3	110.8
27	63.03	20.3	14.0	46.16	46.8	112.5
28	64.29	21.1	11.4	47.03	46.3	110.4
29	66.17	19.0	11.3	51.00	41.9	110.1
31	68.52	19.8	6.0	53.40	39.9	105.7
32	73.55	20.2	2.1	58.08	35.8	103.0
34	84.00	16.9	0.4	66.15	27.0	101.2

[a] Absolute motion Indian plate, rotations according to P. Patriat (pers. comm., 1983, 1989); see also Morgan (1983) and Patriat and Achache (1984).

interpolated over time for individual datum levels. Ages for paleomagnetic samples were estimated by linear interpolation over depth between consecutive biostratigraphic and/or magnetostratigraphic datum levels (Peirce, Weissel, et al., 1989), or were based on ^{39}Ar-^{40}Ar age determinations (Duncan, this volume). Expected directions for individual samples at the site were calculated from the so doubly interpolated pole positions following the axial geocentric dipole assumption.

3. Coercivity and blocking-temperature spectra of individual components were scrutinized for common stability patterns in order to further identify overprint and/or primary magnetization groupings in addition to the evidence gained from the equal-area, density, and stratigraphic plots.

The detailed PCA determination of linear and Hoffman-Day directions commonly showed slight to substantial shifts in declination with little variation in inclination. The regularity of such shifts and the resolution power of our interactive graphics PCA analysis supported the use of this two-cycle analysis approach to separate the determination of more than one subcomponent direction. Splitting of subcomponents and interactive visual appreciation of their reality was based on angular difference, length, and goodness-of-fit of split component directions. Such "split" components have been denoted throughout text, figures, and tables with subscripted component acronyms. For instance the acronym DR indicates a single drilling-induced overprint, but D_1 and D_2 indicate split overprints of softer (1) and harder (2) stability characteristics. Likewise, PP indicates a single primary magnetization component, and P_1 and P_2 distinguish between primary magnetization components of softer and harder stability ranges.

Magnetization Components

We have identified the following primary and multiple overprint components (A–G):

A: Steeply upward-directed components of low coercivity, generally less than 20 mT. These are drilling-induced overprints (DR; D_1, D_2), well established from earlier ODP paleomagnetic studies (Shipboard Scientific Party, 1987, 1988d, 1989d).

B: Components generally pointing 180° (sample reference frame), with shallow inclination (RR; R_1, R_2, etc). These components are generally restricted to the softer sediment samples and are characterized by high coercivity values up to and in excess of the 100-mT peak field obtainable with the Schonstedt GSD-5 AF-demagnetizer. The pervasive presence of these components generally precludes determination of a primary magnetization component, if any. Their origin could not be established with certainty and deserves some discussion. Acquisition as a systematic rotational remanent magnetization (Stephenson, 1976, 1980a, 1980b; Collinson, 1983) can be ruled out. The components are already present during initial NRM measurements (Fig. 2), decay upon AF demagnetization treatment rather than becoming more prominent, and are not related to the orientation of the sample within the two-axis AF tumbler unit. Likewise, acquisition of a viscous remanence upon long-term storage in the refrigerator is unlikely because the measured ambient field did not match the component directions, and initial NRM measurements before and after a 2–3-month storage period showed only limited viscous pickup of low coercivity. The persistent ~180° bias of the directions in the core reference frame strongly suggests that these components were induced during shipboard core handling and/or sampling. The direction of the "180 degree" component parallels the push direction during sampling. Løvlie et al. (1986) and Hailwood et al. (1989) have argued that comparable azimuthally aligned directions were acquired during sampling. However, the "180 degree" component is most prevalent in the softer samples (Fig. 2), and it is not clear why mechanical resetting during insertion of the sample box should be a bulk phenomenon rather than be restricted to the immediate vicinity of the sample-box walls. Systematic alignment of magnetization directions in the declination plane throughout multiple unoriented cores and sections, particularly in sediments with a low shear strength and low intensity of magnetization, was previously noted on board *JOIDES Resolution* during Leg 121 (Shipboard Scientific Party, 1989b) and earlier legs (Shipboard Scientific Party, 1988b, 1988c [fig. 16A], 1989f, 1989g). Our experiments aboard ship indicate that these components do not result from core slicing/sawing. Acquisition during whole-core AF demagnetization, using the AF-demagnetizer attached to the shipboard 2G-Enterprises cryogenic magnetometer, likewise can now be positively excluded because the samples have not undergone such AF demagnetization.

It is possible that mechanical resetting of the softer sediments occurred during operation of the *P*-wave logger with systematic alignment of the 0°–180° direction of the core sections along the transducer orientation. Our limited experiments on board (Shipboard Scientific Party, 1989h) failed, however, to establish a link with operation of the *P*-wave logger. Viscous magnetization pickup was noted during our cruise (Shipboard Scientific Party, 1989h) and on earlier legs (Shipboard Scientific Party, 1988b, 1988c), although directional agreement with the "180 degree" component was not established, nor was such a correlation searched for. This viscous acquisition is attributed to the low shear strength of the samples. Clearly, the acquisition mechanism of the "180 degree" component needs to be established and its cause prevented, as it may lead to unnecessary loss of the primary magnetization signal.

C: Primary magnetization components (PP; P_1, P_2, etc.) were identified through comparison with the pattern of expected inclinations—and declinations, in the case of oriented APC cores—and on the basis of their coercivity and blocking-temperature spectra. We commonly observed split components (e.g., P_1, P_2) with comparable inclinations, but distinct declinations and stability ranges (e.g., see Figs. 3C, 3K_2, 13I, 19D, 19E, 25E, 25M, 29A, 29E, 29K, 29L, 29N, 34A_1, 37A, and 37J). The reason for such declination discrepancies is not clear. In sediments recovered with the extended core barrel (XCB), relative rotations within a sample may occur. There is no reason, however, why characteristic components in such twisted samples should show different stability ranges. In the absence of declination control it is not possible to ascertain which of the split components truly represents a primary magnetization. Simple selection of the hardest split component as the true representation of the primary magnetization, with disregard of the softer splits, would be a somewhat naive approach for which we see no justification. There does not seem to be a fundamental reason why the softer magnetic fraction cannot be as good of a representation of the originating ambient field or would have been more affected by subsequent alteration processes. Examples are the perceived mechanically reset origin for the hard "180 degree" components with a softer primary component remaining (e.g., Holes 756B and 756C) and partial alteration processes leading to components with higher stability ranges (Hole 758A basement flows). We have followed, in our opinion, an objective approach with the separate calculation of mean inclinations (and directions) for all split components and have maintained this separation up to the common-site paleolatitude analysis ("Maximum Likelihood Determination of Breakpoints" section). We refer in the following to these split components rather informally as primary component*s* (a misnomer!) or split components or splits, in the sense that each of the splits could represent the true primary magnetization. With intersplit directional differences residing nearly entirely in the declination, and with the present analysis confined to inclination data only, such a semantic misnomer is irrelevant.

Other secondary components that occur more locally include

D: Recent field components (OV; O_1, O_2; e.g., Figs. 28D, 36F, 39C, and 40D);

E: Overprints reflecting periods of erosion and nondeposition (OV; O_1, O_2), that is, components observed around the lower Oligocene–Eocene hiatus in Hole 758A (Figs. 30C and 31D; see the section on Hole 758A XCB-cored sediments);

F: Thermal or hydrothermal basement reactivation components, such as the reversed polarity overprint (PR) in the normal polarity flow sequence of Hole 758A (e.g., Figs. 35B and 36E; see the section on Hole 758A basement flows);

G: Some spurious magnetization components of limited extent and unknown origin (e.g., Figs. 31E and 36G).

We also have observed in the basement sequence of Site 757 two aberrant and directionally very discrete groupings (HO; H_1, H_2 and LO; L_1, L_2) with very stable magnetic properties (e.g., Figs. 23B, 23C, 24A through 24H). We think that these aberrant directional groupings result from large-scale tectonic disturbances.

MAGNETIZATION PATTERNS AND MAGNETOSTRATIGRAPHY

We proceed here with a site by site description of magnetic observations, and defer interpretation to the following "Paleolatitudes and Breaks in Movement Rate" section.

Site 756

Sediments from Site 756 gave disappointing results (Table 3). The basalt sequence gave high-quality results, but their meaning is not clear.

Hole 756B

AF demagnetization only was applied to samples from this hole (Cores 121-756B-1H to 121-756B-11H; Figs. 3A, 3D, and 4 and Table 3). The magnetization of the APC-cored sediments is dominated by the "180 degree" overprint. Split components (Figs. 3A, 3B, 5A, 5B, 6A, and 6B) were identified with stability ranges up to 50–70 mT. Overprints with the lower AF stability ranges (Figs. 3A, 3B, and 5A) showed a more consistent concentration around 180° declinations and low to equatorial inclinations. Primary magnetization components (Figs. 3C, 3D, and 5C) are less prevalent and are generally as a group, but not always individually (Fig. 3D), of lower stability (Fig. 6) than the harder of the "180 degree" components. This observation is in accordance with the perceived origin of the "180 degree" overprint as a mechanically reset magnetic fraction in the majority of the samples. The occurrence of primary magnetization components throughout the sequence seems too disjointed to attempt a magnetostratigraphic interpretation.

Hole 756C

The magnetization pattern of the sedimentary sequence in Hole 756C (Cores 121-756C-4X to 121-756C-8X, 101–142 m below seafloor [mbsf]; Figs. 3E–3H, 3J, and 7 and Table 3) is comparable to that of the overlying sedimentary sequence drilled in Hole 756B (see previous section). Up to three "180 degree" components (Figs. 3F, 8A, 8B, and 9A–9C) and two primary magnetization components (Figs. $3H_1$, H_2, 8C, and 9D–9G) were identified, with comparable AF stability ranges, which range for the latter slightly higher up to 80 mT (Fig. 9). AF and thermal demagnetization of the samples from the single flow at the base of this hole (151–154 mbsf, Core 121-756C-10N) show two primary magnetization components with blocking-temperature ranges from 100° to 400°C and 300° to 700°C, respectively. We have noted in a few samples only a steeply upward-pointing drilling-induced component of low AF and thermal stability (Figs. 9H and 9J).

Hole 756D

AF and thermal demagnetization of the flow sequence (flow Units 756D-F1–756D-F14) in Hole 756D (Cores 121-756-4R to 121-756D-12R; Figs. 3I–3L, 10, 41E, and 41F and Table 3) showed two reversed polarity primary magnetization components (Figs. $3K_2$ and 11A) with comparable mean inclinations (60°–62°) and coercivity ranges (Figs. 12A and 12C), but with distinct blocking-temperature ranges (Figs. 12B and 12D). A steeply upward-directed drilling-induced component (Figs. 3I and 11B) of low coercivity, less than 15 mT, and a low blocking-temperature range (Fig. 12E, less than 200°C) was observed as well as some low-inclination components (Fig. $3K_1$).

Site 757

Results from the upper half of the sedimentary sequence are of disappointing quality. High-quality results were obtained from the ash and basement sequence. The basement results, however, could not be interpreted because of presumed tectonic problems.

Hole 757B

AF demagnetization of the sediments (Cores 121-757B-1H to 121-757B-19H and 121-757B-20X to 121-757B-23X, 0–211.7 mbsf; Figs. 13A–13H and 14 and Table 3) showed predominantly "180 degree" (Figs. 13A–13G, 15A, 15B, 17A, and 17B) and drilling-induced (Figs. 13B, 13D, 15C, and 17D) overprints. Only in a few samples from the upper part of the APC-cored sequence could we identify primary magnetization components of limited reliability (Figs. 13C and 15D). The various components show overlapping AF stability spectra, generally below 50 mT (Figs. 14, 16, and 18), with high-stability "180 degree" components.

AF and thermal demagnetization of the underlying ash sequence (Cores 121-757B-24X to 121-757B-40X, 211.7–369.3 mbsf; Figs. 13I–13M and Table 3) showed primary magnetization components of an exclusively reversed polarity (Figs. 13I, 13L, 13M, and 17E) with broad stability ranges up to 100 mT and up to 560°–640°C (Figs. 18A–18D and 41D). We observed limited occurrence of drilling-induced overprints of low stability, generally below 20 mT and below 400°C (Figs. 13J, K_1, 17D, 18G, and 18H). In addition, thermal demagnetization and/or thermal continuation of samples previously AF demagnetized showed a harder low-inclination overprint (Figs. $13K_2$, 13L, 17C, 18I, and 18J) of uncertain origin. Its inclination is comparable to the anomalously low inclinations that we observed in the two basal cooling units of Hole 757B (Cores 121-757B-41X to 121-757B-43N, 369.3–374.8 mbsf; Figs. 13N, 13O, and 41E and Table 3) and in the upper part of the flow sequence drilled in Hole 757C. We will argue hereafter (see "Mean Inclination/Latitude Results" section) that these anomalous inclinations probably result from pre-ash tectonic disturbances. If so, the similarity of the low-inclination directions in the ashes and the upper half of the flow sequence may be just fortuitous.

Hole 757C

AF demagnetization of the XCB-cored sediments (Cores 121-757C-2R to 121-757C-5R, 121.5–150.5 mbsf; Figs. 19A–19D and 20A and Table 3) showed limited occurrence of a soft drilling-induced overprint (Figs. 19B, 21C, and 22E), two harder "180 degree" components (Figs. 19B, 21A, 21B, 22C, and 22D), and two high-stability (up to 100 mT) primary components (Figs. 19C, 19D, 20A, 21D, 22A, and 22B). AF and thermal demagnetization of the ashes from wash-recovered Core 121-757C-6W showed a

Table 3. Mean inclination results and 95% confidence intervals (McFadden and Reid, 1982) for the softer (PP, P_1) and the harder (PP, P_2/P_3) primary magnetization components (see "Analysis of Demagnetization Data").

Depth (mbsf)	Components[a]	Type[b]			Age interval (Ma)		Number	Confidence interval: Mean inclination (degrees)	Confidence interval: Lower boundary (degrees)	Confidence interval: Upper boundary (degrees)
121-756B-1H to 121-756B-11H										
[c]15.0–25.0	PP, P_1	N+R	LP	AF	4.50	7.00	8	−40.73	−49.56	−30.76
[c]15.0–25.0	PP, P_1	NOR	LP	AF	4.50	7.00	5	−35.54	−42.36	−28.52
[c]25.0–31.0	PP, P_1	N+R	LP	AF	7.00	8.50	4	−42.34	−50.17	−34.33
[c]25.0–31.0	PP, P_1	NOR	LP	AF	7.00	8.50	3	−41.77	−57.53	−25.80
52.0–65.5	PP, P_1	N+R	LP	AF	16.00	20.50	8	−56.47	−63.65	−47.87
52.0–65.5	PP, P_1	NOR	LP	AF	16.00	20.50	5	−57.00	−72.17	−39.50
52.0–65.5	PP, P_1	REV	LP	AF	16.00	20.50	3	55.64	53.33	57.94
52.0–65.5	PP, P_1	N+R	HD	AF	16.00	20.50	4	−61.70	−79.27	−42.25
65.5–80.0	PP, P_1	N+R	LP	AF	20.50	26.00	7	−54.10	−60.89	−46.46
65.5–80.0	PP, P_1	NOR	LP	AF	20.50	26.00	5	−54.78	−66.20	−42.21
65.5–80.0	PP, P_1	N+R	HD	AF	20.50	26.00	4	−57.41	−80.86	−31.10
90.0–105.0	PP, P_1	NOR	LP	AF	29.50	32.50	9	−58.05	−63.47	−51.60
90.0–105.0	PP, P_2	NOR	LP	AF	29.50	32.50	4	−67.62	−84.71	−48.11
90.0–105.0	PP, P_1	NOR	HD	AF	29.50	32.50	7	−61.41	−68.44	−53.10
121-756C-4X to 121-756C-10N										
101.0–117.0	PP, P_1	REV	LP	AF	31.50	34.50	4	54.84	35.48	72.74
101.0–117.0	PP, P_1	N+R	HD	AF	31.50	34.50	7	−62.27	−73.91	−46.51
101.0–117.0	PP, P_1	REV	HD	AF	31.50	34.50	6	64.14	45.77	77.97
117.0–128.0	PP, P_1	N+R	LP	AF	34.50	36.00	7	−63.18	−72.12	−51.86
117.0–128.0	PP, P_1	REV	LP	AF	34.50	36.00	5	65.03	46.95	79.85
117.0–128.0	PP, P_1	N+R	HD	AF	34.50	36.00	8	−59.96	−68.82	−48.44
117.0–128.0	PP, P_1	NOR	HD	AF	34.50	36.00	5	−56.71	−67.60	−44.68
117.0–128.0	P_2, P_3	N+R	HD	AF	34.50	36.00	3	−62.86	−80.82	−44.32
128.0–143.0	PP, P_1	REV	LP	AF	36.00	43.30	8	60.33	41.16	73.06
128.0–143.0	P_2, P_3	REV	LP	AF	36.00	43.30	3	56.57	39.34	73.40
128.0–143.0	PP, P_1	REV	HD	AF	36.00	43.30	5	59.37	45.89	71.30
128.0–143.0	P_2, P_3	REV	HD	AF	36.00	43.30	3	61.43	55.63	67.17
143.0–155.0	PP, P_1	REV	LP	EV	43.30	43.30	11	60.27	54.55	64.84
143.0–155.0	P_2, P_3	REV	LP	EV	43.30	43.30	8	65.16	58.51	70.62
143.0–155.0	PP, P_1	REV	HD	EV	43.30	43.30	10	64.69	51.53	72.89
143.0–155.0	P_2, P_3	REV	HD	EV	43.30	43.30	6	61.02	45.97	73.20
121-756D-4R to 121-756D-12R										
158.5–168.2	PP, P_1	REV	LP	EV	43.30	43.30	8	56.70	49.51	62.87
158.5–168.2	PP, P_2	REV	LP	EV	43.30	43.30	8	53.50	50.34	56.46
158.5–168.2	PP, P_1	REV	HD	EV	43.30	43.30	7	60.11	47.24	70.29
158.5–168.2	PP, P_2	REV	HD	EV	43.30	43.30	7	60.31	48.98	69.48
168.2–173.8	PP, P_1	N+R	LP	EV	43.30	43.30	7	−59.33	−64.84	−53.13
168.2–173.8	PP, P_1	REV	LP	EV	43.30	43.30	6	60.33	53.80	66.27
168.2–173.8	PP, P_2	N+R	LP	EV	43.30	43.30	7	−65.59	−69.31	−61.47
168.2–173.8	PP, P_2	REV	LP	EV	43.30	43.30	6	65.29	60.27	69.86
168.2–173.8	PP, P_1	N+R	HD	EV	43.30	43.30	7	−61.24	−66.09	−55.82
168.2–173.8	PP, P_1	REV	HD	EV	43.30	43.30	6	61.06	54.31	67.16
168.2–173.8	PP, P_2	N+R	HD	EV	43.30	43.30	7	−63.76	−68.13	−58.87
168.2–173.8	PP, P_2	REV	HD	EV	43.30	43.30	6	64.00	57.91	69.49
177.7–178.3	PP, P_1	REV	LP	EV	43.30	43.30	3	59.08	46.68	71.26
177.7–178.3	PP, P_2	REV	LP	EV	43.30	43.30	3	61.74	45.99	77.08
177.7–178.3	PP, P_1	REV	HD	EV	43.30	43.30	3	61.58	46.50	76.30
177.7–178.3	PP, P_2	REV	HD	EV	43.30	43.30	3	61.58	46.50	76.30
187.4–192.0	PP, P_1	REV	LP	EV	43.30	43.30	7	60.34	57.65	62.89
187.4–192.0	PP, P_2	REV	LP	EV	43.30	43.30	7	60.32	57.46	63.03
187.4–192.0	PP, P_1	REV	HD	EV	43.30	43.30	6	67.25	51.77	78.97
187.4–192.0	PP, P_2	REV	HD	EV	43.30	43.30	6	58.95	50.95	66.12
197.1–202.6	PP, P_1	REV	LP	EV	43.30	43.30	7	60.42	55.07	65.24
197.1–202.6	PP, P_2	REV	LP	EV	43.30	43.30	7	60.97	56.82	64.78
197.1–202.6	PP, P_1	REV	HD	EV	43.30	43.30	6	61.73	49.85	71.70
197.1–202.6	PP, P_2	REV	HD	EV	43.30	43.30	6	60.13	53.03	66.54
206.6–208.6	PP, P_1	REV	LP	EV	43.30	43.30	8	64.43	60.52	67.91
206.6–208.6	PP, P_2	REV	LP	EV	43.30	43.30	8	65.71	61.74	69.21
206.6–208.6	PP, P_1	REV	HD	EV	43.30	43.30	6	70.48	61.03	78.15
206.6–208.6	PP, P_2	REV	HD	EV	43.30	43.30	8	69.15	61.28	75.14
208.6–221.0	PP, P_1	N+R	LP	EV	43.30	43.30	16	−61.28	−62.77	−59.59
208.6–221.0	PP, P_1	REV	LP	EV	43.30	43.30	15	61.51	59.83	63.01
208.6–221.0	PP, P_2	N+R	LP	EV	43.30	43.30	16	−62.41	−63.76	−60.90
208.6–221.0	PP, P_2	REV	LP	EV	43.30	43.30	15	62.69	61.30	63.95
208.6–221.0	PP, P_1	N+R	HD	EV	43.30	43.30	16	−61.27	−63.67	−58.31
208.6–221.0	PP, P_1	REV	HD	EV	43.30	43.30	15	61.15	58.00	63.73
208.6–221.0	PP, P_2	N+R	HD	EV	43.30	43.30	16	−62.56	−65.22	−59.16
208.6–221.0	PP, P_2	REV	HD	EV	43.30	43.30	15	62.53	58.88	65.41

Table 3 (continued).

Depth (mbsf)	Components[a]	Type[b]			Age interval (Ma)		Number	Confidence interval: Mean inclination (degrees)	Confidence interval: Lower boundary (degrees)	Confidence interval: Upper boundary (degrees)
[d]Mean-flow results: Holes 756C and 756D										
	PP, P_1	REV	LP	EV	43.30	43.30	8	60.45	58.20	62.57
	PP, P_2	REV	LP	EV	43.30	43.30	8	62.14	57.82	65.98
	PP, P_1	REV	HD	EV	43.30	43.30	8	63.71	59.81	67.20
	PP, P_2	REV	HD	EV	43.30	43.30	8	62.36	58.98	65.43
121-757B-2H to 121-757B-19H										
6.0–43.8	PP, P_1	N+R	LP	AF	3.70	5.30	10	−40.66	−48.29	−31.76
26.0–43.8	PP, P_1	NOR	LP	AF	3.70	5.30	7	−44.88	−52.73	−36.23
26.0–43.8	PP, P_1	REV	LP	AF	3.70	5.30	3	29.72	11.36	47.91
26.0–43.8	PP, P_2	N+R	LP	AF	3.70	5.30	5	−42.49	−58.24	−25.32
26.0–43.8	PP, P_1	N+R	HD	AF	3.70	5.30	11	−41.64	−47.29	−35.18
26.0–43.8	PP, P_1	NOR	HD	AF	3.70	5.30	8	−43.32	−51.19	−34.45
26.0–43.8	PP, P_1	REV	HD	AF	3.70	5.30	3	37.08	25.31	48.76
26.0–43.8	PP, P_2	N+R	HD	AF	3.70	5.30	4	−39.32	−58.18	−19.55
26.0–43.8	PP, P_2	REV	HD	AF	3.70	5.30	3	35.02	14.83	54.97
43.8–53.0	PP, P_1	N+R	LP	AF	5.30	6.50	4	−35.49	−43.32	−27.54
62.2–70.0	PP, P_1	N+R	LP	AF	8.30	8.80	3	−39.07	−62.76	−14.98
84.5–90.0	PP, P_1	NOR	LP	AF	14.30	16.20	5	−39.29	−48.58	−29.58
152.0–159.5	PP, P_1	NOR	LP	AF	45.50	47.00	2	−58.50	−63.64	−53.36
[e]121-757B-20X to 121-757B-42N										
175.0–186.0	PP, P_1	NOR	LP	EV	50.00	52.70	9	−57.00	−61.35	−52.04
175.0–186.0	PP, P_2, P_3	NOR	LP	EV	50.00	52.70	3	−64.76	−76.06	−53.21
175.0–186.0	PP, P_1	NOR	HD	EV	50.00	52.70	5	−60.28	−73.25	−45.39
186.0–203.5	PP, P_1	N+R	LP	EV	52.70	53.70	7	−62.07	−71.14	−50.68
186.0–203.5	PP, P_1	NOR	LP	EV	52.70	53.70	4	−60.09	−70.77	−48.77
203.5–213.0	PP, P_1	REV	LP	EV	53.70	55.00	4	65.76	61.37	70.03
[f]214.0–250.4	PP, P_1	N+R	LP	EV	58.50	58.50	19	−64.02	−67.39	−57.05
[f]214.0–250.4	PP, P_1	REV	LP	EV	58.50	58.50	18	64.00	56.61	67.60
[f]214.0–250.4	PP, P_2, P_3	REV	LP	EV	58.50	58.50	10	62.42	55.41	67.34
214.0–250.4	LO, L_1	N+R	LP	EV	58.50	58.50	15	−18.09	−23.22	−12.60
214.0–250.4	LO, L_1	NOR	LP	EV	58.50	58.50	4	−17.45	−33.42	−1.23
214.0–250.4	LO, L_1	REV	LP	EV	58.50	58.50	11	18.32	11.19	25.05
214.0–250.4	LO, L_2	N+R	LP	EV	58.50	58.50	8	−21.42	−30.30	−12.04
214.0–250.4	LO, L_2	NOR	LP	EV	58.50	58.50	3	−20.45	−30.63	−10.23
214.0–250.4	LO, L_2	REV	LP	EV	58.50	58.50	5	22.02	3.02	40.21
[f]214.0–250.4	PP, P_1	REV	HD	EV	58.50	58.50	16	62.41	53.17	66.95
[f]214.0–250.4	PP, P_2, P_3	REV	HD	EV	58.50	58.50	9	64.78	48.74	72.90
214.0–250.4	LO, L_1	N+R	HD	EV	58.50	58.50	11	−23.65	−29.62	−17.27
214.0–250.4	LO, L_1	NOR	HD	EV	58.50	58.50	4	−26.87	−40.57	−12.89
214.0–250.4	LO, L_1	REV	HD	EV	58.50	58.50	7	21.76	12.34	30.78
214.0–250.4	LO, L_2	N+R	HD	EV	58.50	58.50	4	−20.22	−42.73	2.85
[f]250.4–367.0	PP, P_1	REV	LP	EV	58.50	58.50	16	63.92	56.63	67.76
[f]250.4–367.0	PP, P_2, P_3	REV	LP	EV	58.50	58.50	15	67.02	61.82	70.01
250.4–367.0	LO, L_1	N+R	LP	EV	58.50	58.50	17	−18.97	−23.96	−13.55
250.4–367.0	LO, L_1	NOR	LP	EV	58.50	58.50	8	−17.43	−29.25	−4.91
250.4–367.0	LO, L_1	REV	LP	EV	58.50	58.50	9	20.27	16.33	24.12
250.4–367.0	LO, L_2	N+R	LP	EV	58.50	58.50	14	−21.33	−26.20	−16.11
250.4–367.0	LO, L_2	REV	LP	EV	58.50	58.50	10	21.02	17.02	24.90
[f]250.4–367.0	PP, P_1	REV	HD	EV	58.50	58.50	8	66.47	58.57	71.88
[f]250.4–367.0	PP, P_2, P_3	REV	HD	EV	58.50	58.50	8	66.17	58.46	71.53
250.4–367.0	LO, L_1	N+R	HD	EV	58.50	58.50	16	−21.11	−28.20	−13.09
250.4–367.0	LO, L_1	NOR	HD	EV	58.50	58.50	7	−25.45	−38.94	−10.86
250.4–367.0	LO, L_1	REV	HD	EV	58.50	58.50	9	17.67	6.90	27.80
250.4–367.0	LO, L_2	N+R	HD	EV	58.50	58.50	15	−21.07	−28.67	−12.50
250.4–367.0	LO, L_2	NOR	HD	EV	58.50	58.50	7	−25.02	−39.51	−9.27
250.4–367.0	LO, L_2	REV	HD	EV	58.50	58.50	8	17.59	5.91	28.65
367.0–374.0	LO, L_1	REV	LP	EV	58.50	58.50	8	18.33	15.81	20.81
367.0–374.0	LO, L_2	REV	LP	EV	58.50	58.50	8	18.33	15.81	20.81
367.0–374.0	LO, L_1	REV	HD	EV	58.50	58.50	7	20.04	12.06	27.75
367.0–374.0	LO, L_2	REV	HD	EV	58.50	58.50	7	20.04	12.06	27.75
[e]121-757C-2R to 121-757C-6W										
127.5–132.0	PP, P_1	NOR	LP	EV	37.90	40.00	5	−56.29	−69.85	−40.95
127.5–132.0	PP, P_1	NOR	HD	EV	37.90	40.00	3	−54.28	−65.74	−42.65
132.0–152.0	PP, P_1	N+R	LP	EV	40.00	45.50	15	−59.24	−64.04	−52.24
132.0–152.0	PP, P_1	NOR	LP	EV	40.00	45.50	13	−59.10	−64.77	−50.98
132.0–152.0	PP, P_2, P_3	NOR	LP	EV	40.00	45.50	11	−57.10	−67.21	−40.47
132.0–152.0	PP, P_1	N+R	HD	EV	40.00	45.50	11	−58.81	−67.27	−45.79
132.0–152.0	PP, P_1	NOR	HD	EV	40.00	45.50	9	−60.91	−71.15	−45.44
132.0–152.0	PP, P_2, P_3	NOR	HD	EV	40.00	45.50	9	−58.92	−71.66	−38.15

Table 3 (continued).

Depth (mbsf)	Components[a]	Type[b]			Age interval (Ma)		Number	Confidence interval: Mean inclination (degrees)	Lower boundary (degrees)	Upper boundary (degrees)
[e]121-757C-2R to 121-757C-6W (Cont.)										
152.0–159.5	PP, P_1	N+R	LP	EV	45.50	47.00	12	−61.74	−68.12	−52.09
152.0–159.5	PP, P_1	NOR	LP	EV	45.50	47.00	8	−54.69	−60.14	−48.54
[c]152.0–159.5	PP, P_1	REV	LP	EV	45.50	47.00	4	72.63	57.72	85.69
152.0–159.5	PP, P_2, P_3	N+R	LP	EV	45.50	47.00	12	−63.67	−70.26	−53.07
152.0–159.5	PP, P_2, P_3	NOR	LP	EV	45.50	47.00	8	−55.47	−60.95	−49.23
[c]152.0–159.5	PP, P_2, P_3	REV	LP	EV	45.50	47.00	4	75.07	68.59	81.11
152.0–159.5	PP, P_1	N+R	HD	EV	45.50	47.00	10	−58.55	−67.80	−44.77
152.0–159.5	PP, P_1	NOR	HD	EV	45.50	47.00	8	−54.98	−65.45	−41.48
152.0–159.5	PP, P_2, P_3	N+R	HD	EV	45.50	47.00	9	−59.88	−70.34	−44.25
152.0–159.5	PP, P_2, P_3	NOR	HD	EV	45.50	47.00	7	−56.17	−68.84	−39.86
[f]159.5–161.5	PP, P_1	REV	LP	EV	58.50	58.50	4	65.08	51.18	76.21
[f]159.5–161.5	PP, P_2, P_3	REV	LP	EV	58.50	58.50	5	62.52	54.68	69.30
159.5–161.5	LO	REV	LP	EV	58.50	58.50	3	33.95	20.73	47.07
[f]159.5–161.5	PP, P_2, P_3	N+R	HD	EV	58.50	58.50	3	−61.68	−73.83	−48.25
[e]121-757C-7R to 121-757C-12R										
363.0–363.5	LO, L_1	N+R	HD	EV	58.50	58.50	3	−9.19	−27.21	8.88
373.2–385.0	LO, L_1	N+R	LP	EV	58.50	58.50	10	−16.07	−21.64	−10.29
373.2–385.0	LO, L_1	REV	LP	EV	58.50	58.50	9	17.04	11.18	22.71
373.2–385.0	LO, L_2	N+R	LP	EV	58.50	58.50	6	−17.84	−20.30	−15.37
373.2–385.0	LO, L_2	REV	LP	EV	58.50	58.50	5	17.65	14.40	20.88
373.2–385.0	LO, L_1	N+R	HD	EV	58.50	58.50	10	−18.47	−23.74	−12.99
373.2–385.0	LO, L_1	REV	HD	EV	58.50	58.50	7	16.40	12.32	20.42
373.2–385.0	LO, L_2	N+R	HD	EV	58.50	58.50	5	−17.19	−21.32	−13.04
373.2–385.0	LO, L_2	REV	HD	EV	58.50	58.50	4	16.84	10.73	22.92
385.0–386.5	LO, L_1	REV	LP	EV	58.50	58.50	7	21.20	16.26	26.02
385.0–386.5	LO, L_2	REV	LP	EV	58.50	58.50	7	18.69	17.10	20.27
385.0–386.5	LO, L_1	REV	HD	EV	58.50	58.50	6	22.57	18.14	26.92
385.0–386.5	LO, L_2	REV	HD	EV	58.50	58.50	6	21.36	15.94	26.69
386.5–387.3	LO, L_1	REV	LP	EV	58.50	58.50	5	21.26	17.00	25.48
386.5–387.3	LO, L_2	REV	LP	EV	58.50	58.50	5	19.72	17.53	21.91
387.3–391.0	LO, L_1	REV	LP	EV	58.50	58.50	11	20.76	16.83	24.54
387.3–391.0	LO, L_2	REV	LP	EV	58.50	58.50	10	20.10	17.18	22.96
387.3–391.0	LO, L_1	REV	HD	EV	58.50	58.50	9	17.60	11.53	23.46
387.3–391.0	LO, L_2	REV	HD	EV	58.50	58.50	9	16.84	11.57	21.95
391.0–393.8	LO, L_1	REV	LP	EV	58.50	58.50	8	20.00	15.61	24.29
391.0–393.8	LO, L_2	REV	LP	EV	58.50	58.50	8	18.60	16.82	20.36
391.0–393.8	LO, L_1	N+R	HD	EV	58.50	58.50	8	−20.59	−24.98	−16.09
391.0–393.8	LO, L_1	REV	HD	EV	58.50	58.50	7	20.80	15.42	26.06
391.0–393.8	LO, L_2	REV	HD	EV	58.50	58.50	8	20.37	15.82	24.80
394.2–394.7	LO, L_1	N+R	LP	EV	58.50	58.50	5	−13.23	−25.91	−0.34
394.2–394.7	LO, L_1	REV	LP	EV	58.50	58.50	4	12.13	−6.84	30.88
394.2–394.7	LO, L_2	N+R	LP	EV	58.50	58.50	5	−13.49	−24.34	−2.47
394.2–394.7	LO, L_2	REV	LP	EV	58.50	58.50	4	11.79	−2.51	25.97
394.2–394.7	LO, L_1	N+R	HD	EV	58.50	58.50	4	−14.30	−27.59	−0.87
394.2–394.7	LO, L_1	REV	HD	EV	58.50	58.50	3	12.60	−11.38	36.46
394.2–394.7	LO, L_2	N+R	HD	EV	58.50	58.50	4	−13.82	−28.53	1.05
394.7–401.7	LO, L_1	N+R	LP	EV	58.50	58.50	7	−23.13	−27.16	−19.01
394.7–401.7	LO, L_1	REV	LP	EV	58.50	58.50	6	22.57	17.83	27.24
394.7–401.7	LO, L_2	N+R	LP	EV	58.50	58.50	7	−20.51	−22.99	−18.01
394.7–401.7	LO, L_2	REV	LP	EV	58.50	58.50	6	20.33	17.25	23.39
394.7–401.7	LO, L_1	N+R	HD	EV	58.50	58.50	7	−17.60	−23.51	−11.56
394.7–401.7	LO, L_1	REV	HD	EV	58.50	58.50	6	17.65	10.04	25.10
394.7–401.7	LO, L_2	N+R	HD	EV	58.50	58.50	7	−20.16	−26.98	−13.13
394.7–401.7	LO, L_2	REV	HD	EV	58.50	58.50	6	19.21	11.13	27.09
[g]401.7–402.3	HO, H_1	REV	LP	EV	58.50	58.50	4	82.40	72.06	90.00
401.7–402.3	HO, H_2	REV	LP	EV	58.50	58.50	4	82.25	74.07	89.18
401.7–402.3	HO, H_1	REV	HD	EV	58.50	58.50	4	77.67	64.05	89.15
[g]402.3–402.7	HO, H_1	REV	LP	EV	58.50	58.50	4	80.53	67.39	90.00
402.3–402.7	HO, H_2	REV	LP	EV	58.50	58.50	3	82.41	74.92	89.54
[g]403.0–403.6	HO, H_1	REV	LP	EV	58.50	58.50	5	81.11	63.22	90.00
403.0–403.6	HO, H_2	REV	LP	EV	58.50	58.50	5	79.65	76.62	82.42
[g]403.0–403.6	HO, H_1	REV	HD	EV	58.50	58.50	4	75.07	56.12	90.00
403.6–404.4	HO, H_1	REV	LP	EV	58.50	58.50	5	80.89	78.53	83.07
403.6–404.4	HO, H_2	REV	LP	EV	58.50	58.50	5	81.79	77.08	85.76
403.6–404.4	HO, H_2	N+R	HD	EV	58.50	58.50	4	−80.91	−88.65	−71.85
404.5–405.0	HO, H_1	REV	LP	EV	58.50	58.50	4	77.37	71.35	82.95
404.5–405.0	HO, H_2	REV	LP	EV	58.50	58.50	4	76.21	72.30	79.95
404.5–405.0	HO, H_1	REV	HD	EV	58.50	58.50	3	76.62	64.69	88.04
404.5–405.0	HO, H_2	REV	HD	EV	58.50	58.50	3	78.94	73.38	84.35
405.0–405.9	HO, H_1	REV	LP	EV	58.50	58.50	5	80.75	70.86	88.10
405.0–405.9	HO, H_2	REV	LP	EV	58.50	58.50	5	80.70	76.61	84.27

Table 3 (continued).

Depth (mbsf)	Components[a]	Type[b]			Age interval (Ma)		Number	Confidence interval: Mean inclination (degrees)	Confidence interval: Lower boundary (degrees)	Confidence interval: Upper boundary (degrees)
[e]121-757C-7R to 121-757C-12R (Cont.)										
[g]405.0–405.9	HO, H_1	REV	HD	EV	58.50	58.50	4	81.64	70.73	90.00
[g]405.0–405.9	HO, H_2	REV	HD	EV	58.50	58.50	3	81.98	68.81	90.00
411.1–413.5	HO, H_1	REV	LP	EV	58.50	58.50	8	80.54	69.84	85.97
411.1–413.5	HO, H_2	REV	LP	EV	58.50	58.50	8	80.14	73.94	84.16
411.1–413.5	HO, H_1	REV	HD	EV	58.50	58.50	6	75.29	59.78	85.54
413.5–417.0	HO, H_1	REV	LP	EV	58.50	58.50	7	82.63	80.13	84.67
413.5–417.0	HO, H_2	REV	LP	EV	58.50	58.50	7	82.28	80.86	83.54
413.5–417.0	HO, H_1	REV	HD	EV	58.50	58.50	5	81.57	79.60	83.40
413.5–417.0	HO, H_2	REV	HD	EV	58.50	58.50	5	84.17	79.47	87.89
121-758A-1H to 121-758A-11H										
0.00–10.9	PP, P_1	NOR	LP	AF	0.00	0.73	13	3.07	-3.00	9.08
0.00–10.9	PP, P_2	NOR	LP	AF	0.00	0.73	13	3.07	-3.00	9.08
0.00–10.9	PP, P_1	NOR	HD	AF	0.00	0.73	12	4.06	-6.79	14.67
0.00–10.9	PP, P_2	NOR	HD	AF	0.00	0.73	12	4.06	-6.79	14.67
10.9–14.2	PP, P_1	REV	LP	AF	0.73	0.91	4	-7.79	-15.29	-0.26
10.9–14.2	PP, P_2	REV	LP	AF	0.73	0.91	4	-7.79	-15.29	-0.26
15.3–24.8	PP, P_1	REV	LP	AF	0.98	1.66	13	-10.16	-14.07	-6.17
15.3–24.8	PP, P_2	REV	LP	AF	0.98	1.66	12	-5.11	-11.90	1.79
15.3–24.8	PP, P_1	REV	HD	AF	0.98	1.66	11	-4.35	-16.60	8.19
15.3–24.8	PP, P_2	REV	HD	AF	0.98	1.66	11	-4.35	-16.60	8.19
26.0–34.2	PP, P_1	REV	LP	AF	1.88	2.47	25	-6.54	-9.61	-3.38
26.0–34.2	PP, P_2	REV	LP	AF	1.88	2.47	24	-3.86	-7.54	-0.12
26.0–34.2	PP, P_1	REV	HD	AF	1.88	2.47	22	-6.41	-12.60	0.07
26.0–34.2	PP, P_2	REV	HD	AF	1.88	2.47	22	-6.41	-12.60	0.07
34.2–39.5	PP, P_1	NOR	LP	AF	2.47	2.92	8	0.55	-5.63	6.72
34.2–39.5	PP, P_2	NOR	LP	AF	2.47	2.92	8	0.22	-6.72	7.15
34.2–39.5	PP, P_1	NOR	HD	AF	2.47	2.92	5	8.98	-7.67	25.39
34.2–39.5	PP, P_2	NOR	HD	AF	2.47	2.92	5	6.61	-12.13	25.12
46.5–56.2	PP, P_1	REV	LP	AF	3.97	4.10	13	-10.72	-18.66	-2.38
46.5–56.2	PP, P_2	REV	LP	AF	3.97	4.10	13	-6.69	-14.68	1.55
46.5–56.2	PP, P_1	REV	HD	AF	3.97	4.10	7	-10.51	-19.71	-1.11
46.5–56.2	PP, P_2	REV	HD	AF	3.97	4.10	7	-14.59	-31.47	3.22
56.2–58.7	PP, P_1	NOR	LP	AF	4.10	4.24	3	-7.36	-28.80	14.14
58.7–61.5	PP, P_1	REV	LP	AF	4.24	4.40	4	-4.27	-22.03	13.56
58.7–61.5	PP, P_2	REV	LP	AF	4.24	4.40	4	-3.79	-23.70	16.20
58.7–61.5	PP, P_1	REV	HD	AF	4.24	4.40	3	-9.95	-22.38	2.52
58.7–61.5	PP, P_2	REV	HD	AF	4.24	4.40	3	-9.95	-22.38	2.52
64.0–66.7	PP, P_1	NOR	HD	AF	4.57	4.77	3	14.46	-8.71	37.52
66.7–76.4	PP, P_1	REV	LP	AF	4.77	5.35	11	-11.10	-16.59	-5.46
66.7–76.4	PP, P_2	REV	LP	AF	4.77	5.35	11	-7.74	-13.37	-2.00
66.7–76.4	PP, P_1	REV	HD	AF	4.77	5.35	8	-13.35	-21.52	-4.92
66.7–76.4	PP, P_2	REV	HD	AF	4.77	5.35	8	-13.96	-21.00	-6.73
76.4–80.5	PP, P_1	NOR	LP	AF	5.35	5.53	4	-7.17	-20.82	6.56
76.4–80.5	PP, P_2	NOR	LP	AF	5.35	5.53	4	0.65	-7.89	9.19
83.9–90.5	PP, P_1	REV	LP	AF	5.89	6.37	7	-6.01	-18.49	6.66
83.9–90.5	PP, P_2	REV	LP	AF	5.89	6.37	7	-3.03	-16.78	10.84
83.9–90.5	PP, P_1	REV	HD	AF	5.89	6.37	5	-0.07	-16.52	16.39
83.9–90.5	PP, P_2	REV	HD	AF	5.89	6.37	5	-0.05	-16.50	16.40
95.0–102.0	PP, P_1	NOR	LP	AF	6.70	6.78	7	-13.94	-29.55	2.41
95.0–102.0	PP, P_2	NOR	LP	AF	6.70	6.78	7	-13.94	-29.55	2.41
95.0–102.0	PP, P_1	NOR	HD	AF	6.70	6.78	5	-0.57	-13.10	11.98
95.0–102.0	PP, P_2	NOR	HD	AF	6.70	6.78	5	-0.57	-13.10	11.98
121-758A-12X to 121-758A-54R										
101.3–115.0	PP, P_1	N+R	LP	AF	8.30	8.90	11	-7.63	-13.91	-1.21
101.3–115.0	PP, P_1	NOR	LP	AF	8.30	8.90	9	-7.89	-15.80	0.18
101.3–115.0	PP, P_2	N+R	LP	AF	8.30	8.90	11	-7.87	-14.03	-1.57
101.3–115.0	PP, P_2	NOR	LP	AF	8.30	8.90	9	-8.18	-15.91	-0.29
101.3–115.0	PP, P_1	N+R	HD	AF	8.30	8.90	6	-7.79	-11.80	-3.77
101.3–115.0	PP, P_1	NOR	HD	AF	8.30	8.90	5	-8.13	-13.36	-2.88
101.3–115.0	PP, P_2	N+R	HD	AF	8.30	8.90	6	-7.25	-13.28	-1.19
101.3–115.0	PP, P_2	NOR	HD	AF	8.30	8.90	3	-6.39	-26.09	13.35
101.3–115.0	PP, P_2	REV	HD	AF	8.30	8.90	3	8.12	-8.92	25.12
115.0–121.0	PP, P_1	NOR	LP	AF	8.90	10.10	6	-15.40	-25.31	-5.26
115.0–121.0	PP, P_2	NOR	LP	AF	8.90	10.10	6	-15.62	-25.52	-5.49
115.0–121.0	PP, P_1	N+R	HD	AF	8.90	10.10	8	-9.28	-13.50	-5.01
115.0–121.0	PP, P_1	NOR	HD	AF	8.90	10.10	5	-9.89	-17.69	-2.03
115.0–121.0	PP, P_1	REV	HD	AF	8.90	10.10	3	8.28	-3.09	19.63
115.0–121.0	PP, P_2	N+R	HD	AF	8.90	10.10	8	-9.28	-13.50	-5.01
115.0–121.0	PP, P_2	NOR	HD	AF	8.90	10.10	5	-9.89	-17.69	-2.03

Table 3 (continued).

Depth (mbsf)	Components[a]	Type[b]			Age interval (Ma)		Number	Confidence interval: Mean inclination (degrees)	Lower boundary (degrees)	Upper boundary (degrees)
121-758A-12X to 121-758A-54R (Cont.)										
115.0–121.0	PP, P_2	REV	HD	AF	8.90	10.10	3	8.28	−3.09	19.63
121.0–131.0	PP, P_1	N+R	LP	AF	10.10	14.40	3	−8.38	−23.30	6.56
121.0–131.0	PP, P_1	REV	LP	AF	10.10	14.40	2	10.75	−0.75	22.25
121.0–131.0	PP, P_2	N+R	LP	AF	10.10	14.40	3	−3.91	−23.91	16.11
121.0–131.0	PP, P_2	NOR	LP	AF	10.10	14.40	2	−0.70	−8.37	6.97
121.0–131.0	PP, P_1	REV	HD	AF	10.10	14.40	4	6.29	−3.76	16.30
121.0–131.0	PP, P_2	REV	HD	AF	10.10	14.40	4	5.66	−5.66	16.95
131.0–144.0	PP, P_1	N+R	LP	AF	14.40	17.20	9	−10.42	−18.40	−2.22
131.0–144.0	PP, P_1	NOR	LP	AF	14.40	17.20	4	−15.95	−37.20	5.69
131.0–144.0	PP, P_1	REV	LP	AF	14.40	17.20	5	6.01	−1.69	13.68
131.0–144.0	PP, P_2	N+R	LP	AF	14.40	17.20	9	−11.46	−19.30	−3.39
131.0–144.0	PP, P_2	REV	LP	AF	14.40	17.20	7	9.74	0.68	18.64
131.0–144.0	PP, P_1	N+R	HD	AF	14.40	17.20	9	−7.77	−14.98	−0.42
131.0–144.0	PP, P_1	NOR	HD	AF	14.40	17.20	4	−6.02	−20.80	8.82
131.0–144.0	PP, P_1	REV	HD	AF	14.40	17.20	5	9.17	−5.21	23.36
131.0–144.0	PP, P_2	N+R	HD	AF	14.40	17.20	9	−6.94	−14.24	0.48
131.0–144.0	PP, P_2	NOR	HD	AF	14.40	17.20	5	−5.62	−15.18	4.00
131.0–144.0	PP, P_2	REV	HD	AF	14.40	17.20	4	8.63	−14.06	31.08
144.0–150.0	PP, P_1	NOR	LP	AF	17.20	20.10	4	−12.57	−23.23	−1.83
144.0–150.0	PP, P_2	N+R	LP	AF	17.20	20.10	3	−11.49	−27.65	4.72
150.0–189.0	PP, P_1	N+R	LP	AF	20.10	23.60	29	−14.74	−18.16	−11.02
150.0–189.0	PP, P_1	NOR	LP	AF	20.10	23.60	26	−15.51	−19.11	−11.60
150.0–189.0	PP, P_1	REV	LP	AF	20.10	23.60	3	8.03	−15.01	31.00
150.0–189.0	PP, P_2	N+R	LP	AF	20.10	23.60	28	−9.31	−11.83	−6.70
150.0–189.0	PP, P_2	NOR	LP	AF	20.10	23.60	21	−9.86	−12.75	−6.87
150.0–189.0	PP, P_2	REV	LP	AF	20.10	23.60	7	7.68	0.56	14.72
150.0–189.0	PP, P_1	N+R	HD	AF	20.10	23.60	25	−10.29	−13.30	−7.16
150.0–189.0	PP, P_1	NOR	HD	AF	20.10	23.60	16	−10.59	−14.77	−6.27
150.0–189.0	PP, P_1	REV	HD	AF	20.10	23.60	9	9.77	4.23	15.21
150.0–189.0	PP, P_2	N+R	HD	AF	20.10	23.60	25	−11.59	−15.23	−7.75
150.0–189.0	PP, P_2	NOR	HD	AF	20.10	23.60	15	−11.23	−16.12	−6.16
150.0–189.0	PP, P_2	REV	HD	AF	20.10	23.60	10	12.13	4.87	19.15
189.0–218.0	PP, P_1	N+R	LP	AF	23.60	30.30	22	−17.35	−20.42	−14.07
189.0–218.0	PP, P_1	NOR	LP	AF	23.60	30.30	13	−17.05	−21.78	−12.09
189.0–218.0	PP, P_1	REV	LP	AF	23.60	30.30	9	17.77	12.70	22.69
189.0–218.0	PP, P_2	N+R	LP	AF	23.60	30.30	23	−16.73	−19.78	−13.48
189.0–218.0	PP, P_2	NOR	LP	AF	23.60	30.30	8	−16.18	−22.78	−9.38
189.0–218.0	PP, P_2	REV	LP	AF	23.60	30.30	15	17.03	12.86	21.00
189.0–218.0	PP, P_1	N+R	HD	AF	23.60	30.30	20	−14.93	−19.76	−9.73
189.0–218.0	PP, P_1	NOR	HD	AF	23.60	30.30	9	−13.36	−20.68	−5.79
189.0–218.0	PP, P_1	REV	HD	AF	23.60	30.30	11	16.23	7.86	24.12
189.0–218.0	PP, P_2	N+R	HD	AF	23.60	30.30	21	−17.49	−21.46	−13.20
189.0–218.0	PP, P_2	NOR	HD	AF	23.60	30.30	11	−15.47	−21.27	−9.43
189.0–218.0	PP, P_2	REV	HD	AF	23.60	30.30	10	19.69	12.74	26.28
218.0–238.0	PP, P_1	N+R	LP	AF	30.30	34.20	17	−20.02	−24.92	−14.70
218.0–238.0	PP, P_1	NOR	LP	AF	30.30	34.20	7	−14.14	−18.34	−9.89
218.0–238.0	PP, P_1	REV	LP	AF	30.30	34.20	10	24.09	16.41	31.23
218.0–238.0	PP, P_2	N+R	LP	AF	30.30	34.20	18	−17.76	−21.75	−13.50
218.0–238.0	PP, P_2	NOR	LP	AF	30.30	34.20	9	−15.04	−19.46	−10.52
218.0–238.0	PP, P_2	REV	LP	AF	30.30	34.20	9	20.48	12.70	27.86
218.0–238.0	PP, P_1	N+R	HD	AF	30.30	34.20	15	−16.86	−22.15	−11.21
218.0–238.0	PP, P_1	NOR	HD	AF	30.30	34.20	8	−13.59	−19.20	−7.86
218.0–238.0	PP, P_1	REV	HD	AF	30.30	34.20	7	20.60	9.05	31.59
218.0–238.0	PP, P_2	N+R	HD	AF	30.30	34.20	15	−18.74	−23.86	−13.25
218.0–238.0	PP, P_2	NOR	HD	AF	30.30	34.20	8	−14.59	−19.35	−9.75
218.0–238.0	PP, P_2	REV	HD	AF	30.30	34.20	7	23.44	12.94	33.41
238.0–248.0	PP, P_1	N+R	LP	AF	34.20	34.60	9	−24.39	−33.61	−14.40
238.0–248.0	PP, P_1	NOR	LP	AF	34.20	34.60	3	−21.21	−37.03	−5.30
238.0–248.0	PP, P_1	REV	LP	AF	34.20	34.60	6	26.02	9.02	41.88
238.0–248.0	PP, P_2	N+R	LP	AF	34.20	34.60	9	−24.39	−33.61	−14.40
238.0–248.0	PP, P_2	NOR	LP	AF	34.20	34.60	3	−21.21	−37.03	−5.30
238.0–248.0	PP, P_2	REV	LP	AF	34.20	34.60	6	26.02	9.02	41.88
238.0–248.0	PP, P_1	N+R	HD	AF	34.20	34.60	7	−22.57	−31.59	−13.13
238.0–248.0	PP, P_1	NOR	HD	AF	34.20	34.60	3	−19.27	−40.01	1.61
238.0–248.0	PP, P_1	REV	HD	AF	34.20	34.60	4	25.04	4.28	45.23
238.0–248.0	PP, P_2	N+R	HD	AF	34.20	34.60	7	−23.92	−34.05	−13.23
238.0–248.0	PP, P_2	NOR	HD	AF	34.20	34.60	3	−19.27	−40.01	1.61
238.0–248.0	PP, P_2	REV	HD	AF	34.20	34.60	4	27.39	4.51	49.49
264.0–266.5	PP, P_1	NOR	HD	AF	59.10	60.00	2	−41.30	−56.55	−26.05
264.0–266.5	PP, P_2	NOR	HD	AF	59.10	60.00	2	−41.30	−56.55	−26.05
276.0–286.0	PP, P_1	N+R	LP	AF	61.60	62.00	8	−53.02	−61.06	−43.45
276.0–286.0	PP, P_1	REV	LP	AF	61.60	62.00	6	55.87	44.82	65.55
276.0–286.0	PP, P_2	N+R	LP	AF	61.60	62.00	8	−53.02	−61.06	−43.45

Table 3 (continued).

								Confidence interval		
Depth (mbsf)	Components[a]	Type[b]			Age interval (Ma)		Number	Mean inclination (degrees)	Lower boundary (degrees)	Upper boundary (degrees)
121-758A-12X to 121-758A-54R (Cont.)										
276.0–286.0	PP, P_2	REV	LP	AF	61.60	62.00	6	55.87	44.82	65.55
276.0–286.0	PP, P_1	N+R	HD	AF	61.60	62.00	6	−48.26	−56.05	−39.83
276.0–286.0	PP, P_1	REV	HD	AF	61.60	62.00	5	49.68	40.45	58.38
276.0–286.0	PP, P_2	N+R	HD	AF	61.60	62.00	6	−48.26	−56.05	−39.83
276.0–286.0	PP, P_2	REV	HD	AF	61.60	62.00	5	49.68	40.45	58.38
286.0–295.0	PP, P_1	N+R	LP	AF	62.00	65.00	7	−52.52	−64.15	−38.36
286.0–295.0	PP, P_1	REV	LP	AF	62.00	65.00	6	53.05	35.25	67.82
286.0–295.0	PP, P_2	N+R	LP	AF	62.00	65.00	7	−52.52	−64.15	−38.36
286.0–295.0	PP, P_2	REV	LP	AF	62.00	65.00	6	53.05	35.25	67.82
286.0–295.0	PP, P_1	N+R	HD	AF	62.00	65.00	4	−56.32	−78.13	−32.18
286.0–295.0	PP, P_2	N+R	HD	AF	62.00	65.00	4	−56.32	−78.13	−32.18
305.0–367.3	PP, P_1	N+R	LP	AF	72.10	76.50	35	−61.28	−63.10	−58.45
305.0–367.3	PP, P_1	NOR	LP	AF	72.10	76.50	18	−59.79	−62.77	−55.82
305.0–367.3	PP, P_1	REV	LP	AF	72.10	76.50	17	62.78	59.18	65.50
305.0–367.3	PP, P_2	N+R	LP	AF	72.10	76.50	35	−60.92	−62.88	−57.76
305.0–367.3	PP, P_2	NOR	LP	AF	72.10	76.50	19	−60.27	−63.21	−56.24
305.0–367.3	PP, P_2	REV	LP	AF	72.10	76.50	16	61.68	56.87	65.18
305.0–367.3	PP, P_1	N+R	HD	AF	72.10	76.50	26	−62.39	−65.74	−55.81
305.0–367.3	PP, P_1	NOR	HD	AF	72.10	76.50	8	−60.04	−65.73	−53.35
305.0–367.3	PP, P_1	REV	HD	AF	72.10	76.50	18	63.53	54.29	68.37
305.0–367.3	PP, P_2	N+R	HD	AF	72.10	76.50	26	−62.39	−65.74	−55.81
305.0–367.3	PP, P_2	NOR	HD	AF	72.10	76.50	8	−60.04	−65.73	−53.35
305.0–367.3	PP, P_2	REV	HD	AF	72.10	76.50	18	63.53	54.29	68.37
367.3–431.2	PP, P_1	NOR	LP	AF	76.50	79.00	23	−61.61	−64.64	−56.78
367.3–431.2	PP, P_2	NOR	LP	AF	76.50	79.00	23	−67.11	−70.38	−60.38
367.3–431.2	PP, P_1	NOR	HD	AF	76.50	79.00	21	−65.04	−68.22	−59.69
367.3–431.2	PP, P_2	NOR	HD	AF	76.50	79.00	21	−65.80	−69.41	−58.93
431.2–491.4	PP, P_1	N+R	LP	AF	79.00	81.90	29	−63.52	−65.73	−59.89
431.2–491.4	PP, P_1	NOR	LP	AF	79.00	81.90	28	−63.38	−65.68	−59.66
431.2–491.4	PP, P_2	NOR	LP	AF	79.00	81.90	27	−67.27	−69.49	−63.43
431.2–491.4	PP, P_1	N+R	HD	AF	79.00	81.90	25	−64.87	−67.68	−59.86
431.2–491.4	PP, P_1	NOR	HD	AF	79.00	81.90	24	−64.33	−67.20	−59.43
431.2–491.4	PP, P_2	N+R	HD	AF	79.00	81.90	24	−66.24	−69.00	−61.34
431.2–491.4	PP, P_2	NOR	HD	AF	79.00	81.90	23	−65.77	−68.60	−60.91
121-758A-55R to 121-758A-73R										
491.4–509.5	PP, P_1	NOR	LP	EV	81.90	81.90	14	−64.70	−70.84	−53.33
491.4–509.5	PP, P_2, P_3	NOR	LP	EV	81.90	81.90	9	−70.05	−76.98	−59.36
491.4–509.5	PR	REV	LP	EV	81.90	81.90	5	55.40	43.84	65.95
491.4–509.5	PP, P_1	NOR	HD	EV	81.90	81.90	8	−64.51	−72.50	−53.81
491.4–509.5	PP, P_2, P_3	NOR	HD	EV	81.90	81.90	6	−60.92	−70.25	−49.99
509.5–520.5	PP, P_1	NOR	LP	EV	81.90	81.90	6	−61.21	−71.58	−48.81
509.5–520.5	PP, P_2, P_3	NOR	LP	EV	81.90	81.90	6	−64.09	−78.49	−44.72
509.5–520.5	PP, P_1	NOR	HD	EV	81.90	81.90	6	−65.10	−81.61	−41.29
509.5–520.5	PP, P_2, P_3	NOR	HD	EV	81.90	81.90	6	−65.10	−81.61	−41.29
520.5–546.7	PP, P_1	NOR	LP	EV	81.90	81.90	30	−62.66	−66.21	−53.27
520.5–546.7	PP, P_2, P_3	NOR	LP	EV	81.90	81.90	21	−58.17	−62.42	−50.99
520.5–546.7	PR	REV	LP	EV	81.90	81.90	13	50.63	40.63	57.84
520.5–546.7	PP, P_1	NOR	HD	EV	81.90	81.90	21	−63.70	−68.02	−54.74
520.5–546.7	PP, P_2, P_3	NOR	HD	EV	81.90	81.90	19	−68.05	−72.41	−57.99
546.7–564.7	PP, P_1	NOR	LP	EV	81.90	81.90	24	−68.40	−72.02	−58.40
546.7–564.7	PP, P_2, P_3	NOR	LP	EV	81.90	81.90	18	−70.81	−75.37	−58.08
546.7–564.7	PR	REV	LP	EV	81.90	81.90	15	56.29	44.85	63.16
546.7–564.7	PP, P_1	NOR	HD	EV	81.90	81.90	22	−64.40	−68.66	−54.72
546.7–564.7	PP, P_2, P_3	NOR	HD	EV	81.90	81.90	22	−66.44	−70.61	−55.99
546.7–564.7	PR	REV	HD	EV	81.90	81.90	6	59.76	33.10	78.89
564.7–567.8	PP, P_1	NOR	LP	EV	81.90	81.90	8	−72.67	−79.11	−63.33
564.7–567.8	PP, P_2, P_3	NOR	LP	EV	81.90	81.90	7	−71.94	−78.50	−63.31
564.7–567.8	PP, P_1	NOR	HD	EV	81.90	81.90	5	−76.99	−88.34	−61.24
564.7–567.8	PP, P_2, P_3	NOR	HD	EV	81.90	81.90	5	−76.99	−88.34	−61.24
573.8–586.2	PP, P_1	NOR	LP	EV	81.90	81.90	19	−65.76	−70.21	−56.49
573.8–586.2	PP, P_2, P_3	NOR	LP	EV	81.90	81.90	21	−67.89	−71.00	−62.17
573.8–586.2	PR	REV	LP	EV	81.90	81.90	11	61.84	47.89	70.28
573.8–586.2	PP, P_1	NOR	HD	EV	81.90	81.90	17	−66.94	−71.12	−59.37
573.8–586.2	PP, P_2, P_3	NOR	HD	EV	81.90	81.90	16	−67.87	−71.52	−61.98
587.1–588.5	PP, P_1	NOR	LP	EV	81.90	81.90	4	−69.76	−89.87	−45.77
593.1–601.0	PP, P_1	NOR	LP	EV	81.90	81.90	11	−65.51	−73.02	−52.70
593.1–601.0	PP, P_2, P_3	NOR	LP	EV	81.90	81.90	12	−65.62	−72.75	−52.72
593.1–601.0	PR	REV	LP	EV	81.90	81.90	5	52.70	34.80	68.50
593.1–601.0	PP, P_1	NOR	HD	EV	81.90	81.90	8	−60.76	−69.56	−49.21
593.1–601.0	PP, P_2, P_3	NOR	HD	EV	81.90	81.90	8	−66.61	−77.71	−48.52
602.4–608.7	PP, P_1	NOR	LP	EV	81.90	81.90	8	−70.61	−80.09	−54.68

Table 3 (continued).

								Confidence interval		
Depth (mbsf)	Components[a]	Type[b]			Age interval (Ma)		Number	Mean inclination (degrees)	Lower boundary (degrees)	Upper boundary (degrees)
121-758A-55R to 121-758A-73R (Cont.)										
602.4–608.7	PP, P_2, P_3	NOR	LP	EV	81.90	81.90	10	−70.62	−76.93	−60.26
602.4–608.7	PP, P_1	NOR	HD	EV	81.90	81.90	6	−67.73	−74.36	−60.01
602.4–608.7	PP, P_2, P_3	NOR	HD	EV	81.90	81.90	6	−70.58	−79.88	−58.52
613.0–614.4	PP, P_2, P_3	NOR	LP	EV	81.90	81.90	5	−75.29	−85.58	−62.04
613.0–614.4	PR	REV	LP	EV	81.90	81.90	3	62.98	48.71	76.89
613.0–614.4	PP, P_2, P_3	NOR	HD	EV	81.90	81.90	5	−71.21	−88.97	−46.03
614.5–616.9	PP, P_2, P_3	NOR	LP	EV	81.90	81.90	5	−56.45	−65.58	−46.55
614.5–616.9	PR	REV	LP	EV	81.90	81.90	4	63.77	44.77	80.80
614.5–616.9	PP, P_1	NOR	HD	EV	81.90	81.90	6	−63.02	−77.01	−44.64
614.5–616.9	PP, P_2, P_3	NOR	HD	EV	81.90	81.90	6	−63.02	−77.01	−44.64
616.9–619.6	PP, P_2, P_3	NOR	LP	EV	81.90	81.90	4	−69.68	−82.02	−55.99
619.6–624.3	PP, P_2, P_3	NOR	LP	EV	81.90	81.90	7	−64.40	−71.06	−56.43
619.6–624.3	PR	REV	LP	EV	81.90	81.90	5	58.88	35.00	78.40
619.6–624.3	PP, P_1	NOR	HD	EV	81.90	81.90	6	−64.54	−80.60	−41.88
619.6–624.3	PP, P_2, P_3	NOR	HD	EV	81.90	81.90	6	−58.91	−73.25	−40.85
624.3–637.5	PP, P_1	NOR	LP	EV	81.90	81.90	12	−60.63	−66.63	−52.02
624.3–637.5	PP, P_2, P_3	NOR	LP	EV	81.90	81.90	19	−63.47	−67.60	−56.19
624.3–637.5	PR	REV	LP	EV	81.90	81.90	12	55.25	38.12	65.32
624.3–637.5	PP, P_1	NOR	HD	EV	81.90	81.90	15	−56.16	−62.31	−46.63
624.3–637.5	PP, P_2, P_3	NOR	HD	EV	81.90	81.90	15	−55.27	−61.11	−46.61
637.7–640.9	PP, P_1	NOR	LP	EV	81.90	81.90	4	−68.29	−86.72	−46.93
637.7–640.9	PP, P_2, P_3	NOR	LP	EV	81.90	81.90	6	−63.53	−76.70	−46.43
637.7–640.9	PP, P_1	NOR	HD	EV	81.90	81.90	4	−63.80	−77.57	−48.78
637.7–640.9	PP, P_2, P_3	NOR	HD	EV	81.90	81.90	4	−60.98	−75.26	−45.52
641.0–642.3	PP, P_2, P_3	NOR	LP	EV	81.90	81.90	3	−54.89	−70.38	−39.09
642.3–650.4	PP, P_2, P_3	NOR	LP	EV	81.90	81.90	4	−50.60	−64.10	−36.39
651.7–652.5	PR	REV	LP	EV	81.90	81.90	5	57.86	43.07	70.92
652.6–654.1	PP, P_2, P_3	NOR	LP	EV	81.90	81.90	3	−54.67	−65.18	−44.02
652.6–654.1	PP, P_1	NOR	HD	EV	81.90	81.90	3	−51.06	−71.09	−30.58
652.6–654.1	PP, P_2, P_3	NOR	HD	EV	81.90	81.90	3	−51.06	−71.09	−30.58
654.1–660.6	PP, P_2, P_3	NOR	LP	EV	81.90	81.90	6	−57.04	−67.55	−44.80
654.1–660.6	PP, P_1	NOR	HD	EV	81.90	81.90	5	−65.41	−77.53	−51.14
654.1–660.6	PP, P_2, P_3	NOR	HD	EV	81.90	81.90	5	−60.99	−71.21	−49.56
660.7–664.0	PP, P_1	NOR	LP	EV	81.90	81.90	4	−62.48	−82.11	−40.37
660.7–664.0	PP, P_2, P_3	NOR	LP	EV	81.90	81.90	6	−58.39	−62.46	−54.07
660.7–664.0	PR	REV	LP	EV	81.90	81.90	7	54.57	40.60	65.90
660.7–664.0	PP, P_1	NOR	HD	EV	81.90	81.90	4	−58.31	−70.59	−45.25
660.7–664.0	PP, P_2, P_3	NOR	HD	EV	81.90	81.90	5	−57.74	−68.18	−46.22
664.0–666.4	PP, P_1	NOR	LP	EV	81.90	81.90	6	−52.28	−70.01	−30.17
664.0–666.4	PP, P_2, P_3	NOR	LP	EV	81.90	81.90	7	−53.66	−67.13	−36.48
664.0–666.4	PP, P_1	NOR	HD	EV	81.90	81.90	6	−54.23	−69.56	−35.44
664.0–666.4	PP, P_2, P_3	NOR	HD	EV	81.90	81.90	7	−57.38	−71.96	−37.45
666.4–669.9	PP, P_1	NOR	LP	EV	81.90	81.90	6	−55.61	−69.43	−38.86
666.4–669.9	PP, P_2, P_3	NOR	LP	EV	81.90	81.90	7	−65.70	−74.57	−54.14
666.4–669.9	PP, P_1	NOR	HD	EV	81.90	81.90	5	−57.54	−74.08	−38.13
666.4–669.9	PP, P_2, P_3	NOR	HD	EV	81.90	81.90	5	−57.54	−74.08	−38.13
671.3–673.3	PP, P_1	NOR	LP	EV	81.90	81.90	4	−68.02	−82.59	−51.70
671.3–673.3	PP, P_2, P_3	NOR	LP	EV	81.90	81.90	8	−63.93	−67.92	−59.38
671.3–673.3	PP, P_1	NOR	HD	EV	81.90	81.90	6	−67.98	−72.67	−62.76
671.3–673.3	PP, P_2, P_3	NOR	HD	EV	81.90	81.90	6	−63.02	−74.87	−48.16
[h]Mean basement results: Hole 758A										
[i]491.4–619.6	PP, P_1	NOR	LP	EV	81.90	81.90	9	−67.08	−70.32	−63.30
[i]491.4–619.6	PP, P_2, P_3	NOR	LP	EV	81.90	81.90	11	−68.01	−72.03	−62.64
[i]491.4–619.6	PP, P_1	NOR	HD	EV	81.90	81.90	9	−66.28	−70.18	−61.61
[i]491.4–619.6	PP, P_2, P_3	NOR	HD	EV	81.90	81.90	10	−68.08	−71.56	−63.79
[j]491.4–673.3	PR	REV	LP	TH	–	–	114	56.79	50.28	58.14
[j]491.4–673.3	PR	REV	HD	TH	–	–	33	55.95	44.38	60.19
121-758B-1H to 121-758B-10H										
0.00–10.7	PP, P_1	NOR	LP	AF	0.00	0.73	13	1.41	−2.91	5.72
0.00–10.7	PP, P_2	NOR	LP	AF	0.00	0.73	13	0.61	−4.29	5.50
0.00–10.7	PP, P_1	NOR	HD	AF	0.00	0.73	9	1.93	−6.86	10.66
0.00–10.7	PP, P_2	NOR	HD	AF	0.00	0.73	9	1.93	−6.86	10.66
10.7–14.2	PP, P_1	REV	LP	AF	0.73	0.91	4	−1.49	−15.56	12.61
10.7–14.2	PP, P_2	REV	LP	AF	0.73	0.91	4	1.13	−9.87	12.12
15.25–24.3	PP, P_1	REV	LP	AF	0.98	1.66	11	−2.22	−8.22	3.82
15.25–24.3	PP, P_2	REV	LP	AF	0.98	1.66	11	−1.44	−7.34	4.49
15.25–24.3	PP, P_1	REV	HD	AF	0.98	1.66	8	−0.07	−12.21	12.07
15.25–24.3	PP, P_2	REV	HD	AF	0.98	1.66	8	−0.07	−12.21	12.07
24.3–26.4	PP, P_1	NOR	LP	AF	1.66	1.88	3	0.00	−15.59	15.59
24.3–26.4	PP, P_2	NOR	LP	AF	1.66	1.88	3	0.53	−18.41	19.47

Table 3 (continued).

								Confidence interval		
Depth (mbsf)	Components[a]	Type[b]			Age interval (Ma)		Number	Mean inclination (degrees)	Lower boundary (degrees)	Upper boundary (degrees)
121-758B-1H to 121-758B-10H (Cont.)										
26.4–34.7	PP, P_1	REV	LP	AF	1.88	2.47	24	−5.53	−9.70	−1.23
26.4–34.7	PP, P_2	REV	LP	AF	1.88	2.47	24	−4.10	−8.72	0.64
26.4–34.7	PP, P_1	REV	HD	AF	1.88	2.47	17	−6.32	−13.88	1.53
26.4–34.7	PP, P_2	REV	HD	AF	1.88	2.47	17	−8.33	−15.47	−0.83
34.75–39.0	PP, P_1	NOR	LP	AF	2.47	2.92	5	−2.92	−8.71	2.87
34.75–39.0	PP, P_2	NOR	LP	AF	2.47	2.92	5	2.80	−11.27	16.81
34.75–39.0	PP, P_1	NOR	HD	AF	2.47	2.92	5	−4.96	−29.15	19.52
34.75–39.0	PP, P_2	NOR	HD	AF	2.47	2.92	5	−2.42	−25.95	21.24
40.25–41.5	PP, P_1	NOR	LP	AF	2.99	3.08	3	−1.73	−10.91	7.44
40.25–41.5	PP, P_2	NOR	LP	AF	2.99	3.08	3	1.34	−20.60	23.26
42.6–45.7	PP, P_1	NOR	LP	AF	3.18	3.40	5	−6.35	−16.43	3.79
42.6–45.7	PP, P_2	NOR	LP	AF	3.18	3.40	5	1.22	−5.48	7.92
42.6–45.7	PP, P_1	NOR	HD	AF	3.18	3.40	5	0.40	−10.02	10.82
42.6–45.7	PP, P_2	NOR	HD	AF	3.18	3.40	5	−1.16	−6.89	4.57
45.7–53.0	PP, P_1	REV	LP	AF	3.40	3.88	9	−4.83	−16.39	6.95
45.7–53.0	PP, P_2	REV	LP	AF	3.40	3.88	9	−7.22	−18.82	4.71
54.5–56.8	PP, P_1	REV	LP	AF	3.97	4.10	3	−4.84	−16.16	6.50
58.3–61.1	PP, P_1	REV	LP	AF	4.24	4.40	4	−8.31	−12.97	−3.63
58.3–61.1	PP, P_2	REV	LP	AF	4.24	4.40	4	−5.20	−11.00	0.60
58.3–61.1	PP, P_1	REV	HD	AF	4.24	4.40	4	−4.89	−26.97	17.30
58.3–61.1	PP, P_2	REV	HD	AF	4.24	4.40	4	−5.00	−27.07	17.20
67.0–76.7	PP, P_1	REV	LP	AF	4.77	5.35	12	−5.39	−9.15	−1.60
67.0–76.7	PP, P_2	REV	LP	AF	4.77	5.35	12	−4.33	−9.87	1.27
67.0–76.7	PP, P_1	REV	HD	AF	4.77	5.35	12	−3.14	−12.68	6.55
67.0–76.7	PP, P_2	REV	HD	AF	4.77	5.35	12	−2.33	−11.83	7.28
82.2–85.3	PP, P_1	NOR	LP	AF	5.68	5.89	3	−2.97	−17.38	11.45
82.2–85.3	PP, P_2	NOR	LP	AF	5.68	5.89	3	−2.87	−16.77	11.03
85.3–89.4	PP, P_1	REV	LP	AF	5.89	6.37	3	−17.59	−42.28	7.28
91.0–96.0	PP, P_1	REV	LP	AF	6.50	6.70	4	9.24	−15.80	33.98
91.0–96.0	PP, P_2	REV	LP	AF	6.50	6.70	4	9.11	−15.89	33.81

[a] NOR = normal polarity results only; REV = reversed polarity results only; N + R = combined normal and reversed polarity results. Throughout the analysis, NOR- and/or REV-type results were used only in the case of single-polarity intervals (e.g., Cores 121-758A-1H to 121-758A-11H, 121-758B-1H to 121-758B-10H) or if both NOR and REV results were available for an interval. In all other cases only N + R results were used. For proper documentation, all available NOR, REV, and N + R results are listed.

[b] LP = linear PCA analysis results; HD = Hoffman-Day results from planar PCA analysis; AF = alternating field demagnetization results only; TH = thermal demagnetization results only; EV = combined AF and TH results.

[c] Results not included in final analysis.

[d] Duncan's (this volume) best age estimate at 43.2 ± Ma is the mean of two $^{40}Ar/^{39}Ar$ plateau ages.

[e] Duncan (this volume) estimated basement age close to 58 Ma.

[f] Results corrected for bedding.

[g] Upper limit reset to 90.00°.

[h] Duncan (this volume) gave a weighted mean site age at 81.8 ± 2.6 Ma.

[i] Mean-flow result, restricted to flow Units 758A-F1 to 758A-F15.

[j] Overall mean result.

well-determinable primary magnetization component (Figs. 19E and 21D) and a low-inclination overprint similar to the component observed in the flow sequence of Holes 757B and 757C.

AF and thermal demagnetization of the basement sequence (Cores 121-757C-7R to 121-757C-12R, 362.9–420.7 mbsf; Figs. 19F–19L$_2$, 20A, 20B, 41E, and 41F and Table 3) showed a remarkably consistent pattern of hard magnetization components. The tuff and upper flow sequence (flow Units 757C-F1–757C-F9, 372.8–401.7 mbsf; Figs. 19F–19J, 20, 23B, and 24A–24D) has an inclination of about 20°, mostly downward, and this is abruptly followed downsection by a uniform about 80° downward inclination (flow Units 757C-F10–757C-F19, 401.7–417.0 mbsf; Figs. 19K–19L, 20, 23C, and 24E–24H). Limited occurrence of a low-inclination component also was observed in some of the basal flows (Fig. 23B). These low and high inclinations cannot be interpreted in terms of primary, drilling-induced, or recent field components. Similarity in inclination across multiple flows and Holes 757B and 757C shows that they are not due to rotation of large blocks in aa-type flows. A tectonically related origin seems most plausible, as will be discussed in the "Mean Inclination/Latitude Results" section. A steeply upward-directed drilling-induced component with a low thermal and AF stability range (below 200°C and 20 mT; Figs. 23A and 24I) was also observed in the lower part of the flow sequence.

Site 758

With the exception of the Miocene sequence, the results from the sediments, the ashes, and the basement are of good to high quality. The sedimentary sequence has an appreciable hiatus, with lower Oligocene to upper Paleocene sediments missing.

Hole 758A

APC-Cored Sediments

This terrigenous, clay-rich sequence (Cores 121-758A-1H to 121-758A-11H) and its replicate sequence from Hole 758B yielded a magnificent magnetostratigraphic profile (Tables 3 and 5). A preliminary magnetostratigraphic interpretation based on whole-core NRM and susceptibility measurements documented previously (Shipboard Scientific Party, 1989i) has now been

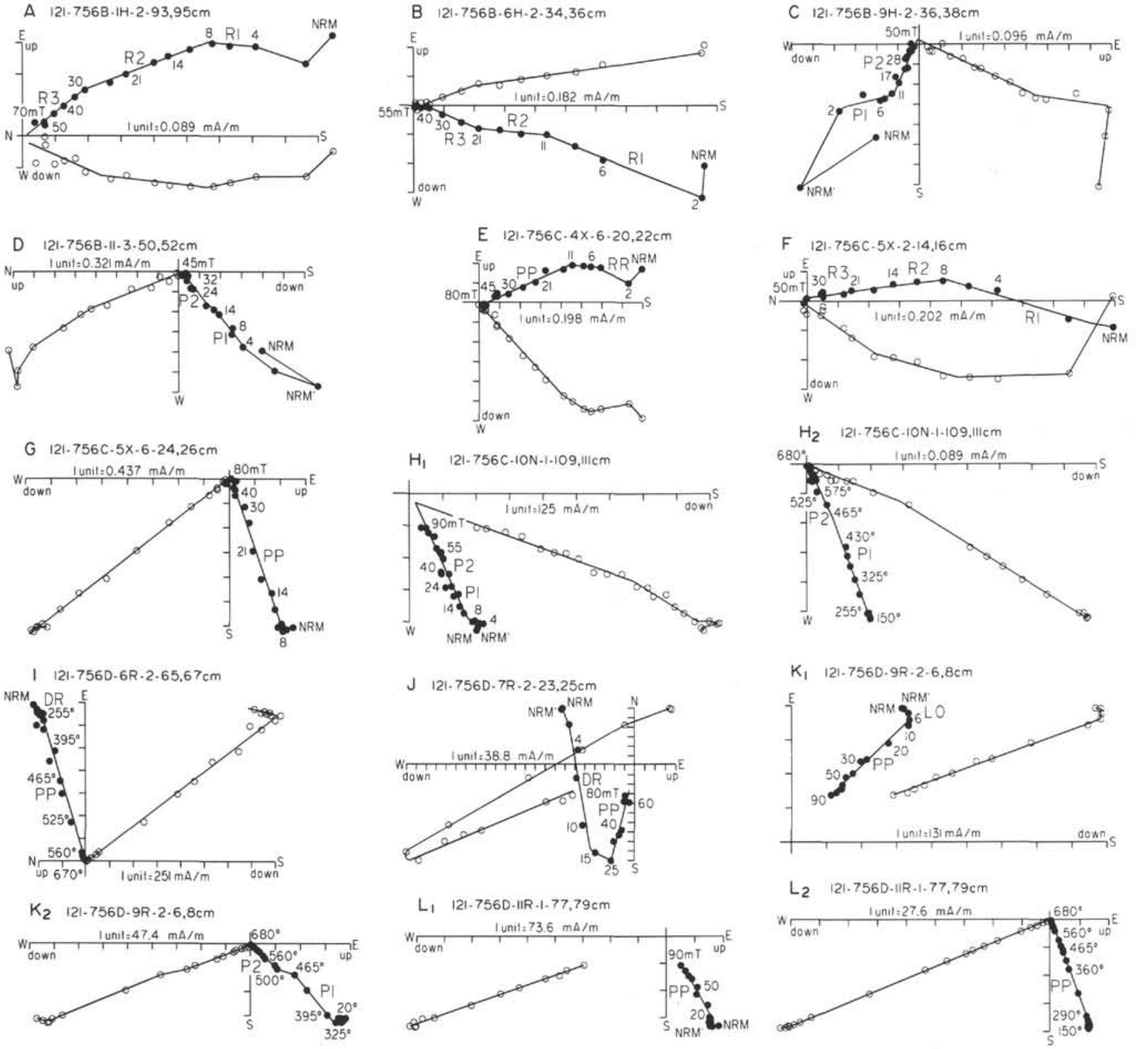

Figure 3. Zijderveld (1967) diagrams of representative samples from Holes 756B, 756C, and 756D during AF and thermal demagnetization. The symbols indicate successive positions (in orthogonal projection) of the end points of the resultant magnetization vector during progressive demagnetization. Open symbols indicate projections on the vertical east-west plane, and solid symbols indicate projections on the horizontal plane. Numbers denote successive peak field values in milliTeslas or °C. PP, P_1, P_2, P_3 = primary magnetization components; DR, D_1, D_2 = drilling-induced overprints; RR, R_1, R_2, R_3 = "180 degree" overprints; LO = low-inclination component.

refined (Farrell and Janecek, this volume). Detailed AF demagnetization of the samples was carried out to confirm this magnetostratigraphic profile. In addition, discrete sample data were necessary to establish whether the observed changes in declination downhole resulted from magnetic overprints not removed by the 9-mT peak field AF-demagnetizer attached to the on-board 2G-Enterprises cryogenic magnetometer or whether this declination shift represents systematic rotation of the cores with depth.

The results show (1) the dominant presence of a very stable (up to 100 mT) primary magnetization component and a polarity pattern fully confirming the whole-core magnetostratigraphic interpretation (Figs. 25, 26A, 27A, 28A, and 28B), (2) limited occurrence of a steep negative-inclination component (drilling induced) with a stability range generally below 10 mT (Figs. 25C, 25E, 25F, 25I–25N, 27B, and 28C), and (3) sporadic occurrence of a recent field overprint with a stability range below 20 mT (Figs. 25H, 25J, and 28D). The intensity of the primary and drilling-induced components varies gradually downhole (Figs. 27A–27C), mainly reflecting variations in concentration of magnetic material, as we had concluded earlier from whole-core NRM and susceptibility measurements (Shipboard Scientific Party, 1989i). Intensities vary over 3 orders of magnitude and decrease sharply at the base of the APC-cored sequence to values of about 10^{-2} mA/m, which is only slightly above the noise level of the ScT cryogenic magnetometer (2×10^{-3} to 5×10^{-3} mA/m).

Linear regression analysis of the oriented samples (Cores 121-758A-3H to 121-758A-11H) shows an increasing discrepancy downhole between observed and expected declinations (Fig.

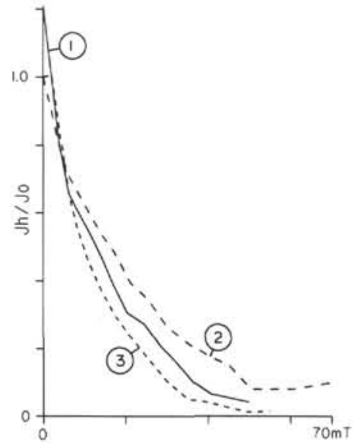

Figure 4. Normalized curves showing the decay of remanent magnetization during AF demagnetization of representative samples from Hole 756B. 1 = Sample 121-756B-9H-2, 38–40 cm; 2 = Sample 121-756B-1H-2, 93–95 cm; 3 = Sample 121-756B-6H-2, 34–36 cm.

27A and Table 4). This discrepancy is more pronounced for reversed polarity declinations than for normal polarit declinations. The reason for this normal/reversed polarity difference is not clear. Hole 758B results, in contrast, show good agreement between the discrepancies for the normal and reversed polarity declinations (Fig. 39A and Table 4). The observed magnitude and trend of the discrepancies (R polarity, Hole 758A; N and R polarity, Hole 758B) are similar to the discrepancies inferred from the whole-core NRM measurements. We reiterate our earlier suggestion (Shipboard Scientific Party, 1989i, fig. 4) that these discrepancies indicate rotation of the drill string during the pressurizing phase of APC coring, that is, between the Eastman-Whipstock orientation observation and the core shooting.

This hypothesis may explain the downhole discrepancy-increase as a result of lengthening of the drill string. The free-water part of the drill string was not reassembled between coring of Holes 758A and 758B. We suggest that the opposing sense of the discrepancy increases—counterclockwise in Hole 758A and clockwise in Hole 758B—results from a different reassembly of the top part of the drill string. It is not clear, however, why the discrepancies should be minimal for the uppermost oriented core in both holes.

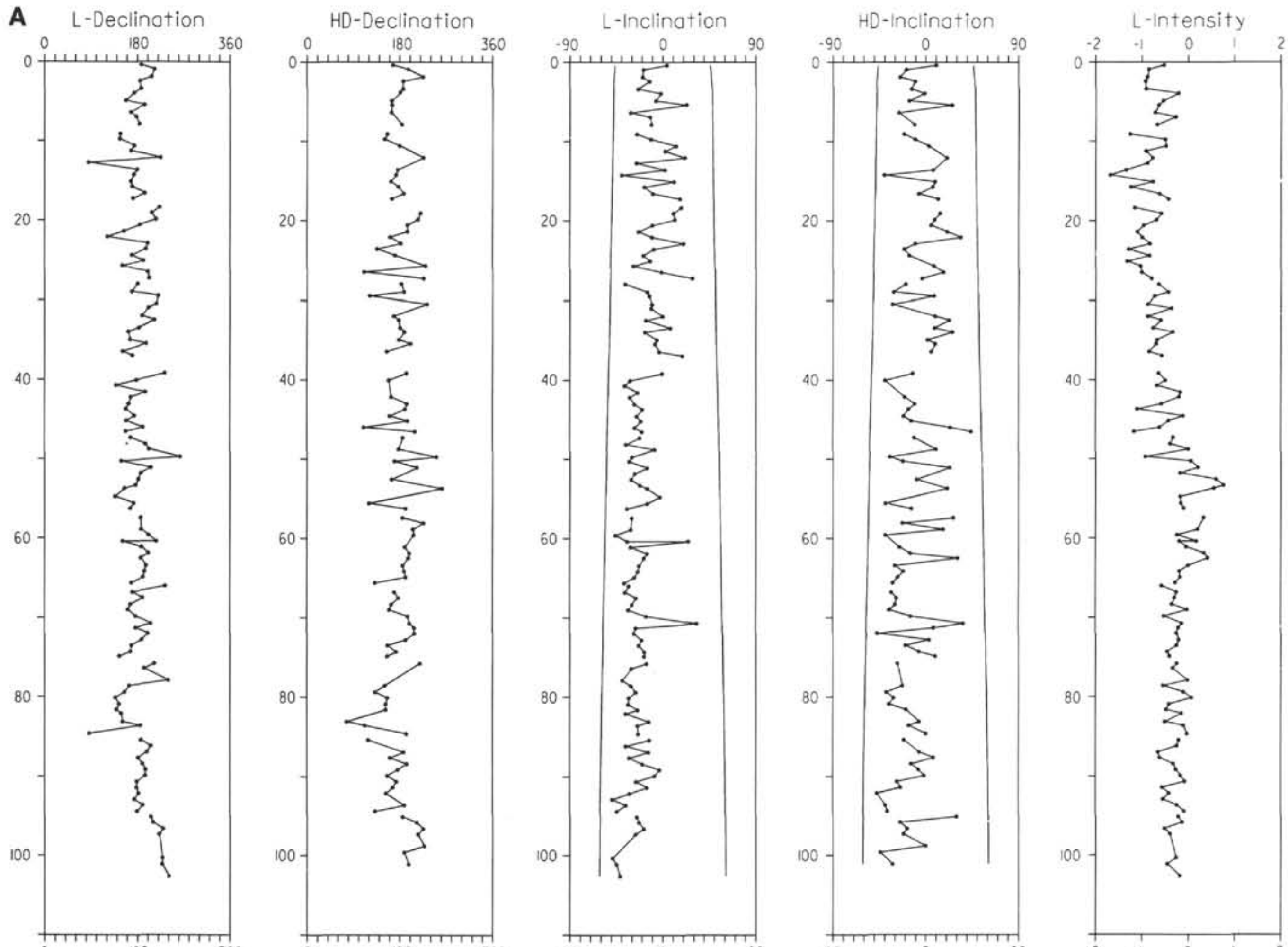

Figure 5. Stratigraphic plots of declination, inclination, and intensity of components determined from linear (L) and planar (HD) PCA of AF demagnetization data for Cores 121-756B-1H to 121-756B-11H. Depth is in meters below seafloor (mbsf), direction in degrees, and intensity in ^{10}log mA/m. Data from individual cores are connected with a solid line. The expected inclination pattern is indicated (see text). **A.** "180 degree" components RR and R_1. **B.** "180 degree" components R_2 and R_3. **C.** Primary components PP, P_1, and P_2.

XCB-Cored Sediments

In the absence of declination control or a clear reversal stratigraphy, we experienced difficulties in interpreting the magnetic components in the weakly magnetized Miocene sequence (Cores 121-758A-12X to 121-758A-20X; Figs. 26A, 26B, 29A–29K, 30A, 31A, and 31B) recovered with the extended core barrel (XCB). Expected inclinations for the primary magnetization component (0°–13°) are comparable to inclinations for recent field (0°–10°) or present field (0°–9°) overprints. The problem is further compounded by the limited occurrence of the "180 degree" overprint, which has a comparable range of inclinations. Presumed primary magnetization components were selected mainly on the basis of a high AF stability range and a declination outside the range expected for the "180 degree" overprint. These selection criteria are less than satisfactory, and obviously risk inclusion of recent or present field components. We will show ("Mean Inclination/Latitude Results" section) that this has indeed occurred.

Interpretation in the underlying Oligocene and older sequence (Cores 121-758A-21X to 121-758A-46X, Table 3) was more straightforward. The expected primary inclination steepens considerably downhole, becoming progressively more distinct from the lower inclination overprint components. In an interval of about 130 m (190–320 mbsf) around the early Oligocene to late Paleocene hiatus (248–257 mbsf) we have identified low-inclination and low-stability (less than 20 mT) components as early Oligocene to Eocene or possibly recent field overprints (Fig. 30C). Note that the inclination of the overprint components directly below the unconformity is not much different from the inclination of the primary components directly above the hiatus. Below this hiatus, the polarity of the higher inclination primary components is well established and defines a mixed polarity sequence down to 338 mbsf (Figs. 29H, 29I, and 30A). The underlying ash and basalt sequence is exclusively of normal polarity (Figs. 29J–29N, 30A, 32, and 35A).

Steeply negative inclinations interpreted as drilling-induced overprints of low AF stability (Figs. 30B and 31C) were identified in the mixed polarity sequence above the Cretaceous/Tertiary boundary (296 mbsf). Below the Cretaceous/Tertiary boundary interpretation of drilling-induced overprints is more problematic, because their inclinations are comparable to normal polarity primary inclinations (Figs. 30A, 32, and 35A). Identification was based exclusively on the notably lower AF stability range of the drilling-induced component (Fig. 31C) vs. that of the primary magnetization components (Figs. 31A, 31B, 33A, 33B, and 36A–36D). Below the Cretaceous/Tertiary boundary and in particular

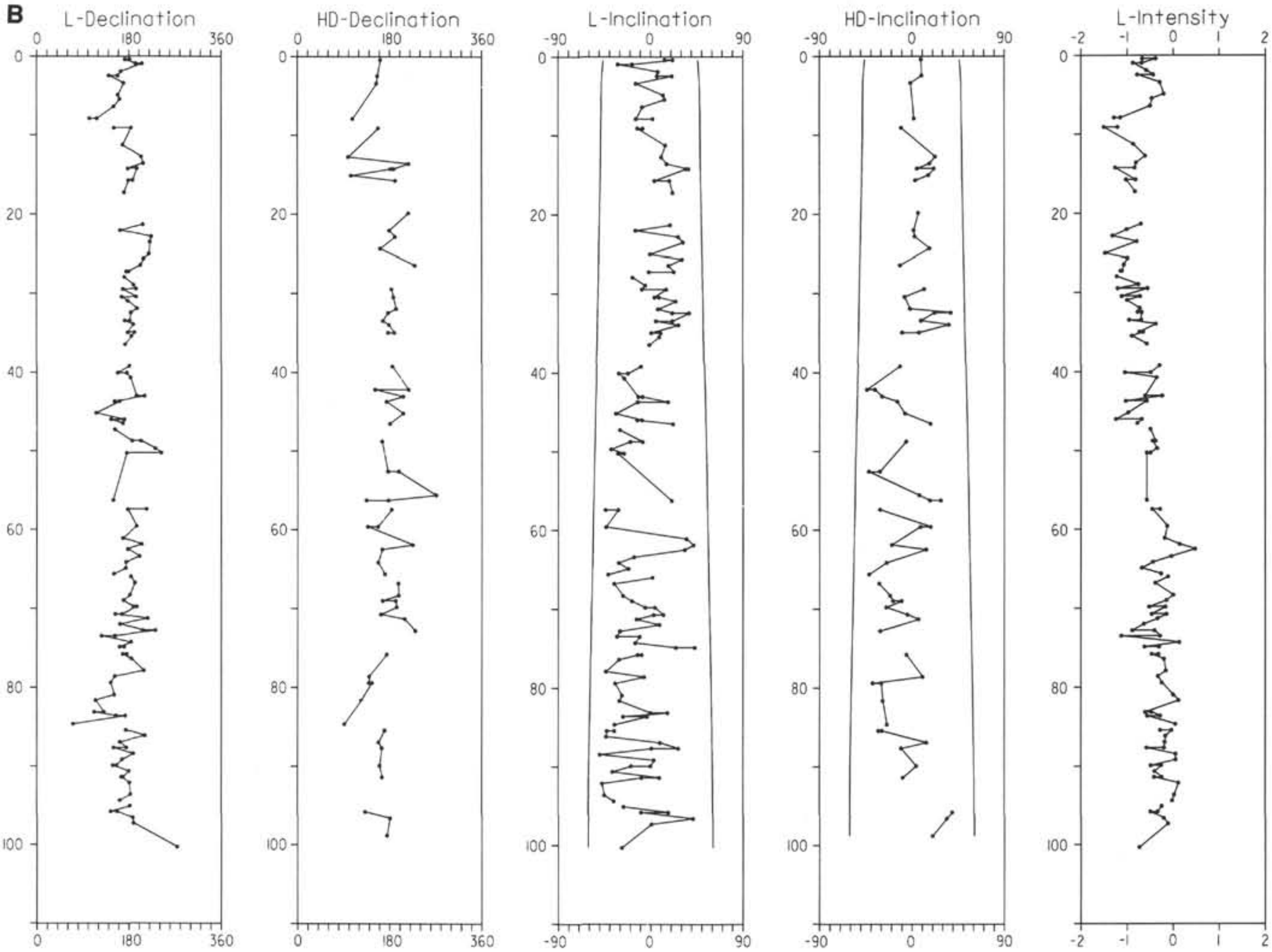

Figure 5 (continued).

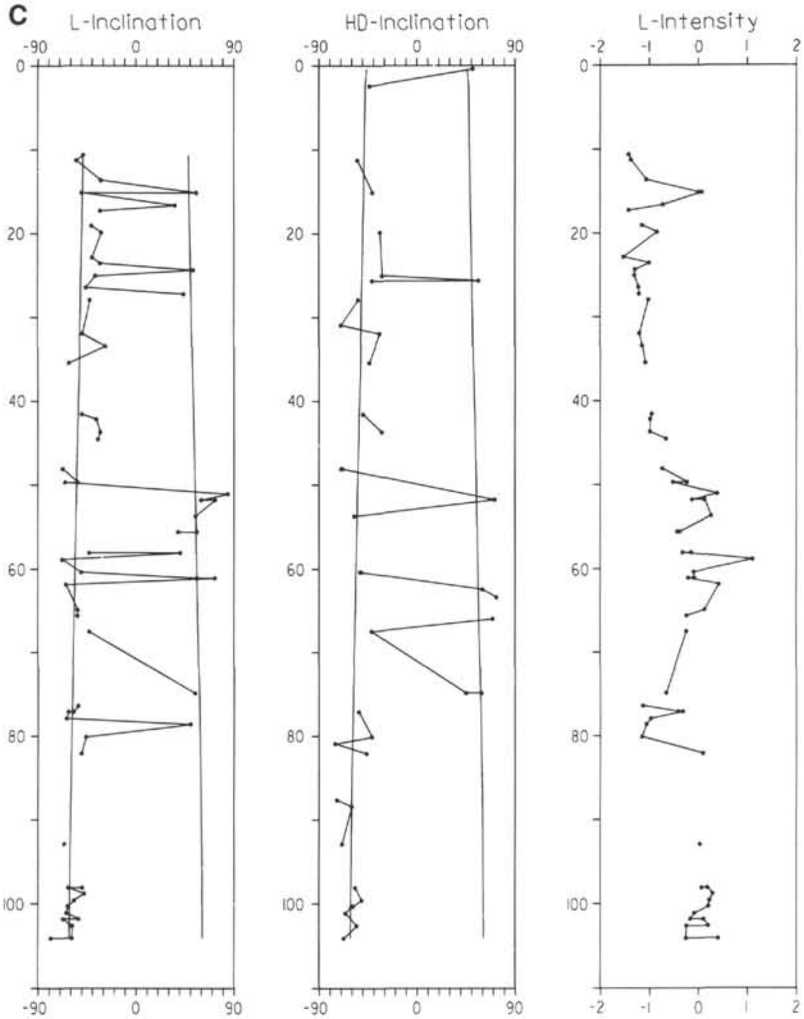

Figure 5 (continued).

in the interval from 312 to 327 mbsf, we observed another overprint of mixed polarity and an about 30° inclination (Fig. 31E). Its origin is not clear.

Ash Sequence

The ash sequence (Cores 121-758A-47R to 121-758A-53R) exhibited exclusively steep negative inclinations of high AF stability (Figs. 26A, 29L–29N, 32, 33A, and 33B and Table 3), which are similar to the primary component observed in the directly overlying sedimentary sequence (337.5–421.5 mbsf). A low-inclination component of presumed recent origin and another shallow (~30° inclination) component occurred sporadically but could easily be distinguished from the primary magnetization component.

Basement Flows

Pilot AF demagnetization showed the presence of only steep negative magnetization components with AF stability generally far below 40 mT in the basement flow sequence (Cores 121-758A-54R to 121-758A-73R; Figs. 26A, 34, 35A, 36A, and 36C and Table 3). These steep inclinations are comparable to those observed in the overlying ash and sedimentary sequence, and may also be interpreted as an exclusively normal polarity primary magnetization component. Their low AF stability range, however, may suggest a drilling-induced origin. AF data alone do not distinguish between these two alternative interpretations. For this reason, pilot and bulk thermal demagnetization and thermal continuation of the already AF-demagnetized samples were undertaken and showed a high thermal stability for this component in the range of 300° to 600°C (Figs. 26C, 26D, $34A_2$, 34C, 34D, $34E_2$–34G, 34I, 34K, 36B, 36D, and 41F). Such a range is clearly outside the low thermal stability ranges previously observed for drilling-induced overprints and we regard such an origin as highly unlikely.

Thermal demagnetization also showed the presence throughout the basalt sequence of an exclusively reversed polarity component with an inclination of about 10° lower than the normal polarity component of presumed primary origin (Figs. $34A_2$, $34E_2$, 34F, 34I, and 35B). This component showed a distinctive bimodal thermal stability range pattern (Fig. 36E), with a higher range at about 400°–550°C and a lower range at about 150°–300°C. The higher range component occurs throughout the basalt sequence (491–637 mbsf). The lower range component is confined to below 579 mbsf and is locally (613–650 mbsf) the more prominent one. We interpret these reversed polarity components as overprints related to thermal and/or hydrothermal activity of a pervasive (higher range) or more local (lower range) origin.

Sporadic overprints with low to equatorial inclinations were observed (Fig. 36F). These represent either a recent field overprint or, more probably, acquisition of a viscous remanence during

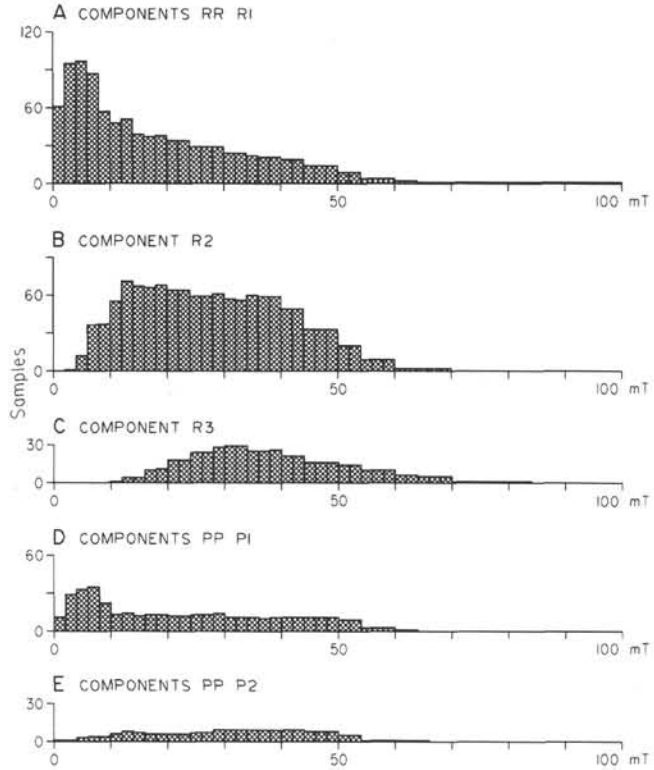

Figure 6. Histograms of stability range distribution upon AF demagnetization for Cores 121-756B-1H to 121-756B-11H. The histograms were constructed by raising the height of individual histogram bars by one unit for every sample whose component stability range, as determined from PCA analysis, covered that bar interval. The 2-mT histogram interval was chosen for optimal resolution only and bears no relation to the interval between demagnetization steps. **A.** "180 degree" components RR and R_1. **B.** "180 degree" component R_2. **C.** "180 degree" component R_3. **D.** Softer primary components PP and P_1. **E.** Harder primary components PP and P_2.

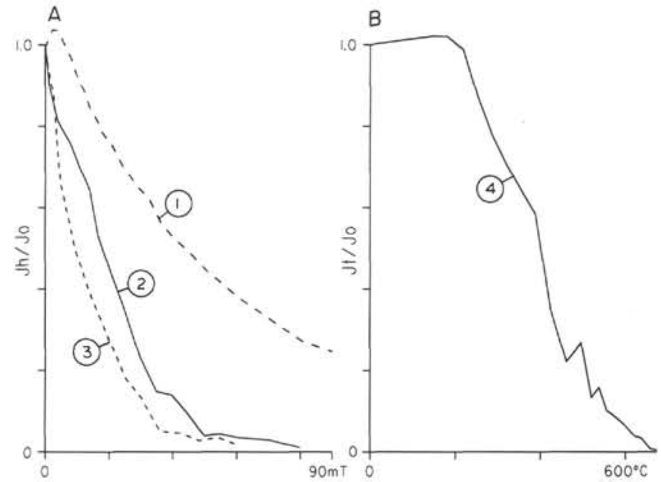

Figure 7. Normalized curves showing the decay of remanent magnetization of representative samples from Hole 756C. **A.** During AF demagnetization. **B.** During thermal demagnetization. 1, 4 = Sample 121-756C-10N-1, 109–111 cm; 2 = Sample 121-756C-4X-6, 20–22 cm; 3 = Sample 121-756C-5X-2, 14–16 cm.

storage, inadvertently in the Earth's magnetic field, prior to thermal continuation treatment of the already AF-demagnetized samples. Locally in the flow sequence we have observed some components with an about 30° inclination (Fig. 36G). These components of unknown origin are similar to the components observed in the ash and sedimentary sequence below the Cretaceous/Tertiary boundary.

Hole 758B

AF demagnetization of the Hole 758B samples (Cores 121-758B-1H to 121-758B-10H; Table 3) showed magnetization components similar to those observed in the equivalent APC-cored upper part of Hole 758A. That is: (1) primary magnetization components stable up to 90 mT (Figs. 37, 38, 39A, 40A, and 40B) that show a reversal pattern fully confirming the whole-core measurements (Fig. 39A; Shipboard Scientific Party, 1989i, fig. 41) and, in addition, probably identify one of the two Réunion subchrons (see "Magnetostratigraphy" section); (2) limited occurrence of a steeply upward-pointing drilling-induced component with an AF stability range generally below 20 mT (Figs. 39B and 40C); and (3) sporadic occurrence of a soft present field overprint (Figs. 39C and 40D).

Magnetostratigraphy

The primary magnetization patterns of Sites 756, 757, and 758 are rather disjointed and have only limited magnetostratigraphic value. A splendid magnetostratigraphic profile was obtained, however, from the terrigenous clay-rich upper 100-m sequence from Site 758 (Cores 121-758A-1H to 121-758A-11H and 121-758B-1H to 121-758B-10H).

Detailed correlation between Holes 758A and 758B, based on whole-core magnetic remanence (5- or 10-cm interval) and susceptibility (3-cm interval) measurements and distinct lithologic markers, produced a unique and nearly complete polarity record from the Brunhes Chron down to Chron 6 (Shipboard Scientific Party, 1989i, figs. 40 and 41). In a subsequent thorough reexamination of these data, Farrell and Janecek (this volume, fig. 3) made a number of minor adjustments, generally less than 5 cm, to the stratigraphic position of the reversal boundaries. In this refined interpretation, which we readily accept here (Table 5), reversal boundaries were placed systematically on polarity transitions. Wherever a reversal boundary was more clearly defined in one hole than in the other, the depth of this boundary and the magnetic susceptibility record were used as a guide to help place the reversal boundary in the opposing hole.

The detailed AF demagnetization results of the samples taken from both APC-cored sequences (Hole 758A, 155 samples; Hole 758B, 145 samples; Table 1) confirm the whole-core magnetostratigraphic record. The two Réunion subchrons were not previously observed in this record. A search for these subchrons was made through detailed sampling, at a 10-cm or smaller interval, of Sections 121-758A-4H-3, 121-758A-4H-4, and 121-758B-4H-1. This search has shown a single normal polarity occurrence (Sample 121-758B-4H-1-85, 87 cm, 29.05 mbsf) within the previously identified Chron 2R. A cross-check with the whole-core magnetostratigraphic record of Hole 758B (Shipboard Scientific Party, 1989i, fig. 41; Farrell and Janecek, this volume, fig. 3; J. Farrell, pers. comm., 1990) showed that a set of three observations between 29.05 and 29.15 mbsf (Section 121-758B-4H-1) could be interpreted as a normal polarity interval with a maximum extent between 28.95 and 29.20 mbsf. Such a normal polarity interval has not been identified, however, in the samples or the whole-core record of Hole 758A. We possibly have missed it there because of its short duration. However, the whole-core record of both holes is rather complex over about 1.5 m around this interval, and the interpreted normal polarity interval of Hole 758B does not necessarily represent reality.

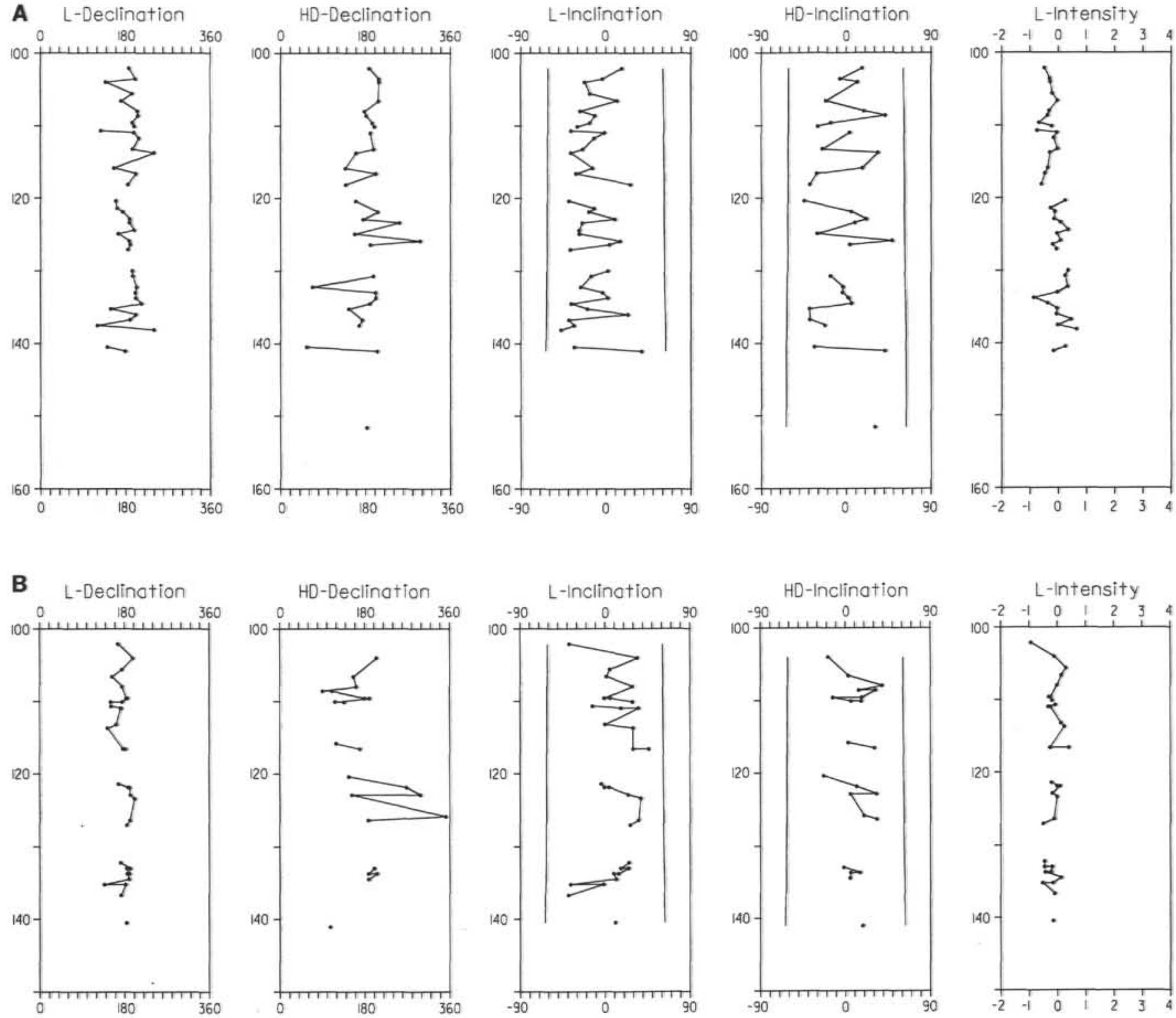

Figure 8. Stratigraphic plots of declination, inclination, and intensity of components determined from linear (L) and planar (HD) PCA from AF (A, B, C) and thermal (C) demagnetization data for Cores 121-756C-4X to 121-756C-12N (see caption to Fig. 5). **A.** "180 degree" components RR and R_1. **B.** "180 degree" components R_2 and R_3. **C.** Primary components PP, P_1, P_2, and P_3 with an attempt at magnetostratigraphic interpretation for part of the sequence. Black = interpreted normal polarity interval; white = interpreted reversed polarity interval; hatchured = undetermined.

Linear interpolation between the two dated bounding polarity reversals in Hole 758B (1.88 Ma at 26.4 mbsf and 2.47 Ma at 34.75 mbsf) dates this normal polarity interval between 2.06 (28.95 mbsf) and 2.07 Ma (29.15 mbsf). This interval falls between Harland's (1982) estimates and Berggren et al.'s (1985) interpolated estimates for the two Réunion subchrons at 2.01–2.04 and 2.12–2.14 Ma and covers a time interval shorter than any of both subchrons. We can reasonably conclude from these data that (1) there is one normal polarity sample in Hole 758B which may correspond to either Réunion Subchron 1 or 2 and (2) the whole-core data may not reasonably be used to establish the presence or duration of any of the Réunion subchrons.

The overall primary magnetization record of the sediments from Sites 756, 757, and 758 is very fragmentary and is obliterated at large by "180 degree" and drilling-induced overprints. A polarity interpretation is presented wherever this could be assessed with some confidence, but we feel that magnetostratigraphic and biostratigraphic control is mostly insufficient to warrant interpretation in terms of the geomagnetic reference time scale (GRTS). Apart from a few clear-cut cases, we have not done so.

Polarity interpretation of the ash and flow sequences was straightforward, with the unexciting occurrence of uniform polarity. In the absence of polarity boundary observations, these single polarity records are correlated with the GRTS according to the closest (minimal) biostratigraphic age control (Peirce, Weissel, et al., 1989) and ^{40}Ar-^{39}Ar dates (R. A. Duncan, pers. comm., 1989, this volume). On this basis, we have interpreted the reversed polarity basement sequence of Site 756 as Chron C18R (^{40}Ar-^{39}Ar date at 42.0 ± 0.6 Ma), possibly Chron C19R (^{40}Ar-^{39}Ar date at 44.6 ± 0.7 Ma). The reversed polarity ash sequence of Site 757 has been interpreted as Chron C24R or C25R (^{40}Ar-^{39}Ar dates at 57.8 and 59.1 Ma, mean age 58.5 Ma). The polarity record of the underlying flow sequence is not readily interpretable because of tectonic problems at Site 757.

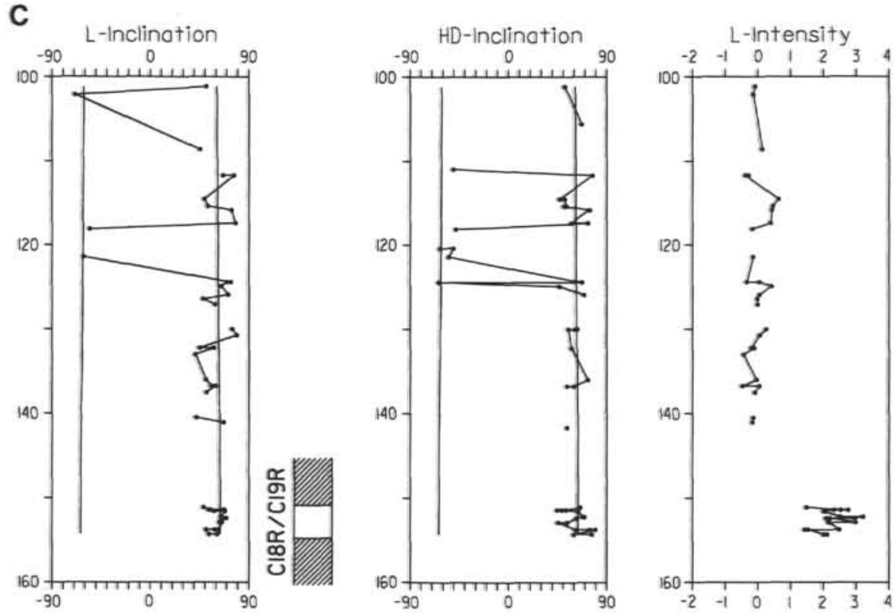

Figure 8 (continued).

The normal polarity ash and flow sequence of Hole 758A down to the base of the hole (673 mbsf), and including the sedimentary sequence below about 340 mbsf, is interpreted as Chron C33N on the strength of biostratigraphic evidence suggesting absence of the lowermost Campanian (Shipboard Scientific Party, 1989i). ^{40}Ar-^{39}Ar dates (Duncan, this volume) for the underlying flow sequence are of rather low quality, with observations of total fusion ages at 80.9 and 82.8 Ma (weighted mean site age at 81.8 ± 2.6 Ma) and plateau ages of suspect reliability (R. A. Duncan, pers. comm., 1989) at 91.5 and 92.9 Ma. The younger dates do not agree with the polarity interpretation (Bolli et al., 1985; Kent and Gradstein, 1986), for the reason that Chron C33N is expected rather than Chron C33R. The older group of dates clearly conflicts with biostratigraphic control. Despite this apparent conflict we have taken the mean total fusion age (81.9 Ma) as representative for the normal polarity sequence with the underlying assumption that the interpolated ages of the GRTS may be up for refinement on the basis of future direct radiometric age determinations.

Susceptibility

Whole-core bulk susceptibility of all cores was measured aboard *JOIDES Resolution* with the Bartington susceptibility meter MS1/CX (Shipboard Scientific Party, 1989b). On-shore measurement of discrete-sample bulk susceptibility was limited to the monitoring of susceptibility changes during thermal demagnetization of the pilot ash and pilot basalt samples. Measurements were carried out with a DIGICO MV16 bulk susceptibility bridge. Three types of behavior were noted: (1) no appreciable variation (e.g., the ashes of Hole 757B, Fig. 41A), (2) gradual reduction above 300°–400°C to less than 50% of initial susceptibility (some of the Site 756 and 757 flows, Fig. 41B), and (3) up to a 100% increase in susceptibility between 250° and 400°C followed by a larger reduction between 500° and 600°C, down to 50% or less of the initial susceptibility (all Site 758 flows and some of the Site 756 and 757 flows, Fig. 41C). In accordance with these generally limited susceptibility changes upon thermal treatment, we experienced only some limited acquisition of viscous magnetization during DIGICO spinner measurements at the 400°–450°C demagnetization steps. Routine nulling of the ambient field at the magnetometer insert prevented any impediment of remanence measurements.

PALEOLATITUDES AND BREAKS IN MOVEMENT RATE

Mean Inclinations

Method

Mean inclinations were determined per hole for every interval between successive datum levels. Datums used are those described in the Leg 121 *Initial Reports* (Peirce, Weissel, et al., 1989). That is: (1) dated polarity reversals for the APC-cored sequences of Holes 758A and 758B, (2) biostratigraphic datum levels for all other sedimentary and ash sequences, and (3) cooling unit boundaries and ^{40}Ar-^{39}Ar determinations (Duncan, this volume) for basement flows.

We followed the McFadden/Reid method (McFadden and Reid, 1982; P. L. McFadden, pers. comm., 1989) in the determination of mean inclinations and associated confidence limits for unoriented and also for oriented cores. AF and thermal demagnetization results were combined, where available, giving unit weight to individual sample data. Dual-treatment demagnetization results from the basement and ash sequences (i.e., thermal continuation data of already AF-treated samples) were combined as if the results represent two separate specimens taken at the same level. This accounts for some apparent inconsistencies between numbers detailed in Table 1. For mixed polarity intervals (see the previous description, for only the second and third types of datums), the equivalent normal polarity mean inclination was calculated.

We previously described that AF and thermal demagnetization treatments alike showed the general presence of a softer and a harder primary magnetization component and explained why we kept such components separated throughout the mean inclination determination and interpretation process. Likewise, mean inclinations were calculated separately for directions obtained from linear and Hoffman-Day analysis. We feel such a separation necessary as there seems no statistically justified criterion available for the integration of linear and Hoffman-Day component directions from the same sample, with proper weighting and without duplication of information. Quality and quantity of the data permitting, we thus calculated four mean directions (linear: soft and hard; Hoffman-Day: soft and hard) per individual inter-

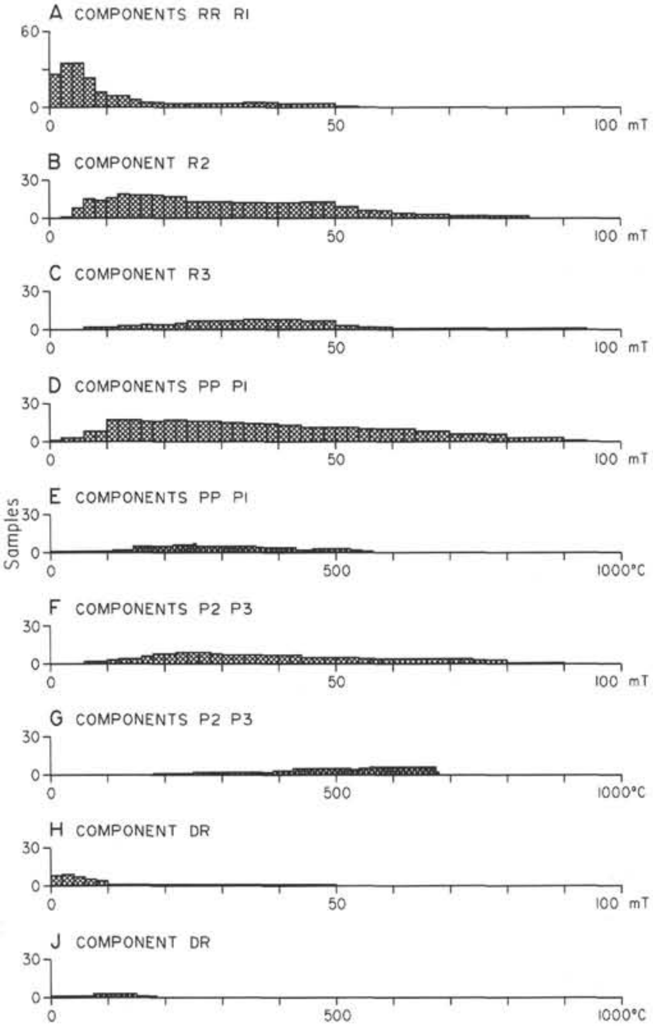

Figure 9. Histograms of stability range distribution upon AF and thermal demagnetization for Cores 121-756C-4X to 121-756C-12N. The histogram intervals of 2 mT for AF demagnetization data and 5°C for thermal demagnetization data were chosen for optimal resolution only and do not correspond with intervals between demagnetization steps (see caption to Fig. 6). **A–C.** "180 degree" components RR, R_1, R_2, and R_3. **D–G.** Primary components PP, P_1, P_2, and P_3. **H, J.** Drilling-induced overprint DR.

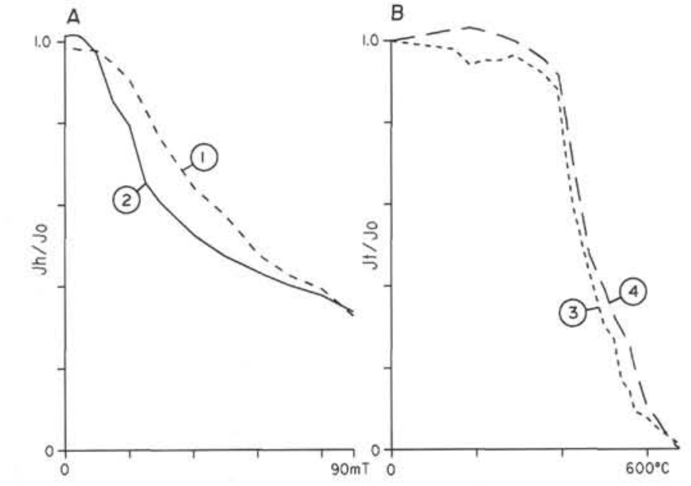

Figure 10. Normalized curves showing the decay of remanent magnetization of representative samples from Hole 756D. **A.** During AF demagnetization. **B.** During thermal demagnetization. 1, 4 = Sample 121-756D-11R-1, 77–79 cm; 2, 3 = Sample 121-756D-9R-2, 6–8 cm.

val. A distinction between these four directions was maintained throughout the subsequent common-site transfer and interpretation process.

For the oriented APC-cored sections of Holes 758A and 758B we also calculated Fisherian mean directions (Fisher, 1953) following the same combination procedures. The so-obtained Fisherian mean inclinations proved indistinguishable from the McFadden/Reid mean inclinations and support the claimed validity of the method (McFadden and Reid, 1982). For procedural consistency, only the McFadden/Reid results were used.

Mean inclinations with an error interval exceeding 25° were arbitrarily excluded from interpretation. For a considerable number of high-inclination basement cooling units a mean inclination could not be obtained because the applied iteration procedures (P. L. McFadden, pers. comm., 1989) did not stabilize. This is due mainly to the inherent declination uncertainty of high-inclination groupings as discussed by McFadden and Reid (1982).

Mean inclination and confidence parameters are listed in Table 3 and are shown as equivalent mean latitudes against depth and/or age in Figures 42–52. The latitude/depth–latitude/age plots show mean latitudes with (1) vertical bars representing the latitude range equivalent of the McFadden/Reid inclination confidence interval and (2) horizontal bars indicating the depth/age interval over which the mean inclination/latitude was obtained. The expected latitude/depth (or age) pattern according to the simulated Morgan/Patriat pole positions (Table 2) is shown for comparison. For the latitude/depth plots this pattern was determined through interpolation over age between the simulated pole positions according to the mean age of each set of two successive datum levels. For latitude/age plots, interpolation of the Morgan/Patriat pole positions was not necessary. Expected directions and equivalent paleolatitudes at the site were calculated following the geocentric axial dipole field model.

Analysis and interpretation of the results were based on latitude/depth and latitude/age plots for the individual holes (see "Mean Inclination/Latitude Results" section). The latitude/depth plots of Site 756 and all latitude/age plots are shown integrated per site. The latitude/depth plots show individual mean results per flow/cooling unit and per ash unit (Table 3). The latitude/age plots show mean-flow inclination/latitude results (Table 3). Only the mean-flow results were carried through in the common-site transfer and overall interpretation process.

Mean Inclination/Latitude Results

Site 756 (Holes 756B–756D)

Results from the upper part of Hole 756B (15–25 and 25–31 mbsf, Fig. 42) show a paleolatitude about 10° lower than expected. Seismic profile data show no measurable dip for the beds, and we suspect that these low-quality results are contaminated by an incompletely eliminated "180 degree" overprint. These results are excluded, therefore, from further interpretation (see Fig. 43). The single-flow mean results from Hole 756C (flow Unit 756C-F1, 143–155 mbsf) were combined with mean-flow results from Hole 756D (flow Units 756D-F5–756D-F7, 756D-F9, and 756D-F12–756D-F14, Table 3). Paleolatitudes indicated by the mean-flow results are about 41°S–45°S, substantially lower than the present-day latitude of the Kerguelen-Heard hot spot (49°S–

53°S). However, these paleolatitudes are not far off the present-day latitude of the Amsterdam–St. Paul hot spot (38°S–39°S) and support observations (Weiss and Frey, this volume; Saunders et al., this volume) for an Amsterdam–St. Paul affinity in the isotope signature of the Site 756 basalts.

Site 757 (Holes 757B and 757C)

Seismic-reflection data show that the ash sequence dips at 10° to the southwest. The dip becomes negligible in the overlying sedimentary sequence. We interpret this dip to represent postemplacement tectonics rather than primary bedding. Correction for bedding brings the observed "steep" inclination into good agreement with the expected inclination of about −65° (Fig. 44 and Table 3). This bedding correction was carried out by combining the observed inclinations(s) with the declination(s) expected according to the simulated Morgan/Patriat pole positions. Expected declinations were used only as a vehicle to restore the observed mean inclination and its confidence interval into a pretilting orientation. Any error in the declination components used is minor compared to the inclination confidence interval, and will not noticeably offset the corrected results. The bedding-corrected paleolatitude of the ash sequence varies upward through the sequence from about 50°S to about 45°S. This lends strong support to the hypothesis that the Kerguelen/Heard hot spot (now at 49°S–53°S) represents the origin of Ninetyeast Ridge (Duncan, this volume; Royer et al., this volume).

Mean inclination/latitude results for the single flow studied at the base of Hole 757B (flow Unit 757B-F1, 367–374 mbsf; Figs. 44 and 46 and Table 3) and all flows of Hole 757C (Figs. 45 and 46 and Table 3) are anomalous. Both AF and thermal demagnetization results show very low, mainly downward inclinations in the upper part of the flow sequence (Unit 757B-F1 and tuff Units 757C-F1–757C-F9, 363.0–401.7 mbsf) and very steep downward inclinations in the lower part of the flow sequence (Units 757C-F10–757C-F19, 401.7–417.0 mbsf). We cannot forward any explanation for these anomalous results other than to attribute them to large-scale tectonic disturbance of the flow sequence, which apparently affected the ash sequence to a much lesser degree. Available seismic-reflection profiles do not allow an estimate for the bedding of the flow sequence. No correction could be made, and these results were excluded from further interpretation. Such a tectonic disturbance of the basement sequence may well be related to the southward jump of the western extension of the Wharton Basin spreading ridge (Sclater and Fisher, 1974; Luyendyk and Rennick, 1977; Peirce, 1978; Royer and Sandwell, 1989; Royer et al., this volume), with transferral of part of the Antarctic plate now at 6°S–16°S to the Indian plate. The ridge jump occurred at about 58 Ma (Chron 25 to 26: Royer and Sandwell, 1989; Royer et al., this volume), contemporaneous or slightly after extrusion of the basement flows (about 58.5 Ma; Duncan, this volume). The new spreading center at 16°S developed close to Site 757 (17°S). Tectonic disturbances associated with formation of this new spreading center may explain the consistently anomalous paleomagnetic results from the basement of Site 757, and may explain the only minor tilt in the overlying ash sequence.

Site 758 (Holes 758A and 758B)

The latitude/depth profile (Fig. 47) clearly shows the discontinuous sedimentary sequence, with a major early Oligocene to late Paleocene hiatus (at about 250 mbsf), and a reduced Cretaceous/Tertiary boundary sequence (at about 296 mbsf). In view of the data gaps, particularly in the Eocene, any constraint on the time of the slowdown of India's northward movement will have to be based on combined evidence from all Ninetyeast Ridge sites under study, rather than on single-site data.

The inclination/latitude data from Site 758 (see the following sections) show three main discrepancies with dipole and nondipole field models and with the expected paleolatitude pattern:

1. The high-quality data from the APC-cored sequence (Figs. 48 and 49, 0–102 mbsf) do not follow the expected inclination/paleolatitude pattern. The data show a discrepancy between normal and reversed polarity inclinations/paleolatitudes, with normal polarity paleolatitudes generally situated farther southward than reversed polarity paleolatitudes. This is particularly clear for Hole 758B (Fig. 49), but less so for Hole 758A (Fig. 48). This discrepancy may result, at least in part, from the presence of a nonidentified local field component (inclination −9°, corresponding to an about 5°S latitude). Most of the normal polarity paleolatitude data, however, fall in the equatorial region rather than at about 5°S and may reflect another origin. Reversed polarity paleolatitudes in Hole 758B are close to expected values, but Hole 758A data show a more prominent discrepancy (Figs. 48 and 49). The base of this APC-cored sequence shows paleolatitudes either constant or more northern than expected, with more southern paleolatitudes at the top. The normal and reversed polarity data do not seem to reflect the pattern of nondipole fields reported to have persisted for at least the last 5 m.y. (Merrill and McElhinny, 1983; Schneider and Kent, 1986, 1988a, 1988b, 1990b; Merrill and McFadden, 1990; Merrill et al., 1990). Such fields would be expected to show an N-R discrepancy, opposite to the one observed here, with lower reversed than normal polarity inclinations, superimposed, of course, on the overall pattern reflecting India's ongoing northward movement. We cannot readily explain this disagreement with nondipole field models based on wider data sets, because our data are of high quality and were fully corrected for azimuthal orientation of the core sections, drift of the drill string, and a further rotation of individual core sections (Figs. 27 and 39).
2. Normal polarity inclinations/paleolatitudes in the upper part of the underlying sedimentary sequence cored with XCB system (100–150 mbsf, Miocene, about 7–20 Ma) are lower than expected and seem more closely aligned with the inclination/"paleolatitude equivalent" of the present local field (−9°/5°S). It appears that we were less than successful in separating a present field overprint from primary magnetization components in this Miocene sequence of admittedly low paleomagnetic intensity and low data quality. It is a puzzling observation, however, that reversed polarity inclinations/paleolatitudes in this Miocene sequence are aberrant like the normal polarity results. We cannot offer any satisfactory explanation for this discrepancy, other than pointing to general sources ranging from an undetermined drift of nonoriented core sections to unidentified overprints like the "180 degree" components.
3. The normal polarity mean inclinations from the lower part of the ash sequence and the upper part of the basalt sequence show a mean paleolatitude at about 50°S. This corresponds closely with the paleolatitude observed in the lower ash sequence from Site 757 and supports the Kerguelen/Heard hot spot origin of Ninetyeast Ridge concluded in earlier studies (e.g., Peirce, 1978; Duncan, 1978; Royer and Sandwell, 1989; Davies et al., 1989). The normal polarity mean inclinations from the lower part of the basalt sequence (flow Units 758A-F16–758A-F29, 619.6–673.3 mbsf), however, are far shallower than expected. This may represent an artifact resulting from insufficient averaging of secular variation and/or unnoticed tilting of the basal part of the basalt sequence only. However, this normal polarity mean inclination and the one for the reversed polarity overprint observed throughout the basalt sequence both indicate an about 40°S paleolatitude (Fig. 50). These two components may reflect a similar overprint origin.

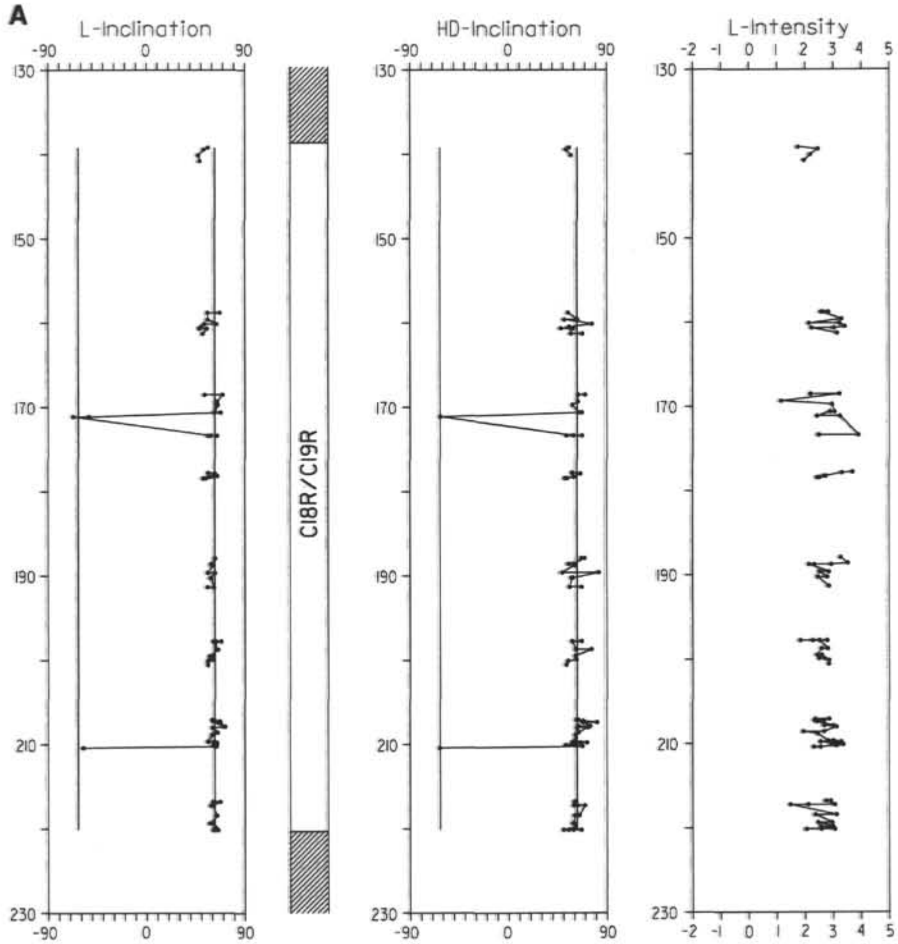

Figure 11. Stratigraphic plots of inclination and intensity of components determined from linear (L) and planar (HD) PCA of AF and thermal demagnetization data for Cores 121-756D-4R to 121-756D-12R (see caption to Fig. 5). **A.** Primary components PP, P_1, and P_2 with an attempt at magnetostratigraphic interpretation for part of the sequence (see caption to Fig. 8). **B.** Drilling-induced overprint DR.

The approximate 40°S paleolatitude indicated by these overprint components is close to the present-day latitude of Amsterdam (~38°S) and St. Paul Island (~39°S). The Site 758 basalt sequence shows some indication of the geochemical signature of the Amsterdam–St. Paul hot spot, though less distinct than at Site 756 (Weiss and Frey, this volume; Saunders et al., this volume). It is possible, therefore, that these overprints were caused by thermal or hydrothermal effects of these hot spots on the Ninetyeast Ridge/Kerguelen hot spot trail, as suggested before from modeling of Indian Ocean plate movements (Luyendyk and Rennick, 1977) and trace elements considerations (Storey et al., 1988, 1989), without considerable contribution to the lava/ash pile. Nearby dikes unnoticed in the core record, or channeling of hydrothermal fluids through zones of weakness, might have led to localized overprint pockets. An alternative interpretation is that these overprints may result from widespread reactivation of zones of weakness like the Ninetyeast Ridge at about Cretaceous/Tertiary boundary time, possibly also expressed in the rift-related volcanism on Broken Ridge observed from dredge samples (^{40}Ar-^{39}Ar age: 63 Ma; Duncan, this volume). Comparison with the expected paleolatitude pattern (Figs. 47, 50, and 51) indicates that these overprints may have originated at that time. A causal relationship between initial India-Asia contact around Cretaceous/Tertiary boundary time, extrusion of the Deccan Traps ("India-Asia Collision and the Deccan Traps Diastrophism" section), and a fundamental reorganization of the Indian Ocean ("Date of Initial Contact and Completion of Suturing" section) will be explored subsequently. It is possible that such a major tectonomagmatic upheaval of the Indian plate left a widespread imprint on the plate's internal and marginal zones of weakness, like Ninetyeast Ridge.

Paleolatitudes for the ash and flow sequence at Site 758 are in agreement with the Kerguelen hot spot (~49°S), but fall about 5° north of paleolatitudes expected from the simulated Morgan/Patriat APWP. Such an offset is consistently evident for the whole of the pre-Cretaceous/Tertiary boundary sequence of sediments, ashes, and basalts (72.1–81.9 Ma). For instance, the observed paleolatitude of the basalt sequence is about 50°S, whereas the expected paleolatitude is 55°S. The observed 50°S paleolatitude is in accord with the Site 757 results, other DSDP studies (Peirce, 1978), and various land-based paleomagnetic studies (Rajmahal Traps: Klootwijk, 1971; Aulis Volcanics/Taltung Formation: Gautam, 1989; Bunbury basalts: Schmidt, 1976b). Inclination errors due to compaction can be excluded (basalts) or are not expected (ashes) following the Site 757 results, and seismic profiles show no measurable dip. This consistent discrepancy between observed and expected inclinations possibly reflects inaccuracies in India-Africa relative motion data prior to Chron 29 (Patriat and Achache, 1984; Patriat and Ségoufin, 1988; Royer et al., 1988; Molnar et al., 1988; Royer and Sandwell, 1989) or

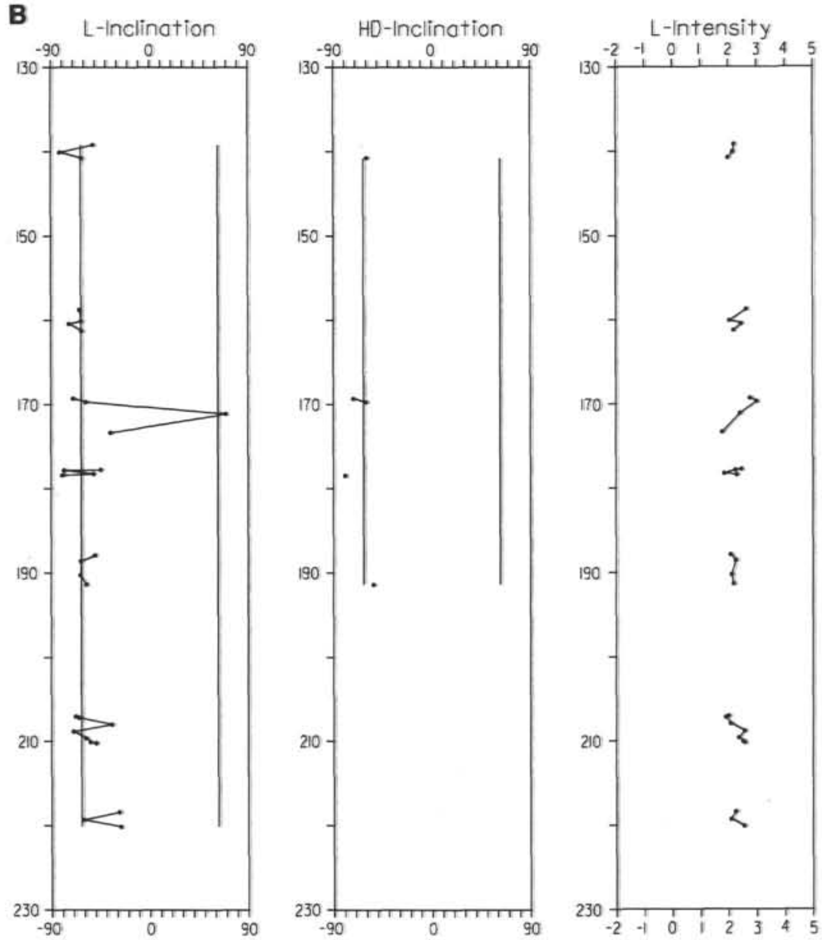

Figure 11 (continued).

offset between the geomagnetic and the hot-spot reference frame observed by some (Harrison and Lindh, 1982; Andrews, 1985; Sager and Bleil, 1987) but not by others (Livermore et al., 1983, 1984; Schneider and Kent, 1990a, 1990b).

Transferral to Common-Site

Mean inclinations from Sites 756 and 757 were transferred to Site 758 over the paleomagnetic pole (Klootwijk, 1979). For every mean inclination result, a pole position was simulated through combination of the observed inclination with the expected declination at the site for the mean age of the studied interval. The expected declinations were calculated from interpolation of the Morgan/Patriat APWP. From these pole positions, equivalent inclinations/paleolatitudes were calculated at the location of Site 758. Simple transferral of observed paleolatitudes on the basis of their present latitudinal separation (e.g., Peirce, 1978) would have resulted in erroneous paleolatitudes up to 2° too far north for the basement sequence of the southernmost Site 756. Such errors would have resulted solely from neglect of the approximately 20° counterclockwise rotation of the Indian plate during the latest Cretaceous and Tertiary.

Site 758 was chosen as the common-site for two main reasons: (1) it has the most extensive time (0–81.9 m.y) and depth (0–673 mbsf) record of the three sites studied and (2) it is more distant than Sites 756 and 757 from the Eulerian poles describing the counterclockwise rotation of the Indian plate, and thus has undergone a larger northward translation. Site 758 results, therefore, have the potential to resolve the pattern of India's northward

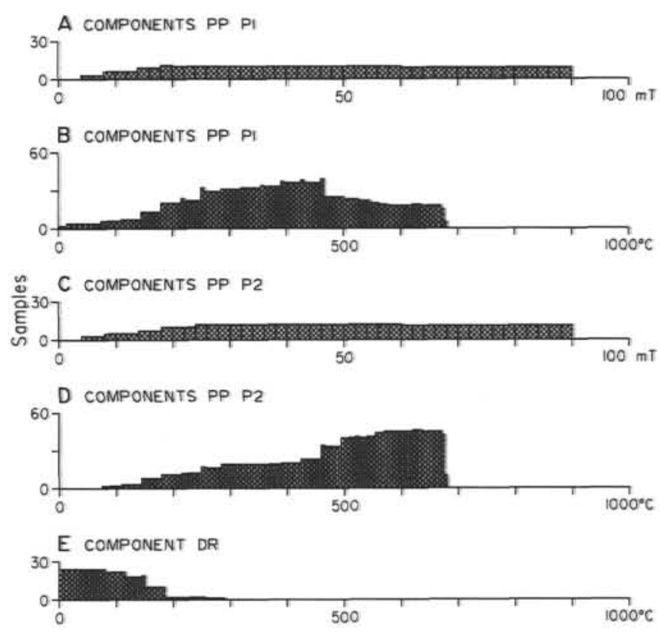

Figure 12. Histograms of stability range distribution upon AF and thermal demagnetization for Cores 121-756D-4R to 121-756D-12R (see captions to Figs. 6 and 9). **A–D.** Primary components PP, P_1, and P_2. **E.** Drilling-induced overprint DR.

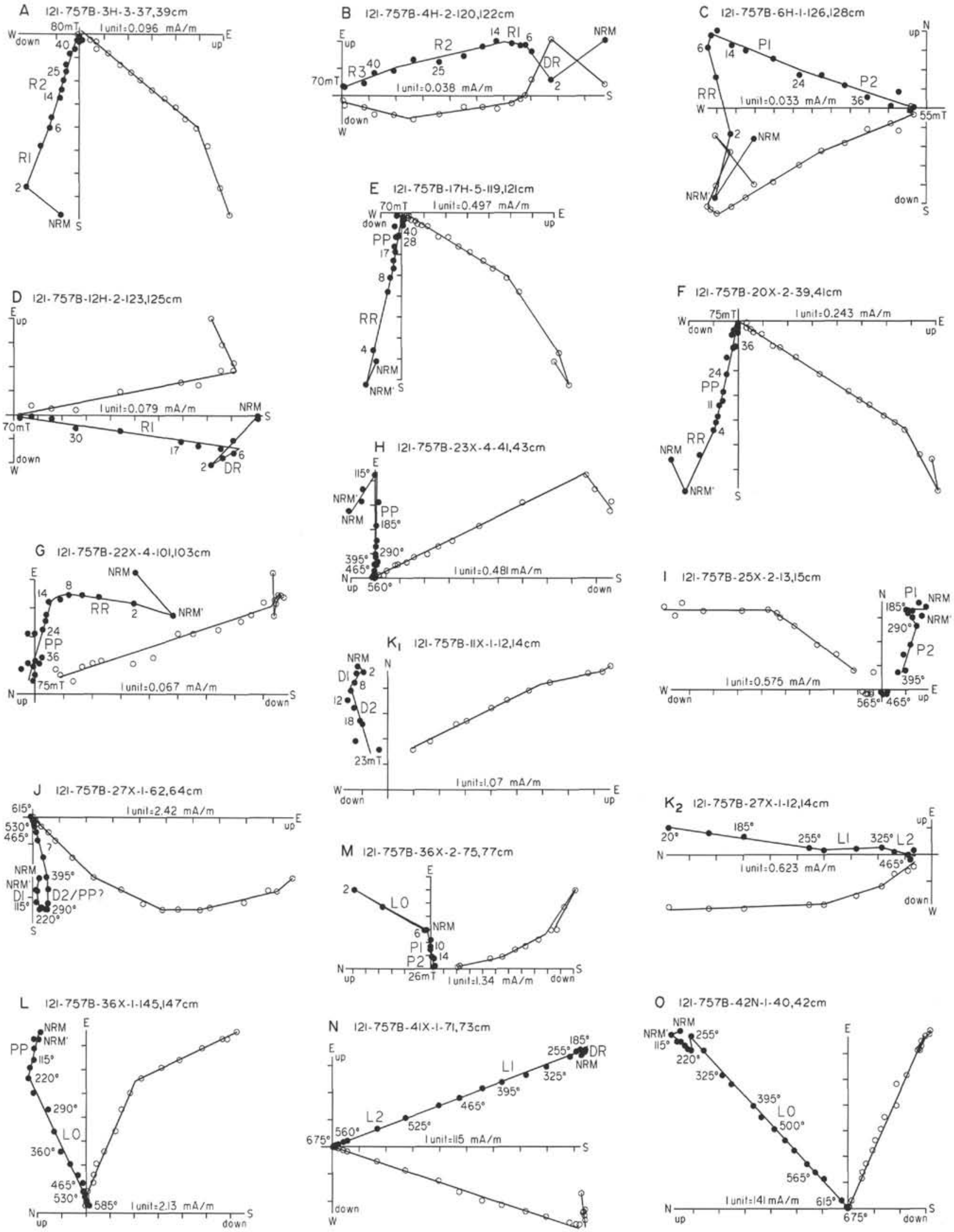

Figure 13. Zijderveld (1967) diagrams of representative samples from Hole 757B during AF and thermal demagnetization (see caption to Fig. 3). LO, L_1, L_2 = low-inclination components.

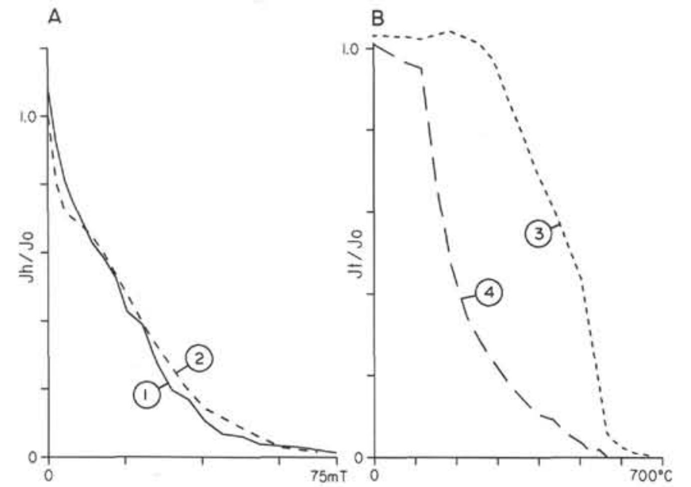

Figure 14. Normalized curves showing the decay of remanent magnetization of representative samples from Hole 757B. **A.** During AF demagnetization. **B.** During thermal demagnetization. 1 = Sample 121-757B-20X-2, 39–41 cm; 2 Sample = 121-757B-4H-2, 120–122 cm; 3 = Sample 121-757B-41X-1, 107–109 cm; 4 = Sample 121-757B-23X-4, 41–43 cm.

movement with a higher degree of resolution than the more southerly Sites 756 and 757 or from results transferred to such sites. The common-site transferral procedure inherently assumes no internal deformation of the Indian plate. In doing so, we have neglected the equatorial zone of distributed lithospheric deformation (Gordon et al., 1990; DeMets et al., 1990) of presumed late Neogene origin (see "Increase in NRM Intensity at 6.5 Ma" section), situated between Site 758 and Sites 756 and 757. Total extension (western part) or shortening (eastern part) across this zone is estimated at no more than 50 km.

Figure 52 shows the combined paleolatitude observations from Sites 756, 757, and 758, transferred to Site 758, in the form of four separate paleolatitude/age plots for linear (soft and hard) and Hoffman-Day (soft and hard) directions. Earlier DSDP paleolatitude data from the Indian plate (see Peirce, 1978; Klootwijk, 1979; Table 6) were not incorporated into this figure. We prefer to analyze these earlier data separately, in order to avoid a bias by comparison of data obtained from different mean inclination reduction methods. These earlier DSDP data were corrected for the absence of declination control following a method developed by Cox (Cox and Gordon, 1984) and summarily described by Peirce (1976). The mean Deccan Traps results, detailed in Klootwijk (1979) (Table 6), were transferred to Site 758 and are incorporated in Figures 52, 55, and 56. Results from a more extensive paleomagnetic review of the Deccan Traps (Vandamme et al., in press) were made available to us recently. These results are in general agreement with Klootwijk's (1979) data, but show some significant improvements in detail. Vandamme et al.'s mean results are included in Table 6 and their implications are referred to wherever appropriate. The results did not form part of the initial analysis leading to Figures 52, 55, and 56, but do not affect the main conclusions reached.

Weighted Linear Regression Analysis

Generalities

The latitude/time plots shown in Figure 52 were analyzed with a weighted linear regression procedure (P. L. McFadden, pers. comm., 1989). The applied weighting factor is inversely proportional to the variance, with the variance approximated by the square of the half-value of the latitude confidence interval. This linear regression method assumes, of course, that northward movement rates (gradients) remained stable over the time intervals for which boundaries are to be determined and do not show appreciable systematic variations. This basic assumption was heuristically tested through a moving window determination of the gradient.

The results show that the wider time windows (10 and 15 m.y) tend to smooth over apparent abrupt changes in the northward movement rate, whereas the narrower time window (5 m.y.) tends toward erratic results (Fig. 53). The latter results suggest, nevertheless, that some gradual decrease in the northward movement rate may have occurred during the critical time interval 40–55 Ma. We have not evaluated whether approximation of the data with a linear regression technique is statistically justified; the data may not be of sufficient quantity and quality for such an evaluation to be successful. Instead, we have preferred to account for more gradual rather than abrupt movement rate variations by interpreting so-determined breakpoints in the northward movement rate/time profile as youngest ages in case of a breakpoint modulated by a gradual slowdown (Eocene) and as oldest ages in case of modulation by a gradual rate increase.

Maximum Likelihood Determination of Breakpoints

Breakpoints in the movement rate profile (Fig. 54 and 55) were determined with the use of a two-stage maximum likelihood procedure (P. L. McFadden, pers. comm., 1989). This method was applied separately to each of the four data sets (linear: soft and hard; Hoffman-Day: soft and hard). First, common breakpoint intervals were estimated visually from the four data sets as described and shown in Figure 54. With limited or absent constraining data points in the breakpoint interval, the actual breakpoints were determined subsequently as the intersection of two weighted least-squares line segments fitted to the two sets of data points between the breakpoint under study and the two adjacent breakpoint intervals. Following this method, maximum likelihood estimates of breakpoint intervals were obtained at about 2.7, 6.7, 18.5, about 53, 63.5–67, and 68–74.5 Ma. The latter two breakpoint intervals and the former three breakpoint estimates were interpreted from well-defined maximum likelihood (MLHD) minima (Fig. 54). However, these breakpoints (intervals) may not reflect a change in movement rate, as discussed subsequently. The breakpoint at about 53 Ma was interpreted from MLHD values (Fig. 54) that show a rather broad low, with an indication of a minimum between 50 and 58 Ma and a very sharp rise at 53 to 58 Ma.

The 63.5–67- and 68–74.5-Ma breakpoint intervals are based largely on the Deccan Traps paleomagnetic data. The Deccan Traps is one of the most studied formations in the world. It will be suggested subsequently ("Some Problematic Paleomagnetic Data" section), however, that the data may not necessarily accurately represent India's paleolatitude at Cretaceous/Tertiary boundary time, when the Deccan Traps presumably extruded. We will not pursue, therefore, the legitimacy or implication of these two breakpoint intervals.

The 2.7-, 6.7-, and 18.5-Ma breakpoint estimates also may not reflect changes in the northward movement rate. These breakpoint estimates closely correspond with breaks in the susceptibility and initial NRM intensity profile of Site 758 (see "Dating the Breaks" section, Fig. 61, and Table 12) at 2.5–2.7, 6.2–6.5, and about 17.5 Ma. They may merely reflect variations in the potential of the sedimentary sequence to accurately reflect and retain a primary magnetization direction. This problem is amply illustrated from the nonintersection of the fitted line segments in the 0–2.7-, 2.7–6.7-, and 6.7–18.5-Ma intervals. The fitted line segments for the 6.7–18.5-Ma interval show for all four data sets (Figs. 52 and 55) a predominant paleolatitude in the 4°S–5°S range. This range corresponds closely to the about −9° inclination of the present

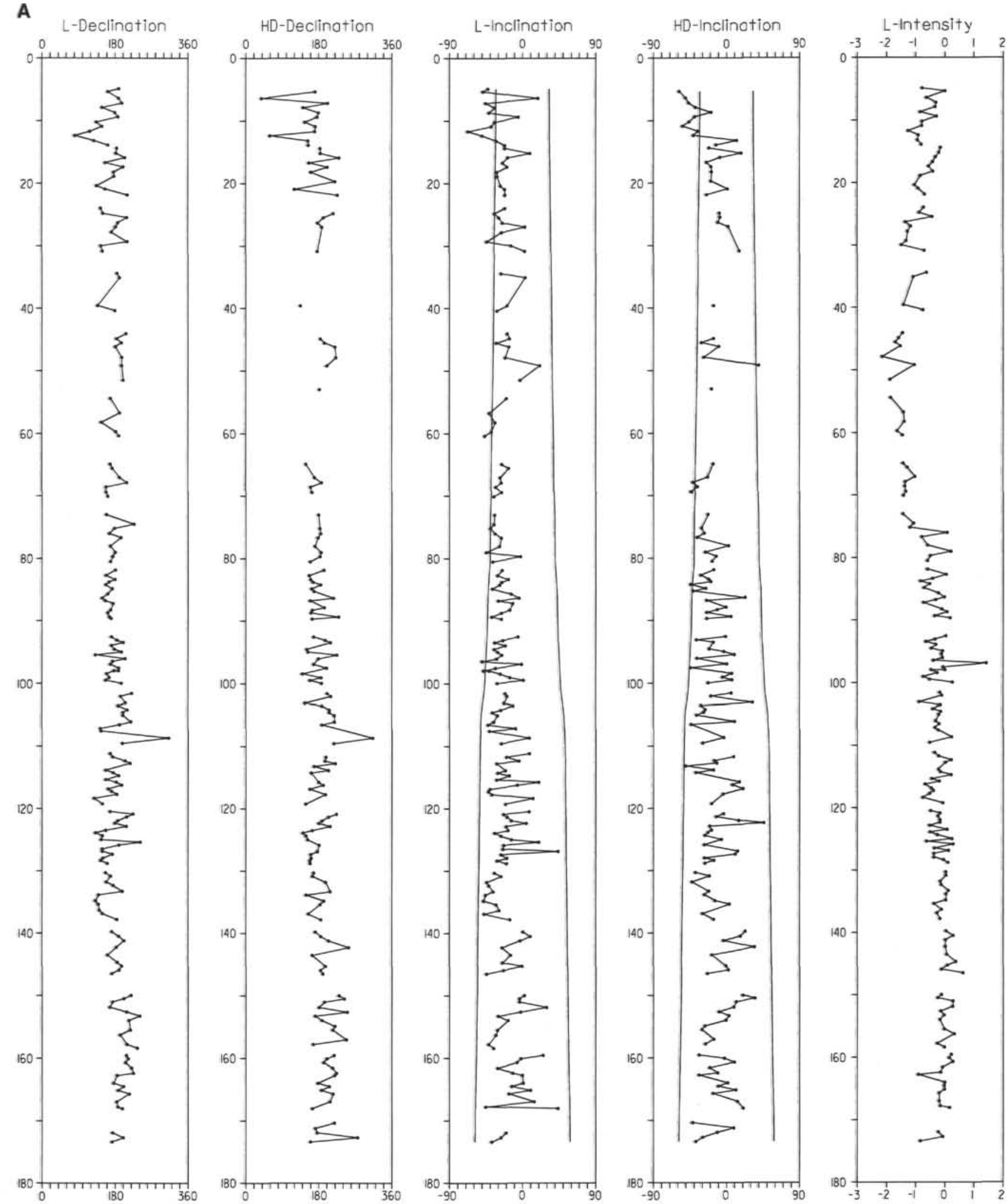

Figure 15. Stratigraphic plots of declination, inclination, and intensity of components determined from linear (L) and planar (HD) PCA of AF demagnetization data for Cores 121-757B-1H to 121-757B-19H (see caption to Fig. 5). **A.** "180 degree" components RR and R_1. **B.** "180 degree" components R_2 and R_3. **C.** Drilling-induced components DR, D_1, and D_2. **D.** Primary components PP, P_1, and P_2 with an attempt at magnetostratigraphic interpretation for part of the sequence (see caption to Fig. 8).

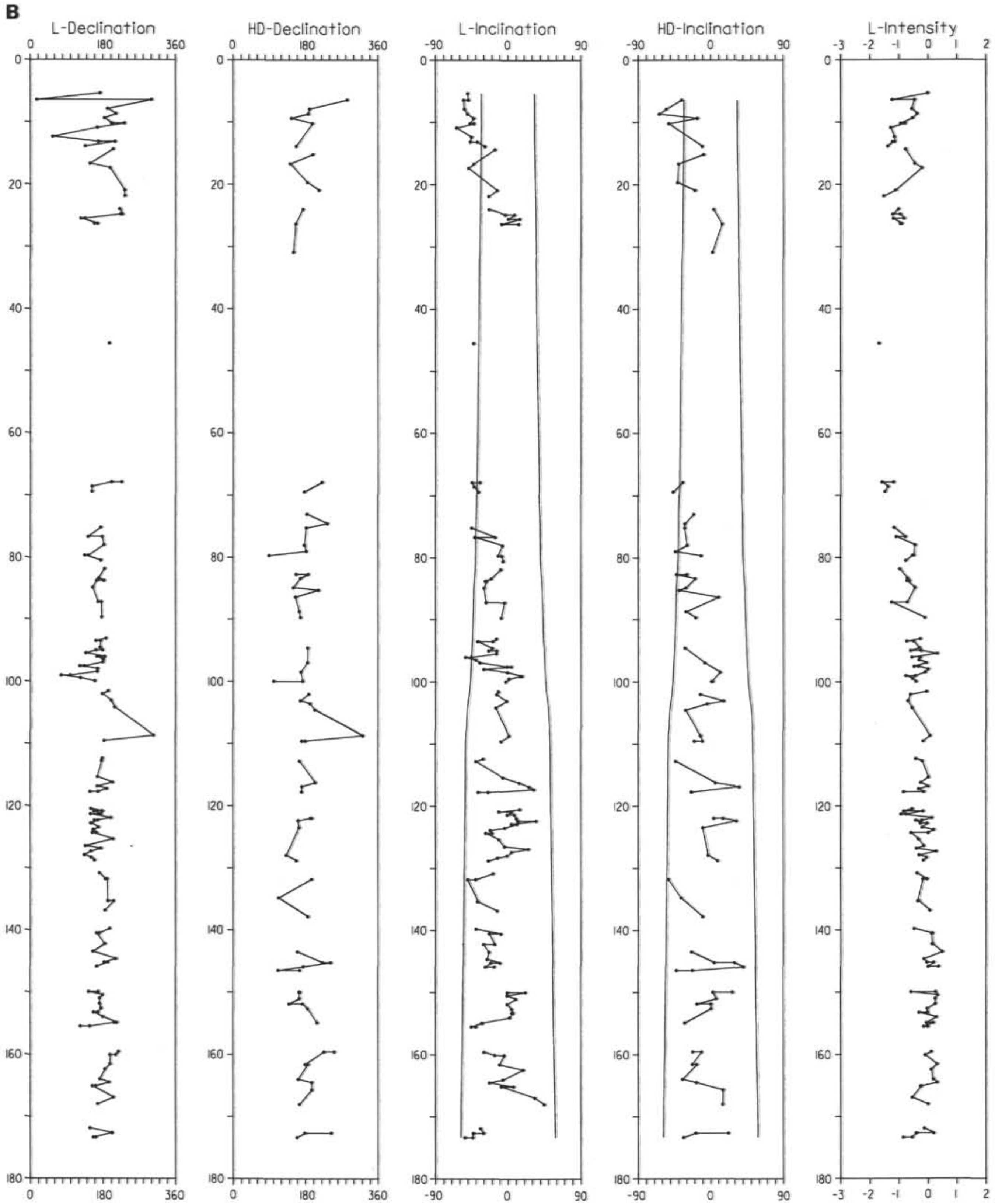

Figure 15 (continued).

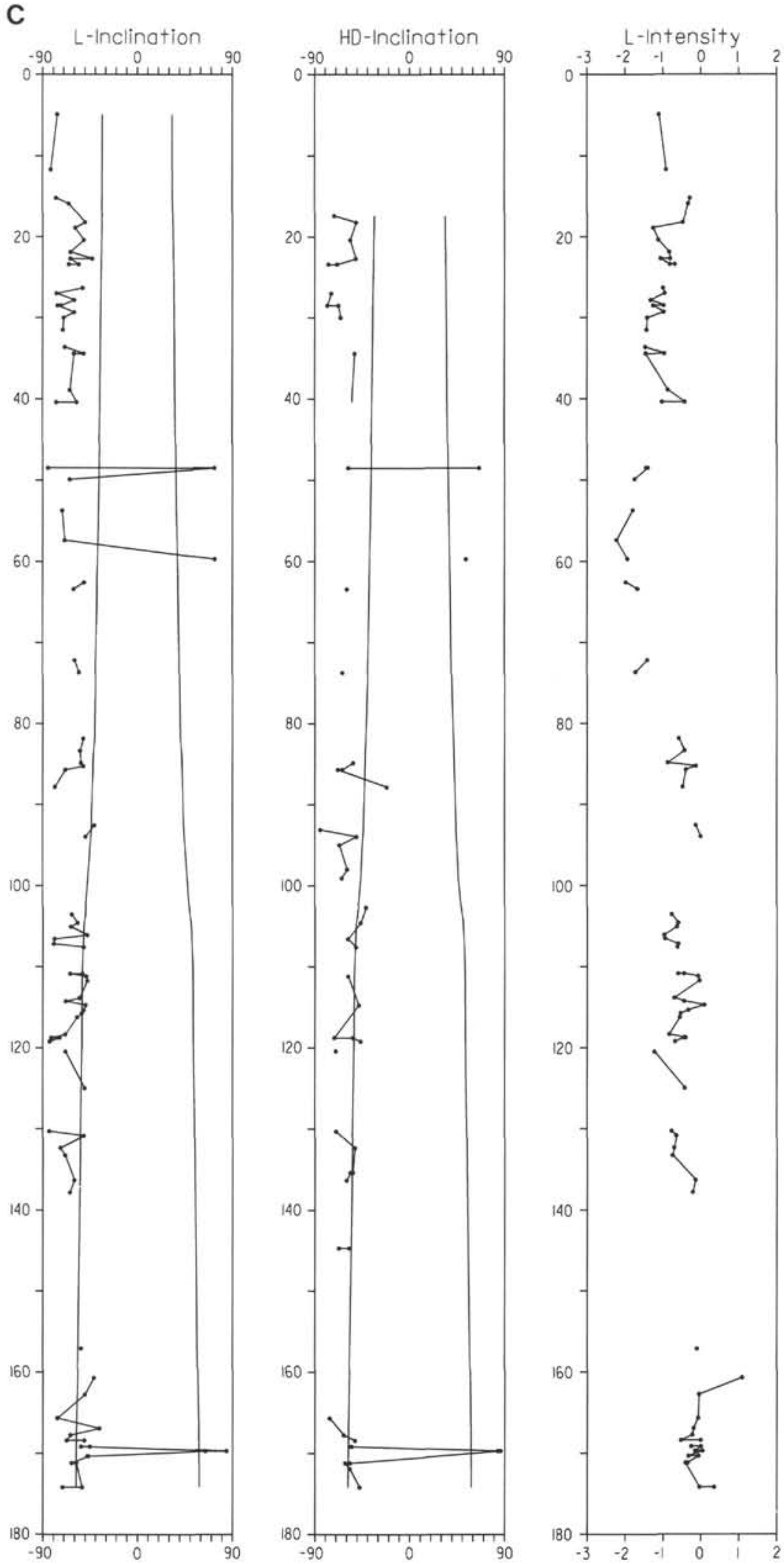

Figure 15 (continued).

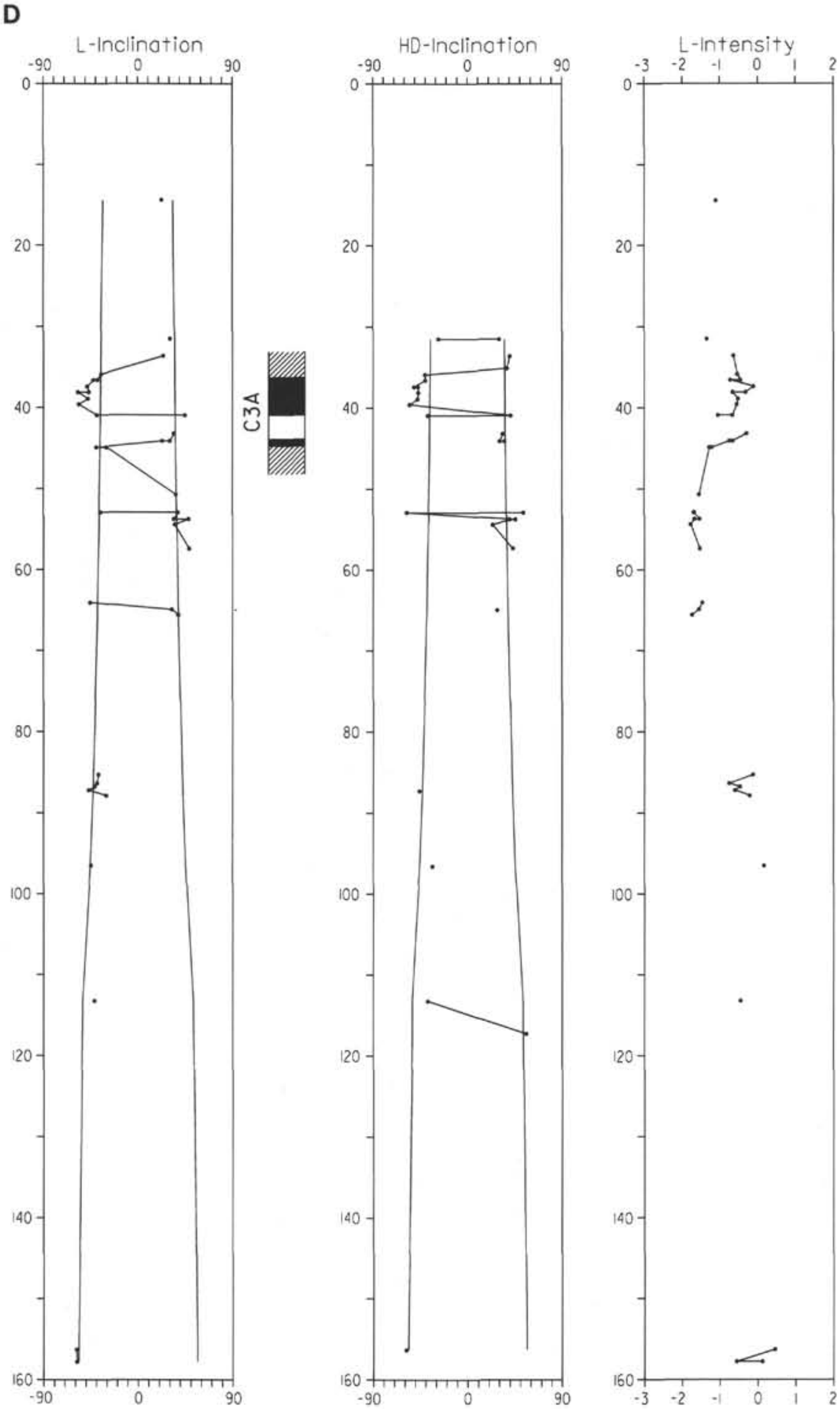

Figure 15 (continued).

field at Site 758, which supports our previous concerns of unidentified present field contaminations in this part of the magnetic record.

Only the breakpoint interval at about 53 Ma may represent a real reduction in the northward movement rate of the Indian plate. Intersection of fitted line segments (Fig. 55, 20–53 and 53–64 Ma) dates this breakpoint more precisely at 55 Ma (combination of the A, B, and C segment intersections in Table 7, whereas the considerably younger [50.4 Ma] intersection of the D segments is considered an outlier), with a reduction in the northward movement rate from about 1.6°–1.8° latitude/m.y. (about 18–19.5 cm/yr; Table 7, mean for segments 5A–5D and 5A–5C, respectively) to 0.4° latitude/m.y (about 4.5 cm/yr; Table 7, mean of 4A–4D). This 55-Ma date has to be taken as a minimal age following the

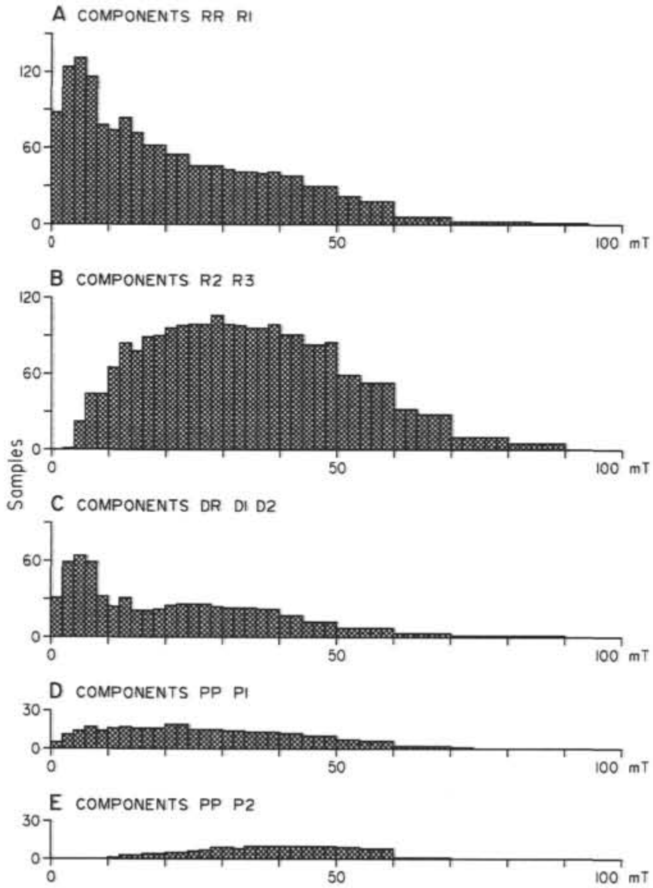

Figure 16. Histograms of stability range distribution upon AF demagnetization for Cores 121-757B-1H to 121-757B-19H (see caption to Fig. 6). **A, B.** "180 degree" overprints RR, R_1, R_2, and R_3. **C.** Drilling-induced overprints DR, D_1, and D_2. **D, E.** Primary components PP, P_1, and P_2.

observation made in the preceding "Generalities" section, and will be referred to as the 55+ Ma breakpoint in the following discussion.

OTHER LINES OF EVIDENCE

Comparison with DSDP, other ODP, and Deccan Traps Data

All DSDP data from the Indian plate (Peirce, 1978; Klootwijk, 1979) and the few other ODP data for Sites 713 and 715 (Vandamme and Courtillot, 1990) were analyzed following similar procedures. All results were transferred to Site 758 (Fig. 56 and Table 6) for compatibility with the Leg 121 data. Peirce's (1978) data from the basement sequence of Site 216 notably agree with the Deccan Traps data (Fig. 56) in showing higher than expected paleolatitudes.

Breakpoint analysis of the data was confined to the interval from 14 to 60 Ma. The Deccan Traps and related data were not included in this analysis, following the observations made in the previous section and in detail in the "Some Problematic Paleomagnetic Data" section on their aberrancy. Using the 55+ Ma breakpoint determined from the Leg 121 data, intersection of the weighted linear regression lines occurs at 53.3 Ma (Table 7). This intersection must be considered inaccurate because of the ill-constrained fit to the pre-55-Ma data, which cover a narrow time range and show a considerable spread in latitude. The date for this intersection may be considered a youngest age. The fitted line in the 14–55-Ma interval shows a paleolatitude about 5° to the north of the expected pattern and also to the north of the paleolatitude pattern determined from the current study of Sites 756, 757, and 758. This more northern than expected paleolatitude pattern seems predominantly based on a few "northern" paleolatitude observations with remarkably low error intervals. The bulk of the data with larger error intervals suggests a more southern paleolatitude during this period, more in line with the Leg 121 results. This would date the reduction in the rate of northward movement somewhat earlier than the 53.3-Ma date obtained. There is thus reasonable agreement between the 55+ Ma date determined from the Leg 121 data and the 53.3+ Ma date determined from all other data.

The Deccan Traps and related DSDP/ODP data span a limited time range at about Cretaceous/Tertiary boundary time but show a considerable spread in latitude. Consequently, there is little control on the slope of the line fitted to these data and its parameters (Table 7, segment 3) must be considered inaccurate.

Comparison with Seafloor-Spreading Data

The 55-Ma (minimal) date for a reduction in the rate of "absolute" northward movement of the Indian plate, based on direct paleolatitude observations, agrees well with the timing of a reduction in the rate of seafloor spreading based on recent interpretations of the magnetic anomaly pattern of the Indian Ocean. Seafloor-spreading interpretations from the Central Indian Ocean anomaly pattern, and also from the southwestern and southern Indian Ocean patterns, generally agree on a spreading-rate reduction at magnetic anomaly 28 (MA28, Patriat and Achache, 1984; MA28, Royer and Sandwell, 1989; MA28, possibly MA27 and MA26, Patriat and Ségoufin, 1988) and at magnetic anomaly 24 (Royer and Sandwell, 1989) or magnetic anomalies 21–23 (Patriat and Achache, 1984; Patriat and Ségoufin, 1988), with MA28 dated at 64.3 Ma, MA24 dated at 56.1 Ma, and MA23 to MA21 dated at 54.7, 52.6, and 50.3 Ma, respectively.

The reduction in the seafloor-spreading rate at 64.3 Ma is not convincingly supported by the paleomagnetically poorly constrained reduction in the rate of northward movement at about that time, as might be concluded from the present (Fig. 55) or earlier data (Fig. 56), which rely heavily on the Deccan Traps results of questionable interpretation (see "Maximum Likelihood Determination of Breakpoints" and "Some Problematic Paleomagnetic Data" sections). The paleomagnetically well-constrained reduction in the rate of northward movement at 55+ Ma agrees closely with at least the seafloor-spreading rate slowdown at MA24 (56.1 Ma). Reductions in the northward movement rate and spreading rate apparently have occurred over a more prolonged period than just at about 55 Ma. This can be concluded from Patriat and coworkers' interpretation for a slowdown at MA23–MA21 and evidence from the moving window gradient analysis (see preceding "Generalities" section) for a further gradual reduction in the northward movement following the 55+ Ma break.

Peirce's (1978) analysis of Ninetyeast Ridge paleomagnetic data argued for a slowdown in India's northward motion at 40 Ma from 14.9 ± 4.5 to 5.2 ± 0.8 cm/yr. The timing and movement rate differ substantially from the Leg 121 conclusion for a slowdown at 55+ Ma from 18–19.5 to 4.5 cm/yr. Peirce pointed out that his data were not well controlled in the crucial 40–55-Ma interval, and his conclusion for the young 40-Ma slowdown seems to depend substantially on a single result from DSDP Site 253 (Cockerham et al., 1975). This result, documented only in abstract form, was transferred via an incorrect procedure to Peirce's common-Site 216. Proper common-site transfer of this single observation and/or restriction of the paleomagnetic analysis to Peirce's own paleomagnetic data (Peirce et al., 1974; Peirce, 1976, 1978) suggests an older timing of the northward movement slowdown, which is more in line with the 55+ Ma slowdown, concluded here from the Leg 121 data.

IMPLICATIONS FOR THE ORIGIN AND EVOLUTION OF NINETYEAST RIDGE

A variety of models for the origin and evolution of Ninetyeast Ridge were proposed over the last decade, mainly based on DSDP results and on seafloor-spreading data. These models explain the geochemical signature of Ninetyeast Ridge basement as a mixture of oceanic island basalt (OIB) and mid-ocean ridge basalt (MORB) sources (Shipboard Scientific Party, 1989c). Ninetyeast Ridge basement ages closely resemble those of the Indian plate to the west; thus, a contributing hot-spot source must have maintained a position close to a spreading ridge. The Antarctic plate has remained in a more or less stationary position and complex ridge-jump models are necessary to assure contiguity of the northward-moving Southeast Indian Ocean Ridge with a mantle-fixed hot spot.

The models proposed involve (1) a fixed Kerguelen hot spot (Duncan, 1978, 1981, this volume; Mahoney et al., 1983; Davies et al., 1989) coupled with ridge jumps (Peirce, 1976, 1978; Royer and Sandwell, 1989) or possibly a slowly, and mainly longitudinally, migrating Kerguelen/Heard (McDonald) hot spot (Royer and Sandwell, 1989; Royer et al., this volume); (2) a leaky transform–spreading ridge junction (Sclater and Fisher, 1974); (3) a combination of both models (Luyendyk and Davies, 1974; Johnson et al., 1976); and (4) a two hot-spot model involving both the Kerguelen-Heard hot spot and the Amsterdam–St. Paul hot spot (Luyendyk and Rennick, 1977).

Peirce's (1978) paleolatitudinal results from basement of DSDP Leg 22 and Leg 26 sites on Ninetyeast Ridge indicated that its volcanic source had remained in an approximately fixed latitudinal position near 50°S, close to the present latitude of the Kerguelėn (50°S)/Heard (53°S) hot spot. Peirce (1978) opted for the first model as the only viable model to explain his observations. The lower ash sequence of Site 757 (about 58.5 Ma) and the lower ash and upper basalt sequence of Site 758 (about 81.9 Ma) likewise indicate an approximate 50°S paleoposition, 49.7°S and 51.1°S, respectively. These paleolatitudes are slightly higher than the well-constrained 46.9°S observed for the Rajmahal Traps, which is not surprising given the expected size of the flood basalts events, but are not significantly different at the 95% confidence level. The overlying ash sequences at both sites (see Figs. 46 and 51 and Table 3) show a gradual northward shift of the Ninetyeast Ridge trail over about 5° of latitude up to 45°S. This paleolatitude pattern strongly supports Peirce's conclusion for a Kerguelen hot spot origin of Ninetyeast Ridge.

The younger basement sequence of Site 756 (about 43.3 Ma), in contrast, indicates a lower paleolatitude of about 43°S. This is, however, not significantly different at the 95% confidence level from the paleolatitudes for Sites 757 and 758 and the Rajmahal Traps. This paleolatitude is also close to the current latitude of the Amsterdam–St. Paul hot spot (38°S–39°S). This paleolatitude, which is lower than expected for a Kerguelen hot spot origin, may be due to an unnoticed tilt of basement. Alternatively, it may represent either a northward shift of the (Kerguelen) hot-spot source associated with the Kerguelen–Broken Ridge breakup prior to a southward rebound to its current position or northward channeling of melts from the Kerguelen hot spot after the site moved off the hot spot. However, the isotope signature of the Site 756 basement shows a distinct affinity to the Amsterdam–St. Paul hot spot (Weiss and Frey, this volume; Saunders et al., this volume). In another alternative view, the about 43°S paleolatitude could be interpreted as a primary, or possible overprint, magnetization caused by this hot spot. Such an overprint was also noted in the basement sequence of Site 758.

IMPLICATIONS FOR THE EVOLUTION OF THE INDIA-ASIA CONVERGENCE

Paleogene Convergence: Paleolatitude Constraints and Speculations

Generalities

The Late Cretaceous and Paleogene latitudinal control on India's northward movement has important implications for the timing of initial India-Asia contact and completion of suturing. We will argue that initial contact was established by Cretaceous/Tertiary boundary time. This bears on topics currently debated in relation to the Cretaceous/Tertiary boundary diastrophism, such as the extrusion of the Deccan Traps and gradual vs. abrupt faunal changes. Following a different approach, the Neogene evolution of the India-Asia convergence zone will be correlated with (and where possible constrained in time) on the basis of the Neogene susceptibility, NRM, and lithostratigraphic profile from Site 758.

Paleolatitudinal control on India's northward movement is shown (Fig. 57) in a series of time steps covering the Late Cretaceous and Tertiary. India's paleopositions for the period 20–65 Ma are based on pole positions (Table 8) derived from line segments fitted to the Leg 121 paleolatitude data and from declinations interpolated from the Morgan/Patriat APWP. Neogene and Late Cretaceous paleopositions are based directly on the Morgan/Patriat pole positions (Table 2). In this reconstruction we assumed no internal deformation of the Indian plate, neglecting possible movements along such zones as the Narmada-Son lineament (see "India-Asia Collision and the Deccan Traps Diastrophism" section) and the equatorial zone of distributed lithospheric deformation.

Greater India is shown in Figures 57 and 58 in its minimal northern extent. Its northwestern outline is extended by 650 km beyond the present-day outline of the Northern Kohistan Suture (NKS). This is based on (1) a minimum of 470 km of crustal shortening south of the Main Mantle Thrust (MMT) estimated from balanced cross sections (Coward, 1983; Coward and Butler, 1985; Butler, 1986; Coward et al., 1987; Butler and Prior, 1988; Coward et al., 1988b; Butler and Coward, 1989) of disputed accuracy (Ramsay, 1988; Butler, 1988; Coward, 1988), (2) a further 130 km of crustal shortening between the MMT and the NKT following estimates of shortening in the Zanskar Range (Searle, 1986; Searle et al., 1988) and the Nanga Parbat–Haramosh Massif (Chamberlain et al., 1989a), and (3) an arbitrary 50 km of initial continental subduction along the NKT (cf. Mattauer, 1986; Searle et al., 1990). Greater India's minimal northern boundary in the Tibetan region is based solely on the magnitude of rotational underthrusting along the Main Central Thrust (MCT), and possibly the Main Northern Thrust (MNT), following the oroclinal bending model (Klootwijk et al., 1985, 1986b). This model postulates minimal magnitudes of underthrusting of 550 km at the longitude of the Krol Belt and 650 km at the longitude of the Thakkhola region.

Date of Initial Contact and Completion of Suturing

The Ninetyeast Ridge paleolatitude data indicate that Greater India's northwestern margin had crossed the equator at approximately 65 Ma (Figs. 57 and 58). This equatorial to very low northern latitude is also recorded by presumably collision-related secondary magnetization components (Table 9), observed both to

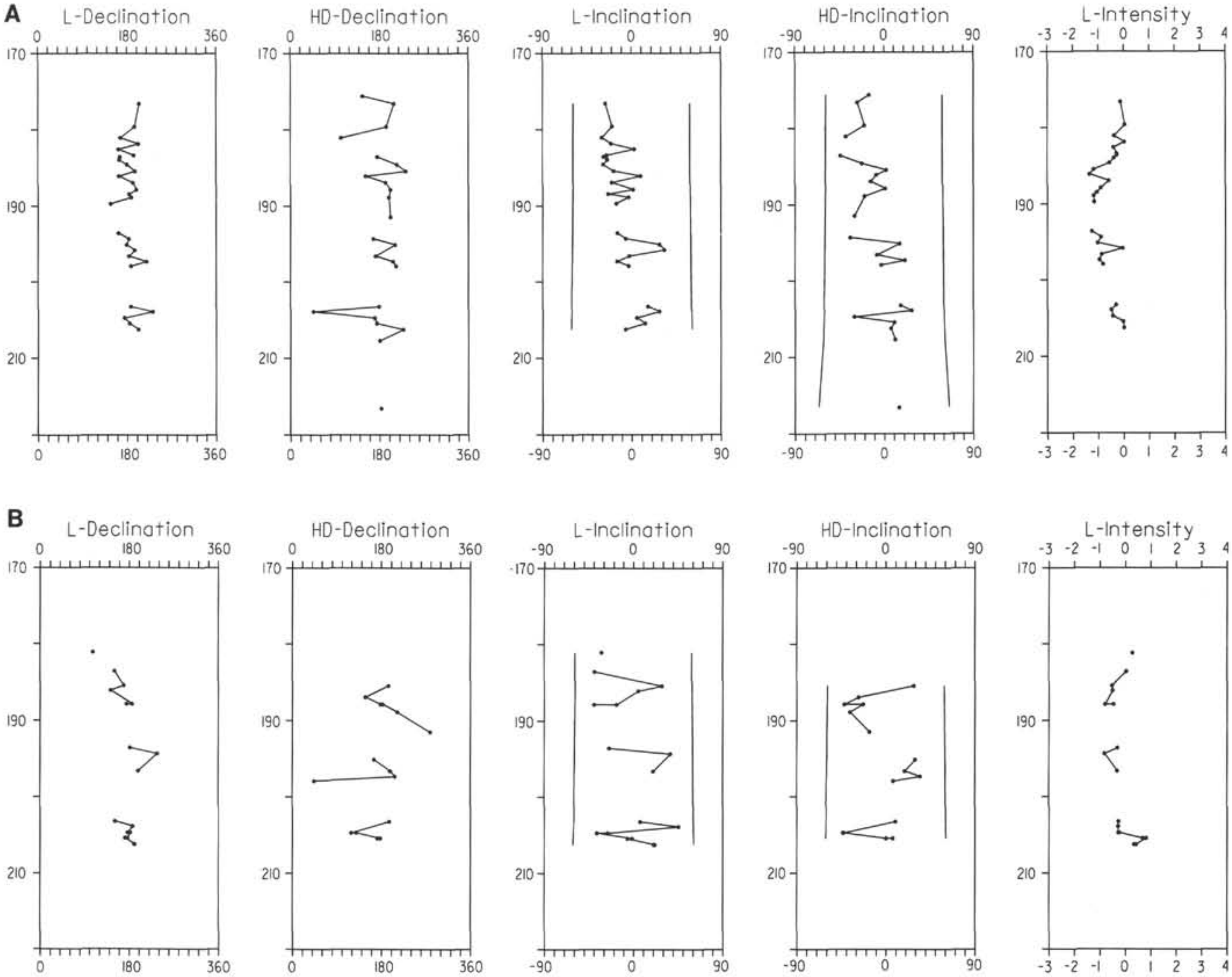

Figure 17. Stratigraphic plots of declination, inclination, and intensity of components determined from linear (L) and planar (HD) PCA of AF (A, B, D) and thermal (C, D, E) demagnetization data for Cores 121-757B-20X to 121-757B-43N (see caption to Fig. 5). **A.** "180 degree" components RR and R_1. **B.** "180 degree" components R_2 and R_3. **C.** Low-inclination components LO, L_1, and L_2. **D.** Drilling-induced components DR, D_1, and D_2. **E.** Primary components PP, P_1, and P_2 with an attempt at magnetostratigraphic interpretation for part of the sequence (see caption to Fig. 8).

the north and to the south of the Northern Kohistan and the Indus-Tsangpo suture zones (e.g., Klootwijk, 1984; Klootwijk et al., 1985, 1986a, 1986b). In the absence of radiometric age control and assuming a collision-related origin, acquisition of these secondary components can be dated only indirectly through comparison of their inclinations/latitudes with paleolatitudinal control on India's northward movement. Acquisition of these secondary components and the initial India-Asia contact have been estimated before at about 60 Ma or slightly earlier (Klootwijk et al., 1985, 1986a, 1986b). The present paleolatitudinal control from Ninetyeast Ridge allows this estimate to be updated. Initial contact was established prior to 65 Ma and probably already at Cretaceous/Tertiary boundary time.

India's reconstructed position at 65 Ma is strongly supported by the remarkable agreement between the expected hot-spot location on the Indian plate at that time and the present latitude of approximately 21°S of the Réunion hot spot. This is demonstrated in Figure 57, which shows the reconstructed 65-Ma position of the Réunion hot spot, both relative to the Indian plate according to Royer et al. (this volume, figs. 9 and 10) with very similar latitudinal positions according to Morgan (1983; see Royer et al., this volume, fig. 8) and Duncan et al. (1989, fig. 2) and also in an absolute frame with the Indian plate positioned according to our paleolatitudinal control from Ninetyeast Ridge (Table 8). Further arguments in support of our paleomagnetically based conclusion for initial India-Asia contact at or before Cretaceous/Tertiary boundary time will be discussed hereafter. These include faunal evidence for a Greater India–southern Asia connection at Cretaceous/Tertiary boundary time, the geologic record of the Zanskar region, and collision-related tectonic disturbances of the Indian shield leading to the Deccan Traps eruptions at about Cretaceous/Tertiary boundary time. Such an early initial contact may have induced the fundamental reorganization of the western Indian Ocean at about 65 Ma (Luyendyk, 1974; Sclater and Fisher, 1974; Norton and Sclater, 1979; Courtillot et al., 1986; Coffin and Royer, in press).

The distinct slowdown of India's northward movement at 55+ Ma is interpreted as completion of suturing, which was initiated

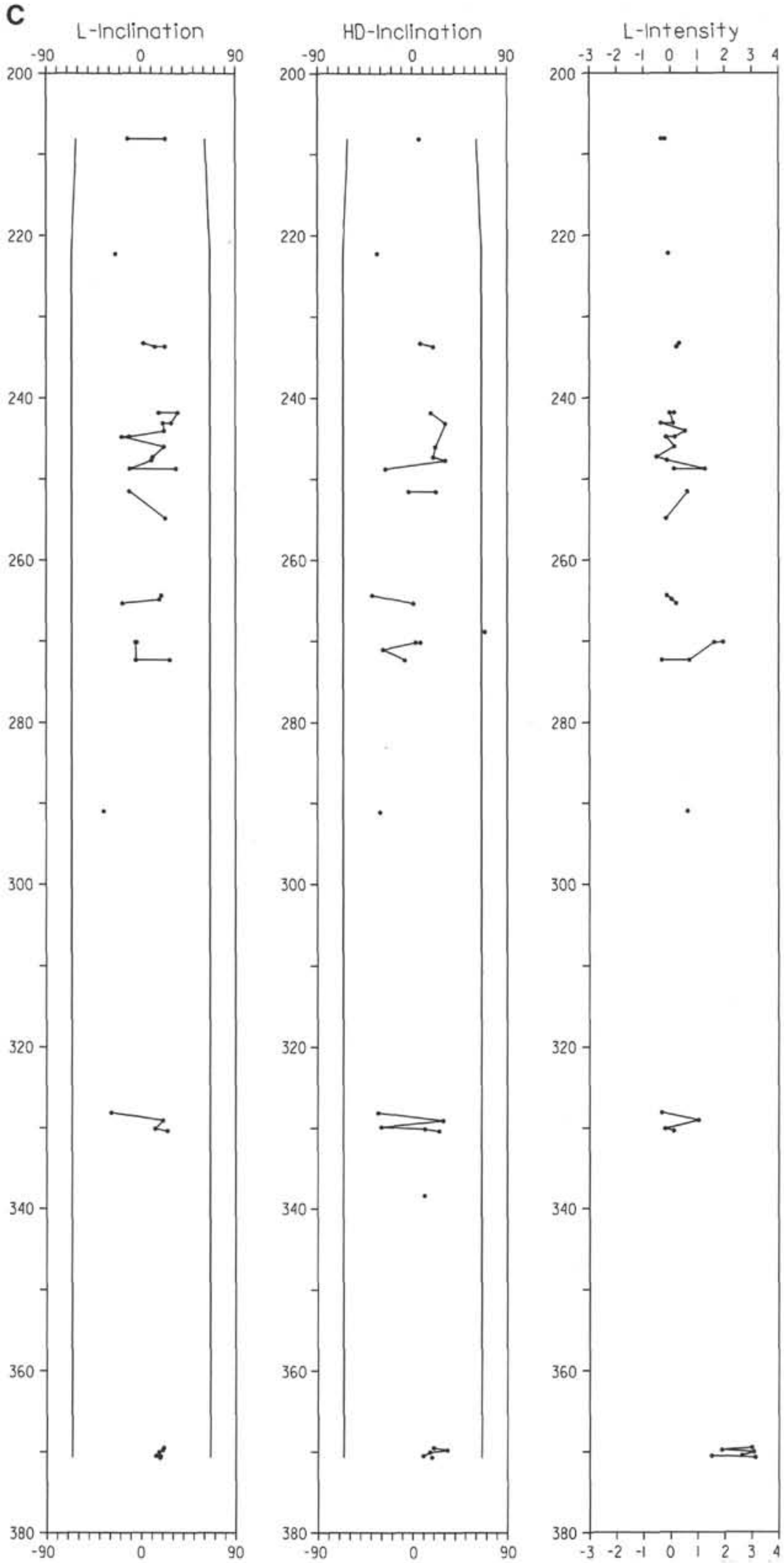

Figure 17 (continued).

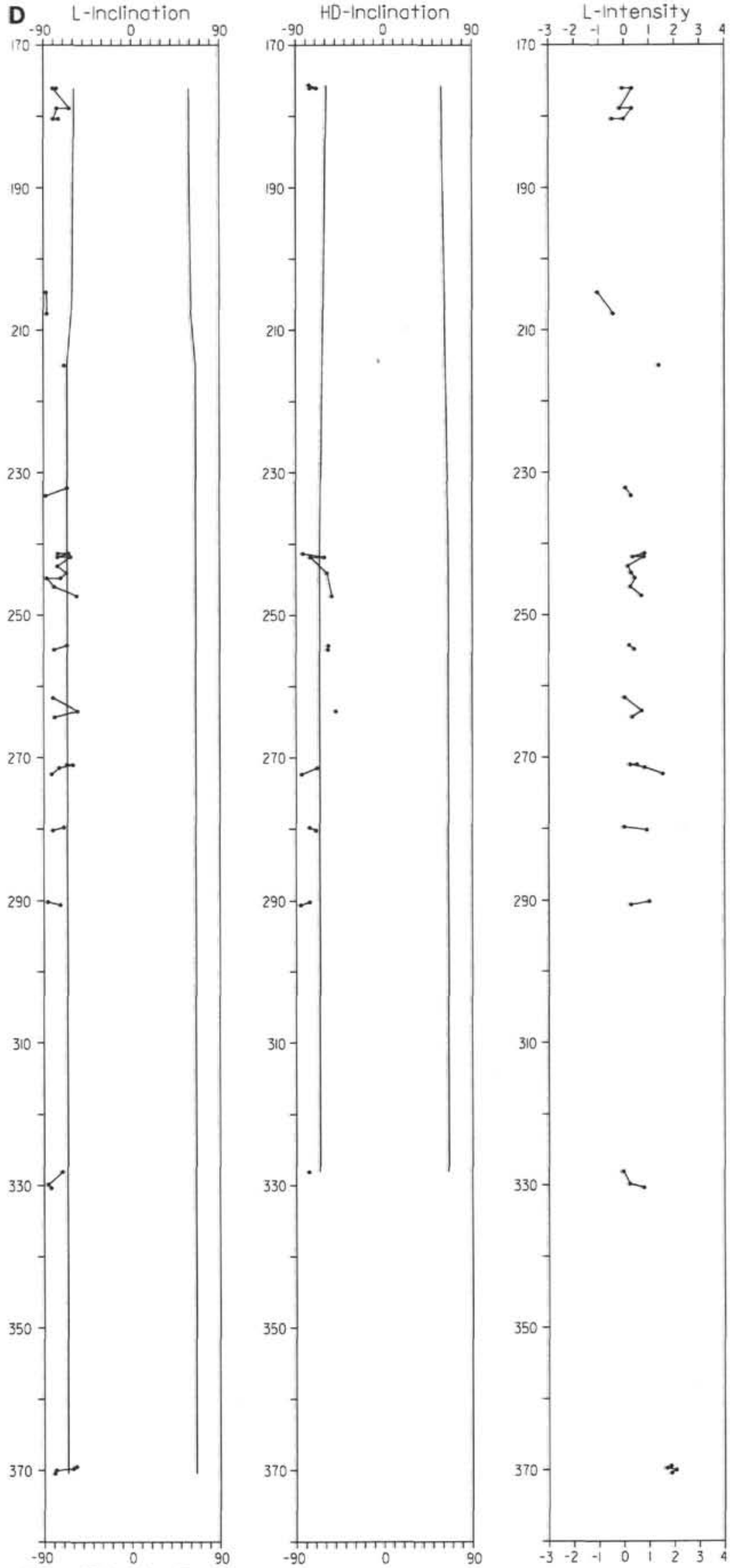

Figure 17 (continued).

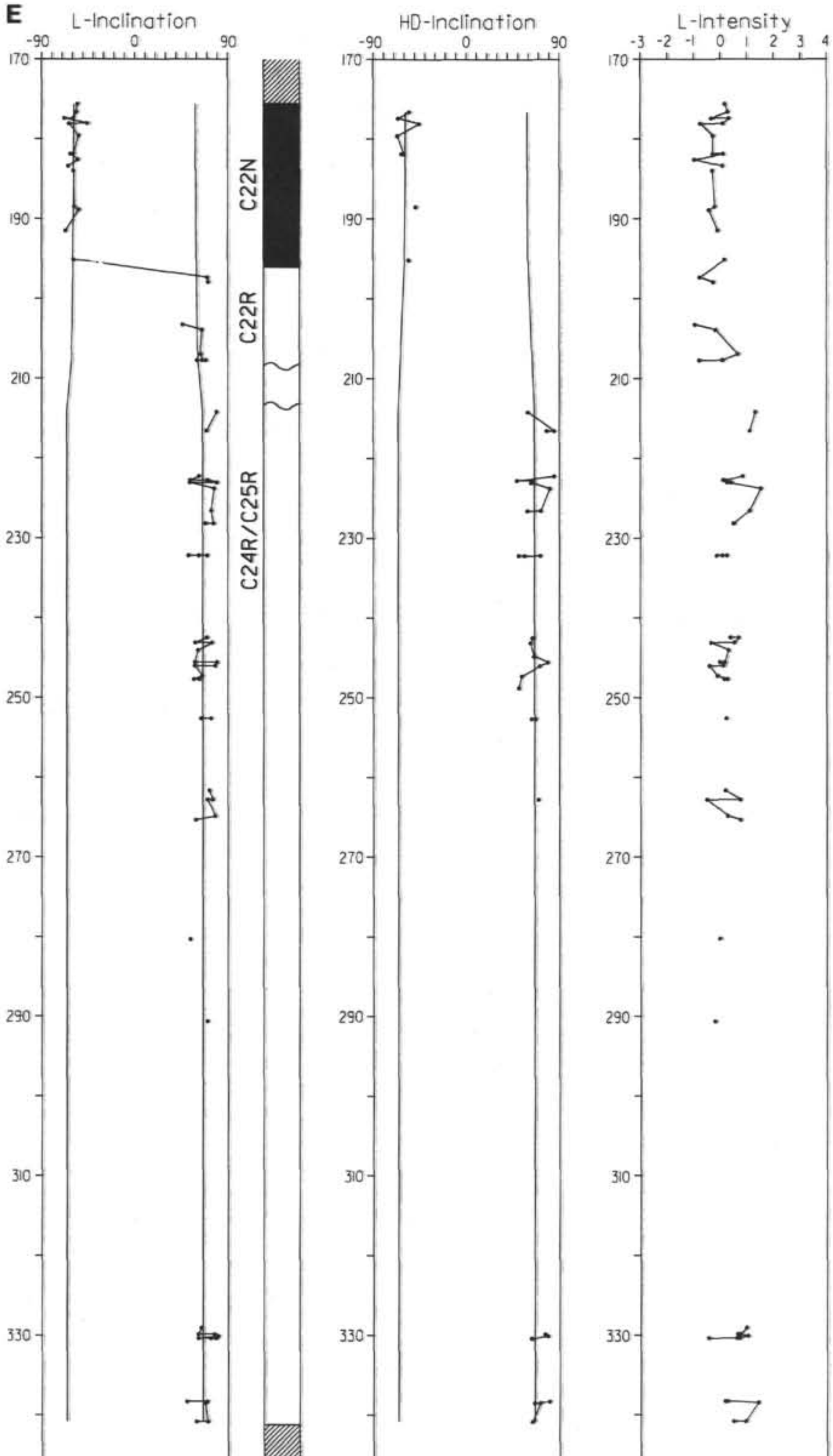

Figure 17 (continued).

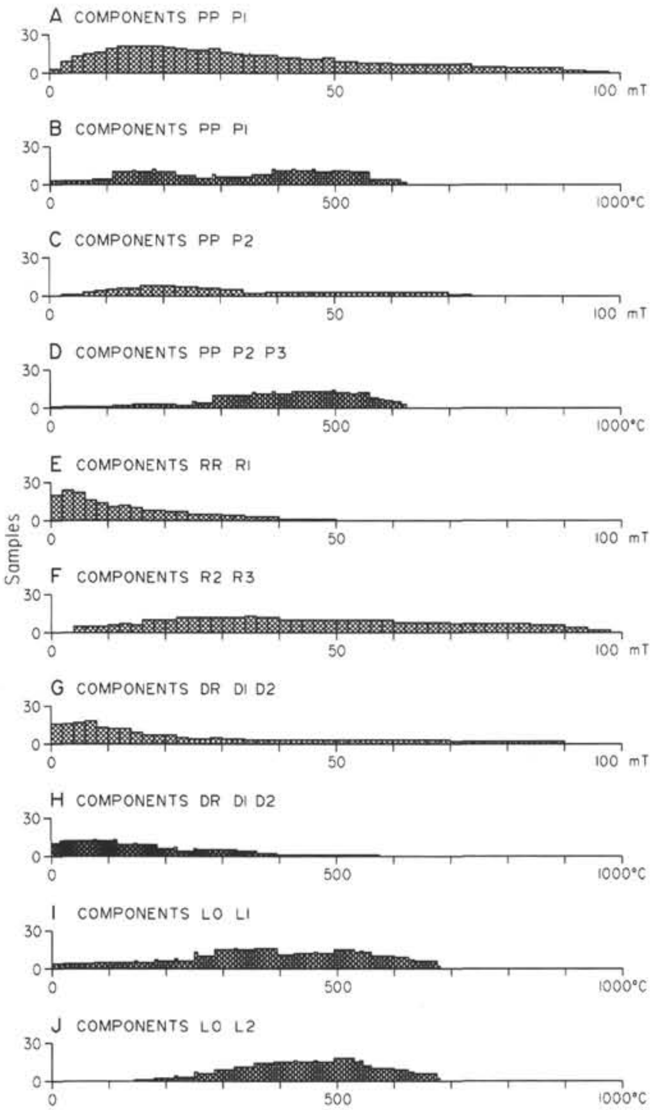

Figure 18. Histograms of stability range distribution upon AF and thermal demagnetization for Cores 121-757B-20X to 121-757B-43N (see captions to Figs. 6 and 9). **A–D.** Primary magnetization components PP, P_1, P_2, and P_3. **E, F.** "180 degree" overprints RR, R_1, R_2, and R_3. **G, H.** Drilling-induced overprints DR, D_1, and D_2. **I, J.** Low-inclination components LO, L_1, and L_2.

in the west and propagated eastward (Powell and Conaghan, 1975; Powell, 1979; Klootwijk et al., 1985). This suturing/slowdown agrees in timing with

1. The temporary loss of the counterclockwise rotational component in India's northward movement. This is clearly demonstrated by the two curved segments of the Morgan/Patriat Indian APWP (Klootwijk et al., 1985; Fig. 60A). Their intersection at about 56–58 Ma is interpreted to represent completion of the India-Asia suturing process.

2. A sedimentary hiatus at about the Eocene/Paleocene time boundary, widely observed in the northeastern Indian Ocean (Curray and Moore, 1971, 1974; Moore et al., 1974; Pimm and Sclater, 1974; Pimm et al., 1974; Curray et al., 1982; Curray and Munasinghe, 1989). Leg 121 data show a similar hiatus covering the lowermost Eocene at Site 757 (Shipboard Scientific Party, 1989h, fig. 4). The early Oligocene to late Paleocene hiatus at Site 758 (Shipboard Scientific Party, 1989i, figs. 5 and 10) is of too wide an age range (about 20 m.y.) to constrain the time of suturing any further.

3. End of spreading in the Tasman and Coral Sea (Weissel and Hayes, 1977; Weissel and Watts, 1979; Veevers, 1984).

4. A marked change in the spreading direction of the Southwest Indian Ocean Ridge and reappearance of magnetic lineations along the Southeastern Indian Ocean Ridge (i.e., magnetic anomaly 24; Patriat and Ségoufin, 1988; Royer et al., 1988).

5. A major climatic change near the Paleocene/Eocene time boundary indicated by a change in deep-sea benthic foraminifers from approximately 61 to approximately 55 Ma (Miller et al., 1987).

Some Problematic Paleomagnetic Data

Two major paleomagnetic data sets do not seem to support an early India-Asia contact at Cretaceous/Tertiary boundary time and were previously interpreted in terms of a latest Paleocene-Eocene initial contact. The data sets come from both sides of the India-Asia convergence zone, the Albian to Cenomanian Takena Formation and the Paleocene Lingzizong Formation (^{40}Ar-^{39}Ar age of 60 Ma; Maluski et al., 1982) of southern Tibet and the Deccan Traps (^{40}Ar-^{39}Ar age of 66.4–68.5 Ma, Duncan and Pyle, 1988a, 1988b; 65–69 Ma, Courtillot et al., 1988; Vandamme et al., in press) of central India.

The southern Tibetan formations have been studied by various groups (Zhu Xian Gyuan et al., 1977; Zhu Zhi Wen et al., 1981; Pozzi et al., 1982; Westphal et al., 1983; Westphal and Pozzi, 1983; Achache et al., 1984; Zhu Zhi Wen and Teng Jiwen, 1984; Lin Jinlu and Watts, 1988a, 1988b) and give a considerable range in paleolatitudes (6°N to 20°N). A stationary Late Cretaceous to early Tertiary paleoposition of southern Tibet at about 13°N has been strongly supported by a positive fold test for part of the Takena Formation data (Achache et al., 1984). The interpretations of Achache et al. were followed by various French groups in recent geodynamic models for the India-Asia convergence. If correct, such data would argue against an initial contact at about Cretaceous/Tertiary boundary time. Klootwijk et al. (1986a) pointed out, however, the discrepancy between these Tibetan data and the collision-related overprints and suggested that the Tibetan data represent middle Tertiary overprints similar to another set of overprints observed in the wider Himalayan region. This view is supported by Besse and Courtillot's (1988) more recent observation that Achache et al.'s paleoposition for southern Tibet disagrees also with a newly determined Eurasian APWP. This APWP suggests a paleoposition some 10° farther south, which would remove the discrepancy with the collision-related overprints. Clearly, the higher paleolatitude data from the Takena and Lingzizong Formations have to be treated with some caution and may not be truly representative of southern Tibet's paleoposition.

More problematic is India's far southern paleoposition according to the Deccan Traps data (Bombay [arbitrary location, not necessarily related to the hot spot] at ~27°S, Besse and Courtillot, 1988; at ~29°S, Vandamme et al., in press; at 32°S to 33°S, Klootwijk, 1979). It has been strongly argued that these flood basalts were extruded in a relatively short time span of less than 1 m.y. around Cretaceous/Tertiary boundary time (Courtillot et al., 1986, 1988; Baksi, 1987, 1989; Baksi and Kunk, 1988; Duncan and Pyle, 1988a, 1988b; Acton and Gordon, 1989; Jaeger et al., 1989; Gallet et al., 1989; Besse et al., 1989; Vandamme et al., in press), with the bulk of the data covering a lower reversed (C29R) and an upper normal (C29N) polarity interval. The Deccan Traps have been studied widely by a number of different groups and a large paleomagnetic data set is available. By virtue of the size of the data set one would expect the mean Deccan Traps

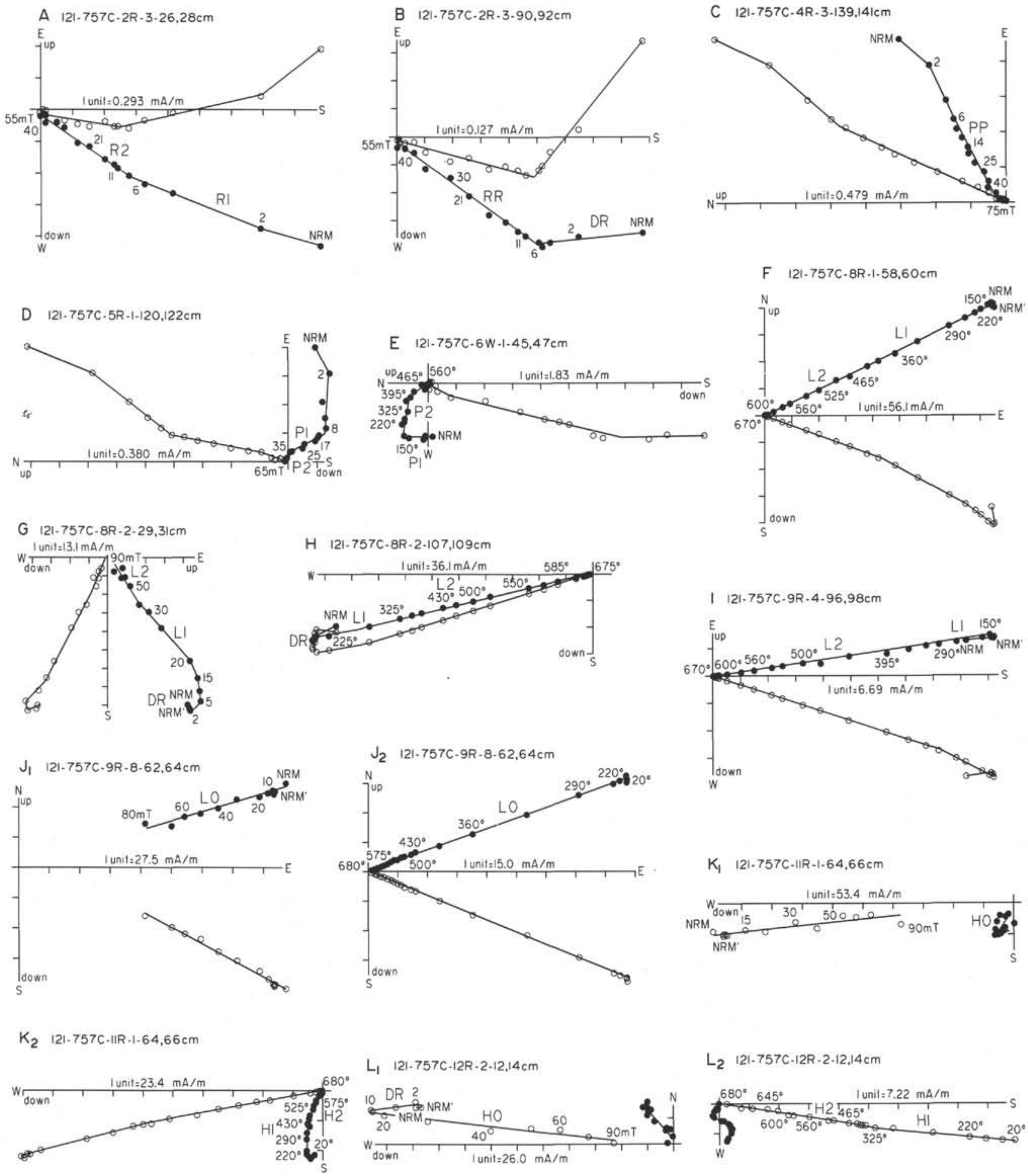

Figure 19. Zijderveld (1967) diagrams of representative samples from Hole 757C during AF and thermal demagnetization (see captions to Figs. 3 and 13). HO, H_1, H_2 = high-inclination components.

paleopole to represent a reliable estimate of the then-ambient geomagnetic field. The data show, however, large and erratic directional variations throughout the flow sequence, and a streaking toward present-day field directions has been observed (Klootwijk, 1979; Vandamme et al., in press). Paleomagnetic analysis of the Deccan Traps results has either tended to counteract the surmised effect of this present-field streaking, particularly prevalent in the main reversed polarity sequence, through mode-type analysis (paleolatitude of Bombay at approximately 32°S–33°S, Klootwijk, 1979; Bombay at 29°S, Vandamme et al., in press) or

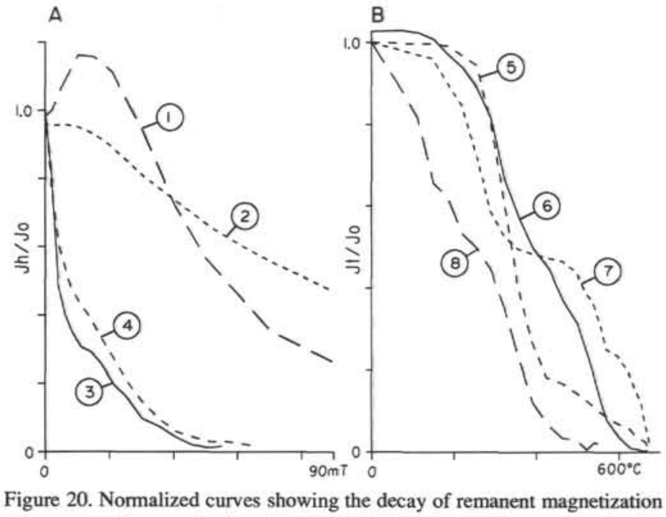

Figure 20. Normalized curves showing the decay of remanent magnetization of representative samples from Hole 757C. **A.** During AF demagnetization. **B.** During thermal demagnetization. 1, 7 = Sample 121-757C-12R-2, 12–14 cm; 2, 5 = Sample 121-757C-9R-8, 62–64 cm; 3 = Sample 121-757C-2R-3, 26–28 cm; 4 = Sample 121-757C-5R-1, 120–122 cm; 6 = Sample 121-757C-8R-1, 58–60 cm; 8 = Sample 121-757C-6W-1, 45–47 cm.

has attempted to identify secular variation effects and observational errors (Bombay at 27°S, Courtillot et al., 1986, 1987; Besse and Courtillot, 1988; Besse et al., 1989).

Such southern paleolatitudes, as exemplified by the 27°S–33°S paleolatitude estimates for Bombay (Fig. 57B), differ substantially from the current location (21°S) of the Réunion hot spot, generally thought to be the feeder for the large-scale extrusions. Besse and Courtillot (1988) and Courtillot et al. (1986) have tried to reconcile this discrepancy with a correction for alleged true polar wander (Courtillot and Besse, 1987). In doing so, it appears, however, that they have incongruously corrected the paleoposition of the Réunion hot spot rather than the Indian plate. The present paleolatitude observations from Ninetyeast Ridge do not show evidence for the systematic deviation between paleomagnetic- and hot-spot-based paleolatitudes, expected from this polar wander model (Fig. 59). This may challenge the validity of Besse and Courtillot's true polar wander correction.

Although systematic discrepancies between observed and expected paleolatitudes are not evident over the 85-m.y. interval covered by the three Ninetyeast Ridge sites, the Deccan Traps paleolatitude observations are higher than the expected paleolatitude (Figs. 52, 57B, and 59) at the time of extrusion (mean ^{40}Ar-^{39}Ar age at about 67.5 Ma: 65–69 Ma, Courtillot et al., 1988; 66.4–68.5 Ma, Duncan and Pyle, 1988a, 1988b). Vandamme et al.'s (in press) data (Fig. 57B and Table 6) indicate a smaller, but substantial, discrepancy than shown by Klootwijk's (1979) data (Figs. 52 and 59). Possible sources for this discrepancy may include (1) a slightly older age than the preferred mean age at 67.4 ± 0.7 Ma (Duncan and Pyle, 1988a, 1988b), with the start of volcanism to be correlated with the steep lower onsets in the K-Ar (70 Ma) and Ar-Ar (69 Ma) age histograms shown by Vandamme et al. (in press, figs. 4 and 5; and with the lower reversed polarity interval [R1, Table 6], perhaps, to be correlated with Chron C31R [Wensink et al., 1979; Wensink, 1987; Courtillot et al., 1987; Stoddard and Jurdy, 1988, 1989]), (2) errors in the determination of the expected paleolatitude, (3) neglect of dip corrections (up to 5° in the Western Ghats) (however, as the predominant flexure axis of the Western Ghats is almost parallel to the mean declination of the Deccan Traps, such a dip correction would have only limited effect on the inclination and thus the paleolatitude; D. Vandamme, pers. comm., 1990), (4) persistent nondipole fields (Acton and Gordon, 1989; Schneider and Kent, 1990b), and (5) more local geomagnetic anomalies at the time of the Deccan Traps eruptions. The good agreement between Peirce's (1978) Site 216 data from Ninetyeast Ridge and the Deccan Traps data (Figs. 56 and 59B) suggests that any geomagnetic anomalies must have been of regional rather than local extent. Whatever the cause for this discrepancy, the far southern paleolatitude of India, as implied by the Deccan Traps data, may not necessarily be a correct representation of India's position *at Cretaceous/Tertiary boundary time*, and should be treated with some caution.

With neglect of the preceding options 2–5, the paleolatitude discrepancy could be solved in assuming a slightly older age for the Deccan Traps at about 70 Ma. This is based on (1) the latitudinal distance (Fig. 57B) between Bombay's position expected at 65 Ma following our Ninetyeast Ridge data and expected according to the Deccan Traps data and (2) backward extrapolation beyond 65 Ma of the fast northward movement rate concluded from our Ninetyeast Ridge data. Such a slightly older age for the Deccan Traps is supported by modeling of the Réunion hot-spot track on the Indian plate. Various reconstructions (Morgan, 1983 [fig. 8 in Royer et al., this volume]; Duncan et al., 1989, fig. 2; Royer et al., this volume, figs. 9 and 10) agree in predicting the 70-Ma position of the hot spot in the vicinity of the Cambay graben and Narmada-Son lineament intersection (Fig. 57B). It is argued hereafter ("India-Asia Collision and the Deccan Traps Diastrophism" section) that the main Deccan Traps flows most likely extruded from this region.

Paleontological arguments against such a slightly older age and in particular against a correlation of the Deccan Traps lower reversed polarity interval (R1) with Chron 31R rather than with Chron 29R are not as conclusive as argued for by Jaeger et al. (1989). These arguments are mainly based on interpretation of data from the Narsapur well on India's eastern coast. This well penetrates three thin trap flows overlying marine Maestrichtian strata belonging to the *Abathomphalus mayaroensis* Zone, which is correlated with Chron 31N. Jaeger et al. concluded that the lower reversed polarity interval (R1), therefore, cannot correspond to Chron 31R. This conclusion is debatable. The relation of the Narsapur trap flows to the main Deccan Traps sequence (N1-R1-N2) is not established in their paper, and the magnetic polarity of the flows is not detailed. A possible correspondence of the Narsarpur trap flows with the upper N1 sequence of the Deccan Traps would allow a correlation of the underlying R1 sequence with Chron 31R.

Faunal Evidence for an India-Asia Connection at Cretaceous/Tertiary Boundary Time

Recent paleontological studies on Intertrappean Beds (Sahni et al., 1982, 1985; Prasad and Sahni, 1988; Rage, 1988; Jaeger et al., 1989; Sahni, 1989; Jaeger and Rage, 1990) have indicated the presence of a microvertebrate fauna with distinct Laurasian affinities, although African affinities have also been suggested (Thewissen, 1990). In particular, pelobatid frogs in the Intertrappean Beds of the Takli Formation at Nagpur and paleoryctic mammals in the Intertrappean Beds of Asifabad (Naskal Intertrappeans) indicate faunal exchange between India and Laurasia. The Intertrappean Beds occur within reversed polarity Deccan Traps sequences, which have been correlated with Chron C29R, which includes the Cretaceous/Tertiary boundary. Such a faunal exchange at Cretaceous/Tertiary boundary time strongly supports our paleomagnetic arguments that India-Asia contact was established at or before Cretaceous/Tertiary boundary time. Absence of Laurasian affinities in the Dinosaur fauna of the Maestrichtian

Lameta beds, which underlie the Deccan Traps, may constrain initial contact to the late Maestrichtian (Buffetaut, 1990; Jaeger and Rage, 1990).

Jaeger et al. (1989) defended their hypothesis of an early initial contact with a paleogeographic reconstruction that figures a greatly enlarged northern extent of Greater India (Powell and Conaghan, 1973; Veevers et al., 1975; Klootwijk et al., 1985; Powell et al., 1988). Paleopositions of Greater India and southern Asia (Jaeger et al., 1989, fig. 3) are very similar to the reconstruction (Fig. 57B) reached on the basis of our paleolatitude control from Ninetyeast Ridge and the equatorial overprints in the India-Asia convergence zone of presumed collision-related origin. Though not expressed explicitly in their paper, it is clear from their reconstruction that Jaeger et al. no longer regarded the Takena and Lingzizong Formation results to accurately reflect the paleoposition of southern Tibet, nor for the Deccan Traps result to accurately reflect India's paleoposition at Cretaceous/Tertiary boundary time.

Geological Record of the Convergence Zone

The evolution of the India-Asia convergence has left its imprint, no doubt, on the geological record of the wider Himalayan region. Whether this record reflects the collision and suturing in the form of erosional unconformity and/or greater sedimentation phase(s) may vary from region to region. The lithostratigraphic and tectonic record of the wider Himalayan region has been interpreted by various authors (e.g., Powell and Conaghan, 1973) as supporting an initial collision at about 55 Ma, the hitherto generally accepted date. Reinterpretation of the geological record of the convergence zone in terms of an initial contact at Cretaceous/Tertiary boundary time is beyond the scope of this paper. Nevertheless, we highlight several (admittedly select) observations that might be interpreted in support of such an early contact.

The Late Cretaceous to early Tertiary sedimentary record of the Zanskar region (Northwestern Himalaya) shows major breaks at the Cretaceous/Tertiary boundary and in the early Eocene (Nicora et al., 1987; Garzanti et al., 1987). The early Eocene erosional unconformity (quoted at about 54 Ma), which coincides in time with the hiatus observed on Ninetyeast Ridge, was interpreted by the authors as a reflection of initial India-Asia contact. Alternatively, this young erosional unconformity may be interpreted to represent completion of suturing. The older erosional unconformity of Cretaceous/Tertiary boundary age, evidenced by erosion of the uppermost Cretaceous Marpo Limestone and deposition of the Stumpata Quartzarenite, was interpreted as a reflection of a lowstand (Vail et al., 1977) at Cretaceous/Tertiary boundary time. It seems more reasonable now to interpret this sedimentary break, which is also evident in the Himalayan foothills of northwestern Pakistan (Yeats and Hussain, 1987; Gee, 1989), as a reflection of initial contact of northwestern Greater India and southern Asia at about Cretaceous/Tertiary boundary time. Such an early contact may have induced a Late Cretaceous to Paleocene phase of south-verging thrusting onto northwestern India (Searle, 1986, 1988; Searle et al., 1987, 1988, 1990) and a metamorphic phase at about 67 Ma in the internal zones of the Western Himalayan Syntaxis (Treloar and Rex, 1990). A further thermal event at about 50 Ma, observed in the same region (Treloar and Rex, 1990) and also in the Gangdese belt of Southern Tibet (Debon et al., 1985), may be related to completion of suturing.

Evidence for tectonic deformation of southern Tibet prior to extrusion of the Paleocene Lingzizong Formation (Tapponnier et al., 1981; Burg et al., 1983; Burg and Chen, 1984; Chang Chen-fa et al., 1986, 1989; Coward et al., 1988b) and emplacement of a tectonic melange (Yamdrock Melange) with exotic fragments no younger than Campanian-Maastrichtian to possibly Danian (Tapponnier et al., 1981; Burg and Chen, 1984; Burg et al., 1984b; Allègre et al., 1984; Searle, 1986, 1988; Searle et al., 1987) likewise can be interpreted in support of initial contact at about Cretaceous/Tertiary boundary time.

India-Asia Collision and the Deccan Traps Diastrophism

A causal relationship between these two events has been argued repeatedly throughout Indian geological literature but has not been substantiated so far on geodynamic grounds. The evolution of the India-Asia convergence documented here suggests that the two events coincided. In what may amount to a recycling of earlier hypotheses, we propose that stresses originating from the initial India-Asia contact in northwestern Greater India led to deformation of the Indian shield along two preexisting major fault systems; that is, the east-northeast–west-southwest trending Narmada-Son/Tapti system (Swaminath et al., 1964; Choubey, 1971; Naqvi et al., 1974; Mishra, 1977; Crawford, 1978; Murthy and Mishra, 1981; Powar, 1981; Das and Patel, 1984; Kaila et al., 1985, 1989; Mahoney, 1988) and the north-northwest–south-southeast system bounding India's west coast and the Western Ghats, which continues into the Cambay graben and into Rajasthan (Biswas and Deshpande, 1973; Ramanathan, 1981; Biswas, 1982, 1987, 1988; Mahoney, 1988). These two deep-reaching fault systems intersect in the Cambay region, the northwestern part of the present-day Deccan Traps outcrop.

Decompression, triggered by collision-initiated movements along these preexisting zones of weakness, probably led to rapid partial melting in a wide sublithospheric region, underplated (Cox, 1980) by the incipient Réunion hot spot (Duncan, 1978, 1981; Morgan, 1981; Duncan et al., 1989; Shipboard Scientific Party, 1988a). The underplated region may have been up to 2000 km in diameter (Cox, 1989; White and McKenzie, 1989; Richards et al., 1989; Griffiths and Campbell, 1990; Campbell and Griffiths, 1990), and the region of flood basalt eruption may have been controlled by the fault zones and far off the actual hot-spot channel. Such an offset may explain the discrepancy between the current 21°S position of the Réunion hot spot and the alleged more southern paleoposition of the wider region of eruption, without appealing to regional geomagnetic anomalies (see "Some Problematic Paleomagnetic Data" section).

In an alternative view, the Deccan Traps extrusion has been related to progressive southward (relative) migration of the volcanic source as India drifted northward over the Réunion hot spot (Beane et al., 1986; Devey and Lightfood, 1986; Mitchell and Cox, 1988; Watts and Cox, 1989; Hooper, 1990), rather than to the fundamental fault systems. Arguments in support of this alternative view appear circumstantial and depend largely on current rather than original outcrop boundaries of successive flow units, with the actual feeder channels not identified. This hot-spot hypothesis is contradicted by various observations other than the paleolatitude discrepancy discussed previously, such as the presence of dike swarms along the Narmada and Tapti Valley (Powar, 1981; Misra, 1981; Deshmukh and Sehgal, 1988) and the west coast, the coincidence of the maximum thickness of the Deccan Traps pile with the east-northeast–west-southwest–trending Narmada-Son/Tapti fault system and the north-northwest–south-southeast–trending coastal fault system (Kaila, 1988), and the occurrence of late-stage acidic and alkalic volcanic centers in the northwestern Deccan Traps region (e.g., Mt. Pavagarh, Mt. Girnar: Verma and Mital, 1972, 1974; Bose, 1980; Misra, 1981; De, 1981; Srivastava, 1983; Mahoney, 1988) rather than in the southern Deccan Traps region.

Arguments for longstanding magmatic activity along the Narmada-Son lineament (e.g., Athavale and Verma, 1970; Saxena, 1986) likewise fail to support the hot-spot hypothesis. In a previous paper, one of us (Klootwijk, 1974) argued against Athavale

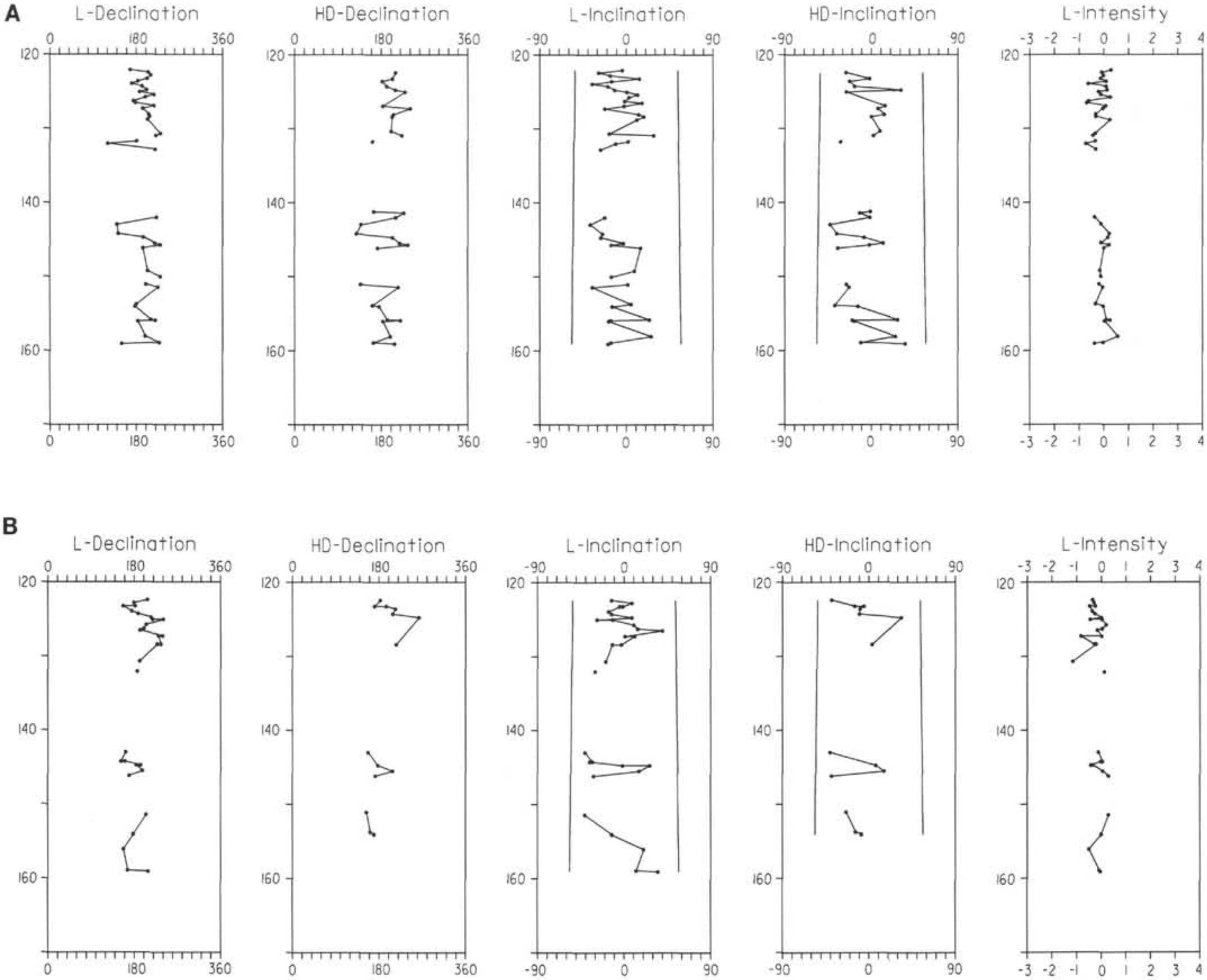

Figure 21. Stratigraphic plots of declination, inclination, and intensity of components determined from linear (L) and planar (HD) PCA of AF (A–D) and thermal (D) demagnetization data for Cores 121-757C-2R to 121-757C-6W (see caption to Fig. 5). **A.** "180 degree" components RR and R_1. **B.** "180 degree" components R_2 and R_3. **C.** Drilling-induced component DR. **D.** Primary components PP, P_1, P_2, and P_3 with an attempt at magnetostratigraphic interpretation for part of the sequence (see caption to Fig. 8).

and Verma's hypothesis on the basis that migration of volcanic activity from the Early Cretaceous Rajmahal Traps (116 Ma; Baksi, 1986, 1987; Baksi et al., 1987) to the Cretaceous/Tertiary boundary Deccan Traps does not agree with a single mantle-fixed hot spot. Reexamination of paleomagnetic data from the Deccan Traps, Rajmahal Traps, and dikes and sills from the intervening Narmada-Son region, however, suggests that a shift in the locus of magmatic activity from east to west may have occurred, with the Narmada-Son fault zone serving as a pathway for easy extrusion of magma (Mahoney, 1988).

Paleomagnetic pole positions from the Gondwana dike and sills (Athavale and Verma, 1970), admittedly not corrected for tectonic deformation, if any, and from the basal normal polarity zone (N2) of the Deccan Traps (Klootwijk, 1979; Vandamme et al., in press), streak between the main Deccan Traps and the Rajmahal Traps pole positions (Fig. 60F and Tables 10 and 11). Some of the basal normal polarity (N2) pole positions (e.g., the Pohor sequence: Wensink, 1973; Wensink et al., 1979) virtually coincide with the Rajmahal Traps poles. This may be purely coincidental, because of the large directional variability of the Deccan Traps results and radiometric control for a Deccan Traps rather than a Rajmahal Traps age. Extrusion of the N2 sequence, which is restricted to the more eastern part of the Deccan Traps outcrop, prior to extrusion of the main Deccan Traps body at about Cretaceous/Tertiary boundary time cannot be excluded. The occurrence of such prolonged and tectonically (re-)activated magmatism along fundamental fault zones such as the Narmada-Son zone with a probable wrench-type displacement component (Bhave et al., 1989) supports our suggested causal relationship between initial India-Asia contact and the Deccan Traps extrusion.

Paleoceanic Circulation at the Cretaceous/Tertiary Boundary

This is not the place to enter into a discussion on the origin of the Cretaceous/Tertiary boundary extinctions, that is, impact-related theories (Alvarez et al., 1980; Smit and Hertogen, 1980; Smit, 1982, 1990; Hut et al., 1987) vs. internal causes such as the Deccan Traps extrusion (McLean, 1982, 1985; Officer and Drake,

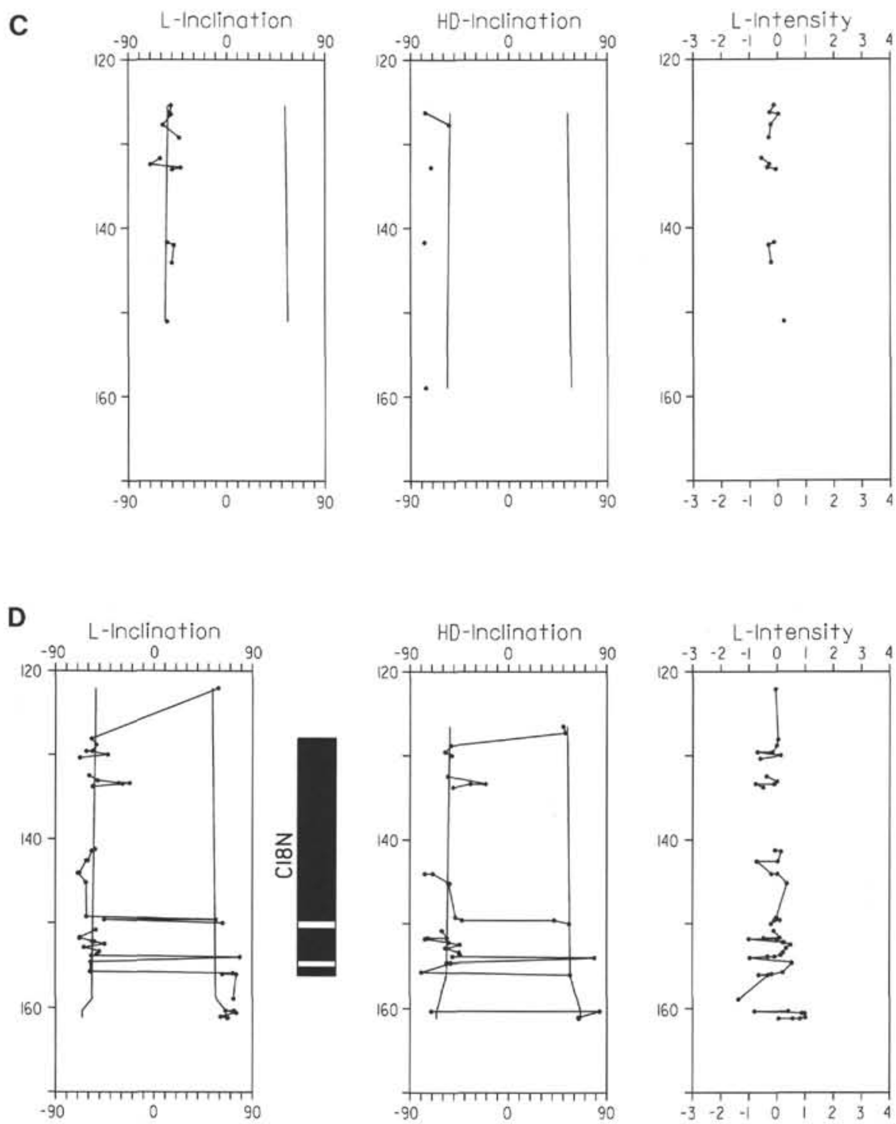

Figure 21 (continued).

1983, 1985; Courtillot et al., 1986; Courtillot and Cisowski, 1986; Officer et al., 1987; Graup and Spettel, 1989). We merely wish to point out that we attribute extrusion of the Deccan Traps and reorganization of the Indian Ocean spreading pattern to deformation of the Indian plate upon initial India-Asia contact at about Cretaceous/Tertiary boundary time. A combination of such geotectonic mechanisms may have resulted in the large-scale lowering of sea level during the earliest Paleocene (Vail et al., 1977; Hallam, 1984, 1987). Complete or partial closure of the Neotethys at about Cretaceous/Tertiary boundary time must have severely disrupted paleoceanic circulation, particularly in the Indian Ocean, Neotethys/Mediterranean region. As part of the ongoing Cretaceous/Tertiary extinction discussion we would like to raise here the possibility that circulation changes may have caused longer term evolutionary changes, observed in a wide range of marine organisms (e.g., Thierstein, 1982; Officer et al., 1987; Hallam, 1987; Keller, 1989; Keller and Lindinger, 1989; Zachos et al., 1989) as background trends to the abrupt mass-extinction events at the Cretaceous/Tertiary boundary (Smit, 1982; Smit and Romein, 1985; Hallam, 1987; Shipboard Scientific Party, 1989a).

Record of the India-Asia Convergence from the Neogene Sedimentary Profile of Site 758

Generalities

The Neogene susceptibility, NRM intensity, and lithostratigraphic profile of Site 758 shows significant long-term changes. In a more detailed analysis than that presented in the *Initial Reports* (Shipboard Scientific Party, 1989i), these changes/breaks will be identified and dated (see following section and Table 12). A correlation with events in the wider Himalayan region and the Indian Ocean will be attempted, to possibly constrain minimal ages of Neogene phases in the orogenic evolution of the India-Asia convergence zone.

Two assumptions need to be validated for this correlation, that (1) tectonic episodes usually are directly reflected in the sedimentary record and (2) susceptibility/remanence data can be used as a proxy for changes in sedimentary flux and content.

1. The breaks most probably represent rather abrupt changes in magnitude and content of terrigenous influx. Petrological studies of Miocene-Pliocene turbidites of the Bengal Fan at DSDP Site

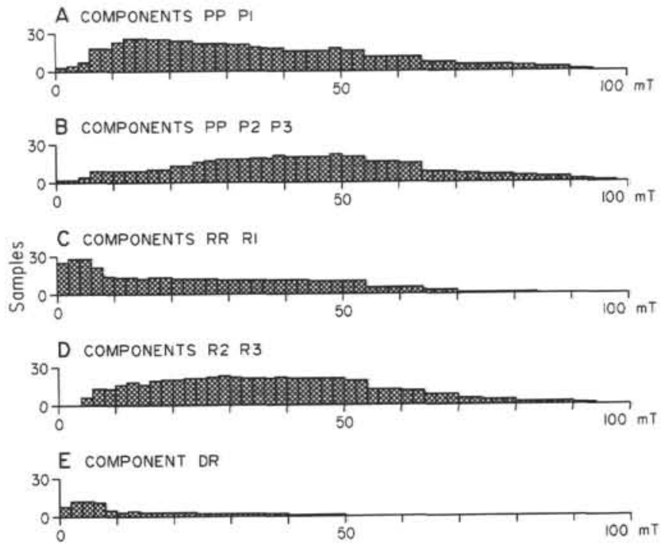

Figure 22. Histograms of stability range distribution upon AF demagnetization for Cores 121-757C-2R to 121-757C-6W (see caption to Fig. 6). **A, B.** Primary magnetization components PP, P_1, P_2, and P_3. **C, D.** "180 degree" overprints RR, R_1, R_2, and R_3. **E.** Drilling-induced overprint DR.

218 led Thompson (1974) and Ingersoll and Suczek (1979) to conclude that these sediments are essentially composed of sands from gneissic, sedimentary, and metasedimentary units in the Himalaya. Site 758 on the northern end of Ninetyeast Ridge is situated at the fringe of the Bengal and Nicobar fans. It is most likely, therefore, that influx of terrigenous material at this site likewise comes from a wider Himalayan source. This must have resulted from runoff of the Ganges and Brahmaputra river systems, and, except for the last few million years, probably also from the ancestral Indus river (Raynolds, 1981; Johnson et al., 1985; LeFort, 1989). In the Leg 121 *Initial Reports* (Shipboard Scientific Party, 1989i) we suggested that the breaks in terrigenous influx, interpreted from the Neogene susceptibility record of Site 758, reflect major changes in the tectonic regime, that is, mainly uplift of the wider Himalayan region north of the MCT and to a lesser extent the southern Tibetan and the Lower Himalayan region (Brookfield, 1989). The general correlation between orogenic uplift and sediment deposition is now firmly established by $^{40}Ar/^{39}Ar$ analysis of detrital K-feldspar and muscovite from Sites 717 and 718 on the southern Bengal Fan (Copeland and Harrison, 1990). This recent study shows that a significant portion of the Bengal Fan is made up of first-cycle detritus resulting from pulses of rapid uplift and erosion of the Himalayan and southern Tibetan region. Such pulses may have been numerous and of regionally variable extent and timing. Although these possibly local pulses may be well detailed in the proximal sedimentary record of the immediately adjacent foredeeps, the distal sedimentary record (Bengal and Nicobar fans, northern Ninetyeast Ridge) has the advantage that it can provide an estimate for spatially integrated changes in the tectonic activity for the entire convergence zone. Sediment petrological (Farrell and Janecek, this volume, fig. 5) and organic geochemical (Littke et al., this volume) studies of the upper Neogene sequence at Site 758 also show significant changes in terrigenous mass-accumulation rates, some of which correlate with the magnetically defined breaks, and a positive correlation between bulk sediment-accumulation rates and the organic carbon content ascribed to inflow of terrigenous organic debris.

2. The applicability of susceptibility as a rapid and sensitive tracer of terrigenous fraction variations was demonstrated recently for cores from Leg 108 in the eastern Atlantic (Bloemendal and deMenocal, 1989) and from Leg 117 in the western Arabian Sea (deMenocal et al., in press; Clemens and Prell, in press; Murray and Prell, in press). Direct correlation of breaks in the Pliocene record of Site 758 with changes in the magnitude of terrigenous influx (Farrell and Janecek, this volume, fig. 5) can be shown for two of the three breaks in that interval (K1/K2 at 1.9 Ma and K3/K4 at 5.1 to 5.4 Ma, see the following text). A prominent decrease in the linear-sedimentation rate and mass-accumulation rate (MAR) of both $CaCO_3$ and non-$CaCO_3$ content at 3.4 Ma (Farrell and Janecek, this volume, fig. 5), however, does not show up in the base-level susceptibility and NRM profile (Fig. 61). This is understandable because the decrease in non-$CaCO_3$ (and magnetic) MAR is masked by a concomitant decrease in $CaCO_3$ dilutant. This prominent decrease in terrigenous influx may not necessarily reflect a Himalayan tectonic phase. The change coincides with the top end of an interval (67, possibly 72, to 45 mbsf) of spikes in the susceptibility profile (Fig. 61), which were correlated (Shipboard Scientific Party, 1989i, table 11) with ash accumulations of a probable Sunda Arc origin. The decrease in the $CaCO_3$ and non-$CaCO_3$ MAR of the overlying sequence can be interpreted, therefore, alternatively as a reduction in biogenic carbonate due to a reduction in volcanic nutrients. If so, the K3/K4 break at the very base of this spike interval could be interpreted likewise as a reflection of the conjugate increase in volcanic activity, rather than a Himalayan/Tibetan tectonic phase.

Correlation of the changes in intensity of remanence and susceptibility (Fig. 61) with variations in magnetic mineralogy and/or grain size, and thus the Himalayan/Tibetan source rocks, can be shown for the upper part of the Pliocene (J. Gee, unpubl. data, 1990) and the basal part (88–93 mbsf), where the very large increase in NRM intensity is not reflected in the susceptibility profile. The Pliocene-Pleistocene magnetostratigraphic profile (see "APC-Cored Sediments" section) is of superb quality with virtually no magnetic overprints. The changes must, therefore, reflect a primary depositional feature and not authigenic formation of secondary magnetic phases. Variations in magnetic mineralogy are also indicated from maximum likelihood analysis of changes in the remanence directional pattern of the Neogene sequence at Site 758 ("Maximum Likelihood Determination of Breakpoints" section and Figs. 54 and 55). Such directional changes at 2.7, 6.7, and about 18.5 Ma correspond closely with the sedimentary breaks at 2.5 to 2.7, 6.2 to 6.5, and 17.5 Ma (see the following and Table 12). These directional changes indicate variations in the capacity of the rocks to adequately represent or retain the Earth's magnetic field direction as a result of variations in their magnetic mineral content and thus indicate variations in source rock. The 2.7-Ma break is particularly illustrative. An upward decrease in remanence intensity over close to 2 orders of magnitude is reflected in no more than an approximately 50% decrease in susceptibility (Fig. 61), but is not really noticeable on the MAR profile (Farrell and Janecek, this volume, fig. 5), which shows a zone of near-constant (low) terrigenous MAR. This implies a change in magnetic mineralogy and, by implication, source rock. This change may be observed in sediment petrology studies, but not from analysis of the MAR alone.

We conclude from these observations that the susceptibility/remanence profile of the Neogene sequence at Site 758 can be used as a proxy for changes in sedimentary flux, indeed. The magnetic profile records changes in both volume and mineralogy of the magnetic content. Its analysis is potentially more powerful than analysis of the MAR, because the magnetic record may trace changes not only in the mass-accumulation rate, but also in the source rock.

The Neogene sedimentary record of Site 758 undoubtedly also records other effects of nontectonic origin. However, we consider these to be of secondary nature only:

1. Correlation of the breaks in the Site 758 record with relative sea-level changes may be shown, but these are themselves probably causally related to the first-order tectonic changes leading to the uplift of the Himalayan-Tibetan region (Vail et al., 1977).

2. Milankovitch cycles were identified in the Pliocene glaciation record (Farrell and Janecek, this volume), but these are of a magnitude and period far less than that of the first-order variations shown in Figure 61.

3. It may be argued that deepening of the northern Ninetyeast Ridge during the Neogene, as determined from benthic foraminiferal assemblages (Shipboard Scientific Party, 1989i, fig. 16) may have led to an only locally increased terrigenous influx through closer association of Site 758 with the Bengal Fan sedimentation system, independent of phases in orogenic evolution. The gradual decline in $CaCO_3$ percentages since the middle Miocene (Shipboard Scientific Party, 1989i, figs. 43–45; Littke et al., this volume) indicates, however, that depth increased gradually. Such a gradual deepening process cannot be related to the sudden changes in susceptibility, NRM, and lithology. Moreover, a regional extent of at least two of the susceptibility breaks observed at Site 758 (K2/K3 and K3/K4) can be demonstrated from correlation with susceptibility breaks observed at Sites 717 and 719 on the southern perimeter of the Bengal Fan (Cochran, Stow, et al., 1989; Shipboard Scientific Party, 1989i, fig. 62).

The progressive Neogene uplift and erosion of the wider Himalayan region is clearly reflected in the Siwaliks sediments of the proximal foredeep (LeFort, 1989). The Lower Siwaliks contain mainly epidote and staurolite, the Middle Siwaliks kyanite (and staurolite), and the Upper Siwaliks hornblende and sillimanite, representing erosion of increasingly higher grade metamorphic terrains. Sedimentation rates for the Siwaliks of the Potwar Basin have been correlated directly with uplift rates of the source area to the north as determined from fission track data, with maximum uplift/sedimentation occurring during Middle Siwalik time (LeFort, 1989). Such changes in content and rate of sedimentation in the proximal record can reasonably be expected to have propagated downstream to appear with a time lag in the distal record of Site 758 at the perimeter of the Bengal Fan. The magnetostratigraphic record of the Holocene to uppermost Miocene sequence at Site 758 is of exceptional quality, and the biostratigraphic record of the underlying Miocene sequence is reasonably detailed. It may be possible, therefore, to place minimal age constraints on at least the younger phases in the Neogene evolution of the convergence zone from the first appearance and/or propagation of the deposition front, with a precision, perhaps, not obtainable from direct observations in the convergence zone itself.

Dating of the Breaks

Distinct changes in the susceptibility record of Holes 758A and 758B (Table 12) were dated on the basis of initial shipboard biostratigraphic control, and a preliminary correlation with phases in the tectonic evolution of the India-Asia convergence zone was presented by the Shipboard Scientific Party (1989i, fig. 61). It has been pointed out that whole-core NRM intensity variations within lithologic Unit I (0–121.7 mbsf) closely reflect whole-core susceptibility variations. Whole-core NRM intensities after 9-mT demagnetization vary over nearly 3 orders of magnitude, from 10^{-2} to 10 mA/m (Shipboard Scientific Party, 1989i, fig. 35). Similar intensity variations are also visible in the primary magnetization record of the samples from the APC-cored sequence of Holes 758A and 758B (Figs. 27 and 39). Therefore, we feel it is more appropriate to identify these breaks using the combined susceptibility, NRM, and lithostratigraphic record, rather than to rely solely on the susceptibility record as done during the shipboard interpretation.

We have dated the younger breaks (<7 Ma) on the basis of the very detailed magnetostratigraphic record and have constrained the age of the older breaks on the basis of post-cruise biostratigraphic control (e.g., P. Gamson, P. Resiwati, and J. Pospichal, pers. comm., 1989, this volume). In addition to the five breaks between susceptibility units K1 to K6 defined before (Shipboard Scientific Party, 1989i) we have also dated the break between lithologic Units I and II (121.7 mbsf) and a break in the basal part of the APC-cored sequence at 88–93 mbsf (Table 12). The break between lithologic Units I and II correlates with a distinct susceptibility peak within unit K5, with the start of influx of more terrigenous clay-rich sediment, and with an overall increase in sedimentation rate (Shipboard Scientific Party, 1989i, fig. 11; Fig. 61). The 88–93-mbsf break correlates with an increase of nearly 2 orders of magnitude in NRM intensity (Shipboard Scientific Party, 1989i, fig. 35; Figs. 27A and 39A) but is not identifiable on the susceptibility profile (Shipboard Scientific Party, 1989i, figs. 60 and 61; Fig. 61).

It ought to be pointed out that identification of some of the breaks may be construed as somewhat subjective. For example, the K5/K6 break is particularly subject to interpretation because core recovery is only about 60% in this part of the record. Likewise, it may be argued that the K3/K4 break could be shifted downward by about 10 m. Such subjective refinements can be settled only through correlation of the breaks over a wider region of the northern Ninetyeast Ridge and the Bengal Fan than the few sites (Shipboard Scientific Party, 1989e, 1989g) for which comparable data are available (Shipboard Scientific Party, 1989i, fig. 62).

Onsets (ends) of evident breaks were dated (Fig. 61 and Table 12) at approximately 17.5, 10–10.4, about 8.8, about 6.5 (6.2), 5.4 (5.1), 2.7 (2.5), and 1.9 Ma. We do not feel it appropriate to quantify error ranges for these dates. The 17.5–8.8-Ma dates are not tightly constrained because of rather limited micropaleontological control. The 6.5–1.9-Ma dates, however, are tightly constrained from the detailed magnetostratigraphic record. These breaks will be discussed and interpreted in the context of one of the more recent tectonic syntheses of the evolution of the India-Asia convergence (Klootwijk et al. 1985; Figs. 57 and 58). This synthesis is one of numerous models that show broad consensus on the sequence and timing of the major tectonic events. It is, currently, the only evolutionary model that accounts for oroclinal bending of the Himalayan Arc.

K5/K6 Break at about 17.5 Ma

The K5/K6 break can be correlated with the first, and probably the most fundamental, phase in the Neogene evolution of the wider Himalayan region. It represents a change in sediment supply related to the initial uplift of the Higher Himalaya and Karakorum region, shortly after latest Oligocene to early Miocene initiation of intercontinental underthrusting along the MCT (Powell and Conaghan, 1973; Seeber et al., 1981), the MNT, and possibly the Main Karakorum Thrust. This large-scale underthrusting event gave rise to intrusion over the full length of the Himalayan Arc and probably the Karakorum of a suite of anatectic leucogranites over a period of about 10 m.y. from about 25 Ma onward (LeFort, 1975, 1986, 1988, 1989; Ferrara et al., 1983; Schärer, 1984; Schärer et al., 1986, 1990a, 1990b; Debon et al., 1986a, 1986b; Searle and Fryer, 1986; LeFort et al., 1987; Deniel

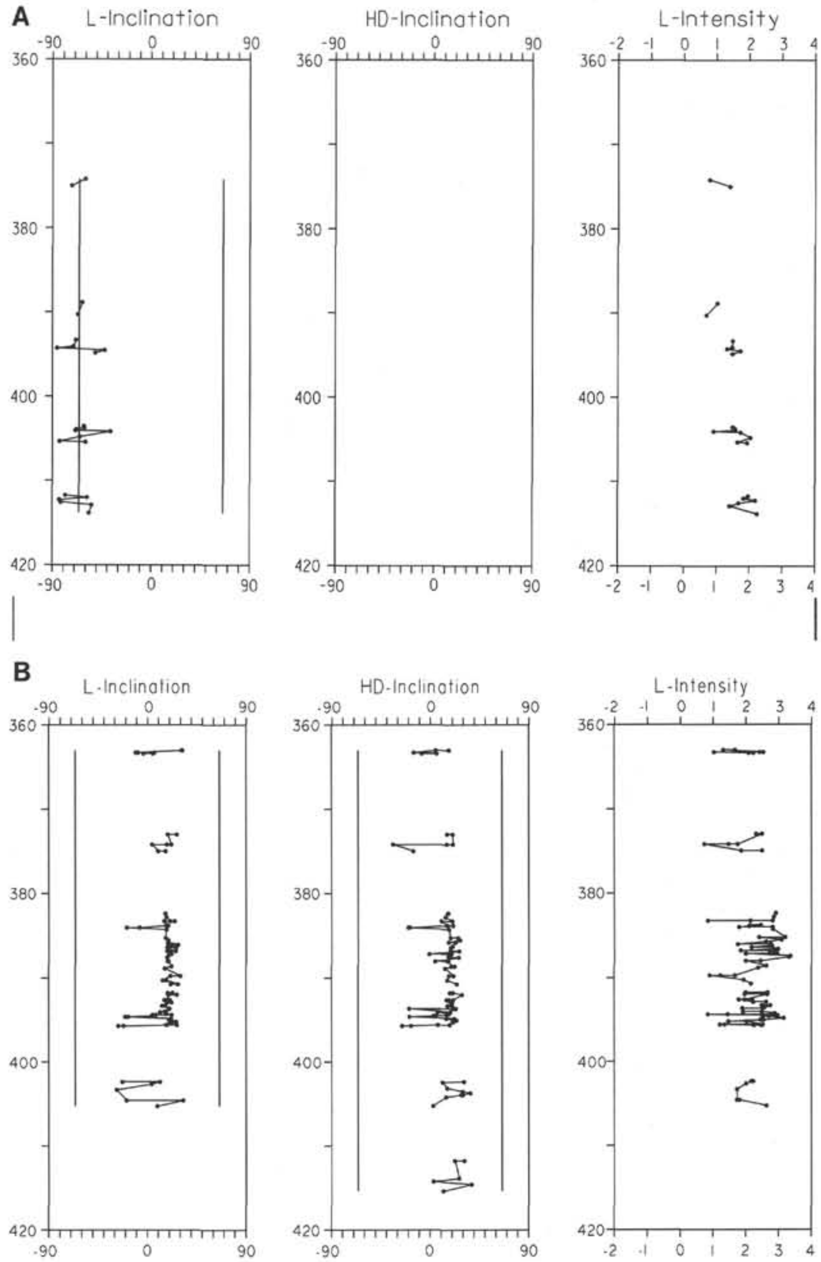

Figure 23. Stratigraphic plots of inclination and intensity of components determined from linear (L) and planar (HD) PCA of AF and thermal demagnetization data for Cores 121-757C-7R to 121-757C-12R (see caption to Fig. 5). **A.** Drilling-induced component DR. **B.** Low-inclination components LO, L_1, and L_2. **C.** High-inclination components HO, H_1, and H_2.

et al., 1987; Maluski et al., 1988; Rex et al., 1988; Searle and Rex, 1989; Hubbard and Harrison, 1989; Stern et al., 1989; Brookfield and Reynolds, 1990). An apparently slightly younger belt of comparable composition was emplaced just north of the surface outcrop of the MNT, the Lhagoi-Kangri belt (Debon et al., 1981, 1986b; Burg et al., 1984a; Schärer et al., 1986; LeFort, 1986, 1988, 1989; Maluski et al., 1988; LeFort et al., 1989). The propagating intercontinental underthrusting below southern Tibet may have given rise to the Miocene calc-alkaline Maquiang Volcanics (10–15 Ma; Coulon et al., 1986; Pearce and Mei Houjun, 1988; Pearce et al., 1989), as suggested before by Bingham and Klootwijk (1980) and Klootwijk and Bingham (1980).

The uplift of the Higher Himalayas associated with this intercontinental underthrusting (e.g., Seeber et al., 1981) is a Himalayan-wide event and is well dated prior to 17 Ma from ^{40}Ar-^{39}Ar studies (Everest region: 17 Ma, Kaneoka and Kono, 1981; about 21 Ma, Hubbard and Harrison, 1989; 17–21 Ma, Copeland et al., 1987b; Gangdese belt: 17–20 Ma, Copeland et al., 1987a; Zanskar: 16.1 Ma, Villa, 1987; Manaslu Granite: 18.5–19 Ma, Copeland and Harrison, 1989; K-feldspars from a sand dune near Quxu containing material from a large part of the upper drainage of the Tsangpo River: age maximum at about 17 Ma, Copeland and Harrison, 1990), from fission track studies (Western Himalayan Syntaxis: just prior to 15 Ma, Zeitler et al., 1982a, 1982b; Nanga Parbat–Haramosh Massif: 16–25 Ma, Zeitler et al., 1989; Chamberlain et al., 1989b), from Rb/Sr, ^{40}Ar-^{39}Ar, and K/Ar mineral studies (internal zones of the Western Himalayan Syntaxis: 15–25 Ma, Treloar and Rex, 1990; Garhwal: 19–21 Ma,

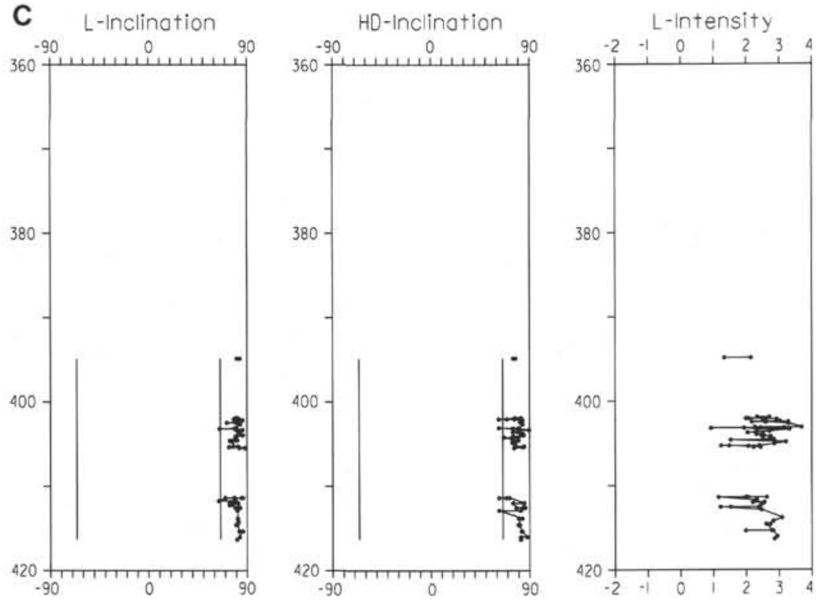

Figure 23 (continued).

Stern et al., 1989; Manaslu Granite: 18.1 Ma, Debon et al., 1987; LeFort, 1989), from U/Pb studies (Karakorum Batholith: 17–25 Ma, Parrish and Tirrul, 1989; Searle et al., 1989; Crawford, 1989; Schärer et al., 1990a; Manaslu Granite: 25 Ma, Deniel et al., 1987; Makalu Granite: 21.9–24.0 Ma, Mt. Everest Granite: 14.3 Ma, Lhagoi-Kangri Granite: 14.3 Ma, Nialam migmatite-granite: 15.1 Ma, Schärer et al., 1986), and from pressure-temperature studies (central Himalayan region: latest Oligocene–middle Miocene, Hodges et al., 1988). The Lower Siwaliks represent the erosional product of this uplift phase, deposited in the proximal southern foredeep. In the Potwar Basin, this uplift is expressed also by a major faunal change dated between 16 and 20 Ma (Barry et al., 1985). The base of the Lower Siwaliks in the Potwar/Salt Range region has been correlated on the basis of detailed magnetostratigraphic studies with the upper part of Chron 17 (Johnson et al., 1985), which corresponds with an age of approximately 18.3 Ma in the Berggren et al. (1985) time scale. Fission track studies (Cerveny et al., 1988) on detrital zircons in the Siwaliks Group have shown that erosion and deposition of the Siwaliks followed uplift of the Higher Himalaya with a consistent delay of no more than 1–5 m.y. Results from recent drilling on the perimeter of the Bengal Fan (Cochran, Stow, et al., 1987, 1989, 1990) indicate that sediments derived from this uplift phase had reached the outer part of the Bengal Fan system by 17 Ma.

The start of the Lower Siwalik sedimentation in the Northwestern Himalayan region is well constrained at 18.3 Ma. The onset of the K5/K6 break in the Site 758 profile is not as precisely known but is still reasonably well constrained at about 17.5 Ma from nannoplanktonic and microplanktonic data (Table 12). In the absence of detailed error control on the latter date it could be argued that the two dates are indistinguishable. However, comparable lags of less than 1 m.y. between the appearance of the break and attributed causative agent are also apparent for the break between lithologic Units I and II (see following section), for the NRM intensity increase at 6.5 Ma (see "Increase in NRM Intensity at 6.5 Ma" section), and possibly for the K4/K5 break (see "K4/K5 Break at about 8.8 Ma" section). On the strength of these recurrent observations we suggest that the time lags are real and that they may represent propagation of the deposition front from the Himalayan foredeep to the perimeter of the Bengal Fan.

Break between Lithologic Units I and II at 10.4–10 Ma

The break between lithologic Units I and II corresponds in time with the base of the Middle Siwaliks. This base is correlated from magnetostratigraphic analysis in the Potwar region with the lower third of Chron 10 (Johnson et al., 1985), at 11.2 Ma in the Berggren et al. (1985) time scale. The sharply increased susceptibility at this level, the upward-increasing clay content of lithologic Unit I (Shipboard Scientific Party, 1989i, fig. 4), and the sharp increase in sedimentation rate (Shipboard Scientific Party, 1989i, fig. 11) reflect the increased uplift and erosion of the wider Himalayan region (Johnson et al., 1982, 1985; Mascle and Hérail, 1982; Cerveny et al., 1988) and Tibetan region. This uplift is dated at about 10 Ma from fission track, K-Ar, and ^{40}Ar-^{39}Ar dates in the Northwestern Himalayan and Karakorum region (Baltoro Granite: Debon et al., 1986a, 1986b; Cerveny et al., 1989a, 1989b; Searle et al., 1989; Brookfield and Reynolds, 1990; Nanga Parbat-Haramosh Massif: Zeitler, 1985; Chamberlain et al., 1989b; Hunza region: Treloar et al., 1989) and from the end of pediplanation and start of increased uplift of the Tibetan Plateau (Shackleton and Chang Chen-fa, 1988).

This phase can be correlated also with a prominent seismic reflector in the Ganges-Brahmaputra delta complex of northwestern Bangladesh (Lindsay et al., in press). This reflector represents a major erosional surface, which Lindsay et al. correlated with the 10.5-Ma lowstand (Vail et al., 1977), which may reflect this phase of increased tectonism in the wider Himalayan region.

The 0.8-m.y. time lag between the appearance of this phase of accelerated uplift and erosion in the form of deposition of the Middle Siwaliks in the Northwestern Himalayan region and appearance of the depositional front on the perimeter of the Bengal Fan may reflect propagation of the depositional front. This Middle Siwalik propagation phase is comparable to the 0.8-m.y. delay concluded in the previous section for propagation of the Lower Siwalik phase.

K4/K5 Break at about 8.8 Ma

The K4/K5 break is very clear from a reduction in susceptibility and NRM intensities. It broadly coincides with isotopic evidence for increased tectonic activity at about 8–9 Ma in the

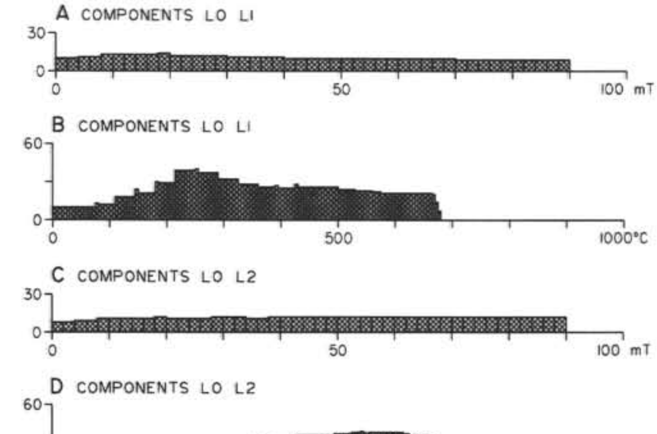

Figure 24. Histograms of stability range distribution upon AF and thermal demagnetization for Cores 121-757C-7R to 121-757C-12R (see captions to Figs. 6 and 9). **A–D.** Low-inclination components LO, L_1, and L_2. **E–H.** High-inclination components HO, H_1, and H_2. **I.** Drilling-induced overprint DR.

Karakorum and Higher Himalaya (Debon et al., 1986b, 1987; Maluski et al., 1988; Hubbard and Harrison, 1989), expressed by a change in sediment supply in the immediately adjacent foreland and ultimately in the Bengal Fan. Whilst the K4/K5 susceptibility break is readily distinguishable from the K3/K4 break, this is not so for radiometric age control on the tectonic phases that they are presumed to portray. Resolution of available radiometric dates is such that tectonic activity at about 8–9 Ma, correlated with the K4/K5 break, is not readily distinguishable from tectonic activity at about 7 Ma (correlated with the subsequent K3/K4 break discussed in the following section). This exemplifies that resolution of the indirect sedimentary control may be superior to currently available direct observational control on evolution of the India-Asia convergence zone.

The K4/K5 break marks a reduction in the influx of magnetic material at Site 758, which may correspond in the Northwestern Himalayan foreland region with a reduction in the sedimentary energy level evidenced by the change in sedimentation from sands in the Nagri Formation to silts in the overlying Dhok Pathan Formation. This formation break is dated from magnetostratigraphic studies (Johnson et al., 1985) at 8.9 Ma in the Berggren et al. (1985) time scale. This date is closely comparable to the date for the K4/K5 break and does not show the apparent propagation delay observed before (see preceding two sections). Alternatively, this K4/K5 break possibly could be correlated with a major faunal change (uplift) observed in the Potwar Plateau at 9.9 Ma (Barry et al., 1985), purportedly showing a propagation delay.

Increase in NRM Intensity at 6.5 Ma

This break is very prominent in the NRM intensity profile, but is not evident in the susceptibility profile. This break can be dated accurately from the splendid magnetostratigraphic profile of Site 758 (Shipboard Scientific Party, 1989i, fig. 41), and is taken at the base of an increase in NRM intensity over nearly 2 orders of magnitude between 6.5 and 6.2 Ma. A marked $\delta^{13}C$ shift in the northern Indian Ocean at 6.3 to 6.2 Ma (Vincent et al., 1985), reflecting an increase in terrigenous organic carbon, may be related to this uplift phase.

As observed for the K5/K6 break and the break between lithologic Units I and II, this break postdates a major phase in the evolution of the convergence zone by between 0.5 and 1 m.y. This phase has been observed in the Indian Ocean from prominent fault block rotations and a major hiatus in the Bengal Fan (Curray and Moore, 1971, 1974; Moore et al., 1974; Curray et al., 1982; Weissel et al., 1980; Geller et al., 1983; Cochran, Stow, et al., 1987, 1989, 1990; Curray and Munasinghe, 1989) dated at about 7 Ma and has been correlated with the formation of a diffuse plate boundary (Wiens et al., 1985, 1986; Wiens, 1986; DeMets et al., 1988, 1990; Neprochnov et al., 1988; Levchenko, 1989; Petroy and Wiens, 1989; Gordon et al., 1990) in the equatorial Indian Ocean south of the subcontinent. In the wider Himalayan region this phase can be correlated with tectonic activity, dated at 7–8 Ma and possibly earlier (Hubbard and Harrison, 1989) and with increased uplift. This uplift is dated directly from fission track, Rb/Sr, and K/Ar data in the Nanga Parbat-Haramosh and Hunza region (Zeitler, 1985) and from ^{40}Ar-^{39}Ar data from the Karakorum Batholith (Brookfield and Reynolds, 1990; Schärer et al., 1990a). In the Potwar Basin/Salt Range region it is dated indirectly from pedological evidence for a marked strengthening of the Asian monsoon system at about 7.7–7.3 Ma (Quade et al., 1989), and also from a related major faunal change at 7.7 Ma (Barry et al., 1985). Studies of TiO_2/Al_2O_3 ratios on the Bengal Fan (Schmitz, 1987) also indicate increased sediment transport since the late Miocene, attributed to uplift-induced increases in the denudation rate and strengthened monsoonal activity. Increased inflow of terrigenous organic debris in the upper Neogene sequence of Site 758 (Littke et al., this volume), and an increase in both non-$CaCO_3$ MAR and magnetic susceptibility since at least 7.3 Ma (Farrell and Janecek, this volume) have been attributed to the same causative factor.

K3/K4 Break at 5.4 to 5.1 Ma

The abrupt increase in susceptibility intensity at 73.8 mbsf is also reflected in a strong increase in NRM intensity between 77 and 72 mbsf. This break falls at the base of the Gilbert Chron (Shipboard Scientific Party, 1989i, fig. 41) and can be dated firmly at 5.1–5.4 Ma. This corresponds in time with initiation of major extensional tectonism in southern Tibet and formation of intramontane basins in the wider Himalayan region (LeFort, 1989). Although initiation of extensional tectonism is commonly estimated at about 4 Ma (Tapponnier et al., 1982, 1986; Rothery and Drury, 1984; Armijo et al., 1986, 1989), one of us has suggested (Klootwijk et al., 1985) a probable earlier initiation in

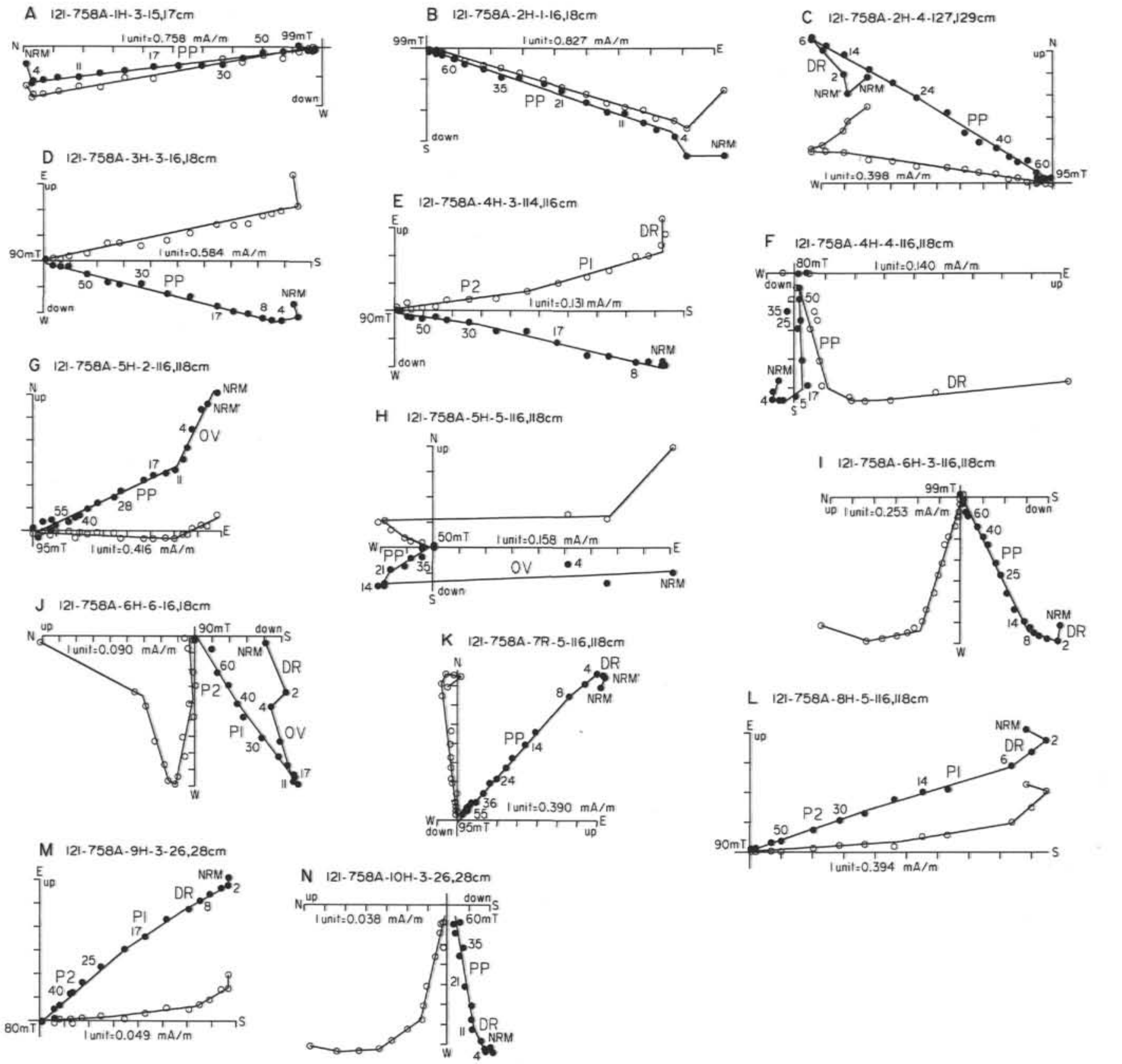

Figure 25. Zijderveld (1967) diagrams of representative samples from Cores 121-758A-1H to 121-758A-11H during AF demagnetization (see caption to Fig. 3). OV = recent field overprint.

the latest Miocene (Mercier et al., 1987) on the basis of a basal sedimentary sequence of that age in the Kali Gandaki Graben of the Nepal Himalaya (Colchen et al., 1980; Fort et al., 1981, 1982; Yoshida et al., 1984; Mercier et al., 1987; Yoshida, 1989). This extensional tectonism has been related causally and in time with oroclinal bending of the Himalayan Arc (Klootwijk et al., 1985; Fig. 1C) and the adjacent southern Tibetan region and outward flow of crustal material toward the western and eastern syntaxial regions (Klootwijk et al., 1985; Brun et al., 1985; Dasgupta et al., 1987; Pêcher and Bouchez, 1987; Otofuji et al., 1989; Molnar and Lyon-Caen, 1989; LeFort, 1989). Bending of the arc may be mimicked in southern Tibet in the deformation of the once continuous Karakorum-Jiali Fault Zone (Tapponnier et al., 1986; Armijo et al., 1989).

This extensional tectonism/oroclinal bending phase is also expressed by young isotopic ages in the wider Himalayan region (Maluski et al., 1988) and by onset of Upper Siwalik sedimentation (5 Ma: Johnson et al., 1982, 1985; Mascle and Hérail, 1982) reflecting increased topographic relief, and it coincides in time with major tectonic upheaval in the Western Himalayan Syntaxis (4–5 Ma: Burbank, 1983; Burbank and Johnson, 1983; Burbank and Raynolds, 1984, 1988; Burbank and Tahirkheli, 1985; Burbank et al., 1986; Johnson et al., 1986; Yeats and Hussain, 1987; Baker et al., 1988; Pennock et al., 1989; Cerveny et al., 1989b; 5 Ma: Burbank and Beck, 1989a; Lillie et al., 1989).

In the Jammu-Kashmir region of the Western Himalayan Syntaxis, clockwise rotations of 7° to 10° were observed in Siwalik beds as young as 7 Ma (Johnson et al., 1983), but no rotation was

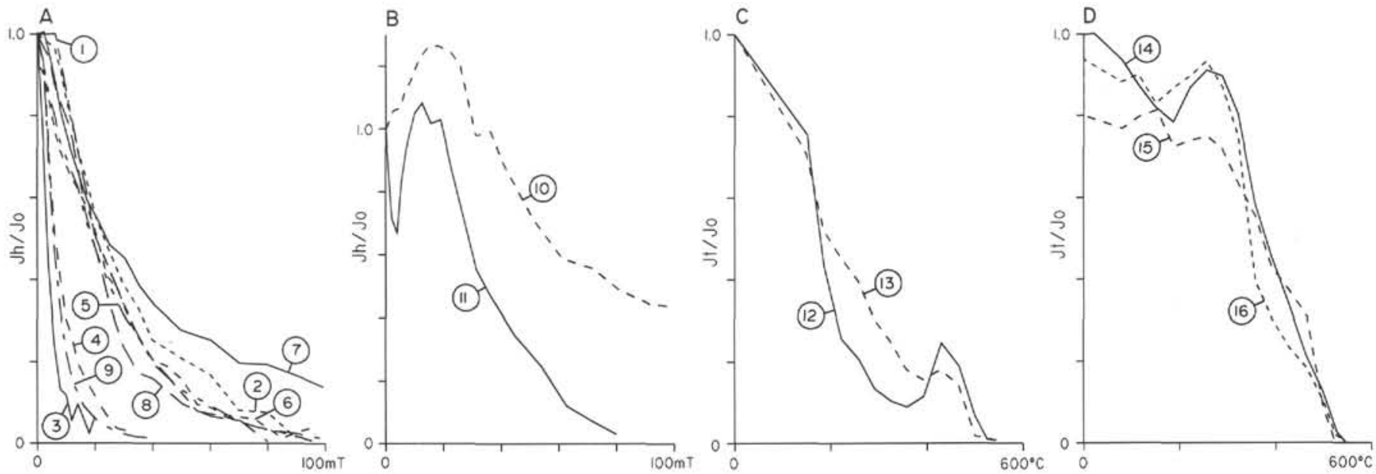

Figure 26. Normalized curves showing the decay of remanent magnetization of representative samples from Hole 758A. **A, B.** During AF demagnetization. **C, D.** During thermal demagnetization. 1 = Sample 121-758A-51R-3, 130–132 cm; 2 = Sample 121-758A-38X-2, 47–49 cm; 3, 12 = Sample 121-758A-60R-6, 28–30 cm; 4, 13 = Sample 121-758A-65R-4, 52–54 cm; 5 = Sample 121-758A-2H-1, 16–18 cm; 6 = Sample 121-758A-5H-2, 116118 cm; 7 = Sample 121-758A-15X-3, 8–10 cm; 8 = Sample 121-758A-9H-3, 26–28 cm; 9 = Sample 121-758A-70R-1, 123–125 cm; 10 = Sample 121-758A-24X-4, 96–98 cm; 11 = Sample 121-758A-6H-6, 16–18 cm; 14 = Sample 121-758A-71R-1, 136–138 cm; 15 = Sample 121-758A-72R-5, 72–74 cm; 16 = Sample 121-758A-67R-3, 137–139 cm.

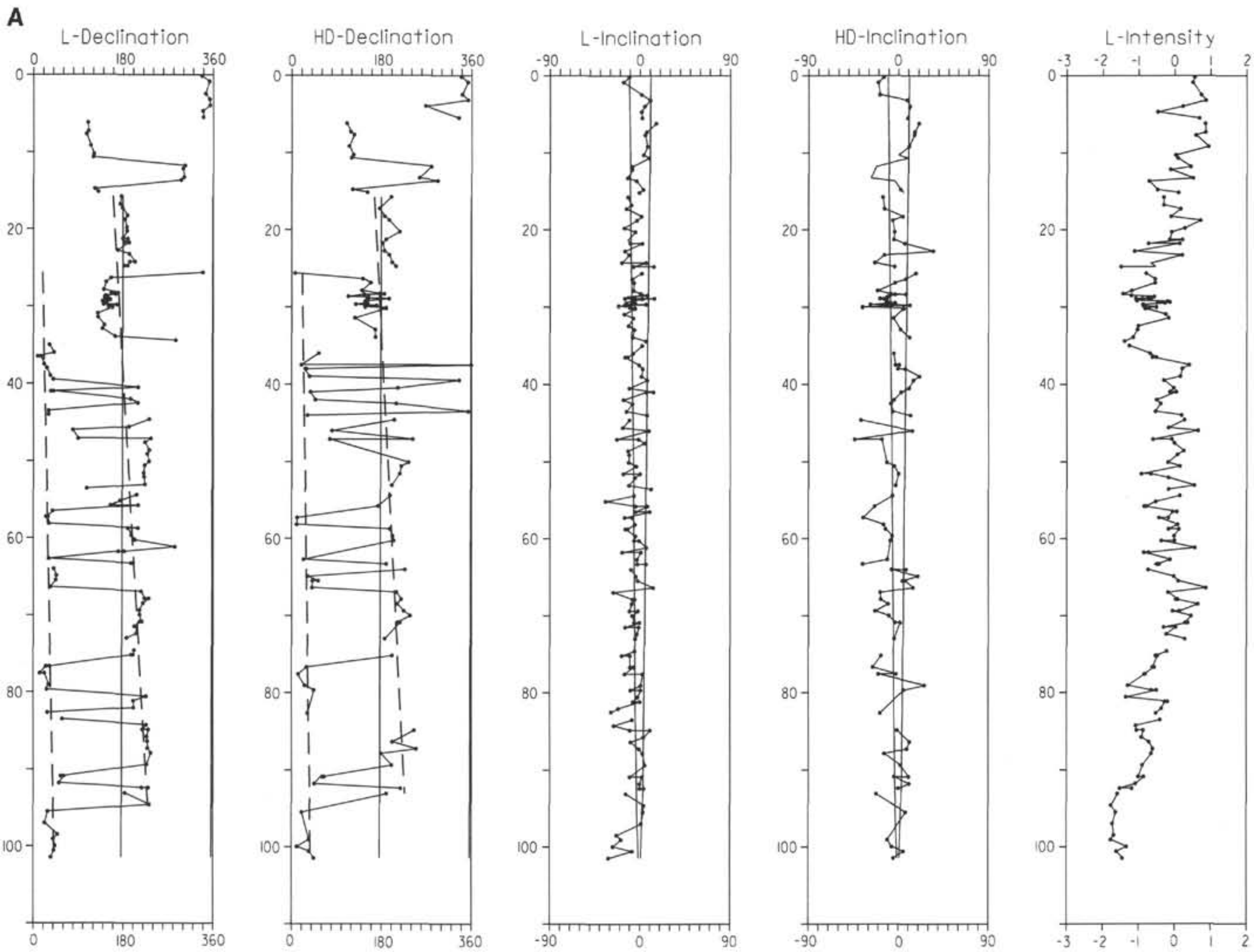

Figure 27. Stratigraphic plots of declination, inclination, and intensity of components determined from linear (L) and planar (HD) PCA of AF demagnetization data for Cores 121-758A-1H to 121-758A-11H (see caption to Fig. 5). Cores 121-758A-3H to 121-758A-11H were corrected for azimuthal orientation and drift of the drill string. **A.** Primary components PP, P_1, and P_2 with expected declinations (solid line) and linear regression of the observed declinations (dashed line) indicated (see "Analysis of Demagnetization Data" and "APC-Cored Sediments" sections and Table 4). **B.** Drilling-induced component DR.

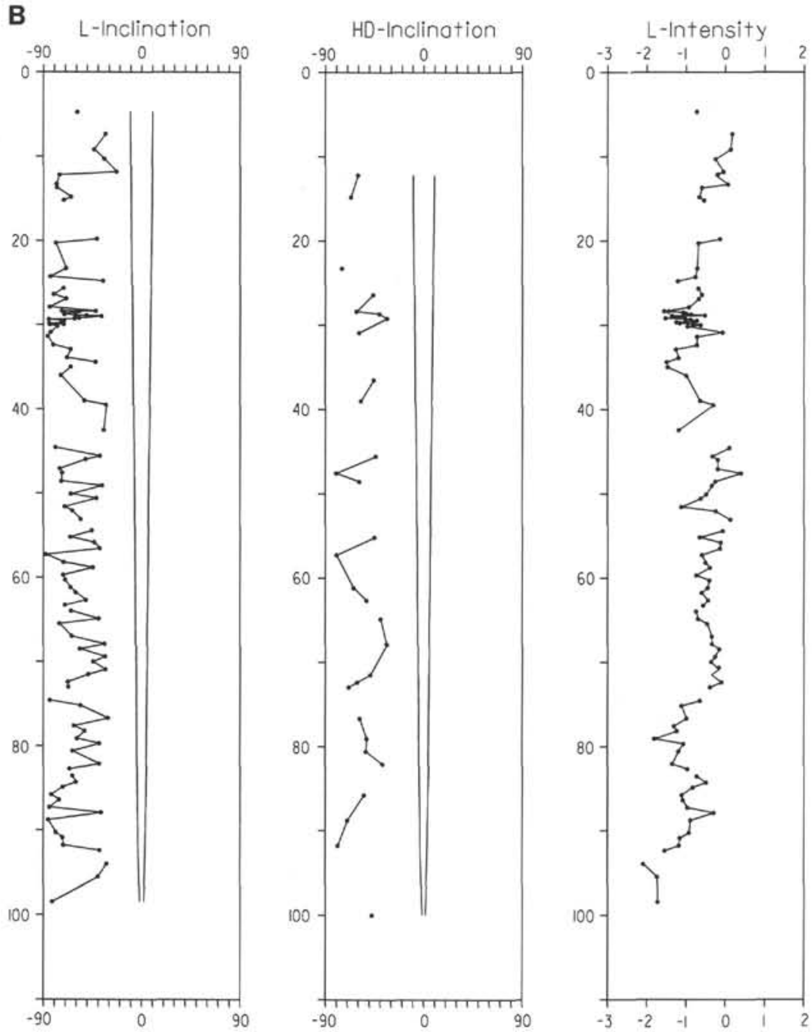

Figure 27 (continued).

observed in the Pliocene-Pleistocene Karewa Beds (Burbank, 1982). This led Burbank et al. (1986) to conclude that regional clockwise rotation is most likely to have occurred between post-middle Miocene and pre-middle Pliocene time (about 10 to 4.5 Ma) and can be constrained, perhaps, to an even narrower time interval between 7 and 5 Ma. Klootwijk et al. (1985) interpreted the clockwise rotation in the region as an integral part of oroclinal bending. The preceding time range may thus be applicable to formation of the wider Himalayan Arc, although confirmation through Himalayan-wide studies of rotation in the Siwalik sequence is needed. Anyway, the age range agrees with the late Miocene–early Pliocene initiation of oroclinal bending postulated by Klootwijk et al. (1985) and correlates well with the 5.4- to 5.1-Ma timing of the K3/K4 break. Establishment of a time lag, if any, in propagation of the sedimentation front associated with this major tectonic phase has to await further dating of rotational deformation along the Himalayan Arc.

K2/K3 Break at 2.7 to 2.5 Ma and the K1/K2 Break at 1.9 Ma

The K2/K3 and K1/K2 breaks are clearly visible in the susceptibility and NRM intensity records at 33–37 and 26–27 mbsf, respectively. These breaks can be related with (1) major phases of uplift and thrusting in the Western Himalayan Syntaxis, indicated by formation of prograding conglomerates (2.8 to 2.6 Ma, part of a cyclus between 3.5 and 1.7 Ma) and thrusting (2.1 to 1.9 Ma) along the MBT (Gansser, 1964, 1981; Zeitler et al., 1982b; Burbank and Johnson, 1983; Burbank and Raynolds, 1984; Zeitler, 1985; Powell, 1986; Burbank et al., 1986; Yeats and Hussain, 1987; Baker et al., 1988; Pennock et al., 1989; Agrawal et al., 1989; Burbank and Beck, 1989a, 1989b; Lillie et al., 1989) and (2) ongoing uplift of the High Himalayas (Hsü, 1976; Li Ji-jun et al., 1981; Zhang Qing-song et al., 1981; Fort et al., 1982; Mercier et al., 1987) and the Tibetan region (Chen Wan-yong, 1981; Guo Shuang-xing, 1981; Kong Zhao-chen and Du Nai-gin, 1981; Li Ji-jun et al., 1981; Song Zhi-chen and Liu Geng-Wu, 1981; Wang Fu-bao et al., 1981; Xu Ren, 1981; Xu Shu-ying, 1981; Zhang Qing-song et al., 1981; Chang Chen-fa et al., 1989) to their present-day heights, particularly since 0.4 Ma (Burbank et al., 1986).

CONCLUSIONS

1. Analysis of the primary paleolatitude pattern of common-Site 758 shows a significant break at 55+ Ma, interpreted as completion of eastward progressive suturing of Greater India and southern Asia. Northward movement of the Indian plate reduced then from 18–19.5 to 4.5 cm/yr at the location of common-Site 758.

2. Comparison of the primary paleolatitude pattern of common-Site 758 and paleolatitudes of presumably collision-related

secondary magnetization components observed both to the north and to the south of the Northern Kohistan and Indus-Tsangpo suture zones indicates that initial contact between northwestern Greater India and southern Asia may have been established already by Cretaceous/Tertiary boundary time. Extrusion of the Deccan Traps may have resulted from ensuing deformation of the Indian plate along preexisting zones of weakness.

3. Significant changes in the susceptibility, NRM intensity, and lithostratigraphic profile of Site 758 were interpreted to reflect Neogene phases in the evolution of the India-Asia convergence zone. The well-established chronostratigraphic control of Site 758 allows for minimal age limits on, and further resolution of, tectonic phases in the Himalayan and wider Tibetan region.

4. The ~50°S primary paleolatitude for the basement of Site 758 and for the ash sequences of Sites 757 and 758 support a Kerguelen hot spot origin for Ninetyeast Ridge. The ~43°S primary paleolatitude for the basement of Site 756 and the ~40°S secondary paleolatitude for the basement of Site 758 may be attributed to contributory activity of the Amsterdam–St. Paul hot spot.

ACKNOWLEDGMENTS

Phil McFadden contributed greatly to this paper by providing, with characteristic enthusiasm, statistical advice and software for the weighted linear regression and maximum likelihood procedures. He and Charlie Barton are thanked for their continuing interest, advice, and support throughout this project. Philippe Patriat is thanked for provision of an updated set of India's absolute motion data. Bob Duncan, Paul Gamson, Purty Resiwati, and Didier Vandamme are thanked for provision of data prior to publication. Didier Vandamme is thanked for some thoughtful suggestions on the Deccan Traps. Chris Pigram and Charlie Barton (BMR) reviewed and improved an early draft. John Convine, Dan Kennedy, Rex Bates, and Angie Jaensch (BMR) are thanked for drafting of the figures. Bob Duncan and Peter Zeitler showed considerable "staying power" in reviewing this lengthy paper. They are thanked for their stimulating criticism and suggestions for improved presentation. Klootwijk publishes with permission of the Director, Bureau of Mineral Resources, Geology and Geophysics.

REFERENCES

Achache, J., Courtillot, V., and Zhou, Y. X., 1984. Paleogeographic and tectonic evolution of southern Tibet since middle Cretaceous time: new paleomagnetic data and synthesis. *J. Geophys. Res.*, 89:10311–10339.

Acton, G. D., and Gordon, R. G., 1989. Limits on the age of the Deccan Traps of India from paleomagnetic and plate reconstruction data and their uncertainties. *J. Geophys. Res.*, 94:17713–17720.

Agrawal, D. P., Dodia, R., Kotlia, B. S., Razdan, H., and Sahni, A., 1989. The Plio-Pleistocene geologic and climatic record of the Kashmir Valley, India: a review and new data. *Palaeogeogr., Palaeoclimatol., Palaeoecol.*, 73:267–286.

Allègre, C. J., Courtillot, V., Tapponnier, P., Hirn, A., Mattauer, M., Coulon, C., Jaeger, J. J., Achache, J., Schärer, U., Marcoux, J., Burg, J. P., Girardeau, J., Armijo, R., Gariépy, C., Göpel, C., Li Tindong, Xiao Xuchang, Chang Chen-fa, Li Guangqin, Lin Baoyu, Teng Jiwen, Wang Naiwen, Chen Guoming, Han Tonglin, Wang Xibin, Den Wanming, Sheng Huaibin, Cao Yougong, Zhou Ji, Qiu Hongrong, Bao Peisheng, Wang Songchan, Wang Bixiang, Zhou Yaoxiu, and Ronghua Xu, 1984. Structure and evolution of the Himalaya-Tibet orogenic belt. *Nature*, 307:17–22.

Alvarez, L. W., Alvarez, W., Asaro, F., and Michel, H. V., 1980. Extraterrestrial cause for the Cretaceous-Tertiary extinction. *Science*, 280:1095–1108.

Andrews, J. A., 1985. True polar wander: an analysis of Cenozoic and Mesozoic paleomagnetic poles. *J. Geophys. Res.*, 90:7737–7750.

Armijo, R., Tapponnier, P., and Han, T. L., 1986. Quaternary extension in southern Tibet: field observations and tectonic implications. *J. Geophys. Res.*, 91:13803–13872.

_______, 1989. Late Cenozoic right-lateral strike-slip faulting in southern Tibet. *J. Geophys. Res.*, 94:2787–2838.

Athavale, R. N., and Verma, R. K., 1970. Palaeomagnetic results on Gondwana dykes from the Damodar Valley coal-fields and their bearing on the sequence of Mesozoic igneous activity in India. *Geophys. J. R. Astron. Soc.*, 20:303–316.

Baker, D. M., Lillie, R. J., Yeats, R. S., Johnson, G. D., Yousuf, M., and Zamin, A.S.H., 1988. Development of the Himalayan frontal thrust zone: Salt Range, Pakistan: *Geology*, 16:3–7.

Baksi, A. K., 1986. $^{40}Ar/^{39}Ar$ incremental heating study of whole rock samples from the Rajmahal and Bengal traps, eastern India. *Terra Cogn.*, 6:161. (Abstract)

_______, 1987. Critical evaluation of the age of the Deccan Traps, India: implications for flood-basalt volcanism and faunal extinctions. *Geology*, 15:147–150.

_______, 1989. Comment on "Age estimate of the Deccan Traps from the North American apparent polar wander path." *Geology*, 17:89–90.

Baksi, A. K., Barman, T. R., Paul, D. K., and Farrar, E., 1987. Widespread Early Cretaceous flood basalt volcanism in eastern India: geochemical data from the Rajmahal-Bengal-Sylhet traps. *Chem. Geol.*, 63:133–141.

Baksi, A. K., and Kunk, M. J., 1988. The age of initial volcanism in the Deccan Traps, India: preliminary $^{40}Ar/^{39}Ar$ age spectrum dating results. *Eos, Trans. Am. Geophys. Union*, 69:732. (Abstract)

Barry, J. C., Johnson, N. M., Raza, S. M., and Jacobs, L. L., 1985. Neogene mammalian faunal changes in southern Asia: correlation with climatic, tectonic and eustatic events. *Geology*, 13:637–640.

Beane, J. E., Turner, C. A., Hooper, P. R., Subbarao, K. V., and Walsh, J. N., 1986. Stratigraphy, composition and form of the Deccan Basalts, Western Ghats, India. *Bull. Volcanol.*, 48:61–83.

Berggren, W. A., Kent, D. V., Flynn, J. J., and Van Couvering, J. A., 1985. Cenozoic geochronology. *Geol. Soc. Am. Bull.*, 96:1407–1418.

Besse, J., and Courtillot, V., 1988. Paleogeographic maps of the continents bordering the Indian Ocean since the Early Jurassic. *J. Geophys. Res.*, 93:11791–11808.

Besse, J., Courtillot, V., Pozzi, P., Westphal, M., and Zhou, Y. X., 1984. Palaeomagnetic estimates of crustal shortening in the Himalayan thrusts and Zangbo suture. *Nature*, 311:621–626.

Besse, J., Courtillot, V., and Vandamme, D., 1989. Comment on "Age estimation of the Deccan Traps from the North American apparent polar wander path." *Geology*, 17:88–89.

Bhave, K. N., Ganju, J. L., and Jokhan Ram., 1989. Origin, nature and geological significance of lineaments. *In* Qureshy, M. N., and Hinze, W. J. (Eds.), *Regional Geophysical Lineaments*. Mem. Geol. Soc. India, 12:35–42.

Bhimasankaram, V.L.S., 1964. Palaeomagnetic directions of the Deccan Traps of Rajahmundry, Andrah Pradesh, India. *Geophys. J. R. Astron. Soc.*, 9:119–133.

Bingham, D. K., and Klootwijk, C. T., 1980. Palaeomagnetic constraints on Greater India's underthrusting of the Tibetan Plateau. *Nature*, 284:336–338.

Biswas, S. K., 1982. Rift basins in western margin of India and their hydrocarbon prospects with special reference to Kutch Basin. *AAPG Bull.*, 66:1497–1513.

_______, 1987. Regional tectonic framework, structure and evolution of the western marginal basins of India. *Tectonophysics*, 135:307–327.

_______, 1988. Structure of the western continental margin of India and related igneous activity. *In* Subbarao, K. V. (Ed.), *Deccan Flood Basalts*. Mem. Geol. Soc. India, 10:371–390.

Biswas, S. K., and Deshpande, S. V., 1973. A note on the mode of eruption of the Deccan Trap lavas with special reference to Kutch. *J. Geol. Soc. India*, 14:134–141.

Bloemendal, J., and deMenocal, P., 1989. Evidence for a change in the peridocity of tropical climate cycles at 2.4 Myr from whole-core magnetic susceptibility measurements. *Nature*, 342:897–899.

Blow, R. A., and Hamilton, N., 1975. Palaeomagnetic evidence from DSDP cores of northward drift of India. *Nature*, 257:570–572.

Bolli, H. M., Saunders, J. B., and Perch-Nielsen, K. (Eds.), 1985. *Plankton Stratigraphy:* Cambridge (Cambridge Univ. Press).

Bose, M. K., 1980. Alkaline magmatism in Deccan volcanic province. *J. Geol. Soc. India*, 21:317–329.

Bossart, P., Ottiger, R., and Heller, F., 1989. Paleomagnetism in the Hazara-Kashmir Syntaxis, NE Pakistan. *Eclogae Geol. Helv.*, 82:585-601.

Brookfield, M. E., 1989. Miocene to Recent uplifts of the Northwestern Himalaya and adjacent areas. *In* Thanasuthipitak, T., and Ounchanum, P. (Eds.), *Intermontane Basins: Geology and Resources:* Chang Mai, 452–467.

Brookfield, M. E., and Reynolds, P. H., 1990. Miocene $^{40}Ar/^{39}Ar$ ages from the Karakorum Batholith and Shyok Mélange, northern Pakistan, indicate late Tertiary uplift and southward displacement. *Tectonophysics*, 172:155–167.

Brun, J.-P., Burg, J.-P., and Chen Guo Ming. 1985. Strain trajectories above the Main Central Thrust (Himalaya) in southern Tibet. *Nature*, 313:388–390.

Buffetaut, E., 1990. Comment on "Paleontological view of the ages of the Deccan Traps, the Cretaceous/Tertiary boundary, and the India-Asia collision." *Geology*, 18:186.

Burbank, D. W., 1982. The chronologic and stratigraphic evolution of the Kashmir and Peshawar intermontane basins, northwestern Himalaya [Ph.D. dissert.]. Dartmouth College, Hannover, N.H.

_______, 1983. The chronology of intermontane-basin development in the northwestern Himalaya and the evolution of the Northwest Syntaxis. *Earth Planet. Sci. Lett.*, 64:77–92.

Burbank, D. W., and Beck, R. A., 1989a. Comment on "Development of the Himalayan frontal thrust zone: Salt Range, Pakistan." *Geology*, 17:378–380.

_______, 1989b. Early Pliocene uplift of the Salt Range: temporal constraints on thrust wedge development, northwest Himalaya, Pakistan. *In* Malinconico, L. L., Jr., and Lillie, R. J., *Tectonics of the Western Himalaya*. Spec. Pap. Geol. Soc. Am., 232:113–128.

Burbank, D. W., and Johnson, G. D., 1983. The late Cenozoic chronologic and stratigraphic development of the Kashmir intermontane basin, northwestern Himalaya. *Palaeogeogr., Palaeoclimatol., Palaeoecol.*, 43:205–235.

Burbank, D. W., and Raynolds, R.G.H., 1984. Sequential late Cenozoic structural disruption of the northern Himalayan foredeep. *Nature*, 311:114–118.

_______, 1988. Stratigraphic keys to the timing of thrusting in terrestrial foreland basins: applications to the Northwestern Himalaya. *In* Paola, C., and Kleinspehn, K. (Eds.), *New Perspectives in Basin Analysis*. Minneapolis (Univ. Minneapolis Press), 331–351.

Burbank, D. W., Raynolds, R.G.H., and Johnson, G. D., 1986. Late Cenozoic tectonics and sedimentation in the northwestern Himalayan foredeep: II. Eastern limb of the Northwest Syntaxis and regional synthesis. *In* Allen, P., and Homewood, P. (Eds.), *Foreland Basins*. Spec. Publ. Int. Assoc. Sedimentol., 8:293–306.

Burbank, D. W., and Tahirkheli, R.A.K., 1985. The magnetostratigraphy, fission track dating and stratigraphic evolution of the Peshawar intermontane basin, northern Pakistan. Geol. Soc. Am. Bull., 96:539–552.

Burg, J. P., and Chen, G. M., 1984. Tectonics and structural zonation of southern Tibet, China. *Nature*, 311:219–223.

Burg, J. P., Guiraud, M., Chen, G. M., and Li, G. C., 1984a. Himalayan metamorphism and deformations in the North Himalayan Belt (southern Tibet, China). *Earth Planet. Sci. Lett.*, 69:391–400.

Burg, J. P., Matte, P., Brunel, M., Andrieux, J., Li Tingdong, Chen Guoming, Li Guangcen, and Xiao Xuchang, 1984b. Présence et signification d'une phase de déformation antérieure au flysch à blocs, réputé d'age Crétacé supérieur, au Sud de la suture du Tsangpo (Tibet, méridional). *In* Mercier, J. L., and Li Guangcen (Eds.), *Mission Franco-Chinois au Tibet 1980*. Paris (Editions CNRS), 351–356.

Burg, J.-P., Proust, F., Tapponnier, P., and Chen Guo Ming, 1983. Deformation phases and tectonic evolution of the Lhasa block (southern Tibet, China). *Eclogae Geol. Helv.*, 76:643–665.

Butler, R.W.H., 1986. Thrust tectonics, deep structure and crustal subduction in the Alps and Himalayas. *J. Geol. Soc. London*, 143:857–873.

_______, 1988. General discussion. *Philos. Trans. R. Soc. London A*, 326:321–323.

Butler, R.W.H., and Coward, M. P., 1989. Crustal thrusting and continental subduction during Himalayan collision tectonics on the N.W. Indian Plate. *In* Sengör, A.M.C. (Ed.), *Tectonic Evolution of the Tethyan Region*. NATO ASI Ser. C, 259:387–413.

Butler, R.W.H., and Prior, D. J., 1988. Anatomy of a continental subduction zone: the Main Mantle Thrust in northern Pakistan. *Geol. Rundsch.*, 77:239–255.

Campbell, I. H., and Griffiths, R. W., 1990. Implications of mantle plume structure for the evolution of flood basalts. *Earth Planet. Sci. Lett.*, 99:79–93.

Cerveny, P. F., Johnson, N. M., Tahirkheli, R.A.K., and Bonis, N. R., 1989a. Tectonic and geomorphic implications of Siwalik Group heavy minerals, Potwar Plateau, Pakistan. *In* Malinconico, L. L., Jr., and Lillie, R. J. (Eds.), *Tectonics of the Western Himalayas*. Spec. Pap. Geol. Soc. Am., 232:129–136.

Cerveny, P. F., Naeser, C. W., Kelemen, P. B., Lieberman, J. E., and Zeitler, P. K., 1989b. Zircon fission-track ages from the Gasherbrum Diorite, Karakorum Range, northern Pakistan. Geology, 17:1044–1048.

Cerveny, P. F., Naeser, N. D., Zeitler, P. K., Naeser, C. W., and Johnson, N. M., 1988. History of uplift and relief of the Himalaya during the past 18 million years: evidence from fission-track ages of detrital zircons from sandstones of the Siwalik Group. *In* Kleinspehn, K. L., and Paola, C. (Eds.), *New Perspectives in Basin Analysis:* New York (Springer-Verlag), 43–61.

Chamberlain, C. P., Jan, M. Q., and Zeitler, P. K., 1989a. A petrologic record of the collision between the Kohistan island-arc and Indian plate, northwest Himalaya. *In* Malinconico, L. L., Jr., and Lillie, R. J. (Eds.), *Tectonics of the Western Himalayas*, Spec. Pap. Geol. Soc. Am., 232:23–32.

Chamberlain, C. P., Zeitler, P. K., and Jan, M. Q., 1989b. The dynamics of the suture between the Kohistan island arc and the Indian plate in the Himalaya of Pakistan. *J. Metamorphic Geol.*, 7:135–149.

Chang Chen-fa, Chen Nansheng, Coward, M. P., Deng Wanming, Dewey, J. F., Gansser, A., Harris, N.B.W., Jin Chengwei, Kidd, W.S.F., Leeder, M. R., Li Huan., Lin Jinlu., Liu Chengjie., Mei Houjun, Molnar, P., Pan Yun, Pan Yusheng, Pearce, J. A., Shackleton, R. M., Smith, A. B., Sun Yiyin, Ward, M., Watts, D. R., Xu Juntao, Xu Ronghua, Yin Jixiang, and Zhang Yuquan, 1986. Preliminary conclusions of the Royal Society and Academia Sinica 1985 geotraverse of Tibet. *Nature*, 323:501–507.

Chang Chen-fa, Pan Yu-Sheng, and Sun Yi-Ying, 1989. The tectonic evolution of Qinghai-Tibet Plateau: a review. *In* Sengör, A.M.C. (Ed.), *Tectonic Evolution of the Tethyan Region*. NATO ASI Ser. C, 259:415–476.

Chen Wan-yong, 1981. Natural environment of the Pliocene basin in Gyirong, Xizang. *In* Liu Dong-sheng (Ed.), *Geology, Geological History and Origin of the Qinghai-Xizang Plateau:* Beijing (Science Press), 343–352.

Choubey, V. D., 1971. Narmada-Son lineament. *Nature*, 232:38–40.

Clemens, S. C., and Prell, W. L., in press. One million year record of summer-monsoon winds and continental aridity from the Owen Ridge (Site 722), northwest Arabian Sea. *In* Prell, W. L., Niitsuma, N., *Proc. ODP, Sci. Results*, 117: College Station, Texas (Ocean Drilling Program).

Cochran, J., Stow, D.A.V., et al., 1987. Collision in the Indian Ocean. *Nature*, 330:519–521.

Cochran, J. R., Stow, D.A.V., et al., 1989. *Proc. ODP, Init. Repts.*, 116: College Station, TX (Ocean Drilling Program).

_______, 1990. *Proc. ODP, Sci. Results*, 116: College Station, TX (Ocean Drilling Program).

Cockerham, R. S., Luyendyk, B. P., and Jarrad, R. D., 1975. Paleomagnetic study of sediments from Site 253 DSDP, Ninetyeast Ridge. *Eos, Trans. Am. Geophys. Union*, 56:78.

Coffin, M. P., and Royer, J.-Y., in press. Jurassic to Eocene plate tectonic reconstructions in the Kerguelen Plateau region. *In* Schlich, R., Wise, S. W., Jr., et al., *Proc. ODP, Sci. Results*, 120: College Station, TX (Ocean Drilling Program).

Colchen, M., Fort, M., and Freytet, P., 1980. Evolution paléogéographique et structurale du fossé de la Thakkhola-Mustang (Himalaya du Nepal): implications sur l'histoire récente de la châine Himalayaènne. *C. R. Acad. Sci. Paris, Ser. D*, 290:11–314.

Collinson, D. W., 1983. *Methods in Rock Magnetism and Palaeomagnetism: Techniques and Instrumentation:* London (Chapman and Hall).

Copeland, P., and Harrison, T. M., 1989. Chronology of the Manaslu Granite: implications for magma segregation. *Terra Abstr.*, 1:174.

_______, 1990. Episodic rapid uplift in the Himalaya revealed by $^{40}Ar/^{39}Ar$ analysis of detrital K-feldspar and muscovite, Bengal Fan. *Geology*, 18:354–357.

Copeland, P., Harrison, T. M., Kidd, W.S.F., Xu, R., and Zwang, Y., 1987a. Rapid early Miocene acceleration of the uplift in the Gandese Belt, Xizang (southern Tibet) and its bearing on accommodation mechanisms of the India-Asia collision. *Earth Planet. Sci. Lett.*, 86:240–252.

Copeland, P., Harrison, T. M., Parrish, R., Burchfiel, B. C., Hodges, K., and Kidd, W.S.F., 1987b. Constraints on the age of normal faulting, north face of Mt. Everest: implications for Oligo-Miocene uplift. *Eos, Trans. Am. Geophys. Union*, 68:1444.

Coulon, C., Maluski, H., Bollinger, C., and Wang, S., 1986. Mesozoic and Cenozoic volcanic rocks from central and southern Tibet: ^{39}Ar-^{40}Ar dating, petrological characteristics and geodynamical significance. *Earth Planet. Sci. Lett.*, 79:281–302.

Courtillot, V., and Besse, J., 1987. Magnetic field reversals, polar wander, and core-mantle coupling. *Science*, 237:1140–1147.

Courtillot, V., Besse, J., Vandamme, D., Montigny, R., Jaeger, J.-J., and Capetta, H., 1986. Deccan flood basalts at the Cretaceous/Tertiary boundary? *Earth Planet. Sci. Lett.*, 80:361–374.

Courtillot, V., Féraud, G., Maluski, H., Vandamme, D., Moreau, M. G., and Besse, J., 1988. Deccan flood basalts and the Cretaceous/Tertiary boundary. *Nature*, 333:843–846.

Courtillot, V., Vandamme, D., and Besse, J., 1987. Reply to comments on "Deccan flood basalts at the Cretaceous/Tertiary boundary?" by H. Wensink. *Earth Planet. Sci. Lett.*, 86:122–123.

Courtillot, V. E., and Cisowski, S., 1987. The Cretaceous-Tertiary boundary events: external or internal causes? *Eos, Trans. Am. Geophys. Union*, 68:193–200.

Coward, M. P., 1983. Thrust tectonics, thin skinned or thick skinned, and the continuation of thrusts to deep in the crust. *J. Struct. Geol.*, 5:113–123.

_______, 1988. General discussion. *Philos. Trans. R. Soc. London A*, 326:323–325.

Coward, M. P., and Butler, R.W.H., 1985. Thrust tectonics and the deep structure of the Pakistan Himalaya. *Geology*, 13:417–420.

Coward, M. P., Butler, R.W.H., Chambers, A. F., Graham, R. H., Izatt, C. N., Khan, M. A., Knipe, R. J., Prior, D. J., Treloar, P. J., and Williams, M. P., 1988a. Folding and imbrication of the Indian crust during Himalayan collision. *Philos. Trans. R. Soc. London A*, 326:89-116.

Coward, M. P., Butler, R.W.H., Khan, M. A., and Knipe, R. J., 1987. The tectonic history of Kohistan and its implications for Himalayan structure. *J. Geol. Soc. London*, 144:377–391.

Coward, M. P., Kidd, W.S.F., Pan Yun., Shackleton, R.M., and Zhang Hu., 1988b. The structure of the 1985 Tibet geotraverse, Lhasa to Golmud. *Phil. Trans. R. Soc. Lond. A*, 327:307–336.

Cox, A., and Gordon, R. G., 1984. Paleolatitudes determined from paleomagnetic data from vertical cores. Rev. Geophys. Space Phys., 22:4772.

Cox, K. G., 1980. A model for flow basalt volcanism. *J. Petrol.*, 21:629-650.

_______, 1989. Hot plumes from the mantle. *Nature*, 340:341–342.

Crawford, A. R., 1978. Narmada-Son lineament of India traced into Madagascar. *J. Geol. Soc. India*, 19:144–153.

Crawford, M. B., 1989. Leucogranites of the northwest Himalaya: melting triggers and the magmatic evolution of collision belts. *Terra Abstr.*, 1:175.

Curray, J. R., Emmel, F. J., Moore, D. G., and Raitt, R. W., 1982. Structure, tectonics and geological history of the northeastern Indian Ocean. *In* Nairn, A.E.M., and Stehli, F. G. (Eds.), *The Ocean Basins and Margins* (vol. 6): New York (Plenum), 399–450.

Curray, J. R., and Moore, D. G., 1971. Growth of the Bengal deep-sea fan and denudation in the Himalayas. *Geol. Soc. Am. Bull.*, 82:563–572.

_______, 1974. Sedimentary and tectonic processes in the Bengal deep-sea fan and geosyncline. *In* Burk, C. A., and Drake, C. L. (Eds.), *The Geology of Continental Margins:* New York (Springer-Verlag), 617-627.

Curray, J. R., and Munasinghe, T., 1989. Timing of deformation, northeastern Indian Ocean. *Earth Planet. Sci. Lett.*, 94:71–79.

Das, B., and Patel, N. P., 1984. Nature of Narmada-Son lineament. *J. Geol. Soc. India*, 25:267–276.

Dasgupta, S., Mukhopadhyay, M., and Nandy, D. R., 1987. Active transverse features in the central portion of the Himalaya. *Tectonophysics*, 136:255–264.

Davies, H. L., Sun, S.-S., Frey, F. A., Gautier, I., McCulloch, M. T., Price, R. C., Bassias, Y., Klootwijk, C. T., and Leclaire, L., 1989. Basalt basement from the Kerguelen Plateau and the trail of the Dupal plume. *Contrib. Mineral. Petrol.*, 103:457–469.

De, A., 1981. Late Mesozoic–lower Tertiary magma types of Kutch and Saurashtra. *In* Subbarao, K. V., and Sukheswala, R. N. (Eds.), *Deccan Volcanism and Related Basalt Provinces in Other Parts of the World.* Mem. Geol. Surv. India, 3:327–339.

Debon, F., LeFort, P., Doubel, D., Sonet, J., and Zimmermann, J. L., 1987. Granites of the Western Karakorum and Northern Kohistan (Pakistan): a composite Mid-Cretaceous to Upper Cenozoic magmatism. *Lithos*, 20:19–40.

Debon, F., LeFort, P., Sheppard, S.M.F., and Sonet, J., 1986a. The four plutonic belts of the Transhimalaya-Himalaya: a chemical, mineralogical, isotopic and chronological synthesis along the Tibet-Nepal section. *J. Petrol.*, 27:219–250.

Debon, F., LeFort, P., and Sonet, J., 1981. Granitoid belts west and south of Tibet: about their geochemical trends and Rb-Sr isotopic studies. *In* Liu Dong-sheng (Ed.), *Geology, Geological History and Origin of the Qinghai-Xizang Plateau:* Beijing (Science Press), 395–405.

Debon, F., Zimmermann, J. L., and Bertrand, J.-M., 1986b. Le granite du Baltoro (batholite axial du Karakorum), nord Pakistan: une intrusion subalcalin d'âge Miocène Supérieur. *C. R. Acad. Sci. Paris*, 303:463-468.

Debon, F., Zimmermann, J. L., Liu Guohue, Jin Chengwei, and Xu Ronghua, 1985. Time relationships between magmatism, tectonics and metamorphism in three plutonic belts in Southern Tibet: new K-Ar data. *Geol. Rundsch.*, 74:229–236.

deMenocal, P., Bloemendal, J., and King, J., in press. A rock-magnetic record of monsoonal dust deposition to the Arabian Sea: evidence for a shift in the mode of deposition at 2.4 Ma. *In* Prell, W. L., Niitsuma, N., et al., *Proc. ODP, Sci. Results*, 117: College Station, TX (Ocean Drilling Program).

DeMets, C., Gordon, R. G., and Argus, D. F., 1988. Intraplate deformation and closure of the Australia-Antarctica-Africa plate circuit. *J. Geophys. Res.*, 93:11877–11897.

DeMets, C., Gordon, R. G., Argus, D. F., and Stein, S., 1990. Current plate motions. *Geophys. J. Int.*, 101:425–478.

Deniel, C., Vidal, P., Fernandez, A., LeFort, P., and Peucat, J.-J., 1987. Isotopic study of the Manaslu granite (Himalaya, Nepal): inferences on the age and source of Himalayan leucogranites. *Contrib. Mineral. Petrol.*, 96:78–92.

Deshmukh, S. S., and Sehgal, M. N., 1988. Mafic dyke swarms in Deccan Volcanic Province of Madhya Pradesh and Maharashtra. *In* Subbarao, K. V. (Ed.), *Deccan Flood Basalts*. Mem. Geol. Soc. India, 10:323–340.

Devey, C. W., and Lightfood, P. C., 1986. Volcanological and tectonic control of stratigraphy and structure in the western Deccan Traps. *Bull. Volcanol.*, 48:195–207.

Duncan, R. A., 1978. Geochronology of basalts from the Ninetyeast Ridge and continental dispersion in the eastern Indian Ocean. *J. Volcanol. Geotherm. Res.*, 4:283–305.

_______, 1981. Hotspots in the southern oceans—an absolute frame of reference for motion of the Gondwana continents. *Tectonophysics*, 74:29–42.

Duncan, R. A., Backman, J., Peterson, L., and Shipboard Scientific Party, 1989. Réunion hotspot activity through Tertiary time: initial results from the Ocean Drilling Program, Leg 115. *J. Volcanol. Geotherm. Res.*, 36:193–198.

Duncan, R. A., and Pyle, D. G., 1988a. Rapid eruption of the Deccan flood basalts at the Cretaceous/Tertiary boundary. *Nature*, 333:841–843.

_______, 1988b. Rapid eruption of the Deccan flood basalts, western India. *In* Subbarao, K. V. (Ed.), *Deccan Flood Basalts*. Mem. Geol. Soc. India, 10:1–9.

Embleton, B.J.J., 1981. A review of the paleomagnetism of Australia and Antarctica. *In* McElhinny, M. W., and Valencio, D. A. (Eds.), *Paleo-*

reconstruction of the Continents. Am. Geophys. Union Geodyn. Ser., 2:77–92.

Ferrara, G., Lombardo, B., and Tonarini, S., 1983. Rb/Sr geochronology of granites and gneisses from the Mount Everest region, Nepal Himalaya. *Geol. Rundsch.,* 72:119–136.

Fisher, R. A., 1953. Dispersion on a sphere. *Proc. R. Soc. London A,* 217:295–305.

Fisher, R. L., and Sclater, J. G., 1983. Tectonic evolution of the Southwest Indian Ocean since the Mid-Cretaceous: plate motions and stability of the pole of Antarctica/Africa for at least 80 Myr. *Geophys. J. R. Astron. Soc.,* 73:553–576.

Fort, M., Freytet, P., and Colchen, M., 1981. The structural and sedimentological evolution of the Thakkhola-Mustang Graben (Nepal Himalaya) in relation to the uplift of the Himalayan Range. *In* Liu Dong-Sheng (Ed.), *Geology, Geological History and Origin of the Qinghai-Xizang Plateau,* Beijing (Science Press), 305–313.

_______, 1982. Structural and sedimentological evolution of the Thakkhola Graben (Nepal Himalayas). *Z. Geomorph. Suppl.,* 42:75–98.

Gallet, Y., Weeks, R., Vandamme, D., and Courtillot, V., 1989. Duration of the Deccan Trap volcanism: a statistical approach. *Earth Planet. Sci. Lett.,* 93:273–282.

Gansser, A., 1964. *The Geology of the Himalayas:* New York (Wiley).

_______, 1981. The geodynamic history of the Himalaya. *In* Gupta, H. K., and Delany, F. M. (Eds.), *Zagros, Hindu Kush, Himalaya Geodynamic Evolution:* Am. Geophys. Union Geodyn. Ser., 3:111–121.

Garzanti, E., Baud, A., and Mascle, G., 1987. Sedimentary record of the northward flight of India and its collision with Eurasia (Ladakh Himalaya, India). *Geodin. Acta (Paris),* 1:297–312.

Gautam, P., 1989. Multi-component remanent magnetization in the Aulis Volcanics, the Lesser Himalaya, Nepal. *J. Geomagn. Geoelectr.,* 41:101–117.

Gautam, P., and Yoshida, M., 1988. On the secondary magnetization observed in the Nawakot Complex rocks, Malekhu area, Central Nepal. *J. Nepal Geol. Soc.,* 5:1–10.

Gee, E. R., 1989. Overview of the geology and structure of the Salt Range, with observations on related areas of northern Pakistan. *In* Malinconico, L. L., Jr., and Lillie, R. J. (Eds.), *Tectonics of the Western Himalayas.* Spec. Pap. Geol. Soc. Am., 232:95–112.

Geller, C. A., Weissel, J. K., and Anderson, R. N., 1983. Heat transfer and intraplate deformation in the Central Indian Ocean. *J. Geophys. Res.,* 88:1018–1032.

Giddings, J. W., 1984. A plotting and interactive graphics package for HP-graphics terminals. *Internal Rep. BMR Palaeomagnetic Group.*

_______, 1985. The palaeomagnetic processing system in the BMR: user's guide. *Internal Rep. BMR Palaeomagnetic Group.*

Giddings, J. W., Klootwijk, C. T., and Percival, P. J., 1985. PALDAS: an integrated data acquisition system for the Black Mountain Palaeomagnetic Laboratory. *Internal Rep. BMR Palaeomagnetic Group.*

Gordon, R. G., DeMets, C., and Argus, D. F., 1990. Kinematic constraints on distributed lithospheric deformation in the equatorial Indian Ocean from present motion between the Australian and Indian plates. *Tectonics,* 9:409–422.

Graup, G., and Spettel, B., 1989. Mineralogy and phase-chemistry of an Ir-enriched pre-K/T layer from the Lattengebirge, Bavarian Alps and significance for the KTB problem. Earth Planet. Sci. Lett., 95:271–290.

Griffiths, R. W., and Campbell, I. H., 1990. Stirring and structure in mantle starting plumes. *Earth Planet. Sci. Lett.,* 99:66–78.

Guo, S., 1981. On the elevation and climatic changes of the Qinghai-Xizang Plateau based on fossil angiosperms. *In* Liu Dong-sheng (Ed.), *Geology, Geological History and Origin of the Qinghai-Xizang Plateau:* Beijing (Science Press), 201–206.

Hailwood, E. A., Stumpp, C., and Zukin, J., 1989. Soft sediment sampling errors in palaeomagnetic and magnetic fabric data. *Bull. Int. Assoc. Geomagn. Aeron.,* 53:199. (Abstract)

Hallam, A., 1984. Pre-Quaternary sea-level changes. *Annu. Rev. Earth Planet. Sci.,* 12:205–243.

_______, 1987. End-Cretaceous mass extinction event: argument for terrestrial cause. *Science,* 238:1237–1242.

Harland, W. B., Cox, A. V., Llewellyn, P. G., Pickton, C.A.G., Smith, D. G., and Walters, R., 1982. *A Geologic Time Scale:* Cambridge (Cambridge Univ. Press).

Harrison, C.G.A., and Lindh, T., 1982. Comparison between hot spot and geomagnetic field reference frames. *Nature,* 300:251–253.

Hodges, K. V., Hubbard, M. S., and Silverberg, D. S., 1988. Metamorphic constraints on the thermal evolution of the central Himalayan orogen. *Philos. Trans. R. Soc. London A,* 326:257–280.

Hooper, P. R., 1990. The timing of crustal extension and the eruption of continental flood basalts. *Nature,* 345:246–249.

Hsü, J., 1976. The palaeobotanical evidence for continental drift and Himalayan uplift. *The Palaeobotanist,* 25:131–145.

Hubbard, M. S., and Harrison, T. M., 1989. $^{40}Ar/^{39}Ar$ age constraints on deformation and metamorphism in the Main Central Thrust zone and Tibetan Slab, Eastern Nepal, Himalaya. *Tectonics,* 8:865–880.

Hut, P., Alvarez, W., Elder, W. P., Hansen, T., Kauffman, E. G., Keller, G., Shoemaker, E. M., and Weissman, P. R., 1987. Comet showers as a cause of mass extinctions. *Nature,* 329:118–126.

Idnurm, M., 1985. Late Mesozoic and Cenozoic palaeomagnetism of Australia—1. A redetermined apparent polar wander path. *Geophys. J. R. Astron. Soc.,* 83:399–418.

Ingersoll, R. V., and Suczek, C. A., 1979. Petrology and provenance of Neogene sand from Nicobar and Bengal fans, DSDP Sites 211 and 218. *J. Sediment. Petrol.,* 49:1217–1228.

Jaeger, J.-J., Courtillot, V., and Tapponnier, P., 1989. Paleontological view of the ages of the Deccan Traps, the Cretaceous/Tertiary boundary and the India-Asia collision. *Geology,* 17:316–319.

Jaeger, J.-J., and Rage, J.-C., 1990. Reply on "Paleontological view of the ages of the Deccan Traps, the Cretaceous/Tertiary boundary, and the India-Asia collision." *Geology,* 18:186–188.

Johnson, B. D., Powell, C. McA., and Veevers, J. J., 1976. Spreading history of the eastern Indian Ocean and Greater India's northward flight from Antarctica and Australia. *Geol. Soc. Am. Bull.,* 87:1560–1566.

_______, 1980. Early spreading history of the Indian Ocean between India and Australia. *Earth Planet. Sci. Lett.,* 47:131–143.

Johnson, G. D., Opdyke, N. D., Tandon, S. K., and Nanda, A. C., 1983. The magnetic polarity stratigraphy of the Siwalik Group at Haritalyangar (India) and a new last appearance datum for Ramapithecus and Sirapithecus in Asia. *Palaeogeogr., Palaeoclimatol., Palaeoecol.,* 44:223–249.

Johnson, G. D., Raynolds, R.G.H., and Burbank, D. W., 1986. Late Cenozoic tectonics and sedimentation in the northwestern Himalayan foredeep: I. Thrust ramping and associated deformation in the Potwar region. *In* Allen, P., and Homewood, P. (Eds.), *Foreland Basins.* Spec. Publ. Int. Assoc. Sedimentol., 8:273–291.

Johnson, N. M., Opdyke, N. P., Johnson, G. D., Lindsay, E. H., and Tahirkheli, R.A.K., 1982. A time framework based on magnetostratigraphy for the Siwaliks sediments of the Khaur area (Peshawar, Pakistan). *Palaeogeogr., Palaeoclimatol., Palaeoecol.,* 37:17–42.

Johnson, N. M., Stix, J., Tauxe, L., Cerveny, P. E., and Tahirkheli, R.A.K., 1985. Paleomagnetic chronology, fluvial processes and tectonic implications of the Siwalik deposits near Chinji village, Pakistan. *J. Geol.,* 93:27–40.

Kaila, K. L., 1988. Mapping the thickness of Deccan Trap flows in India from DSS studies and inferences about a hidden Mesozoic basin in the Narmada-Tapti region. *In* Subbarao, K. V. (Ed.), *Deccan Flood Basalts.* Mem. Geol. Soc. India, 10:91–116.

Kaila, K. L., Murty, P.R.K., and Mall, D. M., 1989. The evolution of the Vindhyan basin vis-à-vis the Narmada-Son lineament, central India, from deep seismic soundings. *Tectonophysics,* 162:277–289.

Kaila, K. L., Reddy, P. R., Dixit, M. M., and Rao, P. K., 1985. Crustal structure across the Narmada-Son lineament, Central India from deep seismic soundings. *J. Geol. Soc. India,* 26:465–480.

Kaneoka, I., and Kono, M., 1981. $^{40}Ar/^{39}Ar$ dating of Himalayan rocks from the Mount Everest region. *J. Geophys.,* 49:207–211.

Keller, G., 1989. Extended period of extinctions across the Cretaceous/Tertiary boundary in planktonic foraminifera of continental-shelf sections: implications for impact and volcanism theories. *Geol. Soc. Am. Bull.,* 101:1408–1419.

Keller, G., and Lindinger, M., 1989. Stable isotope, TOC and $CaCO_3$ record across the Cretaceous/Tertiary boundary at El Kef, Tunisia. *Palaeogeogr., Palaeoclimatol., Palaeoecol.,* 73:243–265.

Kent, D. V., and Gradstein, F. M., 1986. A Jurassic to Recent chronology. *In* Tucholke, B. E., and Vogt, P. R. (Eds.), *The Geology of North America: The Western Atlantic Region.* Geol. Soc. Am. DNAG Ser., 1:45–50.

Kirschvink, J. L., 1980. The least-squares line and plane analysis of palaeomagnetic data. *Geophys. J. R. Astron. Soc.,* 62:699–718.

Klootwijk, C. T., 1971. Palaeomagnetism of the Upper Gondwana–Rajmahal Traps, northeast India. *Tectonophysics,* 12:449–467.

_______, 1974. Palaeomagnetic results on a doleritic sill of Deccan Trap age in the Sonhat coal basin, India. *Tectonophysics,* 22:335–353.

_______, 1979. A review of palaeomagnetic data from the Indo-Pakistani fragment of Gondwanaland. *In* Farah, A., and DeJong, K. A. (Eds.), *Geodynamics of Pakistan.* Geol. Surv. Pakistan, 41–80.

_______, 1984. A review of Indian Phanerozoic palaeomagnetism: implications for the India-Asia collision. *Tectonophysics,* 105:331–353.

Klootwijk, C. T., and Bingham, D. K., 1980. The extent of Greater India III. Palaeomagnetic data from the Tibetan Sedimentary Series, Thakkhola Region, Nepal Himalaya. *Earth Planet. Sci. Lett.,* 51:381–405.

Klootwijk, C. T., Conaghan, P. J., and Powell, C. McA., 1985. The Himalayan Arc: large-scale continental subduction, oroclinal bending and back-arc spreading. *Earth Planet. Sci. Lett.,* 75:167–183.

Klootwijk, C. T., Nazirullah, R., and DeJong, K. A., 1986a. Palaeomagnetic constraints on formation of the Mianwali reentrant, Trans-Indus and Western Salt Range, Pakistan. *Earth Planet. Sci. Lett.,* 80:394–414.

Klootwijk, C. T., Nazirullah, R., DeJong, K. A., and Ahmed, A., 1981. A palaeomagnetic reconnaissance of northeastern Baluchistan, Pakistan. *J. Geophys. Res.,* 86:289–306.

Klootwijk, C. T., Sharma, M. L., Gergan, J., Shah, S. K., and Gupta, B. K., 1986b. Rotational overthrusting of the northwestern Himalaya: further palaeomagnetic evidence from the Riasi thrust sheet, Jammu foothills, India. *Earth Planet. Sci. Lett.,* 80:375–393.

Klootwijk, C. T., Sharma, M. L., Gergan, J., Shah, S. K., and Tirkey, B., 1984. The Indus-Tsangpo suture zone in Ladakh, northwest Himalaya: further palaeomagnetic data and implications. *Tectonophysics,* 106:215–238.

Kong Zhao-chen, and Du Nai-gin, 1981. Preliminary study on the vegetation of the Qinghai-Xizang Plateau during Neogene and Quaternary periods. *In* Liu Dong-sheng (Ed.), *Geology, Geological History and Origin of the Qinghai-Xizang Plateau:* Beijing (Science Press), 239-246.

LeFort, P., 1975. Himalaya: the collided range. Present knowledge of the continental arc. *Am. J. Sci.,* 275A:1–44.

_______, 1986. Metamorphism and magmatism during the Himalayan collision. *In* Coward, M. P., and Ries, A. C. (Eds.), *Collision Tectonics.* Geol. Soc. London Spec. Publ., 19:159–172.

_______, 1988. Granites in the tectonic evolution of the Himalaya, Karakorum and southern Tibet. *Philos. Trans. R. Soc. London A,* 326:281–299.

_______, 1989. The Himalayan orogenic segment. *In* Sengör, A.M.C. (Ed.), *Tectonic Evolution of the Tethyan Region,* NATO ASI Ser. C, 259:289–386.

LeFort, P., Cuney, M., Deniel, C., France-Lanord, C., Sheppard, S.M.F., Upreti, B. N., and Vidal, P., 1987. Crustal generation of the Himalayan leucogranites. *Tectonophysics,* 134:39–57.

LeFort, P., France-Lanord, C., and Pecher, A., 1989. Granites of the Himalayan collision: 1. Petrological constraints. *Terra Abstr.,* 1:173.

Levchencko, O. V., 1989. Tectonic aspects of intraplate seismicity in the northeastern Indian Ocean. *Tectonophysics,* 170:125–139.

Li Ji-jun, Li Bing-yuan, Wang Fu-bao, Zhang Qing-song, Wen Shi-xuan, and Zhen Ben-xing, 1981. The process of the uplift of the Qinghai-Xizang Plateau. *In* Liu Dong-sheng (Ed.), *Geology, Geological History and Origin of the Qinghai-Xizang Plateau:* Beijing (Science Press), 111–118.

Lillie, R. J., Baker, D. M., Yeats, R. S., Johnson, G. D., Yousaf, M., and Zaman, A.S.H., 1989. Reply on "Development of the Himalayan frontal thrust zone: Salt Range, Pakistan." *Geology,* 17:378–380.

Lin Jinlu, and Watts, D. R., 1988a. Palaeomagnetic constraints on Himalayan-Tibetan evolution. Philos. Trans. R. Soc. London A, 326:177–188.

_______, 1988b. Palaeomagnetic results from the Tibetan Plateau. *Philos. Trans. R. Soc. London A,* 327:239–262.

Lindsay, J. F., Holliday, D. W., and Hulbert, A. G., in press. Sequence stratigraphy and the early evolution of the Ganges-Brahmaputra delta complex. *AAPG Bull.*

Livermore, R. A., Vine, F. J., and Smith, A. G., 1983. Plate motions and the geomagnetic field. I. Quaternary and late Tertiary. *Geophys. J. R. Astron. Soc.,* 73:153–171.

_______, 1984. Plate motions and the geomagnetic field. II. Jurassic to Tertiary. *Geophys. J. R. Astron. Soc.,* 79:939–961.

Løvlie, R., Markussen, B., Sejrup, H. P., and Thiede, J., 1986. Magnetostratigraphy in three Arctic Ocean sediment cores: arguments for geomagnetic excursions within oxygen-isotope stage 2-3. *Phys. Earth Planet. Inter.,* 43:173–184.

Luyendyk, B. P., 1974. Gondwanaland dispersal and the early formation of the Indian Ocean. *In* Davies, T. A., Luyendyk, B. P., et al., *Init. Repts. DSDP,* 26: Washington (U.S. Govt. Printing Office), 945–952.

Luyendyk, B. P., and Davies, T. A., 1974. Results of DSDP Leg 26 and the geologic history of the Southern Indian Ocean. *In* Davies, T. A., Luyendyk, B. P., et al., *Init. Repts. DSDP,* 26: Washington (U.S. Govt. Printing Office), 909–943.

Luyendyk, B. P., and Rennick, W., 1977. Tectonic history of aseismic ridges in the eastern Indian Ocean. *Geol. Soc. Am. Bull.,* 88:1347–1356.

Mahoney, J. J., 1988. Deccan Traps. *In* Macdougall, J. D. (Ed.), *Continental Flood Basalts:* Dordrecht (Kluwer Academic Publishers), 151-194.

Mahoney, J. J., Macdougall, J. D., Lugmair, G. W., and Gopalan, K., 1983. Kerguelen hotspot source for Rajmahal Traps and Ninetyeast Ridge? *Nature,* 303:385–389.

Maluski, H., Matte, P., Brunel, M., and Xusheng Xiao, 1988. Argon 39–Argon 40 dating of metamorphic and plutonic events in the North and High Himalaya belts (Southern Tibet–China). Tectonics, 7:299–326.

Maluski, H., Proust, F., and Xiao, X. C., 1982. $^{39}Ar/^{40}Ar$ dating of the trans-Himalaya calc-alkaline magmatism of southern Tibet. *Nature,* 298:152–154.

Mascle, G., and Hérail, G., 1982. Les Siwaliks: le prisme d'accrétion tectonique associé à la subduction intracontinentale himalayènne. *Geol. Alp.,* 58:95–103.

Mattauer, M., 1986. Intracontinental subduction, crust-mantle décollement and crustal-stacking wedge in the Himalayas and other collision belts. *In* Coward, M. P., and Ries, A. C. (Eds.), *Collision Tectonics.* Geol. Soc. London Spec. Publ., 19:37–50.

McElhinny, M. W., Luck, G. R., and Edwards, D., 1971. A large-volume magnetic field-free space for thermal demagnetisation and other experiments in palaeomagnetism. *Pure Appl. Geophys.,* 90:126–130.

McFadden, P. L., and Reid, A. B., 1982. Analysis of palaeomagnetic inclination data. *Geophys. J. R. Astron. Soc.,* 69:307–319.

McKenzie, D., and Sclater, J. G., 1971. The evolution of the Indian Ocean since the Late Cretaceous. *Geophys. J. R. Astron. Soc.,* 25:437–528.

McLean, D. M., 1982. Deccan volcanism: the Cretaceous-Tertiary marine boundary timing event. *Eos, Trans. Am. Geophys. Union,* 63:562.

_______, 1985. Mantle degassing induced dead ocean in the Cretaceous-Tertiary transition. *In* Sundquist, E. T., and Broecker, W. S. (Eds.), *The Carbon Cycle and Atmospheric CO_2: Natural Variations Archean to Present.* Am. Geophys. Union Monogr., 32:493–503.

Mercier, J.-L., Armijo, R., Tapponnier, P., Carey-Gailhardis, E., and Han, T. L., 1987. Change from late Tertiary compression to Quaternary extension in Southern Tibet during the India-Asia collision. *Tectonics,* 6:275–304.

Merrill, R. T., and McElhinny, M. W., 1983. *The Earth's Magnetic Field: Its History, Origin and Planetary Perspective:* London (Academic Press).

Merrill, R. T., and McFadden, P. L., in press. Paleomagnetism and the nature of the Geodynamo. *Science.*

Merrill, R. T., McFadden, P. L., and McElhinny, M. W., in press. Paleomagnetic tomography of the core-mantle boundary. *Phys. Earth Planet. Inter.*

Miller, K. G., Janecek, T. R., Katz, M. E., and Keil, D. J., 1987. Abyssal circulation and benthic foraminiferal changes near the Paleocene/Eocene boundary. *Paleoceanography,* 2:741–761.

Mishra, D. C., 1977. Possible extensions of the Narmada-Son lineament towards Murray Ridge (Arabian Sea) and the eastern syntaxial bend of the Himalayas. *Earth Planet. Sci. Lett.,* 36:301–308.

Misra, K. S., 1981. The tectonic setting of Deccan Volcanics in southern Saurashtra and northern Gujarat. *In* Subbarao, K. V., and Sukheswala, R. N. (Eds.), *Deccan Volcanism and Related Flood Basalt Provinces in Other Parts of the World.* Mem. Geol. Surv. India, 3:81–86.

Mitchell, C., and Cox, K. G., 1988. A geological sketch map of the southern part of the Deccan Province. *In* Subbarao, K. V. (Ed.), *Deccan Flood Basalts,* Mem. Geol. Soc. India, 10:27–33.

Molnar, P., and Lyon-Caen, H., 1989. Fault plane solutions of earthquakes and active tectonics of the Tibetan Plateau and its margins. *Geophys. J. Int.*, 99:123–153.

Molnar, P., Pardo-Casas, F., and Stock, J., 1988. The Cenozoic and Late Cretaceous evolution of the Indian Ocean Basin: uncertainties in the reconstructed positions of the Indian, African and Antarctic plates. *Basin Res.*, 1:23–40.

Molnar, P., and Tapponnier, P., 1975. Cenozoic tectonics of Asia: effects of a continental collision. *Science*, 189:419–426.

_______, 1977. Relation of the tectonics of eastern China to the India-Eurasia collision: application of slip-line field theory to large-scale continental tectonics. *Geology*, 5:212–216.

_______, 1978. Active tectonics of China. *J. Geophys. Res.*, 83:5361–5375.

Moore, D. G., Curray, J. R., Raitt, R. W., and Emmel, F. J., 1974. Stratigraphic-seismic section correlation and implications to Bengal Fan history. *In* von der Borch, C. C., Sclater, J. G., et al., *Init. Repts. DSDP*, 22: Washington (U.S. Govt. Printing Office), 403–412.

Morgan, W. J., 1981. Hotspot tracks and the opening of the Atlantic and Indian oceans. *In* Emiliani, C. (Ed.), *The Sea* (vol. 7): New York (Wiley), 443–487.

_______, 1983. Hotspot tracks and the early rifting of the Atlantic. *Tectonophysics*, 94:123–139.

Murray, D. W., and Prell, W. L., in press. Pliocene to Pleistocene variations in calcium carbonate, organic carbon, and opal on the Owen Ridge, northern Arabian Sea. *In* Prell, W. L., Niitsuma, N., et al., *Proc. ODP, Sci. Results, 117: College Station, TX (Ocean Drilling Program).*

Murthy, T.V.V.G.R.K., and Mishra, S. K., 1981. The Narmada-Son lineament and the structure of the Narmada rift system. *J. Geol. Soc. India*, 22:112–120.

Naqvi, S. M., Rao, V. D, and Narain, H., 1974. The protocontinental growth of the Indian shield and the antiquity of its rift valleys. *Precambrian Res.*, 1:345–398.

Neprochnov, Y. P., Levchenko, O. V., Merklin, L. R., and Sedov, V. V., 1988. The structure and tectonics of the intraplate deformation area in the Indian Ocean. *Tectonophysics*, 156:89–106.

Nicora, A., Garzenti, E., and Fois, E., 1987. Evolution of the Tethys Himalaya continental shelf during Maastrichtian to Paleocene (Zanskar, India). *Riv. Ital. Paleontol. Strat.*, 92:439–496.

Norton, I. O., and Sclater, J. G., 1979. A model for the evolution of the Indian Ocean and the breakup of Gondwanaland. *J. Geophys. Res.*, 84:6803–6830.

Officer, C. B., and Drake, C. L., 1983. The Cretaceous-Tertiary transition. *Science*, 219:1383–1390.

_______, 1985. Terminal Cretaceous environmental events. *Science*, 227:1161–1167.

Officer, C. B., Hallam, A., Drake, C. L., and Devine, J. D., 1987. Late Cretaceous and paroxysmal Cretaceous/Tertiary extinctions. *Nature*, 362:143–149.

Otofuji, Y.-I., Funahara, S., Matsuo, J., Murata, F., Nishiyama, T., Zheng, X., and Yaskawa, K., 1989. Paleomagnetic study of western Tibet: deformation of a narrow zone along the Indus Zangbo suture between India and Asia. *Earth Planet. Sci. Lett.*, 92:307–316.

Parrish, R. R., and Tirrul, R., 1989. U-Pb age of the Baltoro granite, northwest Himalaya, and implications for monazite U-Pb systematics. *Geology*, 17:1076–1079.

Patriat, P., 1983. Reconstruction de l'évolution du système de dorsales de l'Océan Indien par les méthodes de la cinématique des plaques [Thèse d'état]. Univ. de Paris 7.

Patriat, P., and Achache, J., 1984. India-Asia collision chronology has implications for crustal shortening and driving mechanism of plates. *Nature*, 311:615–621.

Patriat, P., and Ségoufin, J., 1988. Reconstruction of the Central Indian Ocean. *Tectonophysics*, 155:211–234.

Patriat, P., Ségoufin, J., Schlich, R., Goslin, J., Auzende, J.-M., Beuzart, P., Bonnin, J., and Olivet, J.-L., 1982. Les mouvements rélatifs de l'Inde, de l'Afrique et de l'Eurasie. *Bull. Soc. Geol. Fr.*, 24:363–373.

Pearce, J., and Mei Houjun, 1988. Volcanic rocks of the 1985 Tibet geotraverse: Lhasa to Golmud. *Philos. Trans. R. Soc. London A*, 327:169–201.

Pearce, J. A., Deng Wanming, Oliver, R. A., Coulon, C., and Keyser, K., 1989. Geochemistry and tectonic significance of post-collision volcanism in Tibet. *Terra Abstr.*, 1:175.

Pêcher, A., and Bouchez, J. L., 1987. High temperature decoupling between the Higher Himalaya crystalline and its sedimentary cover. *Terra Cogn.*, 7:110.

Peirce, J., Weissel, J., et al., 1989. *Proc. ODP, Init. Repts.*, 121: College Station TX (Ocean Drilling Program).

Peirce, J. W., 1976. Assessing the reliability of DSDP paleolatitudes. *J. Geophys. Res.*, 81:4173–4187.

_______, 1978. The northward motion of India since the Late Cretaceous. *Geophys. J. R. Astron. Soc.*, 52:277–311.

Peirce, J. W., Denham, C. R., and Luyendyk, B. P., 1974. Paleomagnetic results of basalt samples from DSDP Leg 26, Southern Indian Ocean. *In* Luyendyk, B. P., Davies, T. A., et al., *Init. Repts. DSDP*, 26: Washington (U.S. Govt. Printing Office), 517–527.

Peltzer, G., Tapponnier, P., and Cobbold, P., 1982. Les grands décrochements de l'Est Asiatique: évolution dans le temps et comparaison avec un modèle expérimental. *C. R. Acad. Sci. Ser. 2*, 294:1341–1348.

Pennock, E. S., Lillie, R. J., Zaman, A.S.H., and Yousaf, M., 1989. Structural interpretation of seismic reflection data from Eastern Salt Range and Potwar Plateau, Pakistan. *AAPG Bull.*, 73:841–857.

Petroy, D. E., and Wiens, D. A., 1989. Historical seismicity and implications for diffuse plate convergence in the Northeast Indian Ocean. *J. Geophys. Res.*, 94:12301–12319.

Pimm, A. C., McGowran, B., and Gartner, S., 1974. Early sinking history of Ninetyeast Ridge, northeastern Indian Ocean. *Geol. Soc. Am. Bull.*, 85:1219–1224.

Pimm, A. C., and Sclater, J. G., 1974. Early Tertiary hiatuses in the north-eastern Indian Ocean. *Nature*, 252:362–365.

Poornachandra Rao, G.V.S., and Bhalla, M. S., 1981. Palaeomagnetism of Dhar traps and drift of the subcontinent during the Deccan volcanism. *Geophys. J. R. Astron. Soc.*, 65:155–164.

Powar, K. B., 1981. Lineament fabric and dyke pattern in the western part of the Deccan Volcanic Province. *In* Subharao, K. V., and Sukheswala, R. N., *Deccan Volcanism and Related Basalt Provinces in Other Parts of the World*. Mem. Geol. Soc. India, 3:45–57.

Powell, C. McA., 1979. A speculative tectonic history of Pakistan and surroundings: some constraints from the Indian Ocean. *In* Farah, A., and DeJong, K. A. (Eds.), *Geodynamics of Pakistan*. Geol. Surv. Pakistan, 5–24.

_______, 1986. Continental underplating model for the rise of the Tibetan Plateau. *Earth Planet. Sci. Lett.*, 81:79–94.

Powell, C. McA., and Conaghan, P. J., 1973. Plate tectonics and the Himalayas. *Earth Planet. Sci. Lett.*, 20:1–12.

_______, 1975. Tectonic models of the Tibetan Plateau. *Geology*, 3:727-731.

Powell, C. McA., Roots, S. R., and Veevers, J. J., 1988. Pre-breakup continental extension in East Gondwanaland and the early opening of the eastern Indian Ocean. *Tectonophysics*, 155:261–283.

Pozzi, J.-P., Westphal, M., Yao Xiu Zhou, Li Sheng Xing, and Xiam Yao Chen, 1982. Position of the Lhasa block, South Tibet, during the Late Cretaceous. *Nature*, 297:319–321.

Prasad, G.V.R., and Sahni, A., 1988. First Cretaceous mammal from India. *Nature*, 332:638–640.

Quade, J., Cerling, T. E., and Bowman, J. R., 1989. Development of Asian monsoon revealed by marked ecological shift during latest Miocene in northern Pakistan. *Nature*, 342:163–166.

Rage, J.-C., 1988. Gondwana, Tethys, and terrestrial vertebrates during the Mesozoic and Cainozoic. *In* Audley-Charles, M. G., and Hallam, A. (Eds.), *Gondwana and Tethys*. Geol. Soc. Spec. Publ. London, 37:255–273.

Ramanathan, S., 1981. Some aspects of Deccan Volcanism of western Indian shelf and Cambay Basin. *In* Subbarao, K. V., and Sukheswala, R. N. (Eds.), *Deccan Volcanism and Related Basalt Provinces in Other Parts of the World*. Mem. Geol. Surv. India, 3:198–217.

Ramsay, J. G., 1988. General discussion. *Philos. Trans. R. Soc. London A*, 326:321.

Rao, A., and Rao, P. S., 1963. Outline of the magnetisation of the Deccan Traps of the Lower Godavari Valley. *In Proceedings Seminar on Geophysical Investigations in the Peninsular Shield*. Osmania Univ., Hyderabad, 65–74.

Raynolds, R.G.H., 1981. Did the ancestral Indus flow into the Ganges drainage? *Geol. Bull. Univ. Peshawar*, 14:141–150.

Rex, A. J., Searle, M. P., Tirrul, R., Crawford, M. B., Prior, D. J., Rex, D. C., and Barnicoat, A., 1988. The geochemical and tectonic evolution of the central Karakorum, North Pakistan. *Philos. Trans. R. Soc. London A*, 326:229–255.

Richards, M. A., Duncan, R. A., and Courtillot, V. E., 1989. Flood basalts and hot-spot tracks: plume heads and trails. *Science*, 246:103–107.

Robertson, W. A., 1963. The palaeomagnetism of some Mesozoic intrusives and tuffs from eastern Australia. J. Geophys. Res., 68:2299–2312.

Rothery, D. A., and Drury, S. A., 1984. The neotectonics of the Tibetan Plateau. *Tectonics*, 3:19–26.

Royer, J.-Y., Patriat, P., Bergh, H. W., and Scotese, C. R., 1988. Evolution of the Southwest Indian Ridge from the Late Cretaceous (anomaly 34) to the middle Eocene (anomaly 20). *Tectonophysics*, 155:235–260.

Royer, J.-Y. and Sandwell, D. T., 1989. Evolution of the Eastern Indian Ocean since the Late Cretaceous: constraints from Geosat altimetry. *J. Geophys. Res.*, 94:13755–13782.

Sager, W., and Bleil, U., 1987. Latitudinal shift of Pacific hotspots during the Late Cretaceous and early Tertiary. *Nature*, 326:488–490.

Sahni, A., 1989. Eurasiatic elements in Indian Cretaceous nonmarine biotas. *Terra Abstr.*, 1:253–254.

Sahni, A., Kumar, K., Hartenberger, J.-L., Jaeger, J.-J., Rage, J.-C., Sudre, J., and Vianey-Liaud, M., 1982. Microvertébrés nouveau des Trapps du Deccan (Inde): mise en évidence d'une voie de communication terrestre probable entre la Laurasie et l'Inde à la limite Crétacé-Tertiaire. *Bull. Soc. Geol. Fr.*, 24:1093–1099.

Sahni, A., Rana, R. S., and Prasad, G.V.R., 1985. New evidence for paleobiogeographic intercontinental Gondwana relationships based on Late Cretaceous–earliest Paleocene coastal faunas from peninsular India. *Am. Geophys. Union Geophys. Monogr.*, 32:207–218.

Saxena, M. N., 1986. Geodynamic synopsis of the Deccan Traps in relation to epochs of volcanic activity of the Indian shield, drift of the continent, and the tectonic development of Southern and Southeastern Asia. *J. Southeast. Asian Earth Sci.*, 1:205–213.

Schärer, U., 1984. The effect of initial ^{230}Th disequilibrium on young U-Pb ages: the Makalu case, Himalaya. *Earth Planet. Sci. Lett.*, 67:191–204.

Schärer, U., Copeland, P., Harrison, T. M., and Searle, M. P., 1990a. Age, cooling history and origin of post-collisional leucogranites in the Karakorum Batholith: a multi-system isotope study. J. Geol., 90:233251.

Schärer, U., Tapponnier, P., Lacassin, R., Leloup, P. H., Zhong Dalai, and Ji Shaocheng, 1990b. Intraplate tectonics in Asia: a precise age for large-scale Miocene movement along the Ailao Shan-Red River shear zone, China. *Earth Planet. Sci. Lett.*, 97:65–77.

Schärer, U., Xu, R. H., and Allègre, C. J., 1986. U-(Th)-Pb systematics and age of Himalayan leucogranites, south Tibet. *Earth Planet. Sci. Lett.*, 77:35–48.

Schmidt, P. W., 1976a. A new palaeomagnetic investigation of Mesozoic igneous rocks in Australia. *Tectonophysics*, 33:1–13.

_______, 1976b. The late Palaeozoic and Mesozoic palaeomagnetism of Australia [Ph.D. dissert.]. Australian National University, Canberra.

Schmidt, P. W., and Embleton, B.J.J., 1976. Palaeomagnetic results from sediments of the Perth Basin, Western Australia and their bearing on the timing of regional laterisation. *Palaeogeogr., Palaeoclimatol., Palaeoecol.*, 19:257–273.

Schmitz, B., 1987. The TiO_2/Al_2O_3 ratio in the Cenozoic Bengal abyssal fan sediments and its use as a paleostream energy indicator. *Mar. Geol.*, 76:195–206.

Schneider, D. A., and Kent, D. V., 1986. Influence of non-dipole field on determination of Plio-Pleistocene true polar wander. *Geophys. Res. Lett.*, 13:471–474.

_______, 1988a. Inclination anomalies from Indian Ocean sediments and the possibility of a standing non-dipole field. *J. Geophys. Res.*, 93:11621–11630.

_______, 1988b. The paleomagnetic field from equatorial deep-sea sediments: axial symmetry and polarity asymmetry. *Science*, 242:252256.

_______, 1990a. Paleomagnetism of Leg 115 sediments: implications for Neogene magnetostratigraphy and paleolatitude of the Réunion hotspot. *In* Duncan, R. A., Backman, J., Peterson, L. C., et al., *Proc. ODP, Sci. Results*, 115: College Station, TX (Ocean Drilling Program), 717–736.

_______, 1990b. The time-averaged paleomagnetic field. *Rev. Geophys.*, 28:71–96.

Sclater, J. G., and Fisher, R. L., 1974. Evolution of the east central Indian Ocean, with emphasis on the tectonic setting of the Ninetyeast Ridge. *Geol. Soc. Am. Bull.*, 85:683–702.

Searle, M. P., 1986. Structural evolution and sequence of thrusting in the High Himalayan, Tibetan-Tethys and Indus suture zones of Zanskar and Ladakh, Western Himalaya. *J. Struct. Geol.*, 8:923–936.

_______, 1988. Structural evolution and sequence of thrusting in the High Himalayan, Tibetan-Tethys and Indus Suture zones of Zanskar and Ladakh, Western Himalaya: reply. *J. Struct. Geol.*, 10:130–131.

Searle, M. P., Cooper, D.J.W., and Rex, A. J., 1988. Collision tectonics of the Ladakh-Zanskar Himalaya. *Philos. Trans. R. Soc. London A*, 326:117–150.

Searle, M. P., and Fryer, B. J., 1986. Garnet, tourmaline and muscovite-bearing leucogranites, gneisses and migmatites of the Higher Himalayas from Zanskar, Kulu, Lahoul and Kashmir. *In* Coward, M. P., and Ries, A. C. (Eds.), *Collision Tectonics*. Geol. Soc. Spec. Publ. London, 19:185–201.

Searle, M. P., Pickering, K. T., and Cooper, D.J.W., 1990. Restoration and evolution of the intermontane Indus Molasse Basin, Ladakh Himalaya, India. *Tectonophysics*, 174:301–314.

Searle, M. P., and Rex, A. J., 1989. Thermal model for the Zanskar Himalaya. *J. Metamorph. Geol.*, 7:127–134.

Searle, M. P., Rex, A. J., Tirrul, R., Rex, D. C., Barnicoat, A., and Windley, B. F., 1989. Metamorphic, magmatic, and tectonic evolution of the central Karakorum in the Biafo-Baltoro-Hushe regions of northern Pakistan. *In* Malinconico, L. L., Jr., and Lillie, L. L. (Eds.), *Tectonics of the Western Himalayas*, Spec. Pap. Geol. Soc. Am., 232:47–73.

Searle, M. P., Windley, B. F., Coward, M. P., Cooper, D.J.W., Rex, A. J., Rex, D., Li Tingdong, Xiao Xuchang, Jan, M. Q., Thakur, V. C., and Kumar, S., 1987. The closing of Tethys and the tectonics of the Himalaya. *Geol. Soc. Am. Bull.*, 98:678–701.

Seeber, L., Armbruster, J. G., and Quittmeyer, R. C., 1981. Seismicity and continental subduction in the Himalayan Arc. *In* Gupta, H. K., and Delaney, F. M. (Eds.), *Zagros-Hindukush-Himalaya*. Am. Geophys. Union Geodyn. Ser., 3:215–242.

Shackleton, R. M., and Chang Chen-fa, 1988. Cenozoic uplift and deformation of the Tibetan Plateau: the geomorphological evidence. *Philos. Trans. R. Soc. London A*, 327:365–377.

Shipboard Scientific Party, 1987. Site 650: Marsili Basin. *In* Kastens, K. A., Mascle, J., et al., *Proc. ODP, Init. Repts.*, 107: College Station, TX (Ocean Drilling Program), 129–286.

_______, 1988a. Introduction. *In* Backman, J., Duncan, R. A., et al., *Proc. ODP, Init. Repts.*, 115: College Station, TX (Ocean Drilling Program), 5–16.

_______, 1988b. Site 661. *In* Ruddiman, W., Sarnthein, M., Baldauf, J. et al., *Proc. ODP, Init. Repts.*, 108: College Station, TX (Ocean Drilling Program), 409–486.

_______, 1988c. Site 667. *In* Ruddiman, W., Sarnthein, M., Baldauf, J., et al., *Proc. ODP, Init. Repts.*, 108: College Station, TX (Ocean Drilling Program), 833–930.

_______, 1988d. Site 709. In Backman, J., Duncan, R. A., et al., Proc. ODP, Init. Repts., 115: College Station, TX (Ocean Drilling Program), 459–588.

_______, 1989a. Cretaceous/Tertiary boundary summary. *In* Peirce, J., Weissel, J., *Proc. ODP, Init. Repts.*, 121: College Station, TX (Ocean Drilling Program), 507–516.

_______, 1989b. Explanatory notes. *In* Peirce, J., Weissel, J., *Proc. ODP, Init. Repts.*, 121: College Station, TX (Ocean Drilling Program), 33–62.

_______, 1989c. Ninetyeast Ridge summary. *In* Peirce, J., Weissel, J., *Proc. ODP, Init. Repts.*, 121: College Station, TX (Ocean Drilling Program), 517–537.

_______, 1989d. ODP Leg 116 (Bengal Fan): explanatory notes. *In* Cochran, J. R., Stow, D.A.V., et al., *Proc. ODP, Init. Repts.*, 116: College Station, TX (Ocean Drilling Program), 13–28.

_______, 1989e. Site 717: Bengal Fan. *In* Cochran, J. R., Stow, D.A.V., et al., *Proc. ODP, Init. Repts.*, 116: College Station, TX (Ocean Drilling Program), 45–90.

_______, 1989f. Site 718: Bengal Fan. *In* Cochran, J. R., Stow, D.A.V., et al., *Proc. ODP, Init. Repts.*, 116: College Station, TX (Ocean Drilling Program), 91–154.

_______, 1989g. Site 719: Bengal Fan. *In* Cochran, J. R., Stow, D.A.V., et al., *Proc. ODP, Init. Repts.*, 116: College Station, TX (Ocean Drilling Program), 155–196.

_______, 1989h. Site 757. *In* Peirce, J., Weissel, J., *Proc. ODP, Init. Repts.*, 121: College Station, TX (Ocean Drilling Program), 305–358.

_______, 1989i. Site 758. *In* Peirce, J., Weissel, J., *Proc. ODP, Init. Repts.*, 121: College Station, TX (Ocean Drilling Program), 359–453.

Singh, J., and Bhalla, M. S., 1972. Preliminary palaeomagnetic studies on igneous rocks of U.P., Andrah Pradesh and Mysore. *Curr. Sci.*, 41:92–94.

Smit, J., 1982. Extinction and evolution of planktonic foraminifera after a major impact at the Cretaceous/Tertiary boundary. *Spec. Pap. Geol. Soc. Am.*, 190:329–352.

_______, 1990. Meteorite impact, extinctions and the Cretaceous-Tertiary boundary. *Geol. Mijnbouw*, 69:187–204.

Smit, J., and Hertogen, J., 1980. An extraterrestrial event at the Cretaceous Tertiary boundary. *Nature*, 285:198–200.

Smit, J., and Romein, A.J.T., 1985. A sequence of events across the Cretaceous-Tertiary boundary. *Earth Planet. Sci. Lett.*, 74:155–170.

Song Zhi-chen, and Liu Geng-Wu, 1981. Tertiary palynological assemblages from Xizang with reference to their paleogeographical significance. *In* Liu Dong-sheng (Ed.), *Geology, Geological History and Origin of the Qinghai-Xizang Plateau:* Beijing (Science Press), 207-214.

Srivastava, R. K., 1983. Temporal status of alkaline rocks of Deccan volcanic province and S.W. Rajasthan. *Geol. Mag.*, 120:303–304.

Staples, C., and Klootwijk, C. T., 1981. Palaeomagnetic results from the Gordon sub-group of Tasmania: further evidence for a Late Cretaceous magnetic overprint in southeastern Australia. *R. Soc. Tasmania*, 115:85–91.

Stephenson, A., 1976. A study of rotational remanent magnetization. *Geophys. J. R. Astron. Soc.*, 47:363–373.

_______, 1980a. Gyromagnetism and the remanence acquired by a rotating rock in an alternating field. *Nature*, 284:48–49.

_______, 1980b. Rotational remanent magnetization and the torque exerted on a rotating rock in an alternating magnetic field. *Geophys. J. R. Astron. Soc.*, 62:113–132.

Stern, C. R., Kligfield, R., Shelling, D., Virdi, N. S., Futa, K., Peterman, Z. E., and Amini, H., 1989. The Bhagirathi leucogranite of the High Himalaya (Garhwal, India): age, petrogenesis, and tectonic implications. *In* Malinconico, L. L., Jr., and Lillie, R. J. (Eds.), *Tectonics of the Western Himalayas*. Spec. Pap. Geol. Soc. Am., 232:33–45.

Stoddard, P. R., and Jurdy, D. M., 1988. Age estimation of the Deccan Traps from the North American apparent polar wander path. *Geology*, 16:296–298.

_______, 1989. Reply on "Age estimation of the Deccan Traps from the North American apparent polar wander path." *Geology*, 17:90–91.

Storey, M., Saunders, A. D., Tarney, J., Gibson, A. L., Norry, M. J., Thirwall, M. F., Leat, P., Thompson, R. N., and Menzies, M. A., 1989. Contamination of Indian Ocean asthenosphere by the Kerguelen-Heard mantle plume. *Nature*, 338:574–576.

Storey, M., Saunders, A. D., Tarney, J., Lear, P., Thirlwall, M. F., Thompson, R. N., Menzies, M. A., and Marriner, G. F., 1988. Geochemical evidence for plume-mantle interactions beneath Kerguelen and Heard Islands, Indian Ocean. *Nature*, 336:371–374.

Swaminath, J., Venkatesh, V., and Sundaram, R. K., 1964. Role of Precambrian lineaments in the evolution of Cenozoic festoons of the Indian subcontinent. *Proc. 22nd Int. Geol. Congr.*, 11:316–333.

Tapponnier, P., Lacassin, R., Leloup, P. H., Shärer, U., Zhong Dalai, Wu Haiwei, Liu Xiaohan, Ji Shaocheng, Zhang Lianshang, and Zhong Jiayou, 1990. The Ailao Shan/Red River metamorphic belt: Tertiary left-lateral shear between Indochina and South China. *Nature*, 343:431–437.

Tapponnier, P., Mercier, J. L., Proust, F., Andrieux, J., Armijo, R., Bassoullet, J. P., Brunel, M., Burg, J. P., Colchen, M., Dupré, B., Girardeau, J., Marcoux, J., Mascle, G., Matte, P., Nicolas, A., Li Tingdong, Xiao Xuchang, Chang Chen-fa, Lin Paoyu, Li Guangcen, Wang Naiwen, Chen Guoming, Han Tonglin, Wang Xibin, Den Wanming, Zhen Haixing, Sheng Huaibin, Cao Yongong, Zhou Ji, and Qiu Hingrong, 1981. The Tibetan side of the India-Eurasia collision. *Nature*, 294:405–410.

Tapponnier, P., and Molnar, P., 1976. Slip-line field theory and large-scale continental tectonics. *Nature*, 264:319–324.

_______, 1977. Active faulting and tectonics in China. *J. Geophys. Res.*, 82:2905-2930.

Tapponnier, P., Peltzer, G., and Armijo, R., 1986. On the mechanics of the collision between India and Asia. *In* Coward, M. P., and Ries, A. C. (Eds.), *Collision Tectonics*, Geol. Soc. Spec. Publ. London, 19:115–157.

Tapponnier, P., Peltzer, G., LeDain, A. Y., Armijo, R., and Cobbold, P., 1982. Propagating extrusion tectonics in Asia: new insights from simple experiments with plasticine. *Geology*, 10:611–616.

Thewissen, J.G.M., 1990. Comment on "Paleontological view of the ages of the Deccan Traps, the Cretaceous/Tertiary boundary, and the India-Asia collision." *Geology*, 18:185.

Thierstein, H. R., 1982. Terminal Cretaceous plankton extinctions: a critical assessment. *In* Silver, L. T., and Schultz, P. H. (Eds.), *Geological Implications of Impacts of Large Asteroids and Comets on the Earth*. Spec. Pap. Geol. Soc. Am., 190:385–405.

Thompson, R. W., 1974. Mineralogy of sands from the Bengal and Nicobar fans, Sites 218 and 211, Eastern Indian Ocean. *In* von der Borch, C. C., Sclater, J. G., et al. (Eds.), *Init. Repts. DSDP*, 22: Washington (U.S. Govt. Printing Office), 711–713.

Treloar, P. J., and Rex, D. C., 1990. Cooling and uplift histories of the crystalline thrust stock of the Indian plate internal zones west of Nanga Parbat, Pakistan Himalaya. *Tectonophysics*, 180:323–349.

Treloar, P. J., Rex, D. C., Guise, P. G., Coward, M. P., Searle, M. P., Windley, B. F., Petterson, M. G., Jan, M. Q., and Luff, I. W., 1989. K-Ar and Ar-Ar geochronology of the Himalayan collision in NW Pakistan: constraints on the timing of suturing, deformation, metamorphism and uplift. *Tectonics*, 8:881–909.

Vail, P. R., Mitchum, R. M., and Thompson, S., III, 1977. Seismic stratigraphy and global changes of sea level. Part 2: the depositional sequence as a basic unit for stratigraphic analysis. *In* Payton, C. E. (Ed.), *Seismic Stratigraphy—Applications to Hydrocarbon Exploration*, AAPG Mem., 26:53–97.

Vandamme, D., and Courtillot, V., 1990. Paleomagnetism of Leg 115 basement rocks and latitudinal evolution of the Réunion hotspot. *In* Duncan, R. A., Backman, J., Peterson, L. C., et al., *Proc. ODP, Sci. Results, 115: College Station, TX (Ocean Drilling Program), 111–117.*

Vandamme, D., Courtillot, V., Besse, J., and Montigny, R., in press. Paleomagnetism and datations of the Deccan Traps: results of a Nagpur-Bombay traverse and review of earlier work. *Rev. Geophys.*

Veevers, J. J. (Ed.), 1984. *Phanerozoic Earth History of Australia:* Oxford (Clarendon Press).

Veevers, J. J., Powell, C. McA., and Johnson, B. D., 1975. Greater India's place in Gondwanaland and in Asia. *Earth Planet. Sci. Lett.*, 27:383-387.

Verma, R. K., and Mital, G. S., 1972. Palaeomagnetism of a vertical sequence of traps from Mount Girnar, Gujrat, India. *Geophys. J. R. Astron. Soc.*, 29:275–287.

_______, 1974. Paleomagnetic study of a vertical sequence of traps from Mount Pavagarh, Gujarat, India. *Phys. Earth Planet. Inter.*, 8:63–74.

Villa, I. M., 1987. Cooling rates of Himalayan Granites and $^{40}Ar/^{39}Ar$ dating. *Terra Cogn.*, 7:109.

Vincent, E., Killingley, J. S., and Berger, W. H., 1985. Miocene oxygen and carbon isotope stratigraphy of the tropical Indian Ocean. *In* Kennett, J. P. (Ed.), *The Miocene Ocean: Paleoceanography and Biogeography*. Mem. Geol. Soc. Am., 163:103–130.

Wang Fu-bao, Li Bing-yuan, and Zhang Qing-song, 1981. The Pliocene and Quaternary environment on the Qinghai-Xizang Plateau. *In* Liu Dong-sheng (Ed.), *Geology, Geological History and Origin of the Qinghai-Xizang Plateau:* Beijing (Science Press), 231–238.

Watts, A. B., and Cox, K. G., 1989. The Deccan Traps: an interpretation in terms of progressive lithospheric flexure in response to a migrating load. *Earth Planet. Sci. Lett.*, 93:85–97.

Weissel, J. K., Anderson, N., and Geller, C. A., 1980. Deformation of the Indo-Australian plate. *Nature*, 287:284–291.

Weissel, J. K., and Hayes, D. E., 1977. Evolution of the Tasman Sea reappraised. *Earth Planet. Sci. Lett.*, 36:77–84.

Weissel, J. K., and Watts, A. B., 1979. Tectonic evolution of the Coral Sea Basin. *J. Geophys. Res.*, 84:4572–4582.

Wensink, H., 1973. Newer paleomagnetic results of the Deccan Traps, India. *Tectonophysics*, 17:41–59.

_______, 1987. Comments on "Deccan flood basalts at the Cretaceous/Tertiary boundary?" by V. Courtillot, J. Besse, D. Vandamme, R. Montigny, J.-J. Jaeger, and H. Capetta. *Earth Planet. Sci. Lett.*, 85:326–328.

Wensink, H., Boelrijk, N.A.I.M., Hebeda, E. H., Priem, H.N.A., Verdurmen, E.A.T., and Verschure, R. H., 1979. Paleomagnetism and radiometric age determinations of the Deccan Traps, India. *In* Laskar, B. and Raja Rao, C. S. (Eds.), *4th Int. Gondwanaland Symp.:* Delhi (Hindustan Publ.), 832–849.

Westphal, M., and Pozzi, J.-P., 1983. Paleomagnetic and plate tectonic constraints on the movement of Tibet. *Tectonophysics,* 98:1–10.

Westphal, M., Pozzi, J.-P., Yao Xiu Zhou, Li Sheng Xing, and Xian Yao Chen, 1983. Palaeomagnetic data about southern Tibet (Xizang), 1. The Cretaceous formations of the Lhasa Block. *Geophys. J. R. Astron. Soc.,* 73:507–521.

White, R., and McKenzie, D., 1989. Magmatism at rift zones: the generation of volcanic continental margins and flood basalts. *J. Geophys. Res.,* 94:7685–7729.

Wiens, D. A., 1986. Historical seismicity near Chagos: a complex deformation zone in the equatorial Indian Ocean. *Earth Planet. Sci. Lett.,* 76:350–360.

Wiens, D. A., DeMets, C., Gordon, R. G., Stein, S., Argus, D., Engeln, F. J., Lundgren, P., Quible, D., Stein, C., Weinstein, S., and Woods, D. F., 1985. A diffuse plate boundary model for Indian Ocean tectonics. *Geophys. Res. Lett.,* 12:429–432.

Wiens, D. A., Stein, S., DeMets, C., Gordon, R. G., and Stein, C., 1986. Plate tectonic models for the Indian Ocean "intraplate" deformation. *Tectonophysics,* 132:37–48.

Xu Ren, 1981. Vegetational changes in the past and the uplift of Qinghai-Xizang Plateau. *In* Liu Dong-sheng (Ed.), *Geology, Geological History and Origin of the Qinghai-Xizang Plateau:* Beijing (Science Press), 139–144.

Xu Shu-ying, 1981. The evolution of the palaeogeographic environments in the Tanggula mountains in the Pliocene-Quaternary. *In* Liu Dong-sheng (Ed.), *Geology, Geological History and Origin of the Qinghai Xizang Plateau:* Beijing (Science Press), 247–256.

Yeats, R. S., and Hussain, A., 1987. Timing of structural events in the Himalayan foothills of northwestern Pakistan. *Geol. Soc. Am. Bull.,* 99:161–176.

Yoshida, M., 1989. Intermontane basins in the Nepal Himalayas. *In* Thanasuthipitak, T., and Ounchanum, P. (Eds.), *Intermontane Basins: Geology and Resources:* Chang Mai, 452–467.

Yoshida, M., Igarashi, Y., Arita, K., Hayashi, D., and Sharma, T., 1984. Magnetostratigraphic and pollen analytic studies of the Takman Series, Nepal Himalayas. *J. Nepal. Geol. Soc., Spec. Iss.,* 4:101–120.

Zachos, J. C., Arthur, M. A., and Dean, W. E., 1989. Geochemical evidence for suppression of pelagic marine productivity at the Cretaceous/Tertiary boundary. *Nature,* 337:61–64.

Zeitler, P. K., 1985. Cooling history of the NW Himalaya, Pakistan. *Tectonics,* 4:127–151.

Zeitler, P. K., Johnson, N. M., Naeser, C. W., and Tahirkheli, R.A.K., 1982a. Fission-track evidence for Quaternary uplift of the Nanga Parbat region, Pakistan. *Nature,* 298:255–257.

Zeitler, P. K., Sutter, J. F., Williams, I. S., Zartman, R., and Tahirkheli, R.A.K., 1989. Geochronology and temperature history of the Nanga-Parbat-Haramosh Massif, Pakistan. *In* Malinconico, L. L., Jr., and Lillier, R. J. (Eds.), *Tectonics of the Western Himalayas.* Spec. Pap. Geol. Soc. Am., 232:1–22.

Zeitler, P. K., Tahirkheli, R.A.K., Naeser, C. W., and Johnson, N. M., 1982b. Unroofing history of a suture zone in the Himalaya of Pakistan by means of fission-track annealing ages. *Earth Planet. Sci. Lett.,* 57:227–240.

Zhang Qing-song, Li Bing-yuan, Yang Yi-chou, Yin Ze-sheng, and Wang Fu-bao. 1981. Basic characteristic of neotectonic movements of Qinghai-Xizang Plateau. *In* Liu Dong-sheng (Ed.), *Geology, Geological History and Origin of the Qinghai-Xizang Plateau:* Beijing (Science Press), 103–110.

Zhu Xian Gyuan, Liu Chung, Ye Sujuan, and Lin Jinlu, 1977. Remanence of red beds from Linzhou, Xizang and the northward movement of the Indian plate. *Scientia Geol. Sin.,* 1:44–51.

Zhu Zhi Wen, Zhu Xiangyuan, and Zhang Yiming, 1981. Paléomagnetisme du Plateau Tibètain et dérive continentale. *Acta Geophys. Sin.,* 24:40–49.

Zhu Zhi Wen, and Teng Jiwen, 1984. Preuves paléomagnétiques de la dérive vers le Nord de fragments de la plaque Indienne après la séparation du continent de Gondwana et de leur collision avec la plaque Eurasiatique. *In* Mercier, J. L., and Li Guangcen (Eds.), *Mission Franco-Chinois au Tibet 1980:* Paris (Editions CNRS), 15–20.

Zijderveld, J.D.A., 1967. AC-demagnetization of rocks: analysis of results. *In* Collinson, D. W., Creer, K. M., and Runcorn, S. K. (Eds.), *Methods in Palaeomagnetism:* Amsterdam (Elsevier), 254–286.

Date of initial receipt: 19 June 1990
Date of acceptance: 25 November 1990
Ms 121B-121

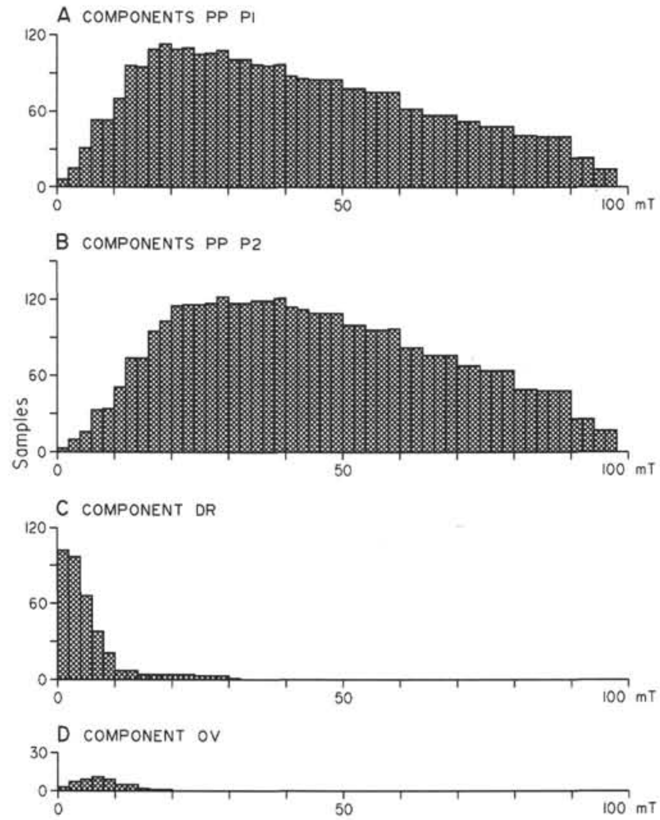

Figure 28. Histograms of stability range distribution upon AF demagnetization for Cores 121-758A-1H to 121-758A-11H (see caption to Fig. 6). **A, B.** Primary magnetization components PP, P_1, and P_2. **C.** Drilling-induced overprint DR. **D.** Recent field overprint OV.

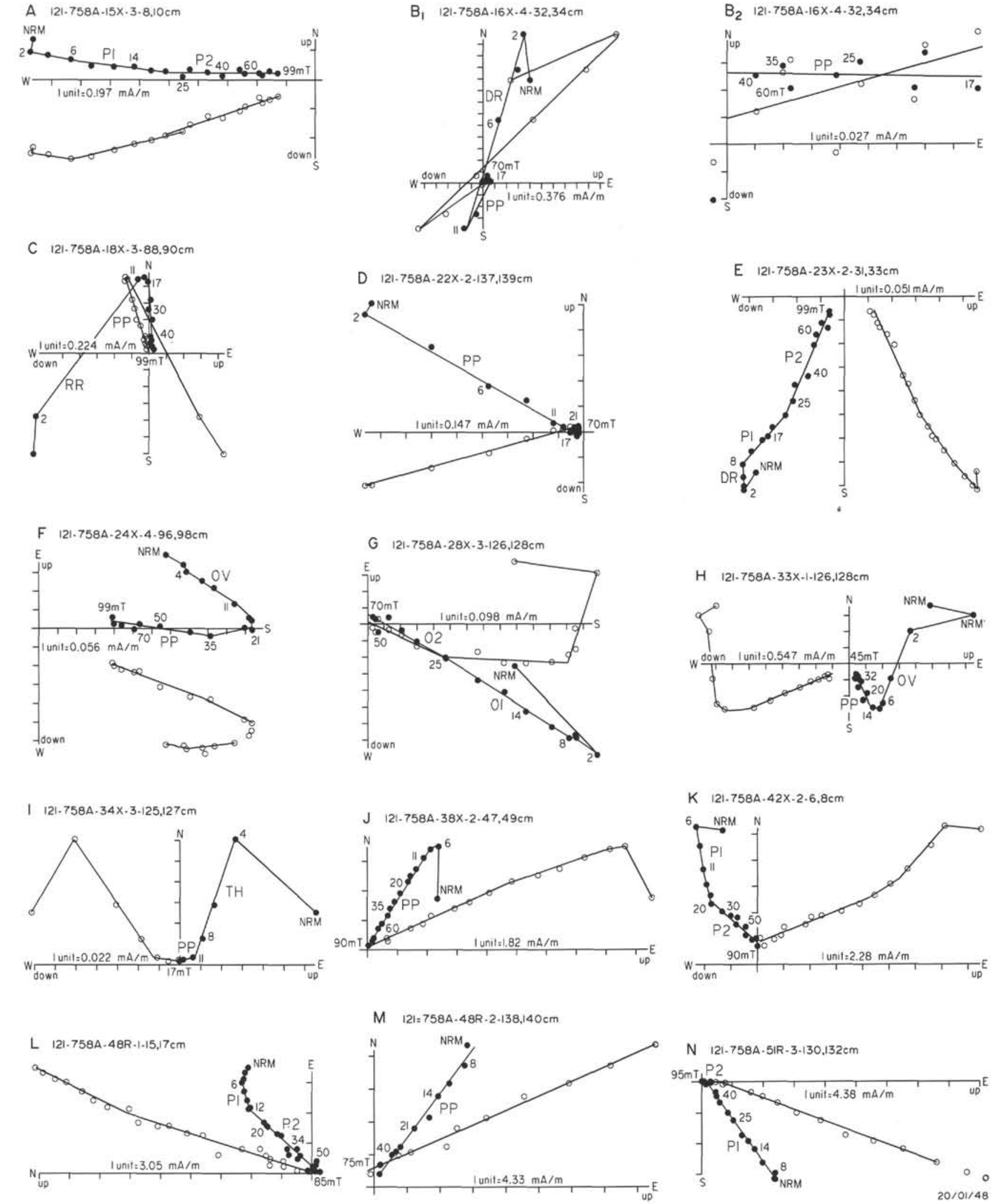

Figure 29. Zijderveld (1967) diagrams of representative samples from Cores 121-758A-12X to 121-758A-54R during AF demagnetization (see captions to Figs. 3, 13, and 19). OV, O_1, and O_2 = overprint of recent or hiatus- (early Oligocene to late Paleocene) related origin; TH = "30 degree inclination" overprint.

Table 4. Linear regression of declinations from primary magnetization components in the double APC-cored sections of Holes 758A and 758B (Figs. 27 and 39).

Core interval	Type	Component	Polarity	Gradient (degrees/ meter)	Intercept (degrees)
121-758A-					
3H to 11H	Linear	PP, P_1, P_2	Normal	0.317	10.2
	Hoffman-Day	PP, P_1, P_2	Normal	0.222	15.6
3H to 11H	Linear	PP, P_1, P_2	Reversed	0.880	145.7
	Hoffman-Day	PP, P_1, P_2	Reversed	0.784	153.7
121-758B-					
3H to 10H	Linear	PP, P_1, P_2	Normal	−0.678	36.2
	Hoffman-Day	PP, P_1, P_2	Normal	−0.754	39.0
3H to 10H	Linear	PP, P_1, P_2	Reversed	−0.599	216.5
	Hoffman-Day	PP, P_1, P_2	Reversed	−0.406	207.7

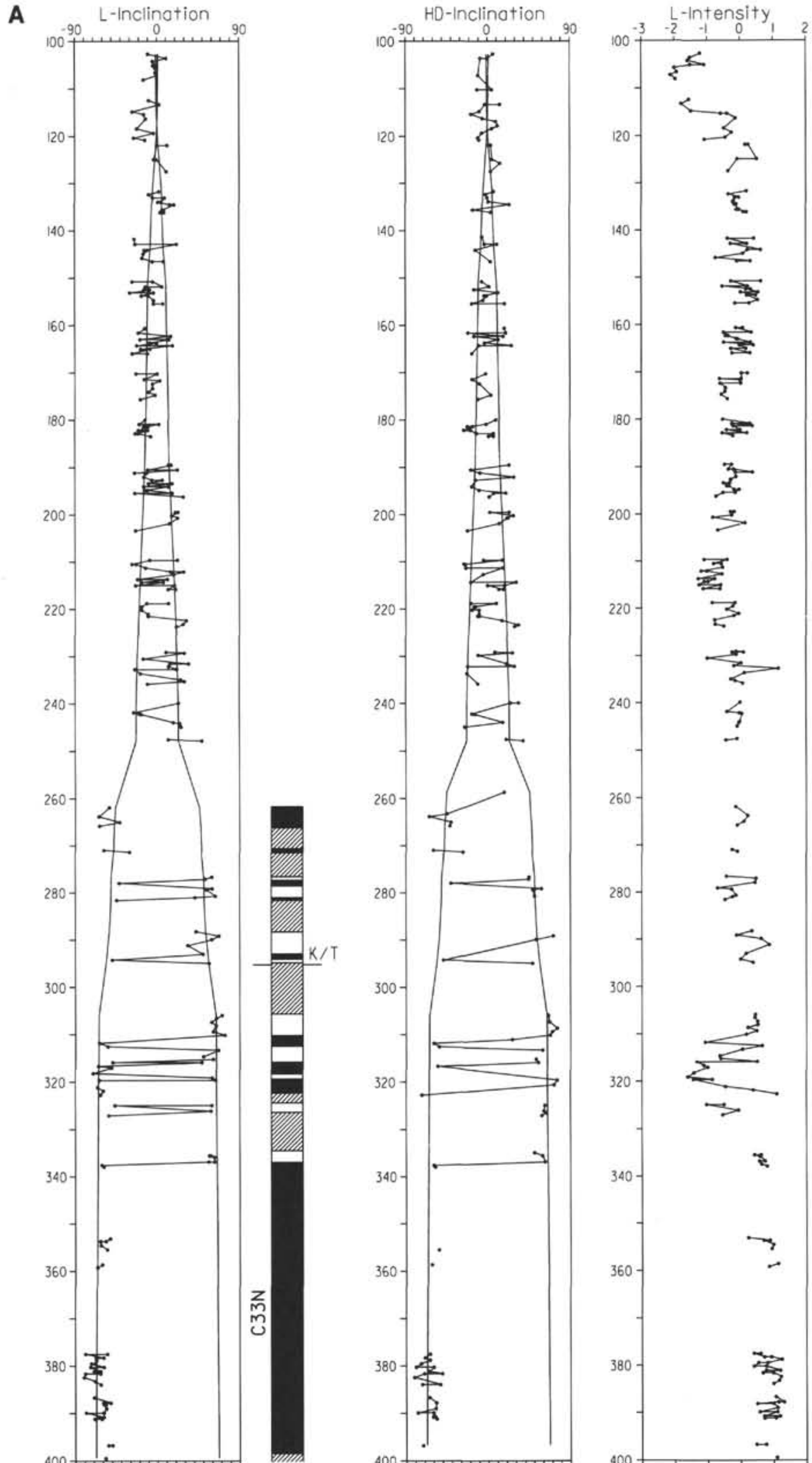

Figure 30. Stratigraphic plots of inclination and intensity of components determined from linear (L) and planar (HD) PCA of AF demagnetization data for Cores 121-758A-12X to 121-758A-43X (see caption to Fig. 5). **A.** Primary components PP, P_1, and P_2 with an attempt at magnetostratigraphic interpretation for part of the section (see caption to Fig. 8). **B.** Drilling-induced component DR. **C.** Hiatus- (early Oligocene to late Paleocene) related overprints OV, O_1, and O_2 (see "XCB-Cored Sediments" section).

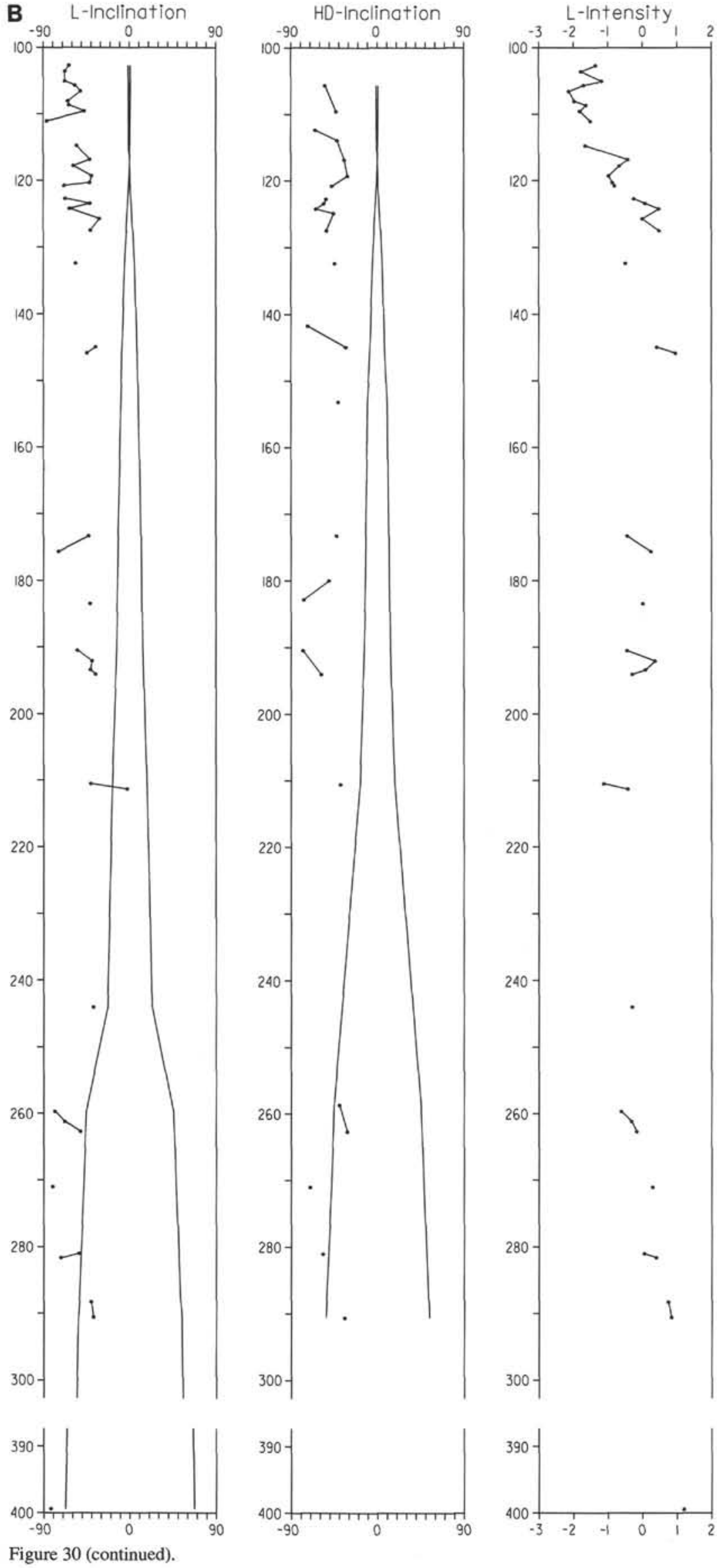

Figure 30 (continued).

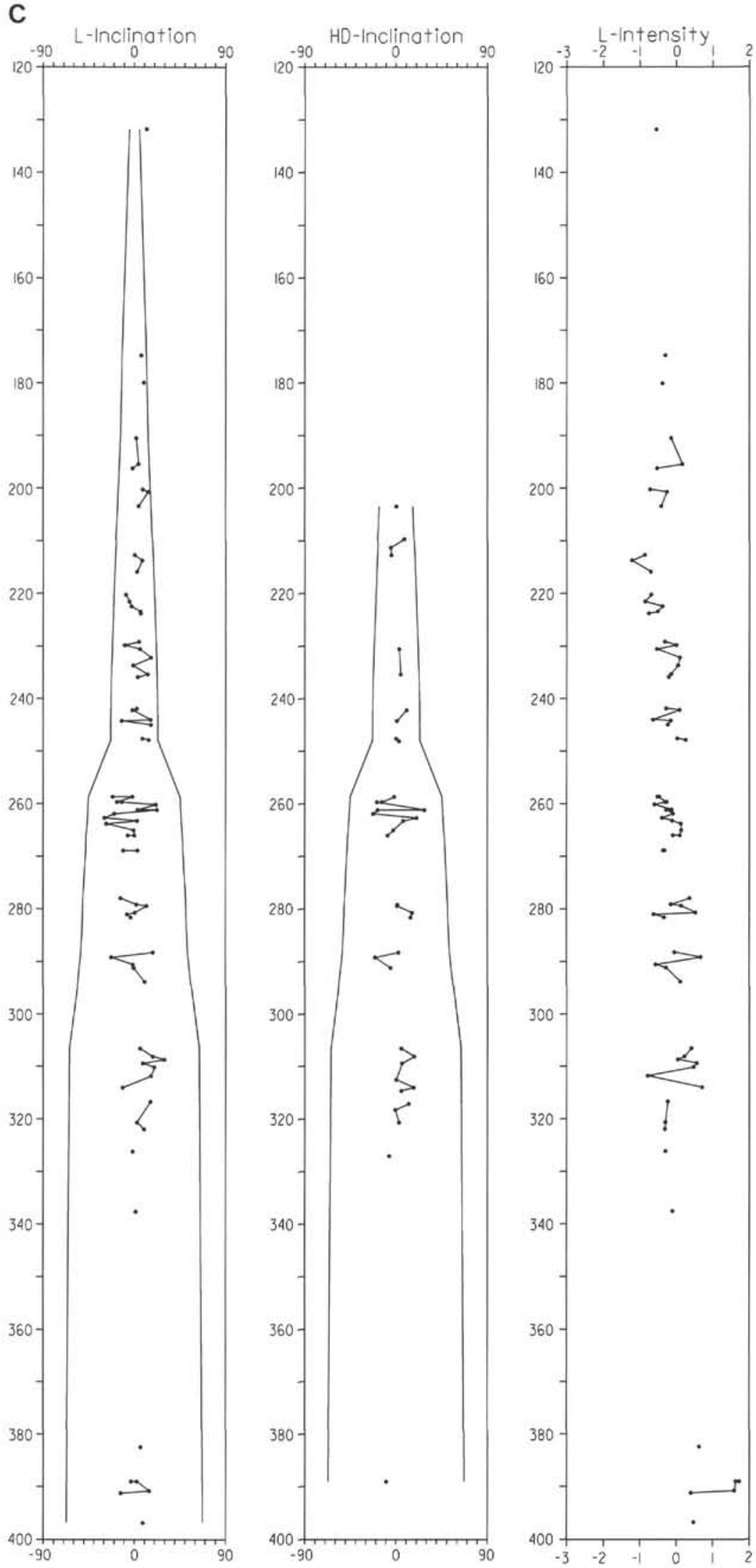

Figure 30 (continued).

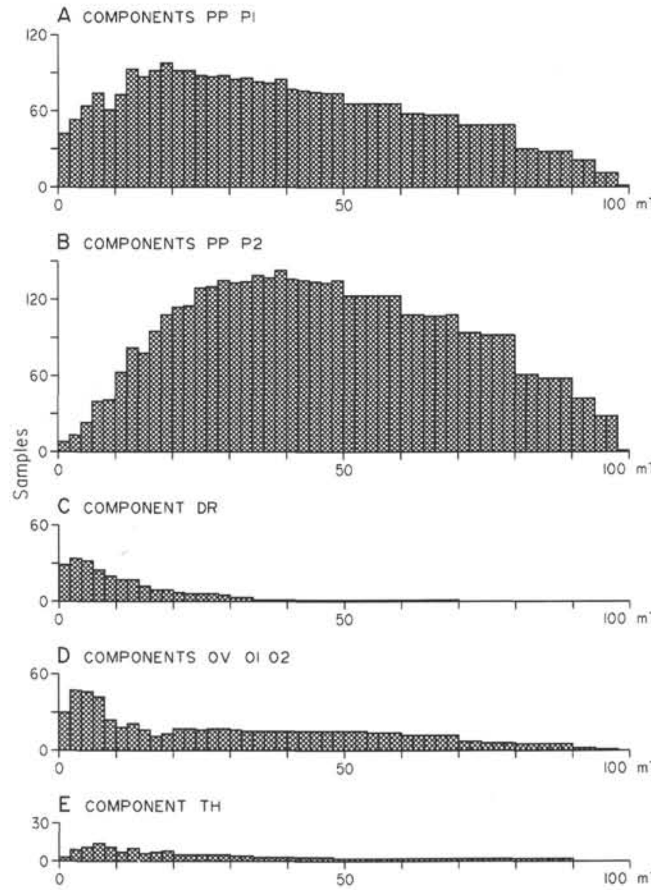

Figure 31. Histograms of stability range distribution upon AF demagnetization for Cores 121-758A-12X to 121-758A-43X (see caption to Fig. 6). **A, B.** Primary magnetization components PP, P_1, and P_2. **C.** Drilling-induced overprint DR. **D.** Hiatus- (early Oligocene to late Paleocene) related overprints OV, O_1, and O_2 (see "XCB-Cored Sediments" section). **E.** "30 degree inclination" overprint.

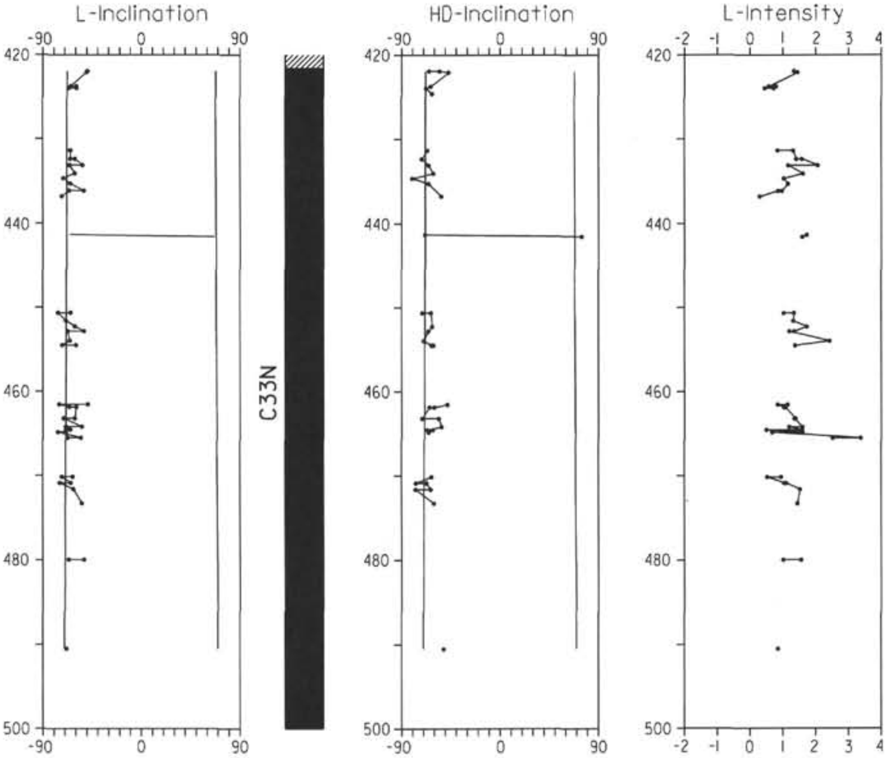

Figure 32. Stratigraphic plots of inclination and intensity of components determined from linear (L) and planar (HD) PCA of AF demagnetization data for Cores 121-758A-47R to 121-758A-54R (see caption to Fig. 5). Primary components PP, P_1, and P_2 with an attempt at magnetostratigraphic interpretation (see caption to Fig. 8).

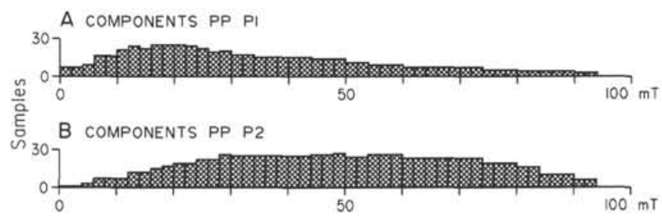

Figure 33. Histograms of stability range distribution upon AF demagnetization for Cores 121-758A-47R to 121-758A-54R (see caption to Fig. 6). **A, B.** Primary magnetization components PP, P_1, and P_2.

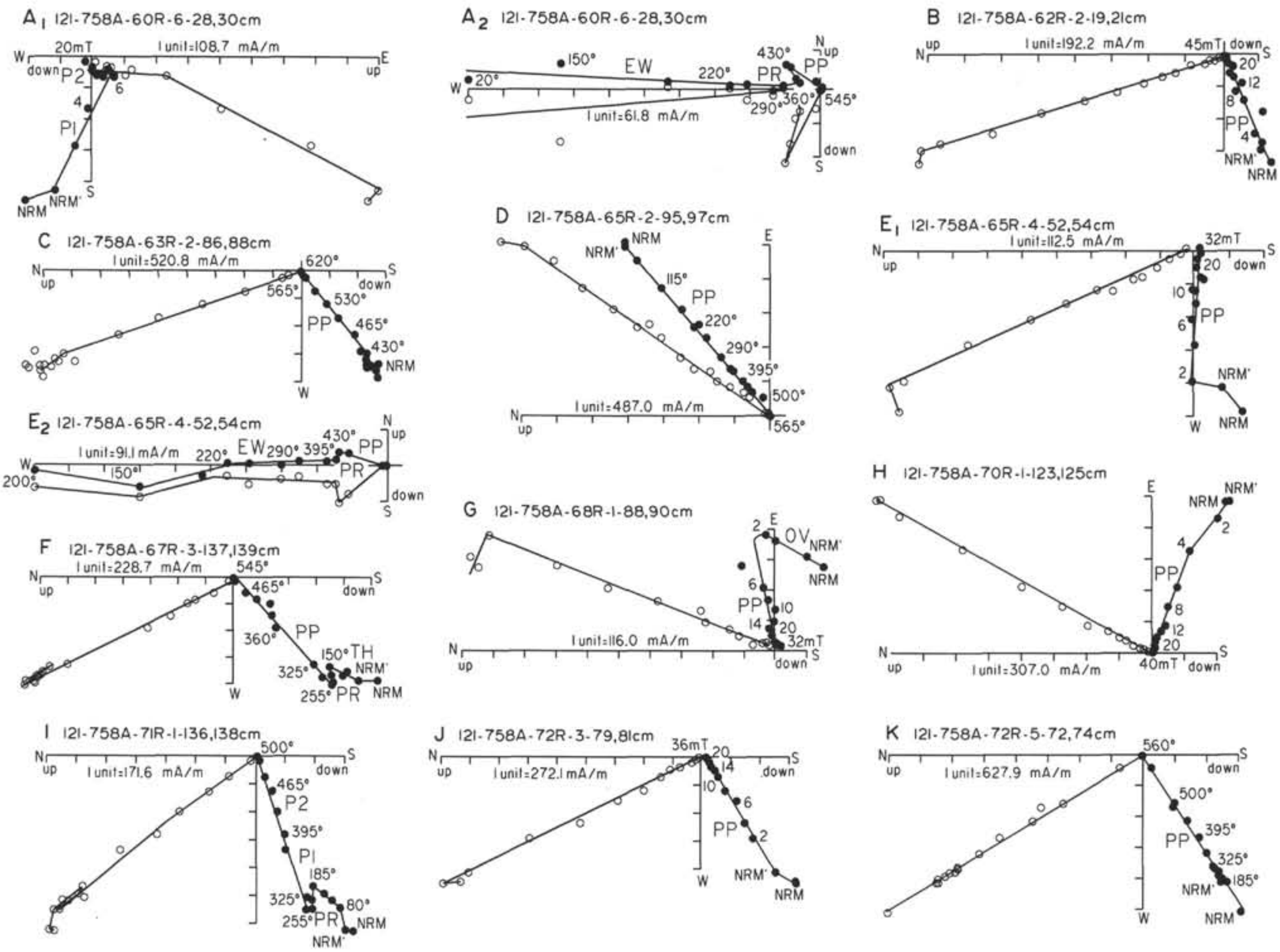

Figure 34. Zijderveld (1967) diagrams of representative samples from Cores 121-758A-55R to 121-758A-73R during AF demagnetization (see captions to Figs. 3 and 25). EW = east-west–oriented low-inclination component.

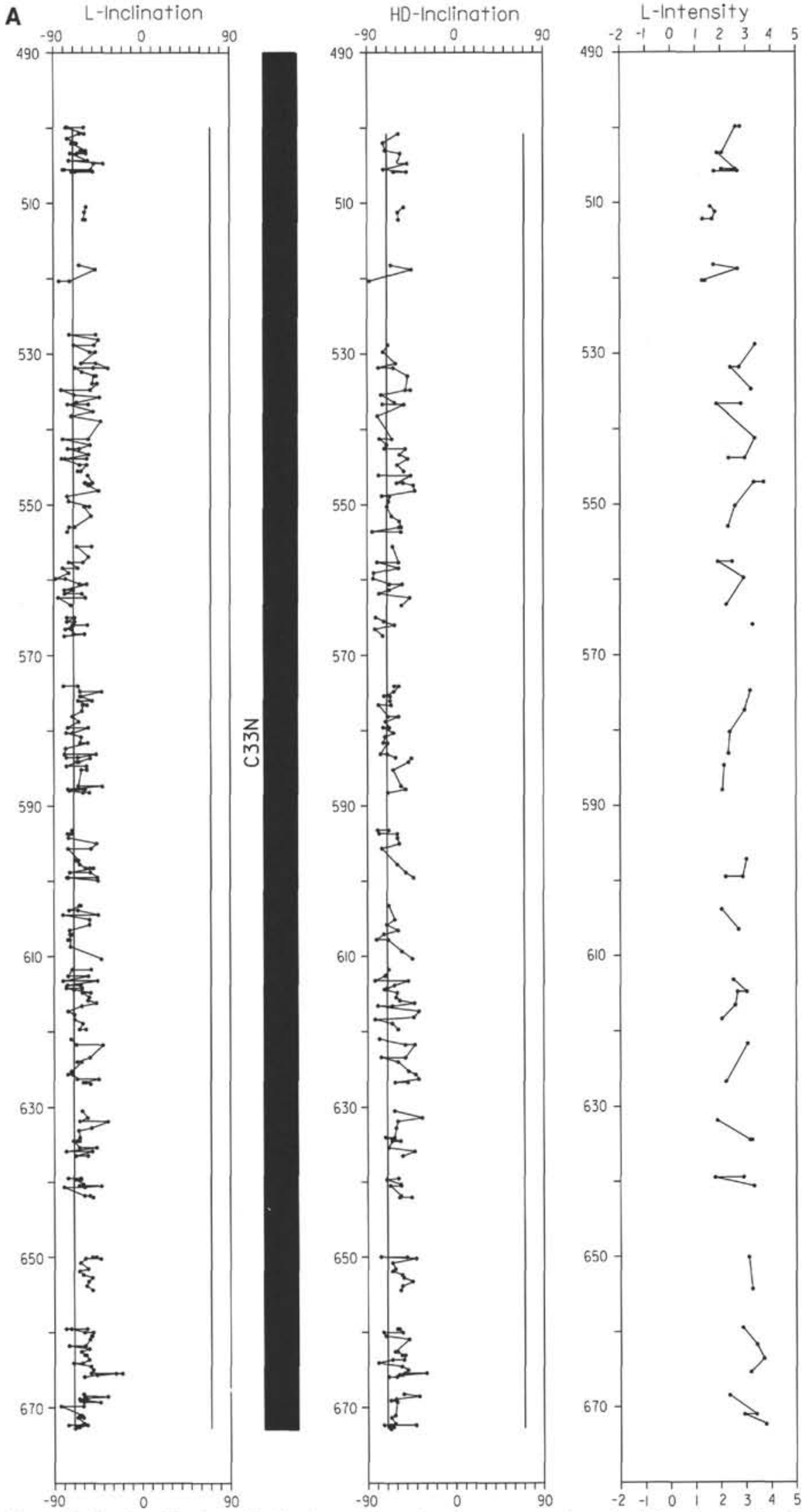

Figure 35. Stratigraphic plots of inclination and intensity of components determined from linear (L) and planar (HD) PCA of AF (A) and thermal (A, B) demagnetization data for Cores 121-758A-55R to 121-758A-73R (see caption to Fig. 5). **A.** Primary components PP, P_1, P_2, and P_3 with an attempt at magnetostratigraphic interpretation (see caption to Fig. 8). **B.** Reversed polarity overprint PR.

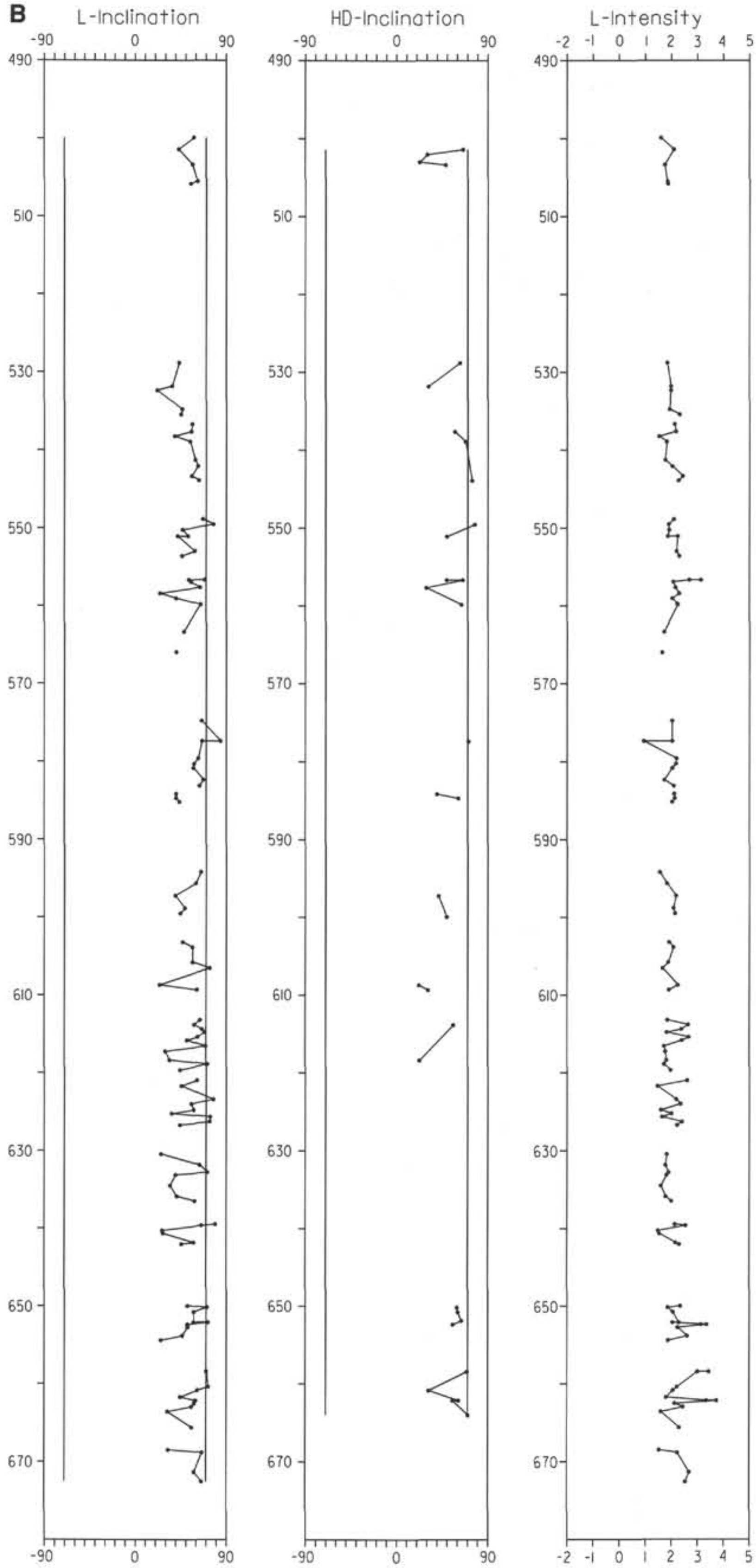

Figure 35 (continued).

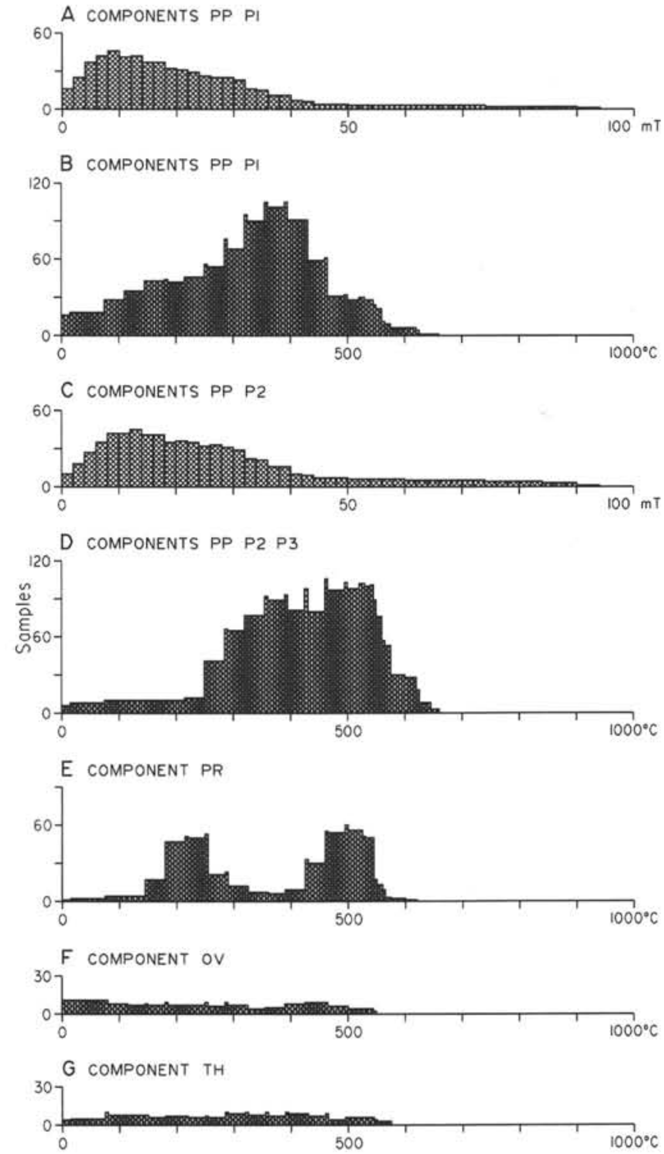

Figure 36. Histograms of stability range distribution upon AF and thermal demagnetization for Cores 121-758A-55R to 121-758A-73R (see caption to Fig. 6). **A–D.** Primary magnetization components PP, P_1, P_2, and P_3. **E.** Reversed polarity overprint PR. **F.** Viscous or recent field overprint OV. **G.** "30 degree inclination" overprint.

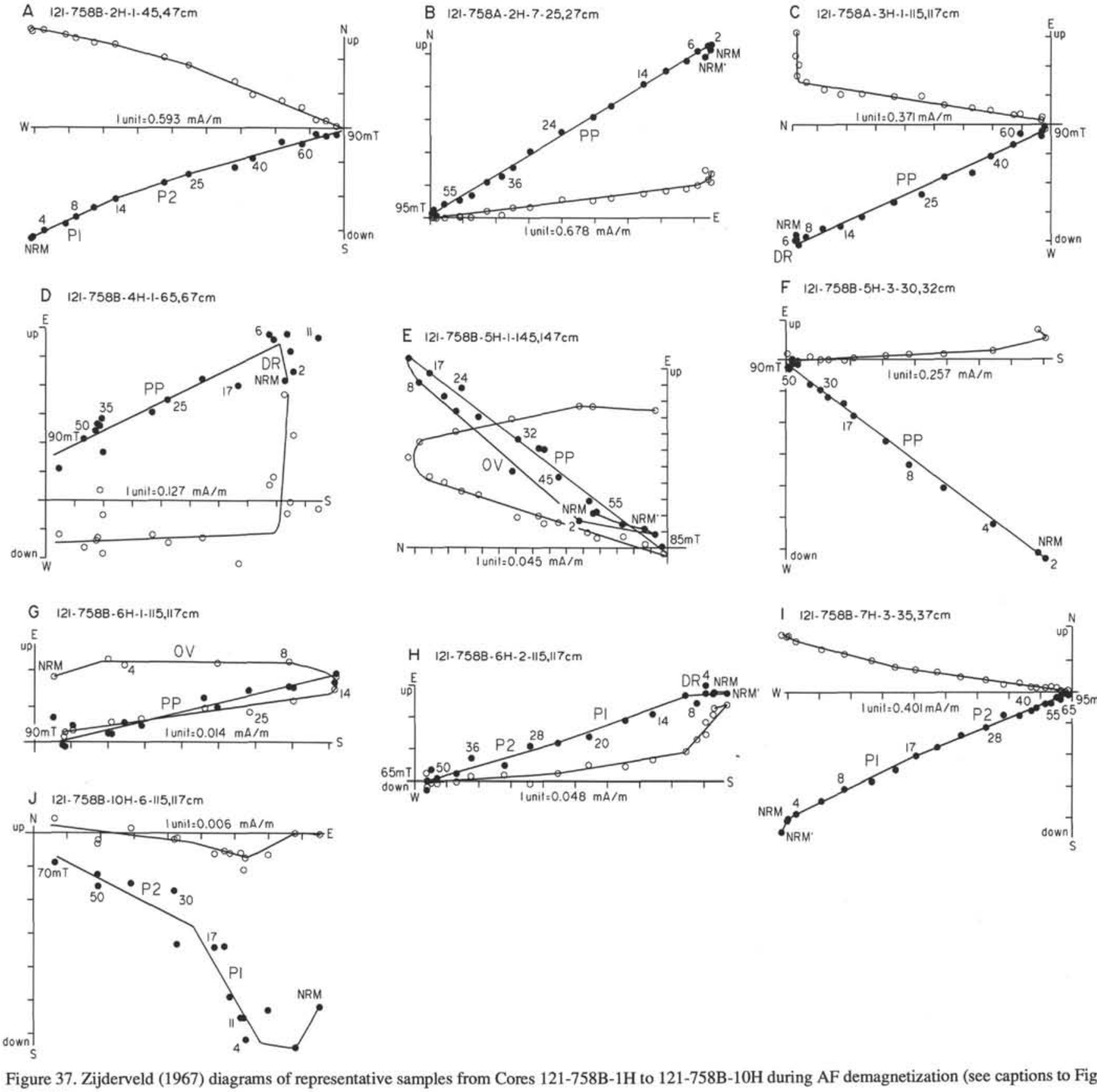

Figure 37. Zijderveld (1967) diagrams of representative samples from Cores 121-758B-1H to 121-758B-10H during AF demagnetization (see captions to Figs. 3 and 25).

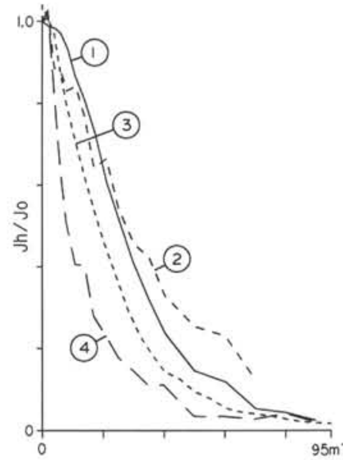

Figure 38. Normalized curves showing the decay of remanent magnetization during AF demagnetization of representative samples from Cores 121-758B-1H to 121-758B-10H. 1 = Sample 121-758B-3H-1, 115–117 cm; 2 = Sample 121-758B-10H-6, 115–117 cm: 3 = Sample 121-758B-7H-3, 35–37 cm; 4 = Sample 121-758B-5H-3, 30–32 cm.

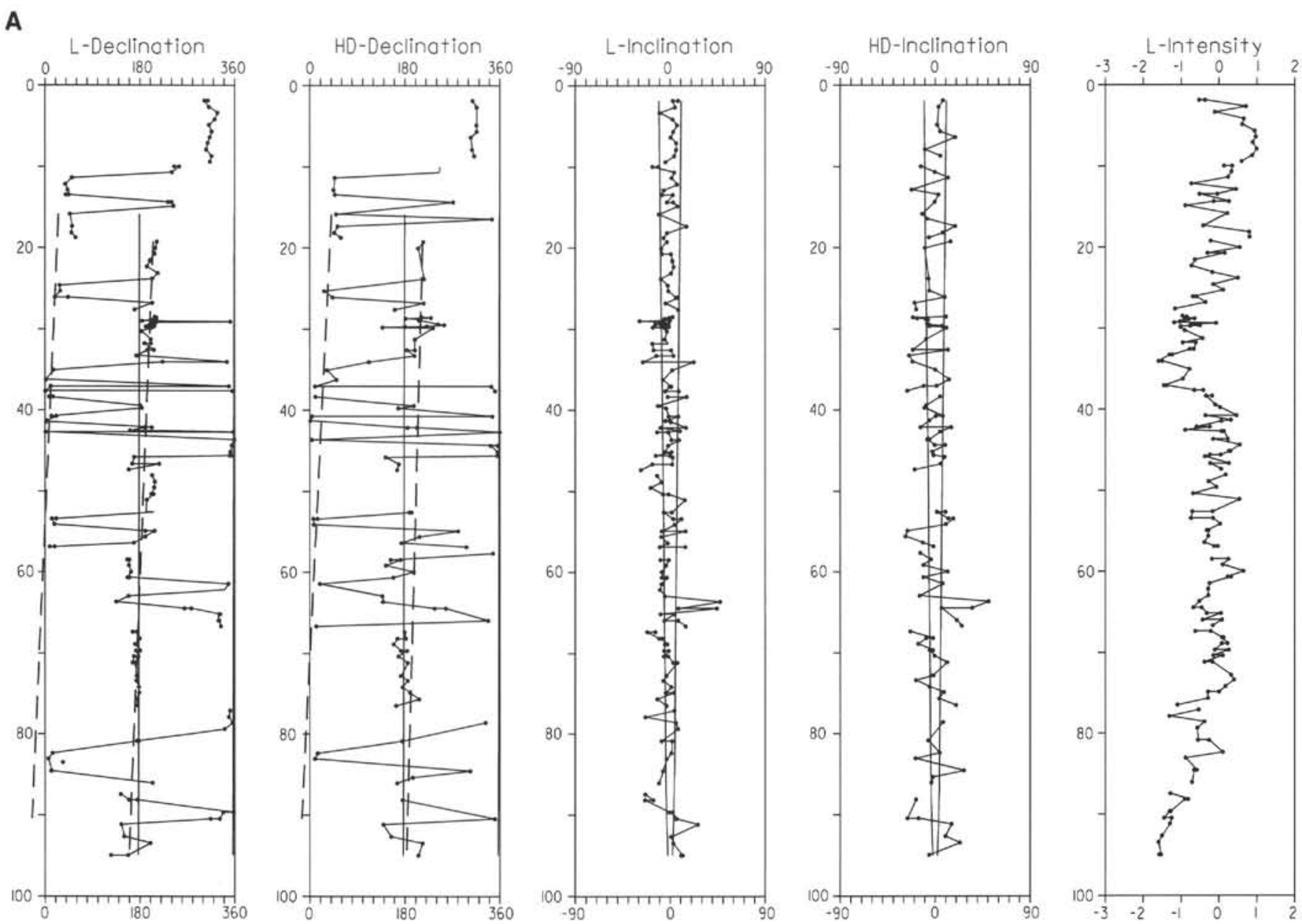

Figure 39. Stratigraphic plots of declination, inclination, and intensity of components determined from linear (L) and planar (HD) PCA of AF demagnetization data for Cores 121-758B-1H to 121-758B-10H (see caption to Fig. 5). Cores 121-758B-3H to 121-758B-10H were corrected for azimuthal orientation and drift of the drill string. **A.** Primary components PP, P_1, and P_2 with expected declinations (solid line) and linear regression of the observed declinations (dashed line) indicated (see "Analysis of Demagnetization Data," "APC-Cored Sediments," and "Hole 758B" sections and Table 4). **B.** Drilling-induced component DR. **C.** Recent field overprint.

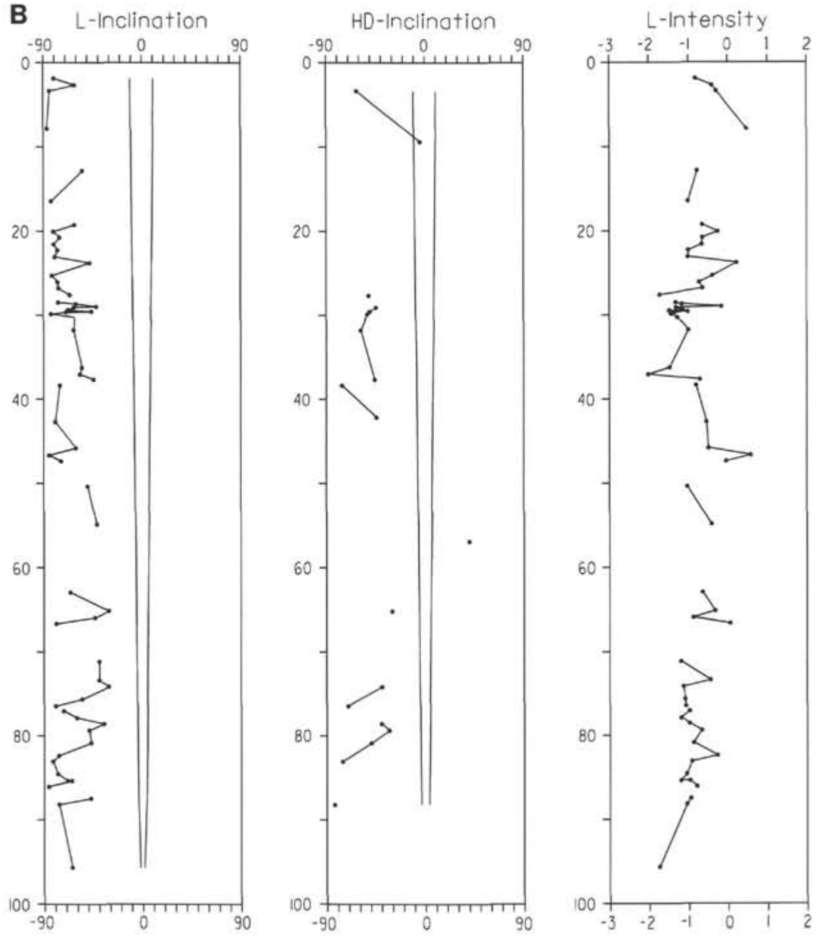

Figure 39 (continued).

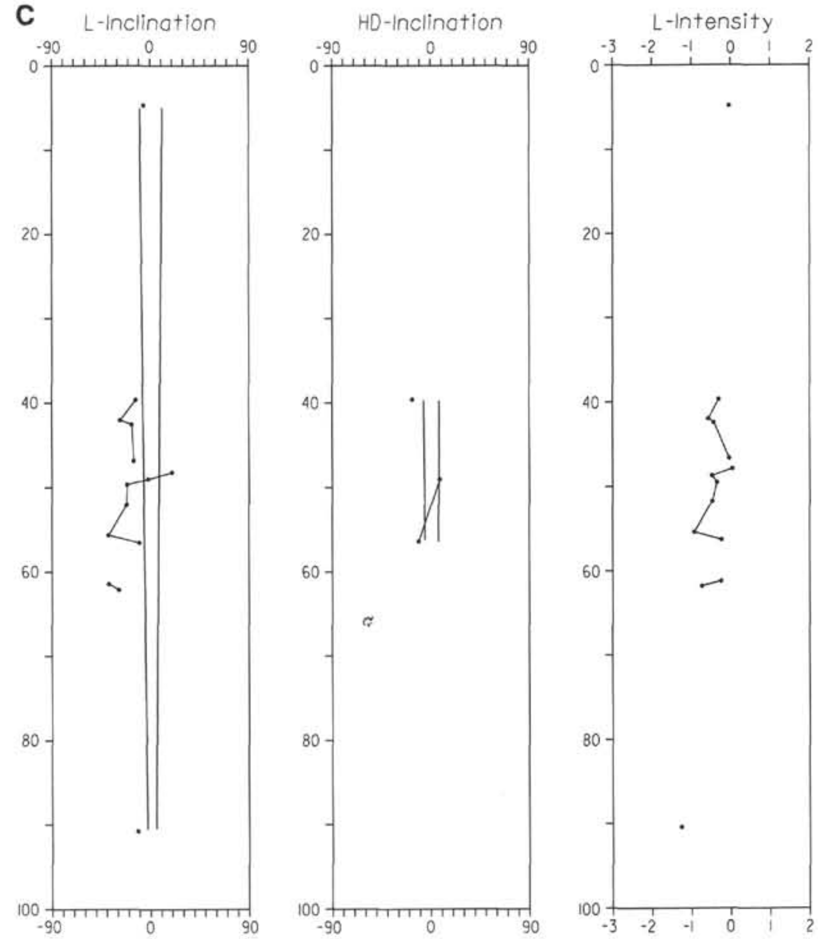

Figure 39 (continued).

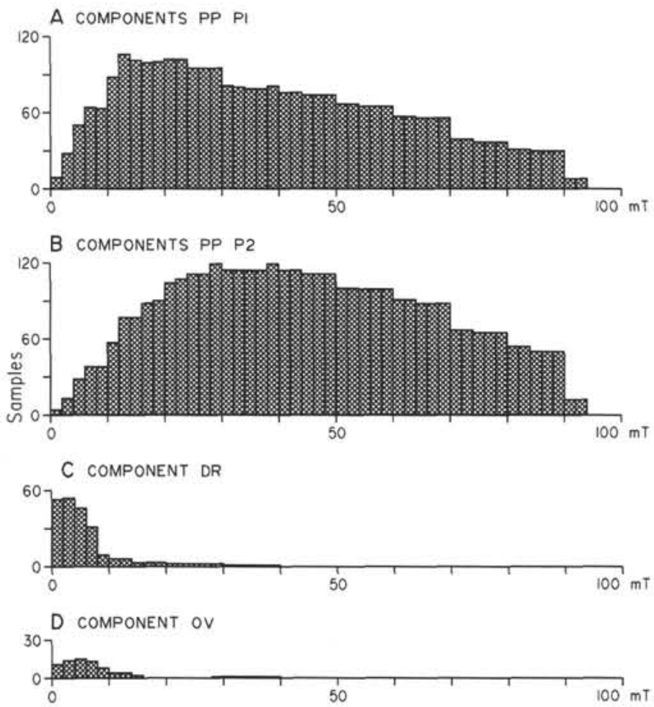

Figure 40. Histograms of stability range distribution upon AF demagnetization for Cores 121-758B-1H to 121-758B-10H (see caption to Fig. 6). **A, B.** Primary magnetization components PP, P_1, and P_2. **C.** Drilling-induced overprint DR. **D.** Recent field overprint OV.

Table 5. Stratigraphic position of reversal boundaries identified in the double APC-cored sequence of Holes 758A and 758B (see Farrell and Janecek, this volume).

Magnetic reversal	Age (Ma)	Type	Depth (mbsf) Hole 758A	Depth (mbsf) Hole 758B
Brunhes/Matuyama	0.73	N-R	10.75	10.70
Upper Jaramillo	0.91	R-N	14.15	14.20
Lower Jaramillo	0.98	N-R	15.35	15.28
Upper Olduvai	1.66	R-N	—	24.25
Lower Olduvai	1.88	N-R	26.00	26.40
Upper Réunion Event 1	2.01	R-N	—	28.95
Lower Réunion Event 1	2.04	N-R	—	29.15
Upper Réunion Event 2	2.12	R-N	—	—
Lower Réunion Event 2	2.14	N-R	—	—
Matuyama/Gauss	2.47	R-N	34.20	34.75
Upper Kaena	2.92	N-R	39.50	39.03
Lower Kaena	2.99	R-N	40.50	40.20
Upper Mammoth	3.08	N-R	41.90	41.40
Lower Mammoth	3.18	R-N	42.95	42.57
Gauss/Gilbert	3.40	N-R	—	45.65
Upper Cochiti	3.88	R-N	—	52.95
Lower Cochiti	3.97	N-R	—	54.60
Upper Nunivak	4.10	R-N	56.20	56.80
Lower Nunivak	4.24	N-R	58.65	58.30
Upper Sidjufall	4.40	R-N	61.50	61.10
Lower Sidjufall	4.47	N-R	63.05	62.45
Upper Thvera	4.57	R-N	—	63.20
Lower Thvera	4.77	N-R	66.80	—
Gilbert/Chron 5	5.35	R-N	76.35	—
Upper Chron 5 Event 1	5.53	N-R	80.45	80.15
Lower Chron 5 Event 1	5.68	R-N	82.65	82.20
Chron 5/Chron 6	5.89	N-R	84.35	85.45
Upper Chron 6 Event 1	6.37	R-N	90.15	89.35
Lower Chron 6 Event 1	6.50	N-R	92.05	91.05

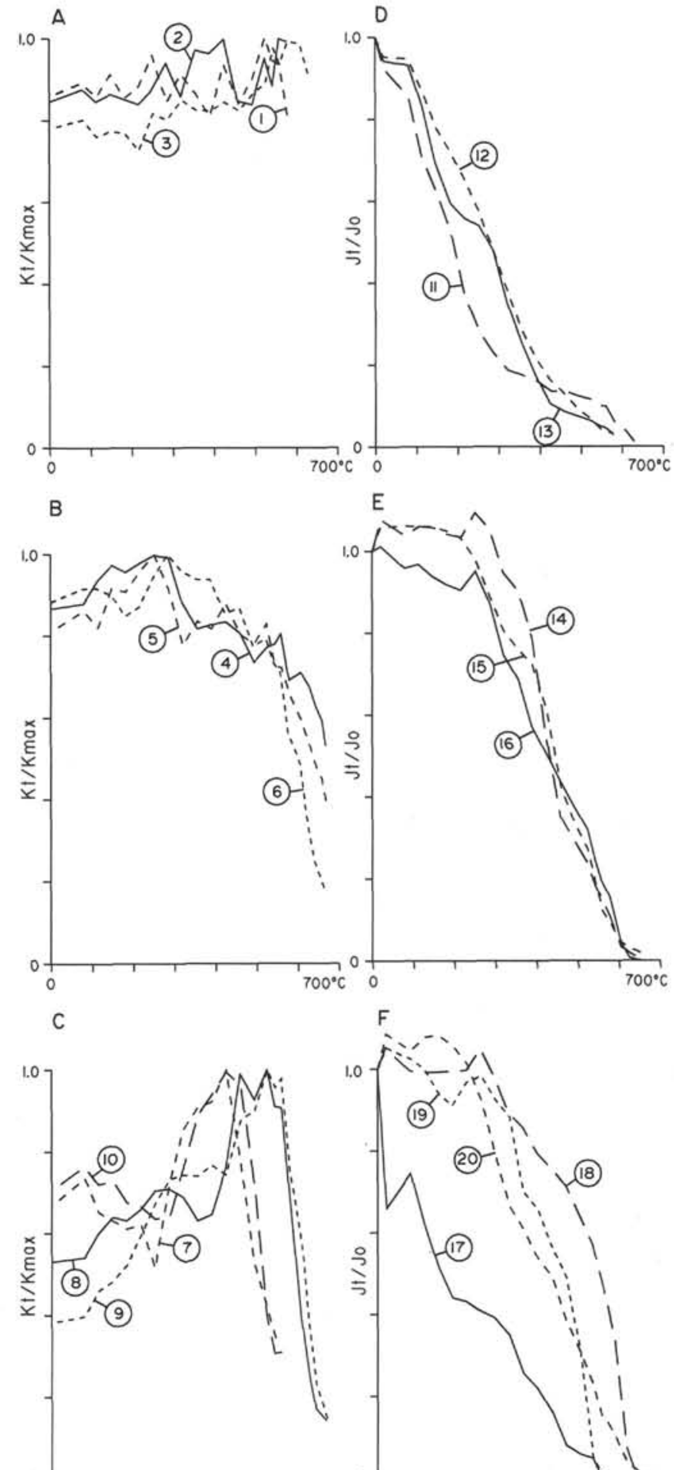

Figure 41. Normalized curves showing changes in susceptibility (**A–C**) and the decay of remanent magnetization (**D–F**) during thermal demagnetization of representative basement samples from Sites 756 to 758. 1, 11 = Sample 121-757B-25X-2, 13–15 cm; 2, 12 = Sample 121-757B-36X-1, 145–147 cm; 3, 13 = Sample 121-757B-28X-3, 144–146 cm; 4, 14 = Sample 121-756D-11R-1, 123–125 cm; 5, 15 = Sample 121-757C-9R-6, 99–101 cm; 6, 16 = Sample 121-757B-42N-1, 40–42 cm; 7, 17 = Sample 121-758A-61R-6, 60–62 cm; 8, 18 = Sample 121-756D-12R-1, 57–59 cm; 9, 19 = Sample 121-757C-11R-1, 75–77 cm; 10, 20 = 121-758A-72R-2, 99–101 cm.

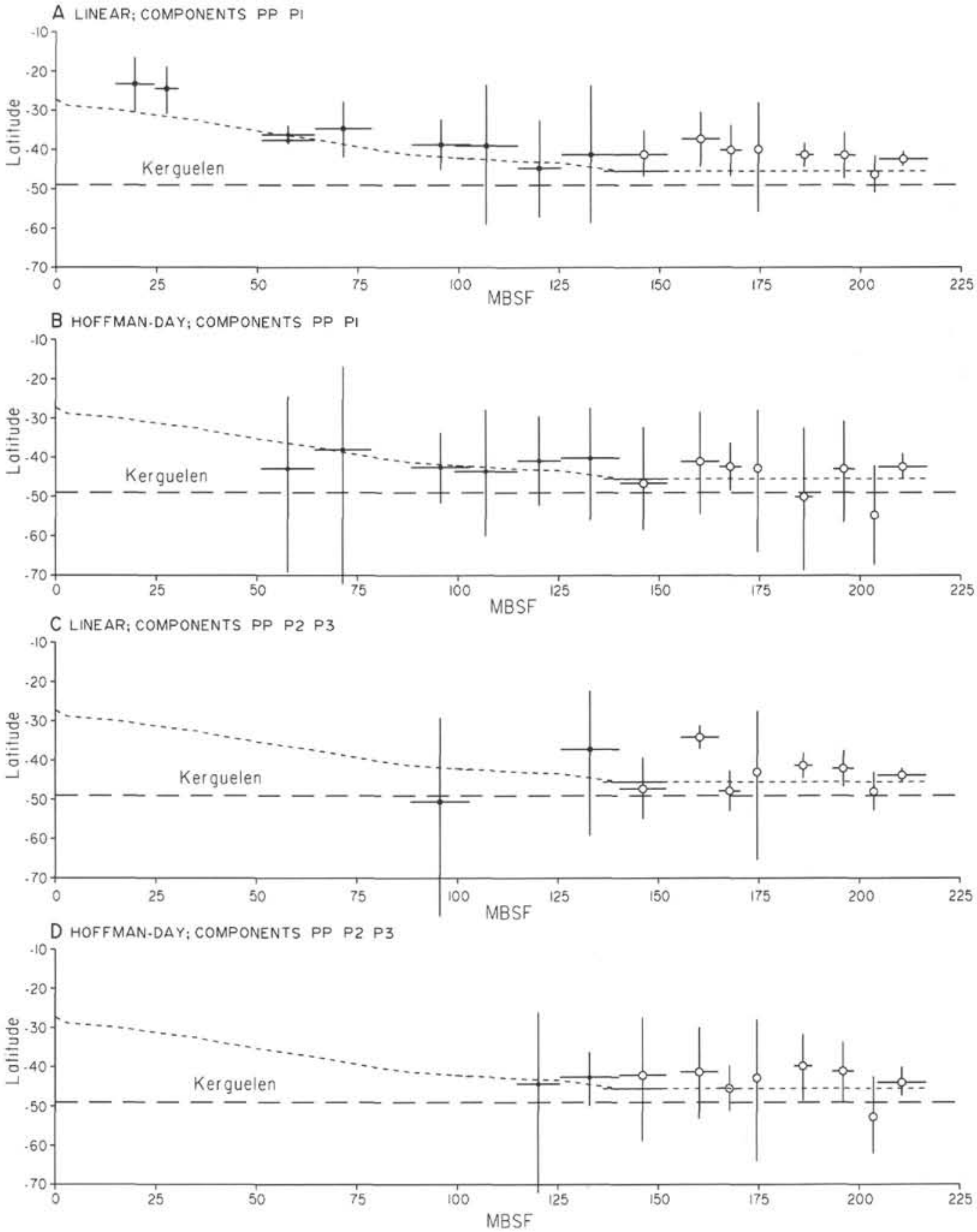

Figure 42. Mean paleolatitude vs. depth profile for Site 756 (Holes 756B, 756C, and 756D combined). The vertical bars indicate the latitude uncertainty and the horizontal bars indicate the depth interval over which the means of the results were calculated. The solid symbols indicate results obtained from AF demagnetization only, and the open symbols indicate results obtained from combined AF and thermal demagnetization data (see "Method" section and Table 3). The dashed line indicates the expected paleolatitude pattern (see "Analysis of Demagnetization Data" section and Table 2). The present-day latitude of the Kerguelen hot spot (49°S) is also indicated.

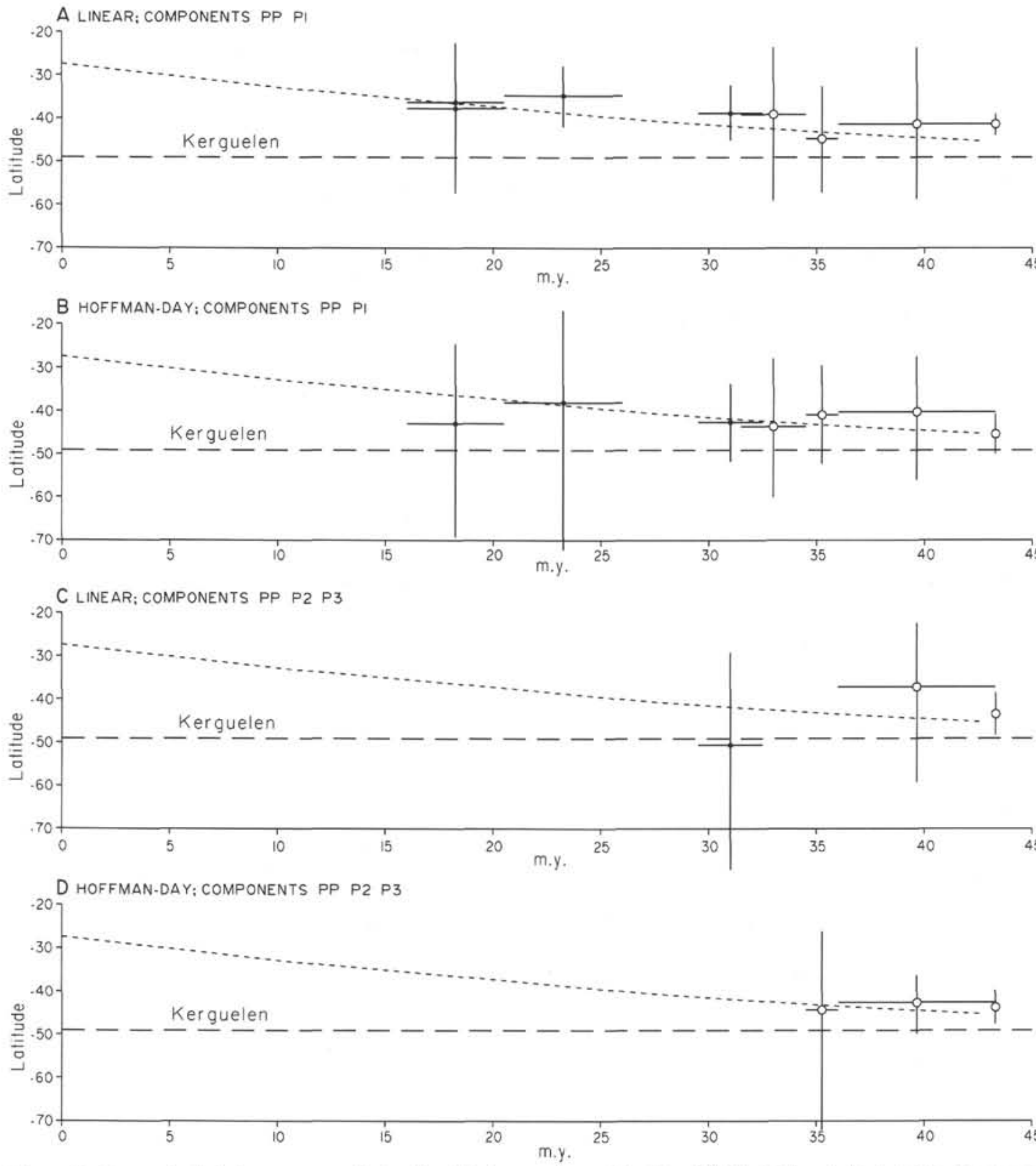

Figure 43. Mean paleolatitude vs. age profile for Site 756 (see caption to Fig. 42 and Table 3). Results for individual basement flows were combined.

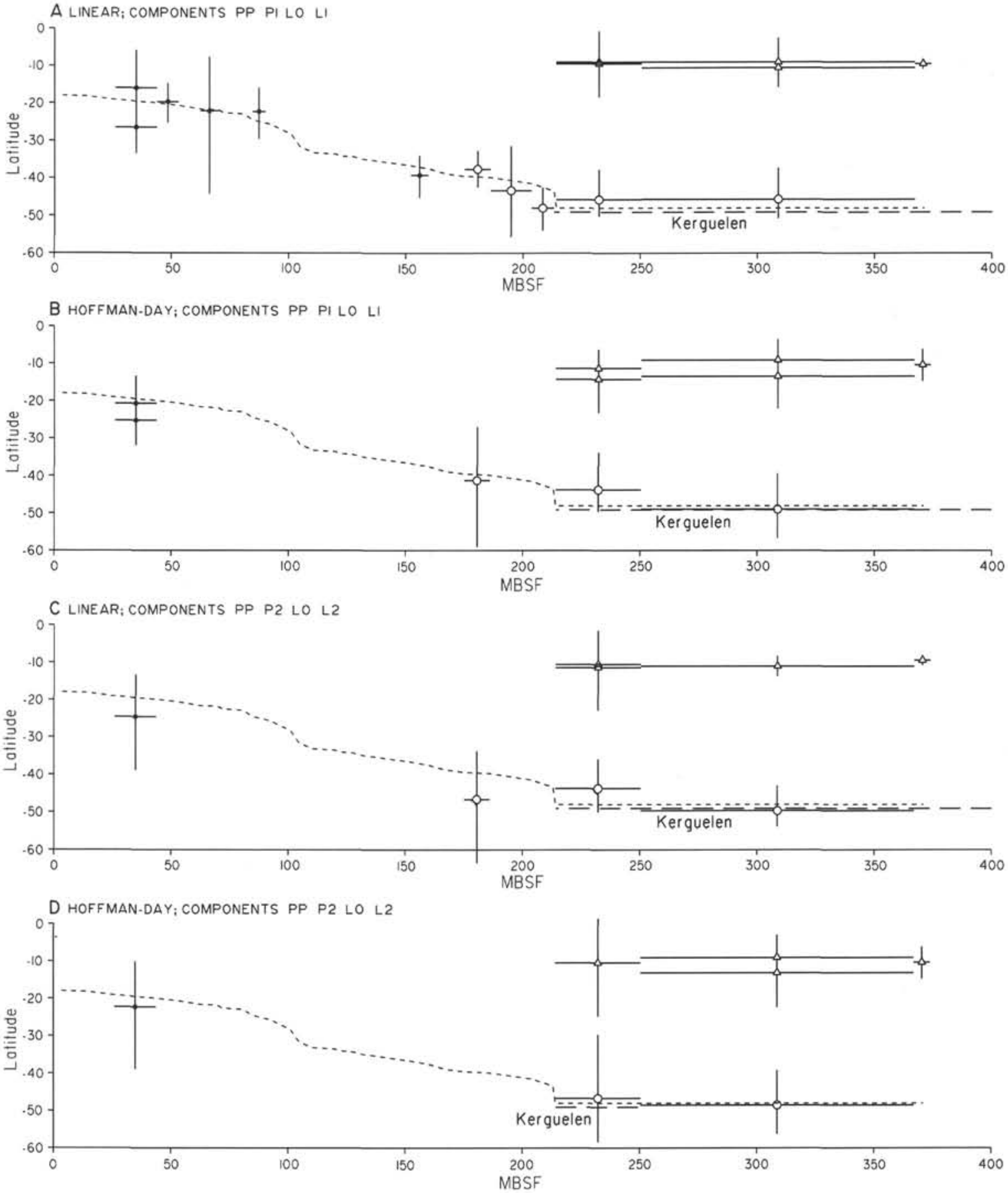

Figure 44. Mean paleolatitude vs. depth profile for Hole 757B (see caption to Fig. 42 and Table 3). The open triangles indicate the low-inclination overprints LO, L_1, and L_2.

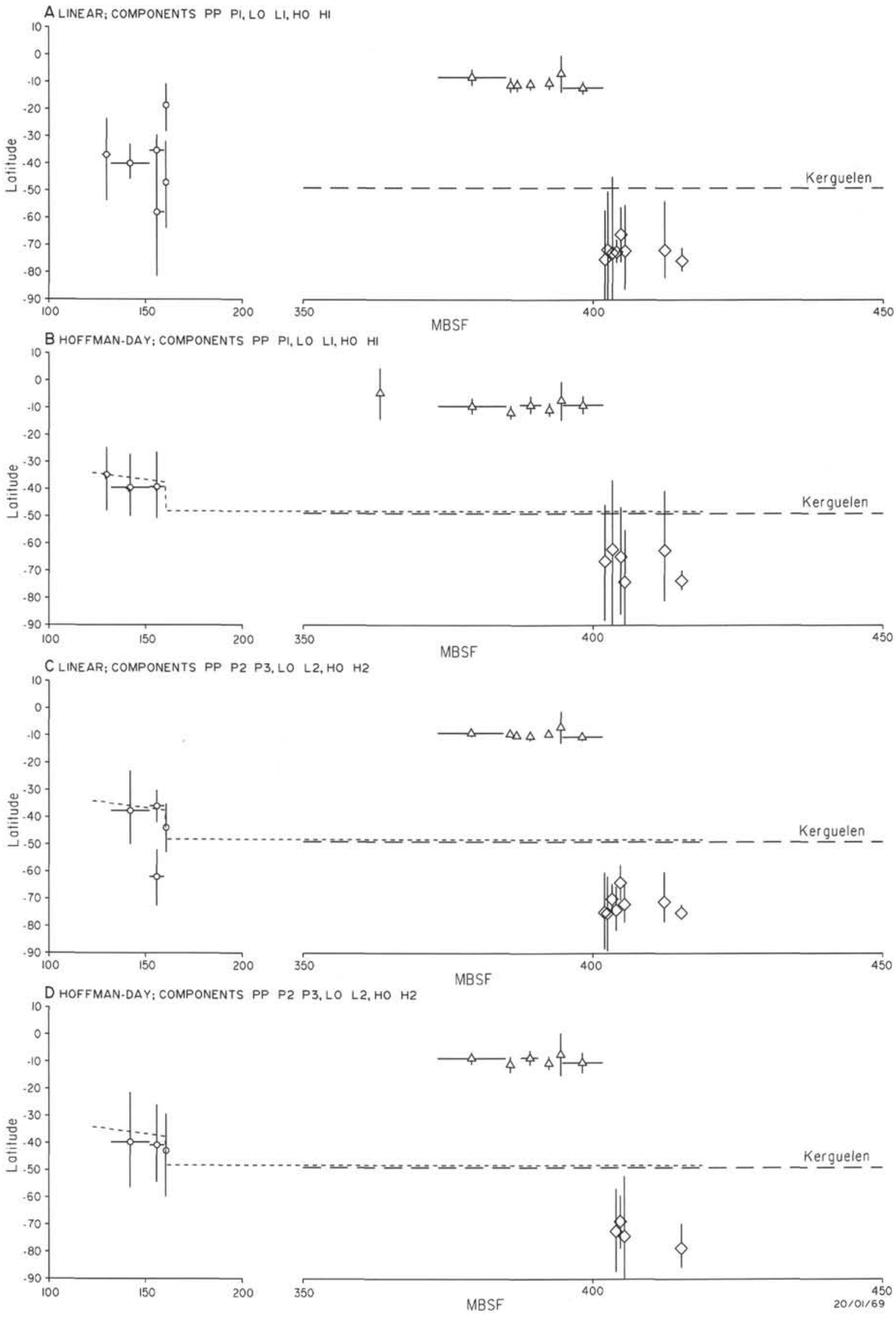

Figure 45. Mean paleolatitude vs. depth profile for Hole 757C (see caption to Fig. 42 and Table 3). The open triangles indicate the low-inclination overprints LO, L_1, and L_2, and the open diamonds indicate the high-inclination overprints HO, H_1, and H_2.

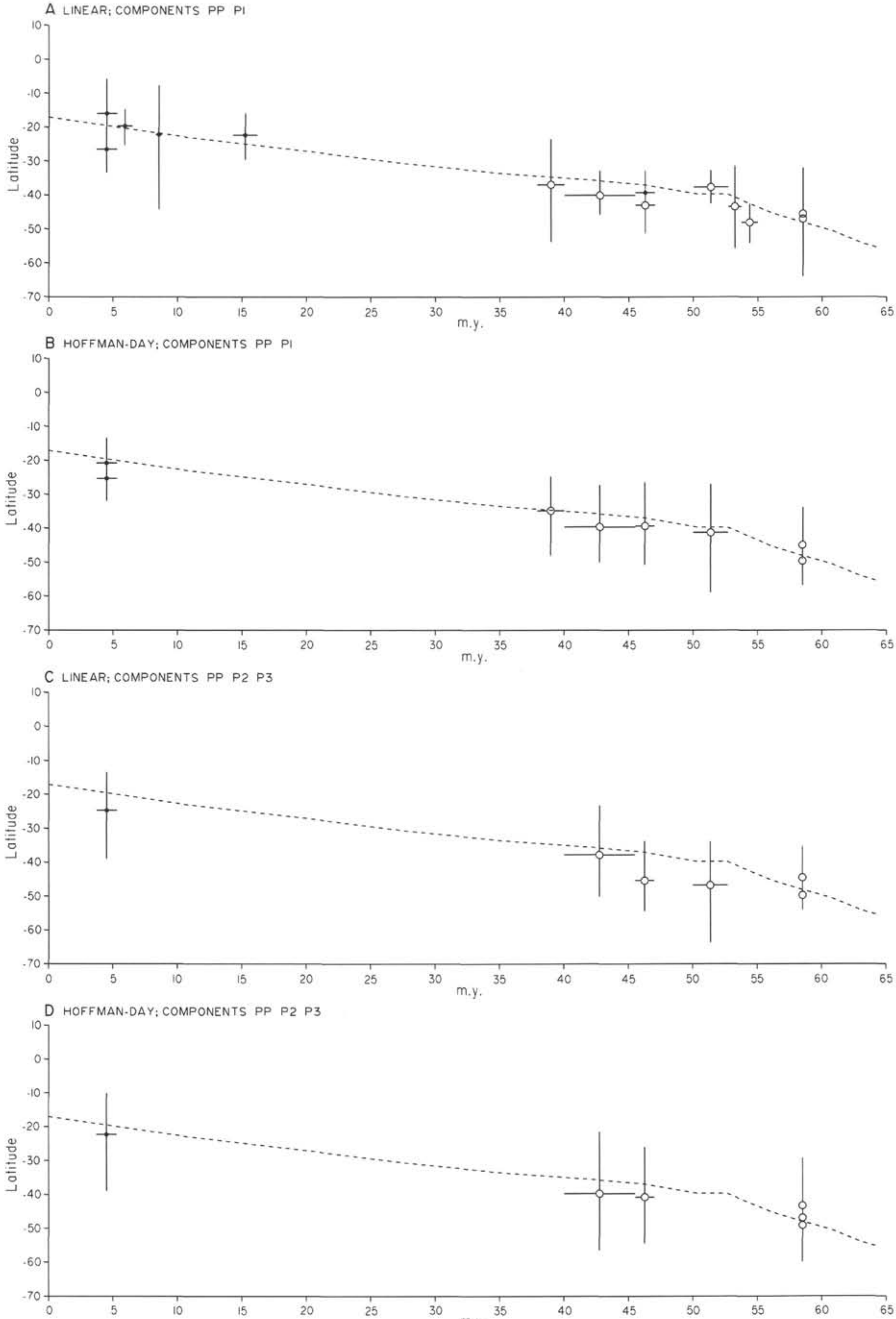

Figure 46. Mean paleolatitude vs. age profile for Site 757 (see caption to Fig. 42 and Table 3).

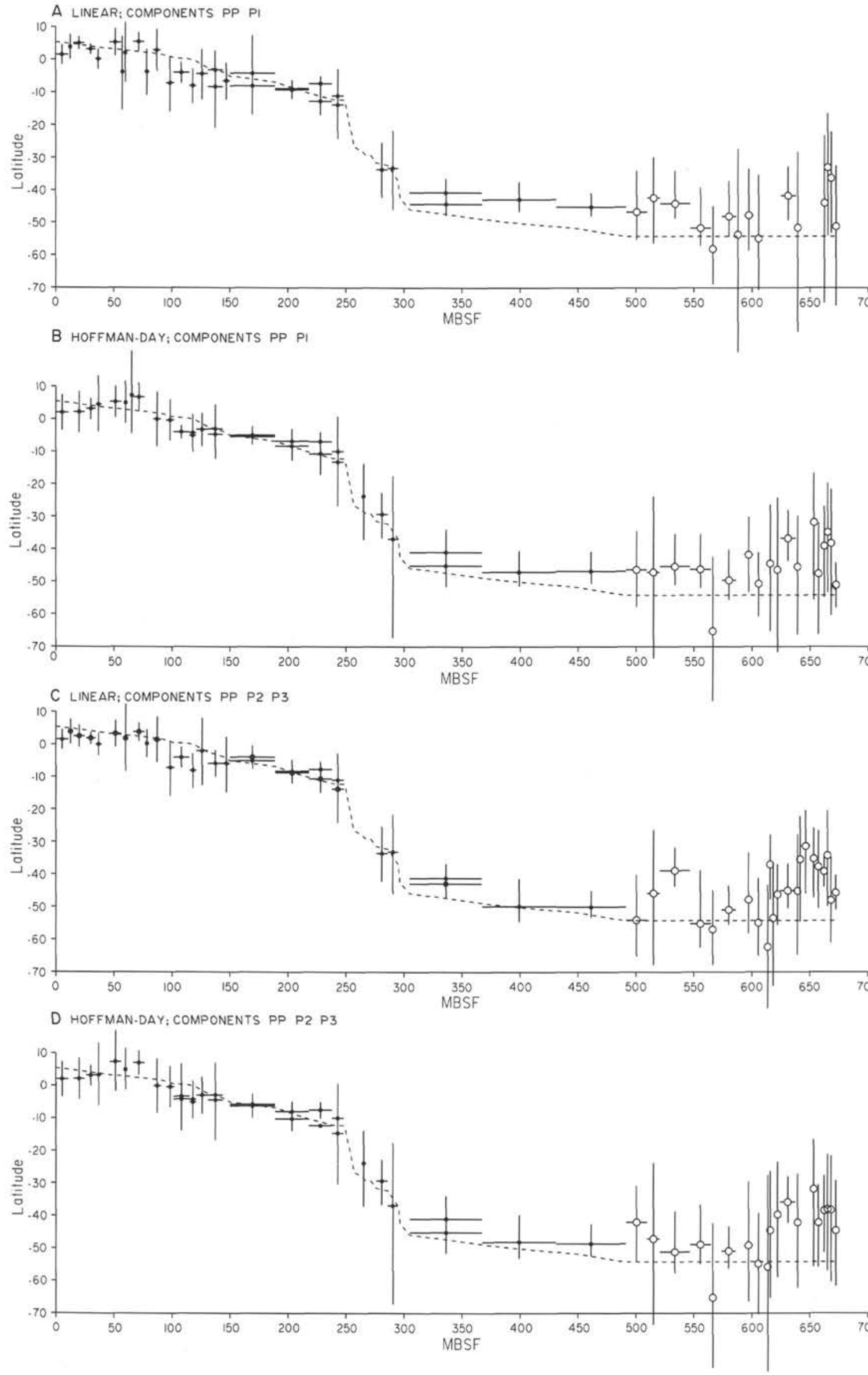

Figure 47. Mean paleolatitude vs. depth profile for Hole 758A (see caption to Fig. 42 and Table 3).

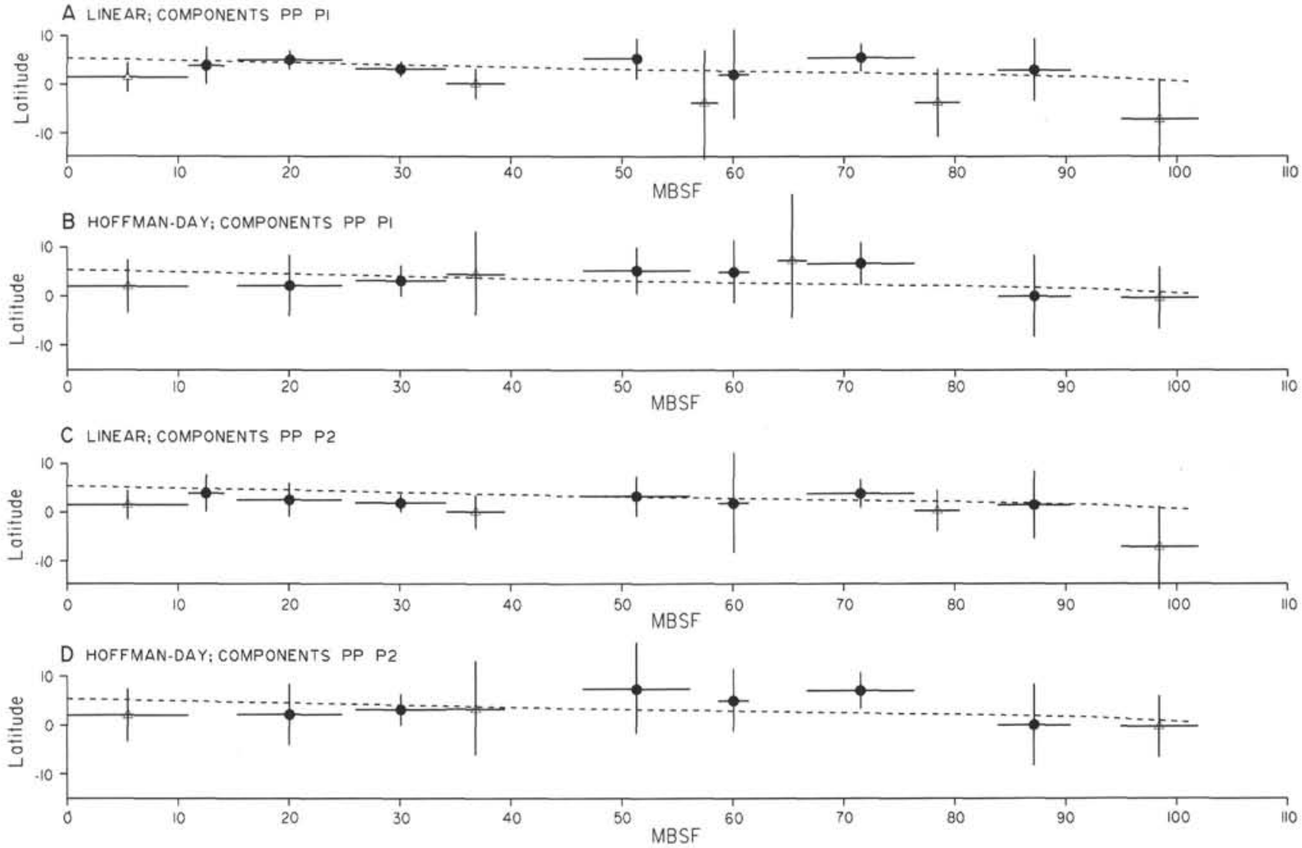

Figure 48. Mean paleolatitude vs. depth profile for the APC-cored section of Hole 758A (Cores 121-758A-1H to 121-758A-11H) from AF demagnetization data only (see caption to Fig. 42 and Tables 3 and 5). The triangles indicate normal polarity results and the dots indicate reversed polarity results. Compare with Figure 49.

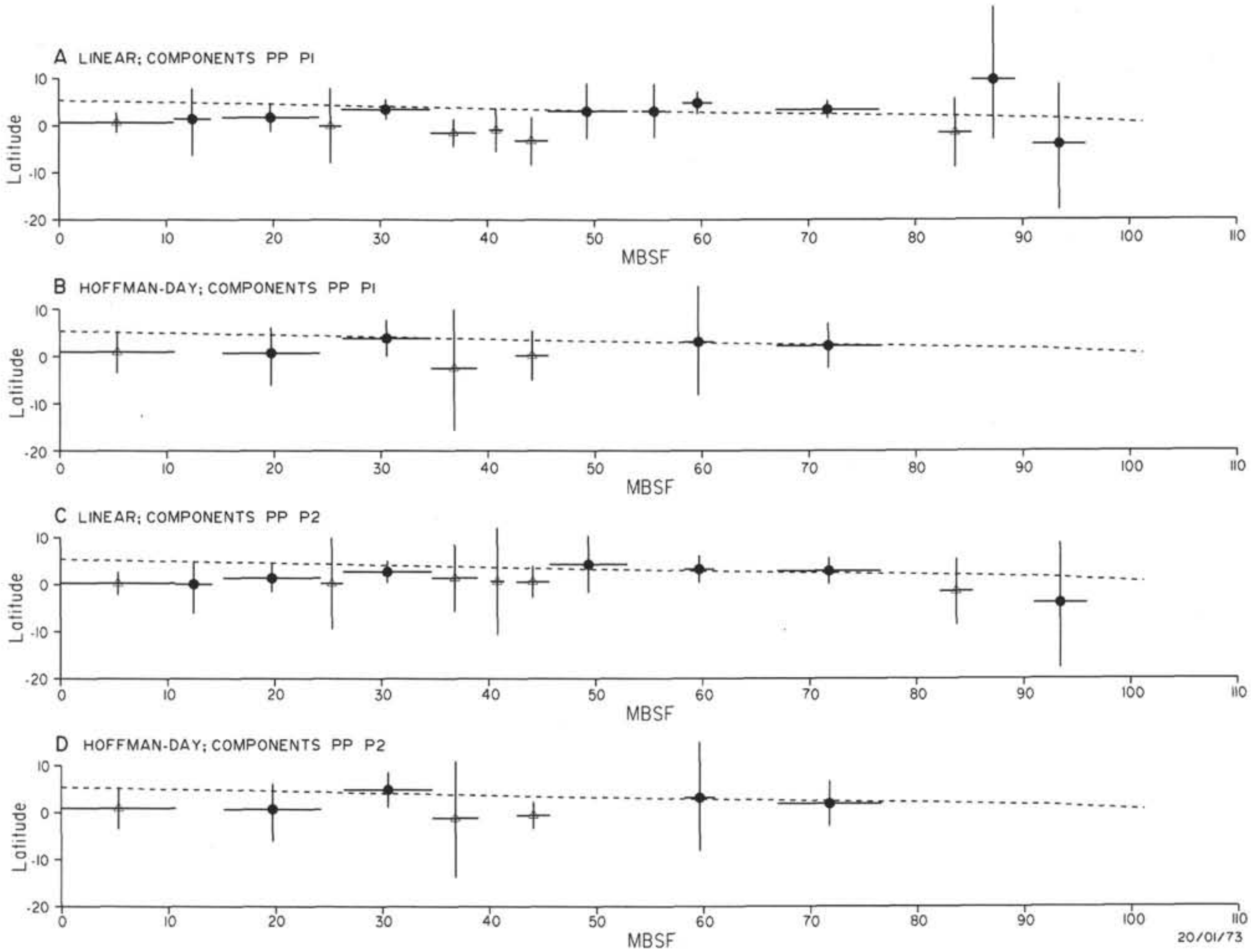

Figure 49. Mean paleolatitude vs. depth profile for the APC-cored section of Hole 758B (Cores 121-758B-1H to 121-758B-10H) from AF demagnetization data only (see captions to Figs. 42 and 48 and Tables 3 and 5). Compare with Figure 48.

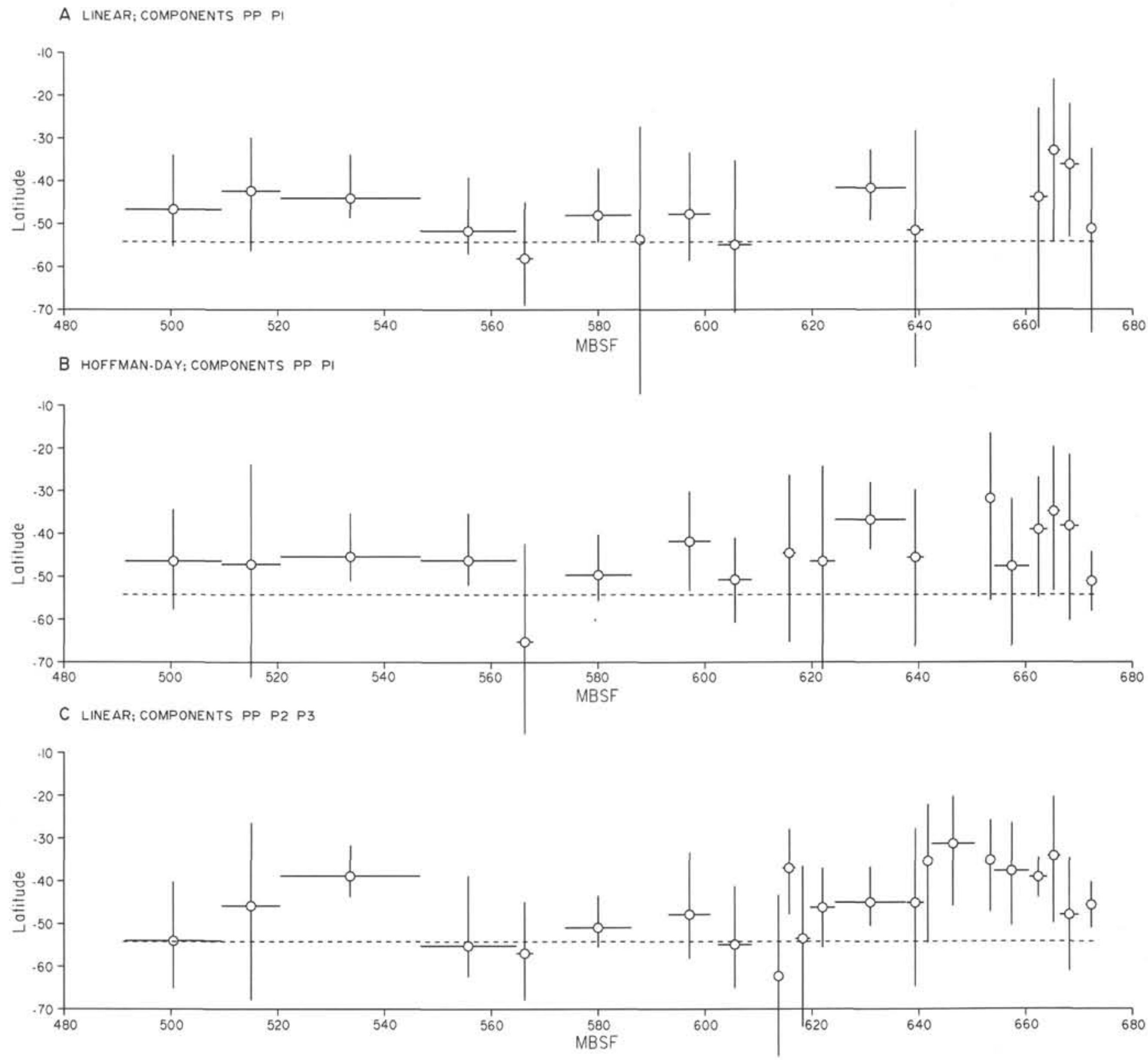

Figure 50. Mean paleolatitude vs. depth profiles for the basement sequence of Hole 758A (Cores 121-758A-55R to 121-758A-73R) from AF and thermal demagnetization data combined (see caption to Fig. 42 and Table 3). The mean results per cooling unit (**A–E**) comprise normal polarity primary magnetization results (open symbols; A–D) and reversed polarity overprint results (solid symbols; E). The overall (sample) mean result for the reversed polarity overprint is shown in **F**.

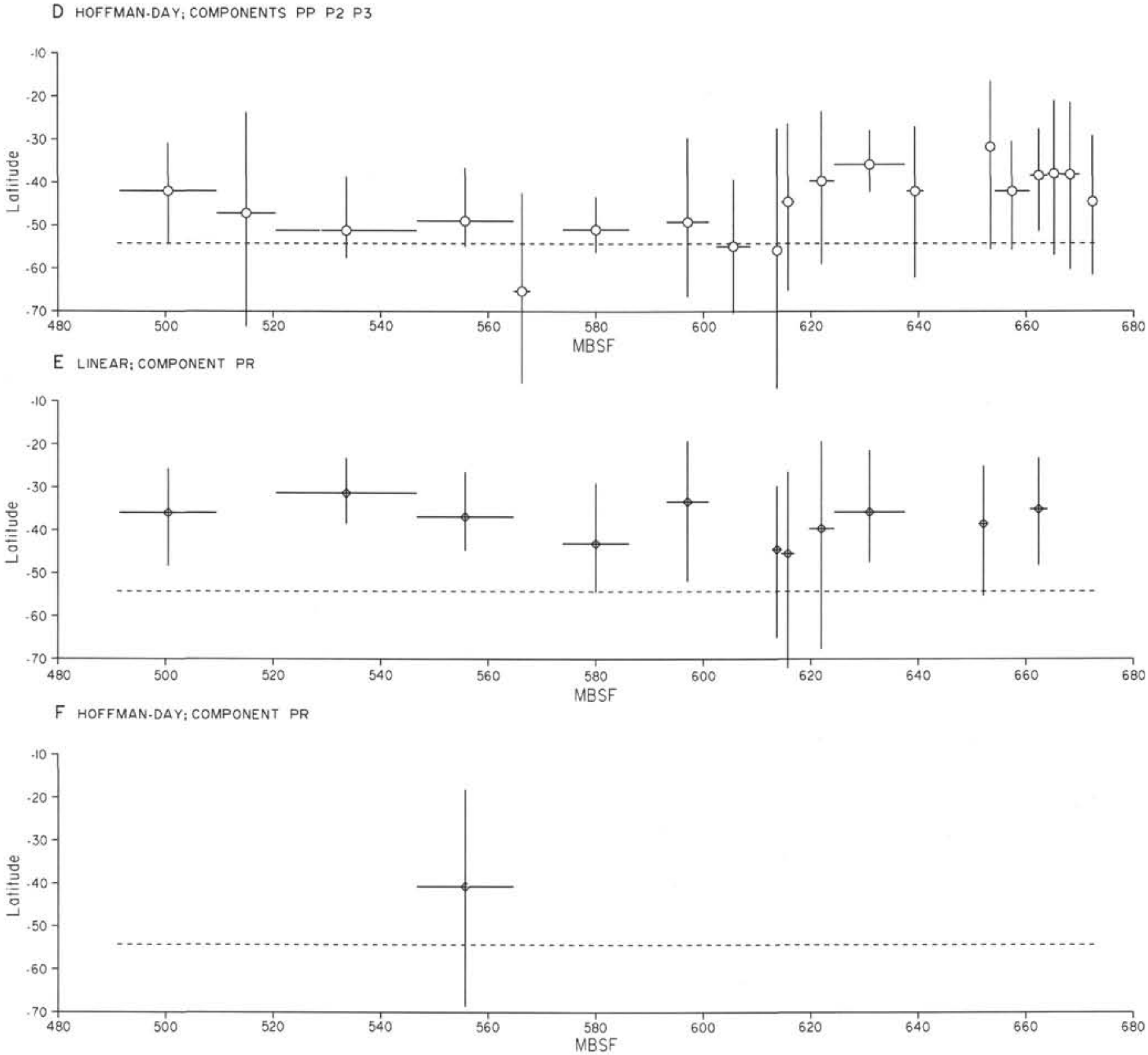

Figure 50 (continued).

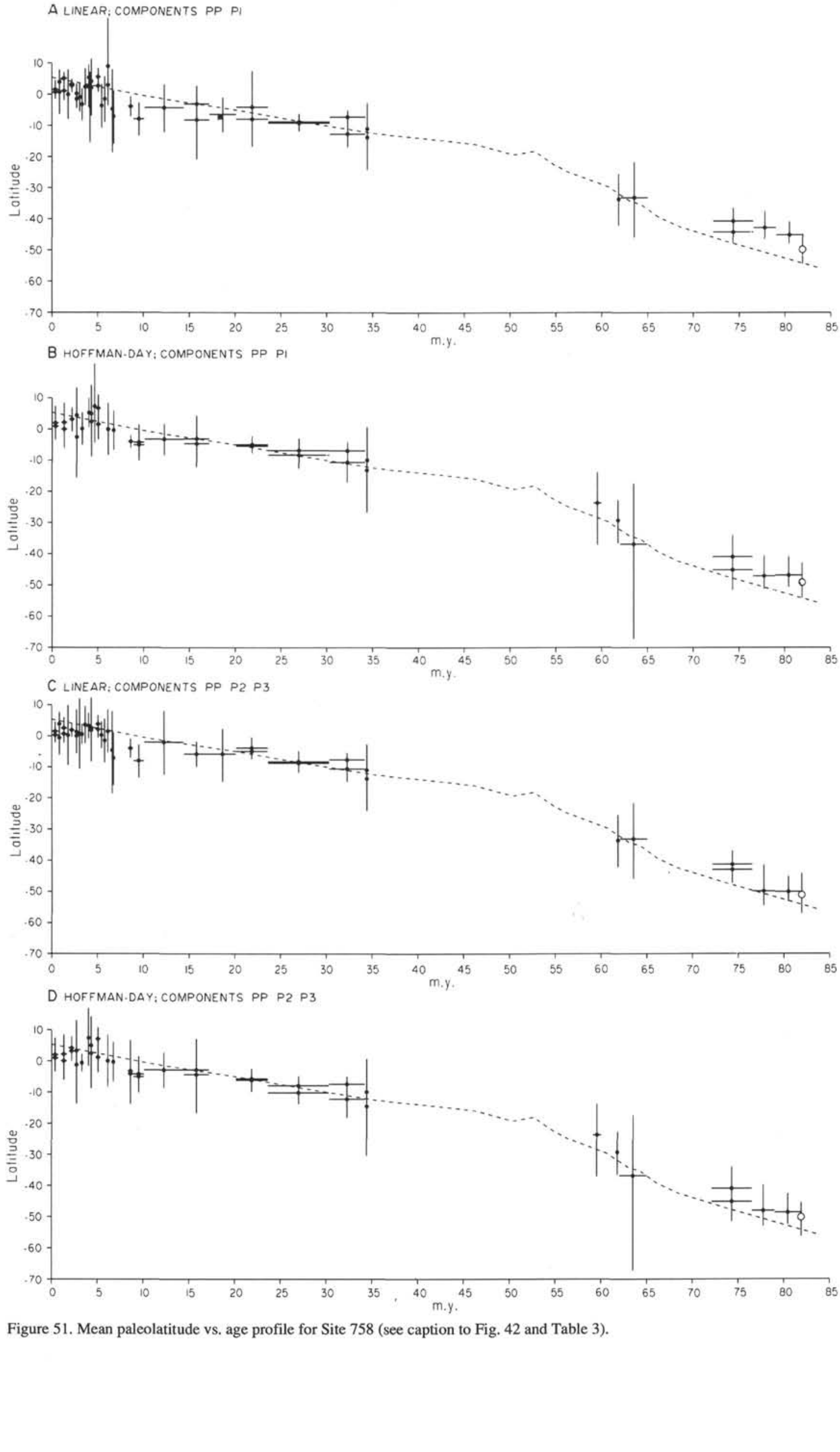

Figure 51. Mean paleolatitude vs. age profile for Site 758 (see caption to Fig. 42 and Table 3).

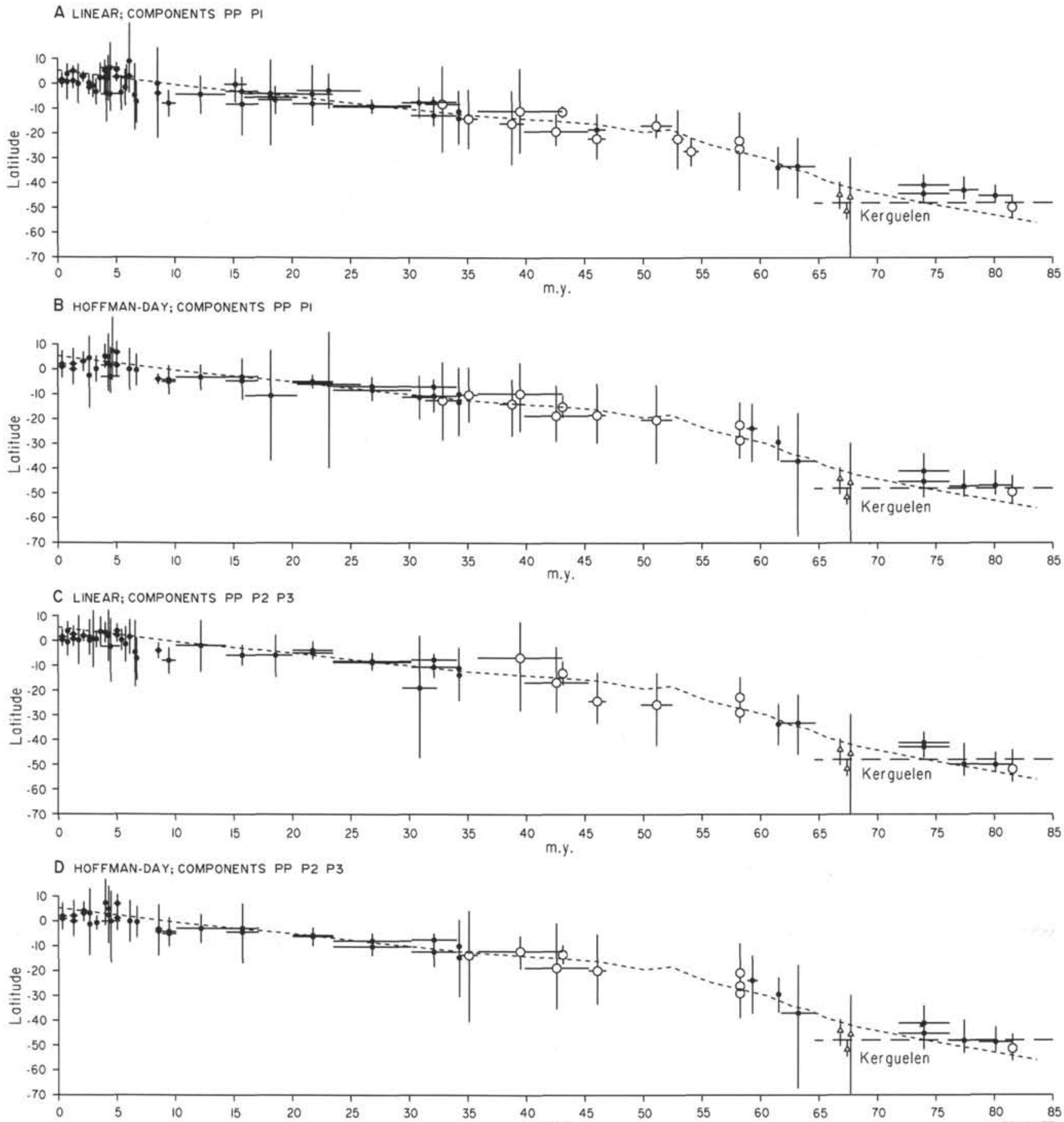

Figure 52. Combined mean paleolatitude vs. age profile for Sites 756, 757, and 758. All data were transferred over the pole to Site 758 (see caption to Fig. 42). The open triangles represent the Deccan Traps data (Fisherian mean; Klootwijk, 1979) (see "Transfer to Common-Site" section and Table 6), likewise transferred to Site 758.

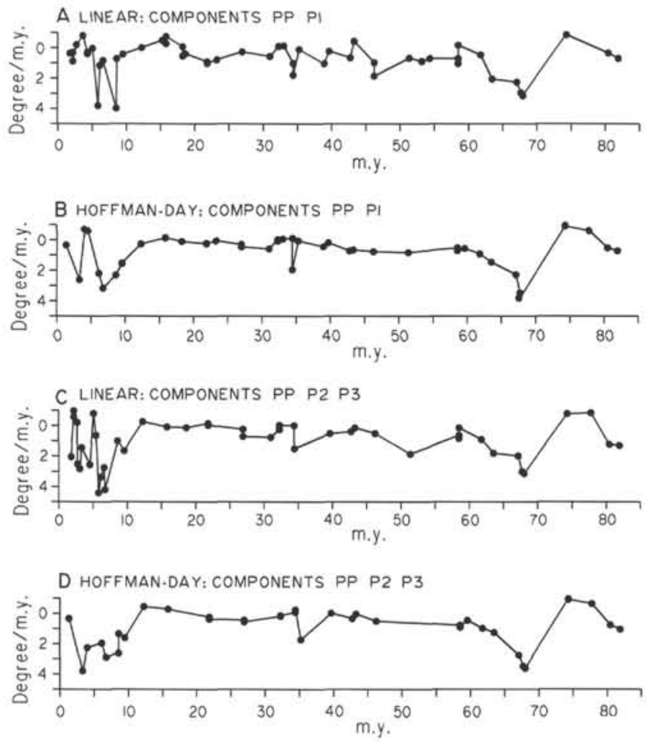

Figure 53. Northward movement rate of Site 758 calculated from the data represented in Figure 52 as a 5-m.y. moving window average.

Table 6. Mean inclination and 95% confidence intervals for DSDP/ODP results other than from Leg 121 and Deccan Traps data.

Site	Component[a]	Type			Age interval (Ma)		Number	Mean (degrees)	Confidence interval: Lower boundary (degrees)	Confidence interval: Upper boundary (degrees)
Site 214	BA	N+R	LP	AF	57.00	60.00	30	−65.20	−72.40	−57.30
Site 215	SE	N+R	LP	AF	57.00	58.00	29	−57.80	−52.40	−62.70
Site 216	BA	REV	LP	AF	67.00	72.00	42	68.70	60.30	76.20
Site 216	SE	N+R	LP	AF	22.00	30.00	9	−18.10	−34.20	0.20
Site 216	SE	N+R	LP	AF	26.00	34.00	13	−24.10	−36.80	−8.90
Site 216	SE	N+R	LP	AF	37.50	43.00	11	−28.40	−41.40	−12.80
Site 216	SE	N+R	LP	AF	65.00	68.00	16	−70.50	−75.60	−64.80
Site 217	SE	N+R	LP	AF	15.00	21.00	8	5.20	−14.40	24.40
Site 217	SE	N+R	LP	AF	26.00	30.00	13	−11.30	−26.20	4.00
Site 219	SE	N+R	LP	AF	54.00	59.00	11	−30.00	−35.60	−24.40
Site 220	SE	N+R	LP	AF	45.00	54.00	13	−27.30	−29.80	−24.80
Site 220	BA	N+R	LP	AF	49.00	54.00	17	−11.40	−12.80	−10.10
Site 221	BA	N+R	LP	AF	45.00	49.00	3	−31.40	−37.60	−25.20
Site 222	SE	N+R	LP	AF	5.00	22.50	49	15.70	8.00	23.20
Site 238	SE	N+R	LP	AF	19.00	30.00	22	−29.80	−33.00	−26.60
Site 238	BA	N+R	LP	AF	34.00	38.00	48	−28.20	−29.20	−27.20
Site 253	SE	N+R	LP	AF	46.00	48.00	49	−68.60	−71.20	−66.00
Site 254	BA	REV	LP	AF	30.00	40.00	9	68.80	81.30	54.80
Site 713	BA	REV	LP	AF	46.20	48.80	32	23.55	18.36	27.80
Site 715	BA	N+R	LP	EV	55.00	60.00	11	−43.03	−49.40	−35.53
Deccan Traps, N1	FI-1	NOR	LP	EV	67.10	[b]67.10	32	−63.08	−67.44	−58.72
Deccan Traps, R1	FI-1	REV	LP	EV	67.70	[b]67.70	47	68.16	65.92	70.40
Deccan Traps, N2	FI-1	NOR	LP	EV	68.00	[b]68.00	6	−64.08	−79.42	−48.74
Deccan Traps, N1	DD	NOR	LP	EV	67.10	[b]67.10	32	−65.48	—	—
Deccan Traps, R1	DD	REV	LP	EV	67.70	[b]67.70	47	68.15	—	—
Deccan Traps, N2	DD	NOR	LP	EV	68.00	[b]68.00	6	−58.19	—	—
Deccan Traps, N1	FI-2	NOR	LP	EV	67.10	[b]67.10	39	−62.36	−66.26	−58.00
Deccan Traps, R1	FI-2	REV	LP	EV	67.70	[b]67.70	120	65.33	63.14	67.40
Deccan Traps, N2	FI-2	NOR	LP	EV	68.00	[b]68.00	11	−64.67	−75.03	−50.53

Note: Results according to Peirce et al. (1974), Blow and Hamilton (1975), Cockerham et al. (1975), Peirce (1976, 1978), Klootwijk (1979), Vandamme and Courtillot (1990), and Vandamme et al. (in press). Results from Sites 214 to 254 were calculated according to Cox's method described in Peirce (1978) and Gordon and Cox (1984); see also Klootwijk (1979). Results for Sites 713 and 715 were recalculated following McFadden and Reid (1982). Deccan Traps data represent Fisherian (1953) means. All data were transferred to Site 758 over the pole (see "Transferral to Common-Site" section and Table 2).

[a] BA = basalts; SE = sediments; FI-1 = Fisherian mean at locality level (Klootwijk, 1979); DD = alternative estimate from the same data set of mean results from density distribution analysis at locality level (Klootwijk, 1979), which is presumed more accurate than the Fisherian mean, but was excluded from the analysis because no estimate of the confidence interval was available; FI-2 = Fisherian analysis (Vandamme et al., in press) at flow level.

[b] Token age intervals, based on alleged 1-m.y. duration of Deccan Traps activity at about 67.5 Ma (Duncan and Pyle, 1988a, 1988b; Courtillot et al., 1988).

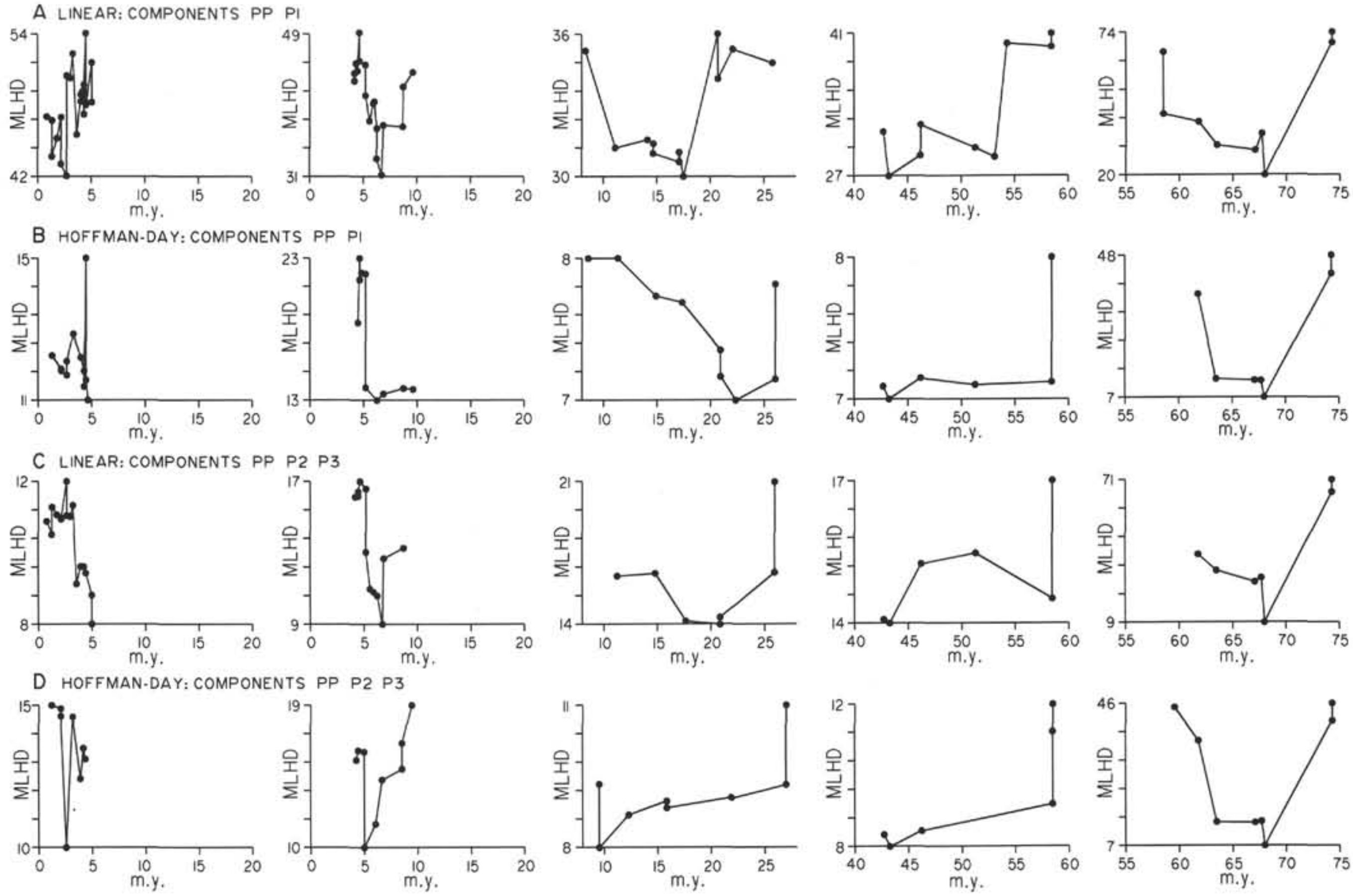

Figure 54. Maximum likelihood determination of breakpoints in the paleolatitude vs. age profile shown in Figure 52. In this method, chi-square values were determined for sets of two intersecting fitted-line segments with each set maintaining the same external end data points, but with the common data point varying between the two external end data points. The shifting common data points have covered most of the 0–85-Ma time span, with full coverage of the periods of particular interest. The maximum likely time interval of individual breakpoints was estimated visually as the interval showing minimal values of the sum of the chi-square values, plotted against the age of the variable common data point. (See "Maximum Likelihood Determination of Breakpoints" section for discussion of the procedure.) MLHD represents the sum of the chi-square values for the two intersecting weighted linear regression lines. The MLHD plot for the 68–74.5-Ma breakpoint interval is not reproduced here. This breakpoint is presumably not related to a change in northward movement rate (see "Mean Inclination/Latitude Results" section).

Table 7. Weighted least-squares fit parameters of paleolatitude/inclination data for Sites 756, 757, and 758 and the Deccan Traps, transferred to Site 758 (see "Transferral to Common-Site" section, Fig. 55, and Table 3), and for all other DSDP/ODP data for the Indian plate and Deccan Traps data (see "Comparison with DSDP, Other ODP, and Deccan Traps Data" section, Fig. 56, and Table 6).

Segment	Type	Components	Nominal regression age interval (Ma)	Number	Intercept latitude (degrees)	Gradient (degrees of latitude/ m.y.)	Intercept error	Gradient error	Chi-square value	Probability[a]
Leg 121 and Deccan Traps										
4A	Linear	PP, P_1	20–55	21	1.7	−0.37	1.65	0.049	37.4	0.007
4B	Hoffman-Day	PP, P_1	20–55	18	4.6	−0.44	2.39	0.083	5.44	0.993
4C	Linear	PP, P_2/P_3	20–55	14	5.0	−0.46	2.14	0.078	11.3	0.503
4D	Hoffman-Day	PP, P_2/P_3	20–55	13	1.4	−0.34	2.58	0.086	6.90	0.807
5A	Linear	PP, P_1	55–64	5	94.0	−2.04	61.38	1.030	0.33	0.954
5B	Hoffman-Day	PP, P_1	55–64	5	59.6	−1.44	76.18	1.271	1.17	0.759
5C	Linear	PP, P_2/P_3	55–64	5	79.4	−1.80	59.29	0.998	2.53	0.467
5D	Hoffman-Day	PP, P_2/P_3	55–64	6	46.1	−1.22	80.07	1.333	0.95	0.917
6A	Linear	PP, P_1	70–82	5	9.6	−0.70	22.85	0.294	3.78	0.286
6B	Hoffman-Day	PP, P_1	70–82	5	9.0	−0.70	36.91	0.469	0.98	0.806
6C	Linear	PP, P_2/P_3	70–82	5	54.5	−1.30	27.04	0.350	1.33	0.721
6D	Hoffman-Day	PP, P_2/P_3	70–82	5	34.0	−1.04	36.63	0.465	0.89	0.827
Other DSDP/ODP legs and Deccan Traps										
1	Linear	All	<55	14	9.4	−0.46	0.93	0.022	350.5	0.000
2	Linear	All	55–60	4	155.3	−3.19	112.57	1.973	0.825	0.662
3	Linear	[b]All	65–71	5	16.9	−0.98	142.01	2.102	4.712	0.194
3	Linear	[c]All	65–71	5	−21.4	−0.38	139.41	2.063	2.920	0.404
Intersection			Age (Ma)							
4A-5A			55.3							
4B-5B			54.6							
4C-5C			55.2							
4D-5D			50.4							
1-2			53.3							
[d]2-3										

[a] Goodness-of-fit probability, that the fit would have a chi-square value this large or larger.
[b] Mean Deccan Traps data according to Klootwijk (1979).
[c] Mean Deccan Traps data according to Vandamme et al. (in press).
[d] Calculation not made because of inherent inaccuracy of segment 3.

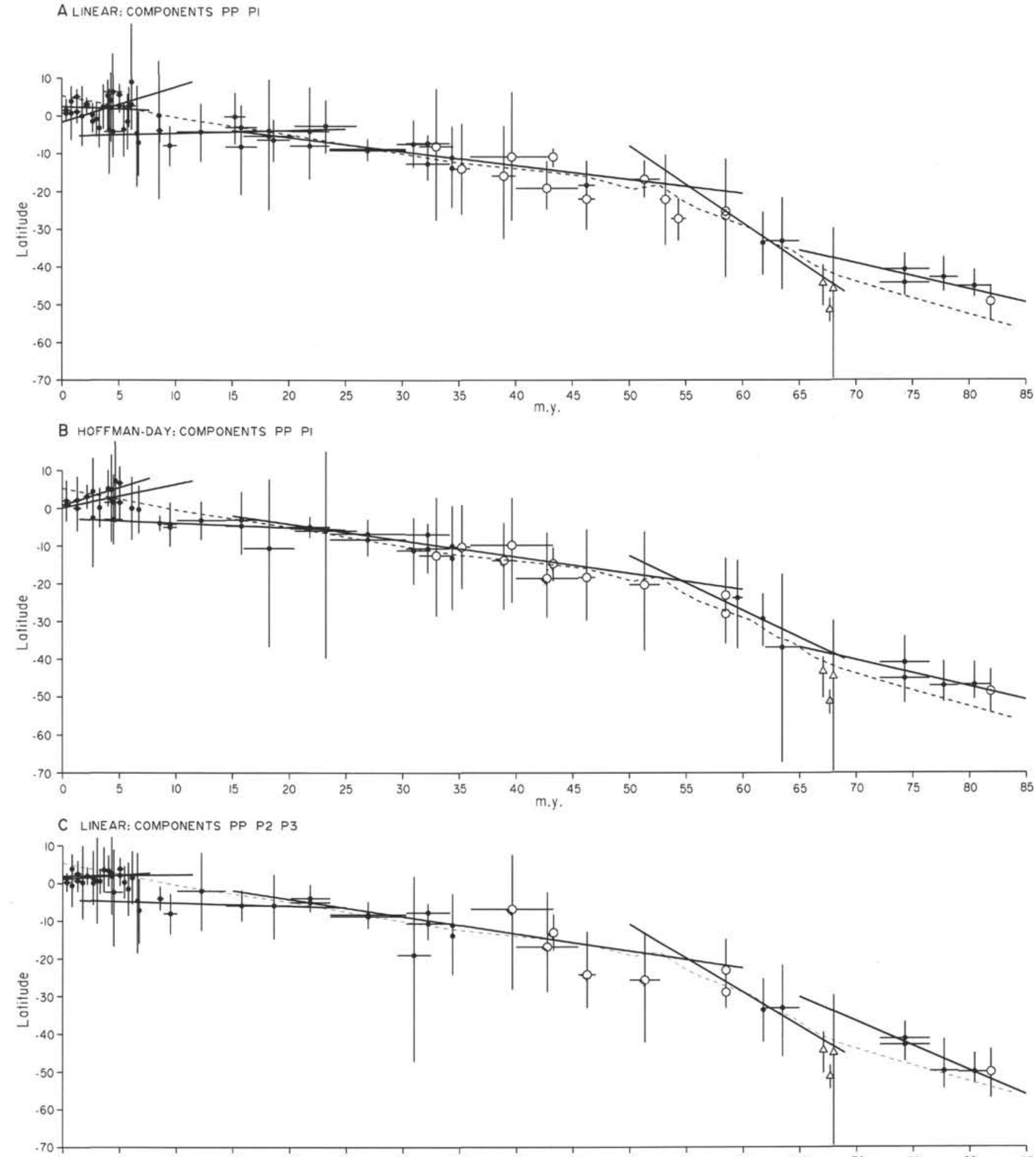

Figure 55. Weighted linear regression lines fitted to the data shown in Figure 52 (**A–D**), combined in Figure 55E. Northward movement rates for Site 758, as calculated from Figures 55**A**–55**D**, are shown in Figure 55**F**. The fitted lines were extended over 5 m.y. at both ends to visualize intersection. Intervals are 0–2.7, 2.7–6.5, 6.5–20.0, 20.0–55.0, 55.0–64.0, and 70.0-82.0 m.y. (see caption to Fig. 42 and Table 7). Confidence intervals for the weighted least-squares fitted lines (**A–D**) are confined by higher order trendlines, with confidence intervals increasing toward both ends. Because of their complexity no attempt was made to formalize confidence intervals on breakpoint ages (**A–D** and **E**) or on northward movement rates (**F**).

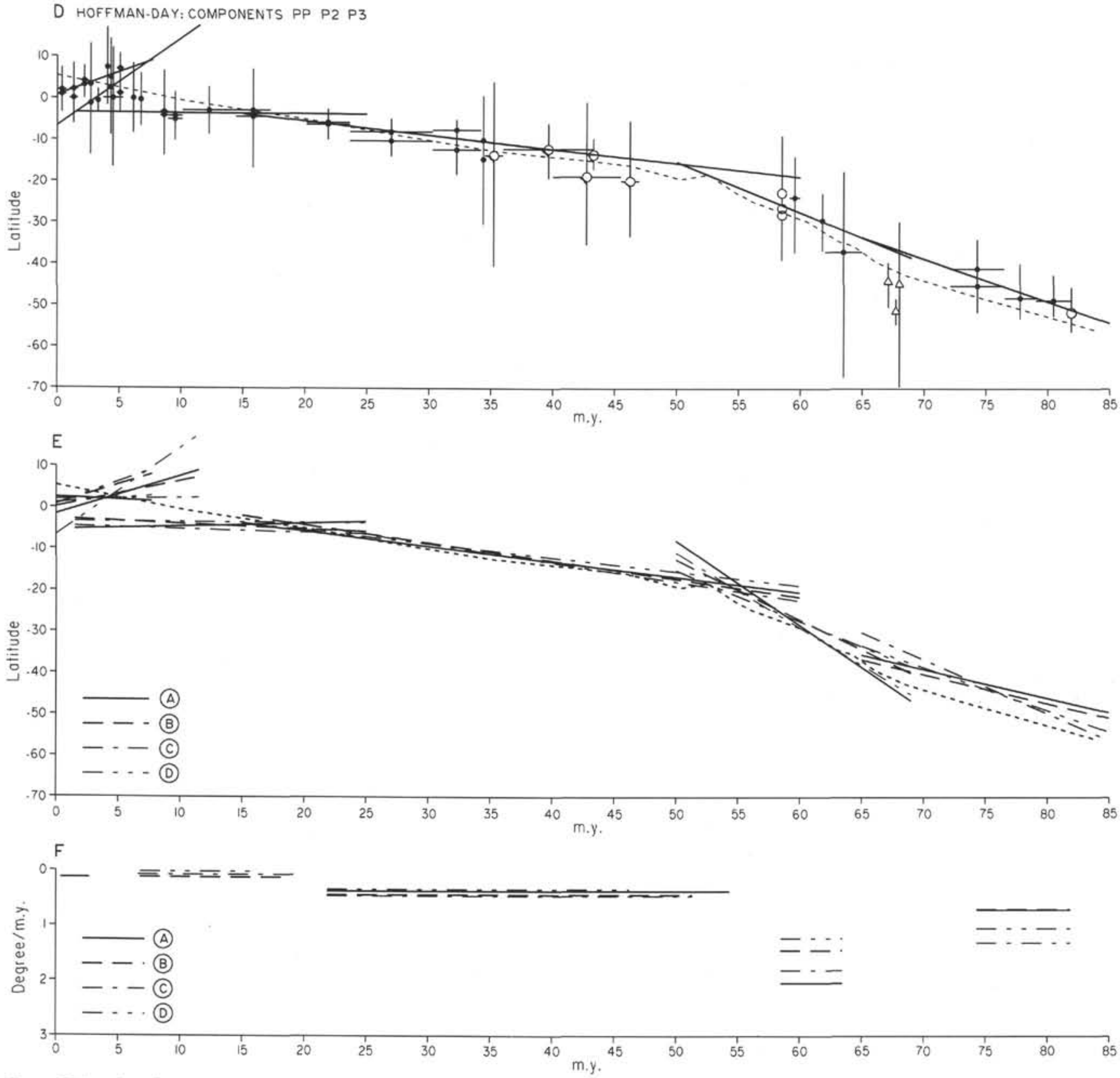

Figure 55 (continued).

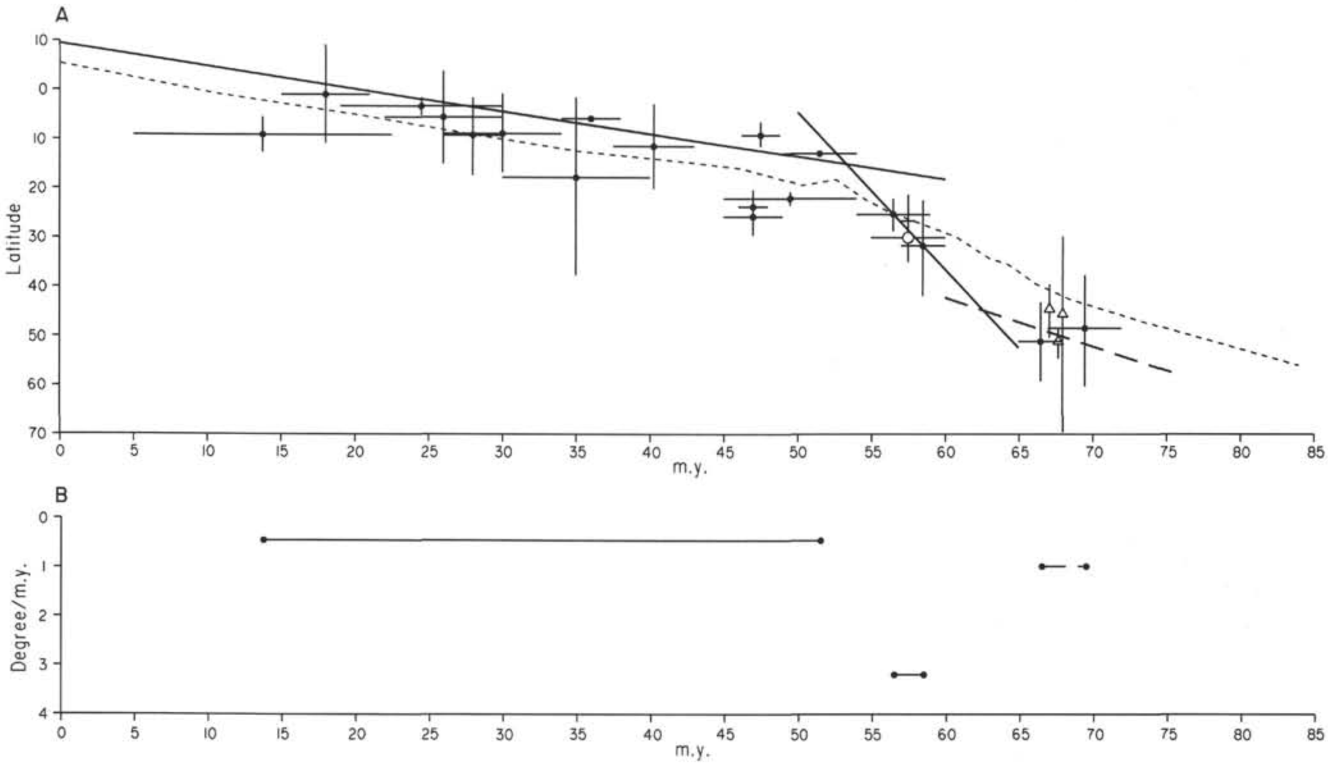

Figure 56. **A.** Weighted linear regression line fitted to all DSDP/ODP results other than Leg 121 data from the Indian plate and the Deccan Traps data (Table 6). **B.** Northward movement rates of Site 758 calculated from Figure 56A. Intervals are 0–55.0, 55.0–60.0, and 65.0–71.0 m.y. (inherently imprecise fit). (See captions to Figs. 42, 52, and 55 and Table 7.)

Table 8. Pole positions for the Indian plate in the interval 20–65 Ma.

Time (Ma)	Site 758 paleolatitude (S, degrees) 4A	4B	4C	4D	Mean[a]	Declination (E, degrees)	South Pole position Longitude (E, degrees)	Latitude (S, degrees)
20	5.7	4.0	4.2	5.5	4.63	354.35	119.87	78.51
25	7.55	6.2	6.5	7.1	6.75	352.35	122.63	75.67
30	9.4	8.4	8.8	8.7	8.87	349.85	125.80	72.52
35	11.25	10.6	11.1	10.3	11.0	346.75	129.19	68.97
40	13.1	12.8	13.4	11.9	13.1	345.92	127.38	66.82
45	14.95	15.0	15.7	13.5	15.2	345.80	124.53	65.07
50	16.80	17.2	18.0	15.1	17.33	345.65	122.04	63.23
55	18.65	19.4	20.3	16.7	19.45	345.55	119.79	61.39
	5A	5B	5C	5D	Mean[a]			
55	18.2	19.6	19.6	21.0	19.13	345.55	120.14	61.66
60	28.4	26.8	28.6	27.1	27.93	345.77	112.03	53.97
65	38.6	34.0	37.6	33.2	36.64	342.34	110.44	44.85

Note: Pole positions obtained from inclination data according to weighted least-squares fits (Table 7 and Fig. 55) and declinations simulated according to the Morgan/Patriat pole positions (Table 2).

[a] Based on data from segments 4A–4C and 5A–5C (Table 7) only. Data from segments 4D and 5D seem aberrant.

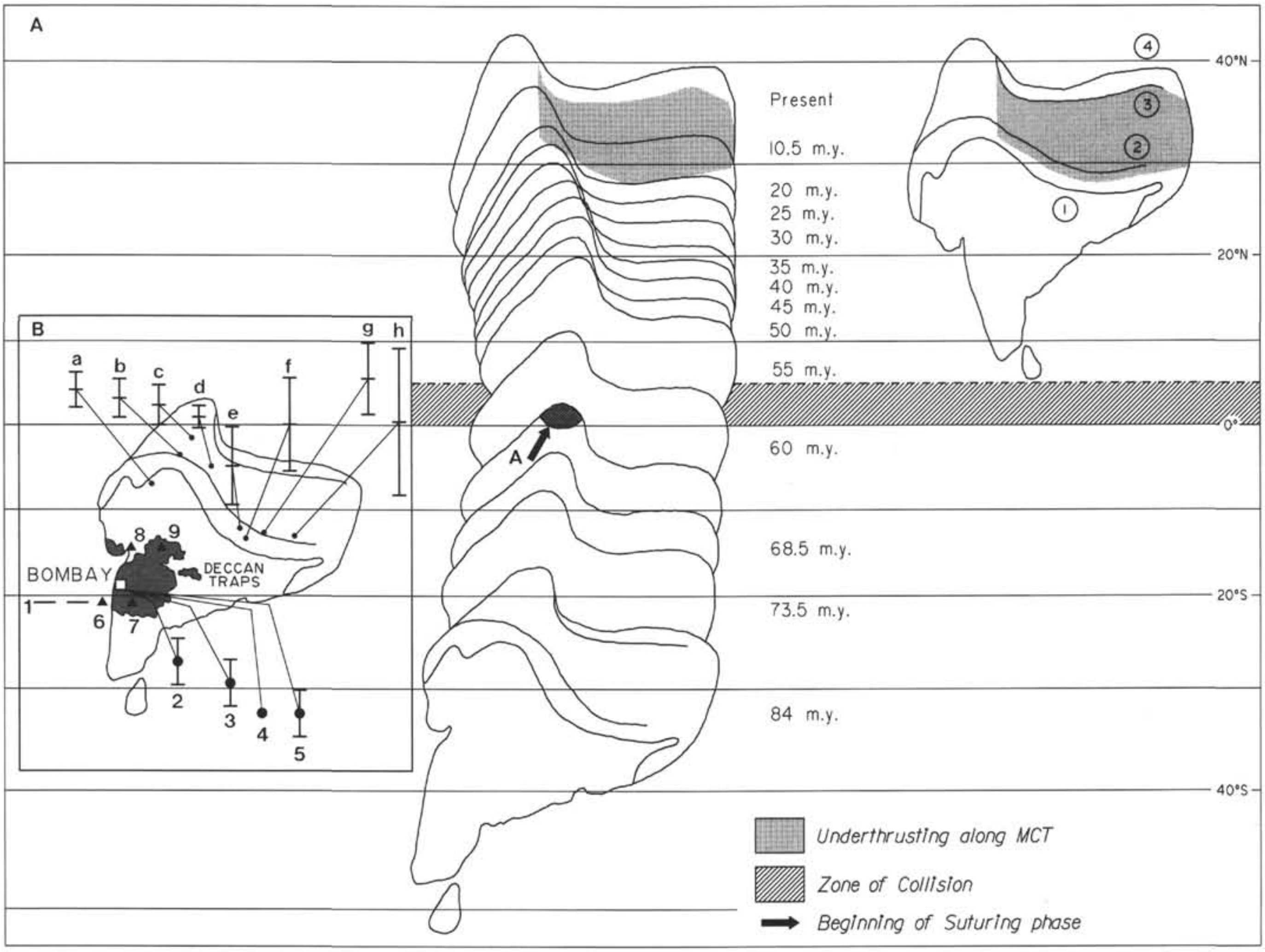

Figure 57. **A.** Northward movement of the Indian plate according to the Morgan/Patriat pole positions (84.0, 73.5, 68.5, and 10.5 Ma; Table 2) and weighted linear regression data (5-m.y steps between 65 and 20 Ma; Tables 7 and 8). Outlines within Greater India represent (from south to north): 1 = Himalayan mountain front; 2 = present-day position of the Indus-Tsangpo suture rotated with the outline of Peninsular India; 3 = reconstructed southern boundary of the Tethyan Himalayan region along the Main Central Thrust (MCT); 4 = minimal northern extent of Greater India as described in text. The equatorial to low northern paleolatitudinal belt (heavily shaded) is based on collision-related secondary magnetization components detailed in Figure 57B and Table 9. **B.** Greater India's paleoposition at 65 Ma (see Fig. 57A) and paleolatitudes defined by the collision-related secondary magnetization components detailed in Table 9 and the text. 1 = present-day latitude of Réunion hot spot; 2 = paleolatitude for Bombay (arbitrary locality, not necessarily related to hot-spot location) according to mean Deccan Traps results (Besse and Courtillot, 1988); 3 = paleolatitude for Bombay according to mean result for the reversed polarity sequence (R1) of the Deccan Traps (Vandamme et al., in press) (Table 6), with unit value given to flow means; 4 = as for 3, according to density distribution analysis (Klootwijk, 1979), with unit value given to locality means and confidence intervals not determined; 5 = as for 3, according to Fisherian analysis (Klootwijk, 1979), with unit value given to locality means; 6, 7 = expected location relative to the Indian plate of the Réunion hot spot at 65 Ma, uncorrected (6) or corrected (7) for late Neogene movement along the diffuse India/Australia plate boundary (Royer et al., this volume, figs. 9 and 10); 8, 9 = as for 6 and 7, at 70 Ma. Sample locations a–h (Table 9) are shown in their present position relative to the Indian shield, not in their original position within Greater India.

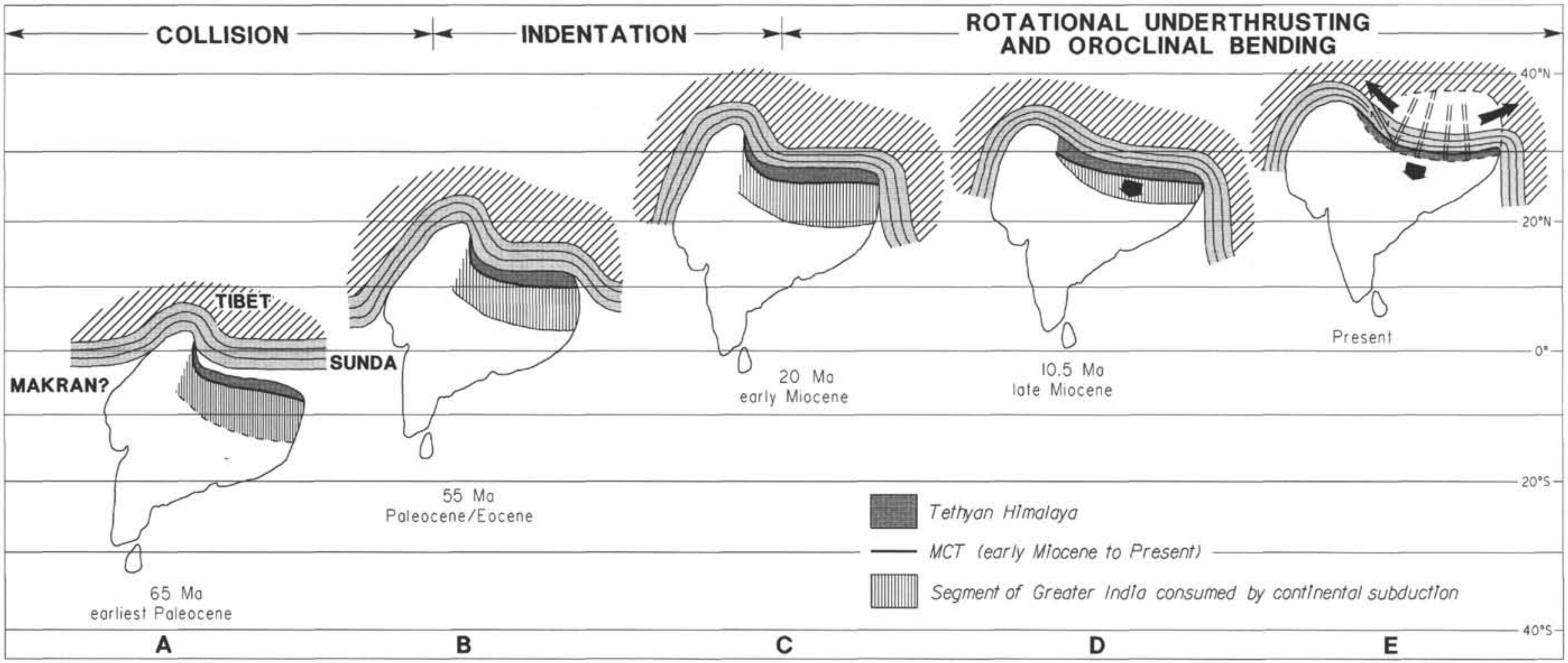

Figure 58. Five stages in the India-Asia convergence, modified from Klootwijk et al. (1985, fig. 6) on the basis of our new paleolatitudinal data (Tables 2 and 6–8). Note development at stage C of the Main Central Thrust (MCT) at about 150–200 km to the south of the leading edge of Greater India (Tethyan Himalaya) and its clockwise propagation with respect to the Indian Shield up to the present-day position of the Boundary Thrust Fault (Seeber et al., 1981). Also note the causal relationship between rotational underthrusting, oroclinal bending, extension in southern Tibet north of the MCT, and (E) dextral displacement on the Pamir-Karakorum Fault. The five stages represented are (**A**) initial collision (about Cretaceous/Tertiary boundary time); (**B**) completion of suturing (55 Ma); (**C**) onset of intercontinental underthrusting (early Miocene); (**D**) late Miocene stage of large-scale rotational underthrusting; and (**E**) initiation of oroclinal bending during the late Miocene/early Pliocene, probably continuing during the Pliocene/Quaternary.

Table 9. Paleolatitudes of collision-related secondary components observed within the India-Asia convergence zone.

Formation	Location[a] (longitude: E, degrees; latitude: N, degrees)	Mean direction: Declination (degrees)	Inclination (degrees)	K	α_{95} (degrees)	Paleo-latitude (degrees)	Reference
Indian plate							
Nawakot Complex	f (84.8, 27.7)	28	1	36	11	0.5N	Gautam and Yoshida (1988)
Tibetan sediments	e (83.7, 28.7)	352.6	−8.9	64.6	8.4	4.5S	Klootwijk and Bingham (1980)
Dingri Limestone	g (87.1, 28.7)	19.7	11.8	132	8.0	6.0N	Besse et al. (1984)
Moghul Kot Formation	a (70.5, 29.6)	20.5	8.5	22	4	4.3N	Klootwijk et al. (1981)
Nowshera Reef	b (72.0, 34.2)	157.7	−6.3	13.8	4.6	3.2N	C. T. Klootwijk et al. (unpubl. data)
Trans-Indian plate							
Indus Molasse/Dras Flyshoids	d (76.9, 34.3)	–	2.9	–	3	1.4N	Klootwijk et al. (1984)
Chitral (combined)	c (72.6, 36.5	–	5.6	–	4.9	2.8N	C. T. Klootwijk et al. (unpubl. data)
Jurassic limestone, Lhasa	h (91.1, 29.7)	175	2	5	17	1.0S	Zhu Zhi Wen et al. (1981) and Zhu Zhi Wen and Teng Jiwen (1984)

Note: See "Date of Initial Contact and Completion of Suturing" section and Figure 57B.
[a] Sample locations shown on Figure 57B.

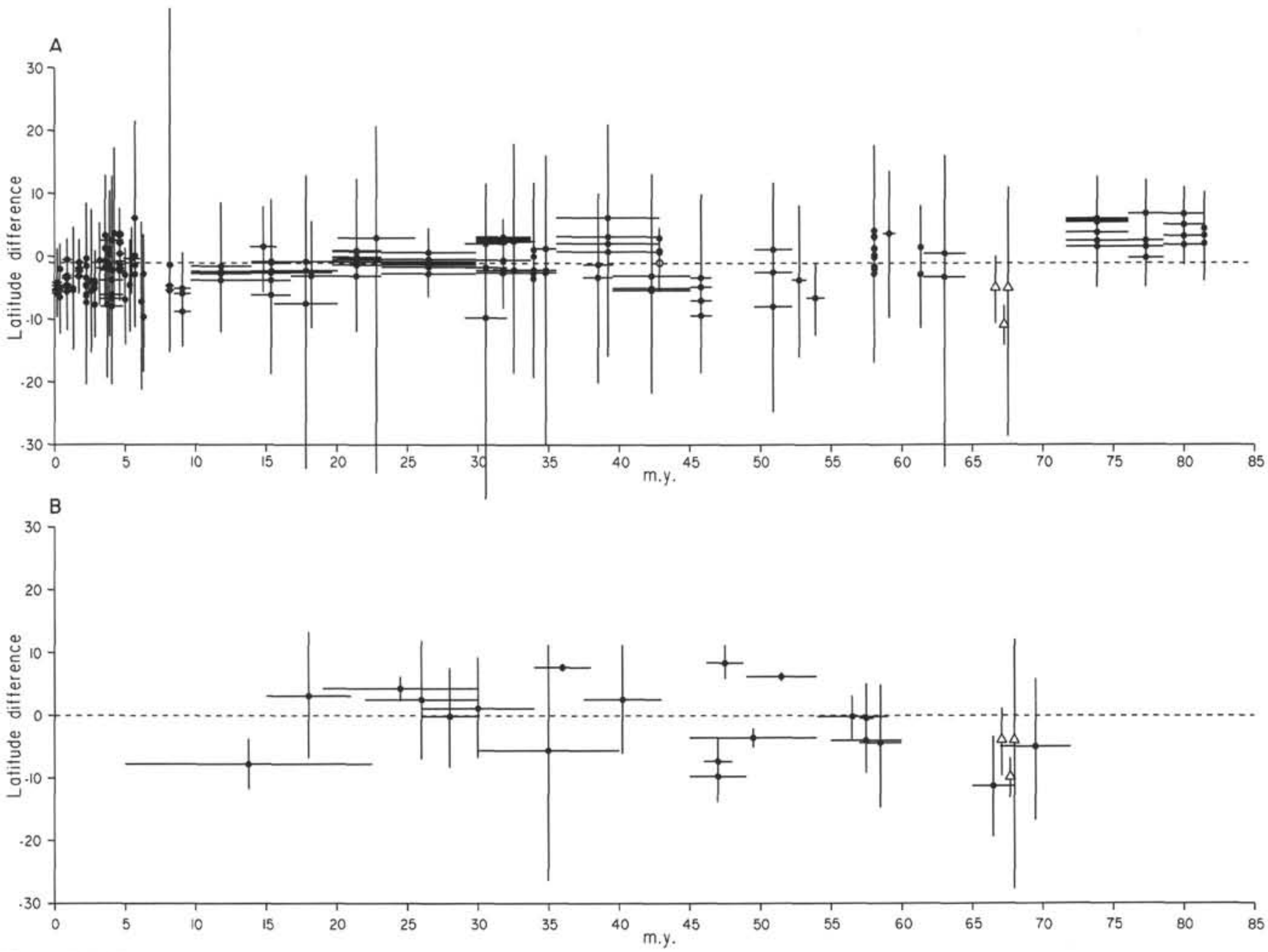

Figure 59. Difference between observed (A: Fig. 52; B: Fig. 53) and expected (Table 2) paleolatitudes for Leg 121 data (**A**) and other DSDP/ODP data from the Indian plate (**B**) (Table 6). Deccan Traps data are included (see caption to Fig. 52).

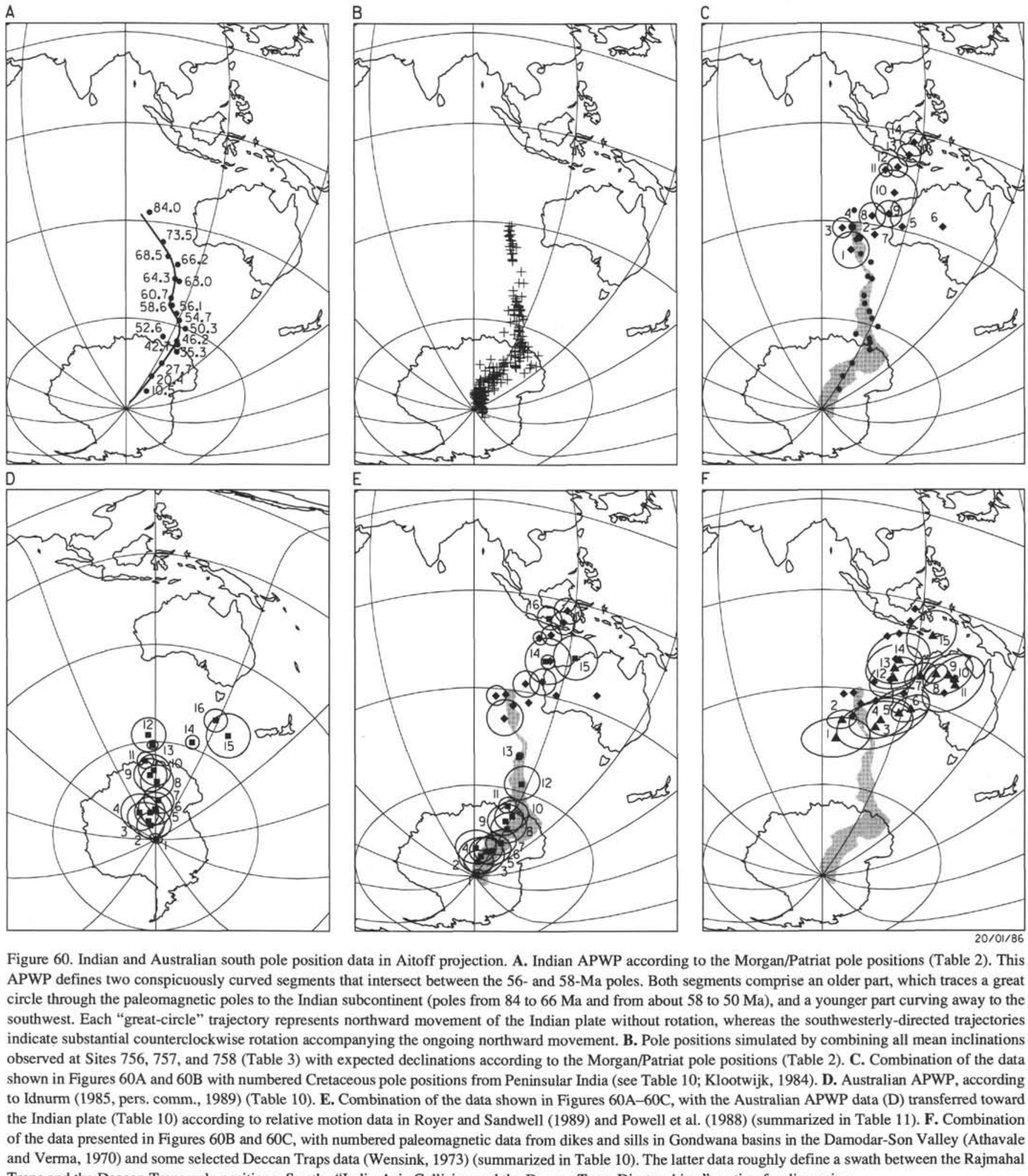

Figure 60. Indian and Australian south pole position data in Aitoff projection. **A.** Indian APWP according to the Morgan/Patriat pole positions (Table 2). This APWP defines two conspicuously curved segments that intersect between the 56- and 58-Ma poles. Both segments comprise an older part, which traces a great circle through the paleomagnetic poles to the Indian subcontinent (poles from 84 to 66 Ma and from about 58 to 50 Ma), and a younger part curving away to the southwest. Each "great-circle" trajectory represents northward movement of the Indian plate without rotation, whereas the southwesterly-directed trajectories indicate substantial counterclockwise rotation accompanying the ongoing northward movement. **B.** Pole positions simulated by combining all mean inclinations observed at Sites 756, 757, and 758 (Table 3) with expected declinations according to the Morgan/Patriat pole positions (Table 2). **C.** Combination of the data shown in Figures 60A and 60B with numbered Cretaceous pole positions from Peninsular India (see Table 10; Klootwijk, 1984). **D.** Australian APWP, according to Idnurm (1985, pers. comm., 1989) (Table 10). **E.** Combination of the data shown in Figures 60A–60C, with the Australian APWP data (D) transferred toward the Indian plate (Table 10) according to relative motion data in Royer and Sandwell (1989) and Powell et al. (1988) (summarized in Table 11). **F.** Combination of the data presented in Figures 60B and 60C, with numbered paleomagnetic data from dikes and sills in Gondwana basins in the Damodar-Son Valley (Athavale and Verma, 1970) and some selected Deccan Traps data (Wensink, 1973) (summarized in Table 10). The latter data roughly define a swath between the Rajmahal Traps and the Deccan Traps pole positions. See the "India-Asia Collision and the Deccan Traps Diastrophism" section for discussion.

Table 10. Late Cretaceous Indian pole positions (Fig. 60C), Tertiary and Late Cretaceous pole positions for Australia (Fig. 60D), and selected Indian pole positions with ages and pole positions spread between the Deccan Traps (Cretaceous/Tertiary boundary) and the Rajmahal Traps (~116 Ma) (Fig. 60F).

			South Pole position					
Number	Formation	Age	Longitude (E, degrees)	Latitude (S, degrees)	Dp[f] (degrees)	Dm[f] (degrees)	E95[g] (degrees)	Reference[a]
Indian pole position								
1	Deccan Traps, N1[b]	~Cretaceous/ Tertiary boundary	101.5	39			5.5	6
2	Deccan Traps, N1[c]	~Cretaceous/ Tertiary boundary	104	35			–	6′
3	Deccan Traps, R1[b]	~Cretaceous/ Tertiary boundary	97.5	32.5			3	7
4	Deccan Traps, R1[c]	~Cretaceous/ Tertiary boundary	101	32			–	7′
5	Deccan Traps, N2[b]	~Cretaceous/ Tertiary boundary?	118.5	29.5			18.5	8
6	Deccan Traps, N2[c]	~Cretaceous/ Tertiary boundary?	132	26			–	8′
7	Tirupati Sandstone	Early Cretaceous		109.5	33.5	10.5	15	10
8	Tirupati Sandstone	Early Cretaceous		107.5	28	4.5	6	11
9	Satyavedu beds	Early Cretaceous		113	26.5	4.5	6	12
10	Sylhet Traps	Early Cretaceous?		113.5	20	8	10.5	13
11	Rajmahal Traps	~116 Ma	110	13.5	2.5	3		14
12	Rajamahal Traps	~116 Ma	113.5	12	4	5		15
13	Rajmahal Traps	~116 Ma	116.5	7.5	3	3.5		16
14	Rajmahal Traps	~116 Ma	117.5	3.5	5.5	6.5		17
Australian pole position								Reference[d]
1	Holocene lake sediments	0.005 Ma	144.6	89.4			1.5	1
2	Newer volcanics	~3 Ma	100.9	85.4			4.0	2
3	Newer volcanics/Werriko Limestone	2.9 Ma	103.6	83.2			6.2	1
4	Springfield basin	–	90.5	80.4			5.6	3
5	Perth basin	–	108.8	81.2			4.5	4
6	Sequence 2	–	119.2	80.4			<5	1
7	Glenample Formation/Port Campbell Limestone	12 Ma	123.5	77.2			4.2	1
8	Sequence 3	–	121.4	72.1			<5	1
9	Sequence 1	–	115.3	70.1			<5	1
10	Point Addis Limestone	26 Ma	118.7	68.4			4.8	1
11	Browns Creek Clay	43? Ma	112.5	65.5			2.5	2
12	Morney profile	–	116.2	57.8			5.2	1
13	North Rankin 1	58 Ma	118.4	61.7			–	1
14	Lower Cretaceous overprint	–	141.8	58.2			2.1	5
15	100 Ma	100 Ma	157.6	51.7			6.7	6
16	Otway Group	110–115 Ma	148.7	48.9			3.6	1
Indian pole position: Deccan Traps–Rajmahal Traps spread								
1	Gondwana dikes #25	–	99.5	46.4	6.0	10.4		7
2	Gondwana dikes #28	–	97.3	40.4	2.8	4.5		7
3	Gondwana dikes #30	–	111.2	41.5	6.9	11.7		7
4	Gondwana dikes #10	–	112.6	38.9	5.8	9.6		7
5	Rajahmundry Traps	~Deccan Traps	118.7	35.8	6.4	10.1		8
6	Gondwana dikes #27	–	122.5	33.6	3.6	6.0		7
7	Gondwana dikes #36	–	122.7	23.4	3.4	5.2		7
8	Gondwana dikes #37	–	127.3	21.4	2.4	3.8		7
9	Gondwana dikes #16	–	131.4	20.6	5.3	8.3		7
10	Rajahmundry Traps	Deccan Traps	133.5	21.0	–	–		9
11	Rajahmundry Traps	Deccan Traps	134.4	22.7	6.8	10.9		10
12	Dhar Traps Unit DF	Deccan Traps	114.1	25.7	5.2	8.0		11
13	Gondwana dikes #20	–	113.7	22.8	6.4	8.9		7
14	Gondwana dikes #14	–	114.7	20.1	7.3	9.9		7
15	Pohor Traps	[e]59.6 Ma (Deccan Traps)	123.6	10.5	6.2	8.8		12

[a] Numbers correspond to table 1 in Klootwijk (1984).
[b] Fisherian mean.
[c] Mean obtained from density distribution analysis.
[d] 1 = Idnurm (1985); 2 = M. Idnurm (pers. comm., 1989); 3 = Schmidt (1976b); 4 = Schmidt and Embleton (1976); 5 = mean from Patonga Claystone, Hornsby Breccia (Embleton, 1981), Gordon Sub-Group (Staples and Klootwijk, 1981), and Brisbane Tuff (Robertson, 1963); 6 = Embleton (1981); 7 = Athavale and Verma (1970); 8 = Rao and Rao (1963); 9 = Bhimasankaram (1964); 10 = Singh and Bhalla (1972); 11 = Poornachandra Rao and Bhalla (1981); 12 = Wensink (1973), Wensink et al. (1979).
[e] ^{40}K-^{40}Ar.
[f] Half angles of the oval of 95% confidence about the pole position.
[g] Half angle of the circle of 95% confidence about the pole position.

Table 11. India-Australia relative motion data used to transfer Australian pole positions (Table 10 and Fig. 60D) to the Indian plate (Fig. 60E).

Time span (Ma)	Chron	Latitude (N, degrees)	Longitude (E, degrees)	Angle (degrees)	Reference
0.0–42.7	0–18	90.0	0.0	0.00	Royer and Sandwell (1989)
42.7–46.2	18–20	17.6	−32.8	−1.47	Royer and Sandwell (1989)
46.2–56.1	20–24	0.7	2.8	−9.28	Royer and Sandwell (1989)
56.1–64.3	24–28	−0.1	3.1	−10.95	Royer and Sandwell (1989)
64.3–68.5	28–31	3.6	−11.1	−7.16	Royer and Sandwell (1989)
68.5–80.2	31–33	−1.2	−6.5	−11.03	Royer and Sandwell (1989)
80.2–84.0	33–34	−2.2	−4.1	−2.73	Royer and Sandwell (1989)
84.0–96.0		−6.00	−9.33	−13.02	Powell et al. (1988)
96.0–132.5		−58.37	67.42	−25.81	Powell et al. (1988)
132.5–160.0		58.0	116.0	0.33	Powell et al. (1988)

Table 12. Depth and age of breaks in the magnetic, susceptibility, and lithologic profile of the Neogene sequence at Site 758.

	Depth (mbsf)				Age[a] (Ma)	
	Intensity change					
		NRM				
Break	Suscept-ilibity	(9 mT)	(100 mT)	Litho-stratigraphy	Magneto-stratigraphy	Biostra-tigraphy
K1/K2	26.5	Not clear	26–27	–	1.9	[b]1.9
K2/K3	36.3	35–37	35–37	–	2.5–2.7	[c]2.2–2.6
K3/K4	73.8	72–77	71–78	–	5.1–5.4	[d]5.6+
NRM increase	–	88–93	88–93	–	6.2–6.5	
K4/K5	112	Not clear	112	–		[e]8.8
Unit I/II boundary	121–125	Not clear	Not clear	121.5		[f]10–10.4
K5/K6	144–145	Not clear	Not clear	–		[g]17.5

[a] Magnetostratigraphic ages are preferred to biostratigraphic ages.
[b] Last occurrence (LO) of *D. brouweri* at 26.45 mbsf (P. Resiwati, pers comm., 1989).
[c] LO of *D. pentaradiatius* at 34.95 mbsf and LO of *D. tamalis* at 40.55 mbsf (P. Resiwati, pers. comm., 1989).
[d] LO of *D. quinqueramus* at 71.2 mbsf (P. Resiwati, pers. comm., 1989).
[e] LO of *D. hameatus* (8.85 Ma) at 114.85 mbsf (P. Resiwati, pers. comm., 1989); microplanktonic dates: 5.2–7.7 Ma at 102 mbsf and 7.7–10.2 Ma at 112 mbsf (P. Gamson, pers. comm., 1989).
[f] Age at 121.5 mbsf, according to Shipboard Scientific Party (1989i).
[g] LO of *S. belemnos* (17.4 Ma) at 143.75 mbsf (P. Resiwati, pers. comm., 1989); microplanktonic dates: 15.2–16.6 Ma at 140 mbsf and 17.6–20.9 Ma at 150 mbsf (P. Gamson, pers. comm., 1989).

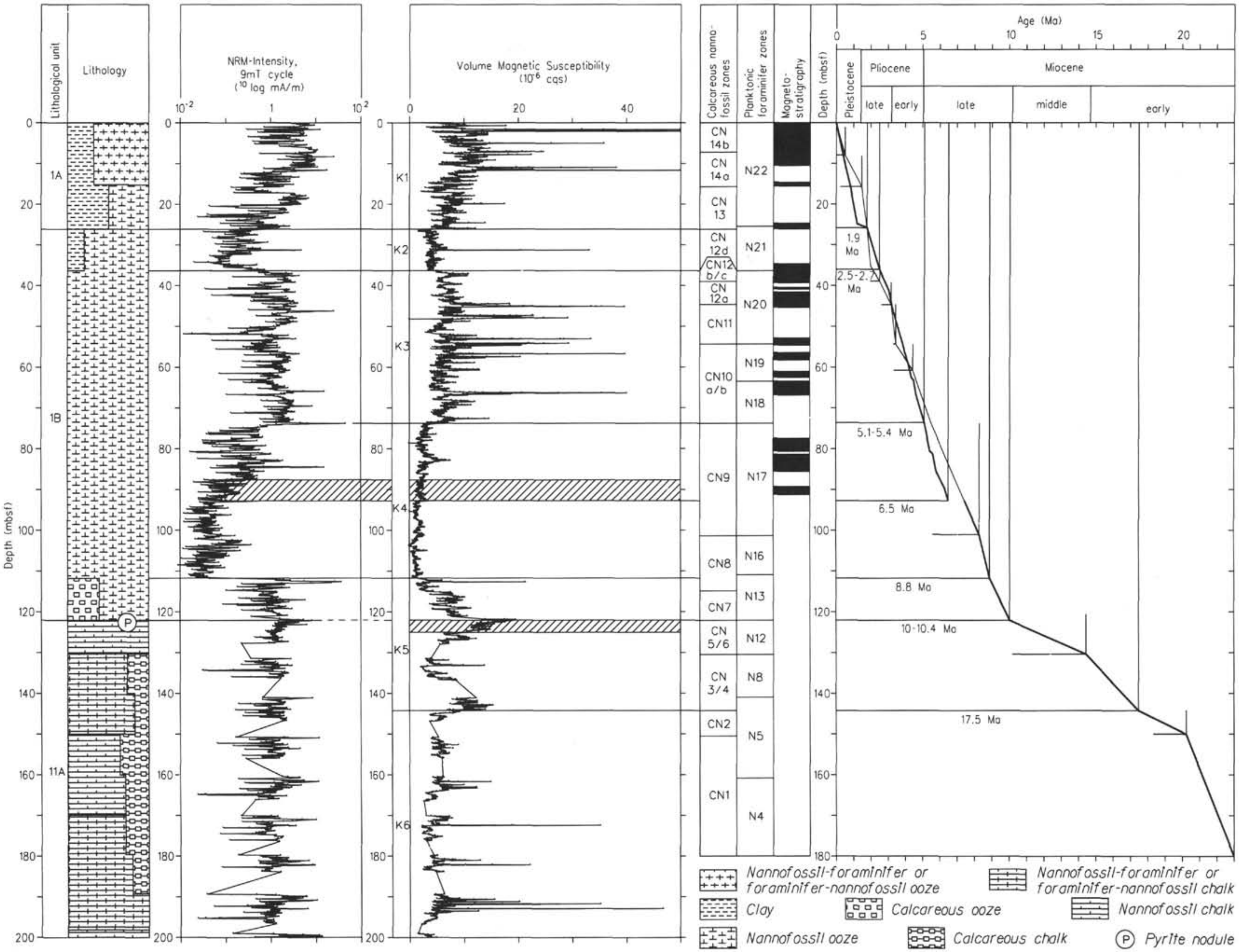

Figure 61. Relation between lithostratigraphic marker levels, remanence intensity, susceptibility, and the Neogene age/depth record of Hole 758A, with K-unit boundaries and other breaks indicated (Table 12). The age/depth record is based on magnetostratigraphic and biostratigraphic results from shipboard studies only (Shipboard Scientific Party, 1989i).